Petrophysical characterization of paleokarst and effect on reservoir properties

Master Thesis

Katrine Slotnæs

Department of Physics and Technology/Department of Earth Science

University of Bergen

June 2012

Abstract

Karst is a geological process that can enhance porosity and permeability within a carbonate succession, thus affecting the heterogeneity producing a substantial effect on the fluid flow. The subject is not widely explored in the petroleum-related literature and hydrocarbon exploration depends on recognizing geological structures. In this case, paleokarst within the Northern Billefjorden, Svalbard, have been used as an analog for classifying paleokarst structures and estimate the petrophysical properties.

Samples were collected from 21 separate breccia bodies. They show a wide range in texture and brecciation. Petrophysical properties were determined using the saturation method for estimating the porosity, and air – and water measurements for estimating the permeabilities.

Samples that were unaffected by brecciation gave low effective porosity values. Whereas the voids and vuggy pore space of the brecciated samples yield also low porosity which indicated that the pores were rarely connected. Cements within the brecciated samples could be observed visually and occluded the fractures traces as much as 100 % in some areas. Flow permeability values determined from the samples gave low permeabilities (< 10 mD) for all of the samples. However the permeability of the samples did not always reflect the outcrops, which were highly fractured. Visual estimations of the outcrops would yield higher permeabilities, as some fractures had larger aperture than the diameter of a core plug (1 inch).

The paleokarst within this study would be classified as a fractured reservoir, with low porosities band high permeabilities. Connectivity between the breccia bodies would establish if the area has a reservoir potential. Exploration of a single breccia pipe, would be a too high risk and not economical. The Minkinfjellet Formation would yield good connectivity, whereas the unbrecciated parts of Wordiekammen consisting of micritic limestone would yield low permeability between the breccia bodies. However, the Minkinfjellet Formation was covered by scree in the study area so the connectivity is uncertain, whereas a fractured wackestone/packstone layer within the Wordiekammen Formation, could imply good reservoir potential covering the studied areas.

Acknowledgements

Table of contents

1 Introduction

1.1 Background

Hydrocarbon reservoirs with enhanced porosity and permeability which result from karstification due to prolonged subaerial exposure of carbonate rock are common in many petroliferous basins in the world (Mazzullo and Chilingarian 1996). Collapsed-paleocave systems are an important class of this type and consist of a complex array of rock textures, fabrics, structures, and pore networks (Kerans 1988; Loucks and Mescher 2001; Loucks 1999, 2001; Loucks and Handford 1992). These can create complex petrophysical heterogeneities in petroleum reservoirs (Loucks 1999), which may affect the fluid flow behavior significantly. This is because paleocave reservoirs have a complex history of formation, including dissolution, fracturing, burial, compaction and coalescing (Hammes et al. 1996; Loucks 1999, 2001, 2007; Loucks and Handford 1992), often occurring in several stages (Hammes et al. 1996). Paleokarst reservoir can be large scale features, extending for hundreds to thousands of meters (Loucks 1999).

The aim of reservoir characterization is to describe the spatial distribution of the petrophysical parameters such as porosity, permeability and saturation within paleocave reservoir (Lucia 1999). The objective of this study is to improve our understanding of karst reservoir by using a well-known outcrop example, a paleokarst area situated at the northernmost part of Billefjorden, Spitsbergen (e. g Eliassen and Talbot 2005). A suite of samples were sampled from different breccia deposits in this area and characterized, and the petrophysical properties measured. The focus has been on interpreting the development of collapsed paleokarst structures, and how it has affected the petrophysical properties within a breccia body.

Several studies of paleokarst have been made, (Kerans 1988; Loucks and Mescher 2001; Loucks 1999), and petrophysical properties have mostly been estimated by the use of thin sections. The study area at Billefjorden has been documented by several authors (Aase 2006; Braathen et al. 2011; Eliassen 2002; Eliassen and Talbot 2003b; Eliassen and Talbot 2005; Lønøy 1995; Maher and Braathen 2011; Nordeide 2008). This thesis can be considered a continuation of the work begun by (Nordeide 2008). However this study will give a more quantitative description of the petrophysical properties to karst deposit through laboratory testing.

1.2 From Karst to paleokarst

This chapter will give an introduction to the development of paleokarst structures. The transition from karst to paleokarst can occur over a period up to millions of years. The processes involved in the transition can be burial of cave systems, collapse of cave systems, sediment infilling, fracturing and cementation (Ford and Williams 1989). A paleokarst landscape gives information about an earlier geological setting dominated by karstification.

1.2.1 Karst

Karst is defined as comprising terrain with distinctive hydrology and landforms that arising from a combination of high solubility rocks and well developed secondary (fracture) porosity, **Figure 1.1** (Ford and Williams 1989). Karst areas are characterized by sinking streams, caves, enclosed depressions, fluted rock outcrops, and large springs. Important factors in the formation of karst are rock structure and lithology such as massive, pure, and coarsely fractured rocks (Ford and Williams 1989).

Many sequences of carbonate rocks are found to contain or get terminated by unconformities that are karst solutional surfaces or cavities that are now inactive, these are called paleokarst (Ford and Williams 1989). Paleokarst can be defined as a karstified surface and karst features associated with it, such as caves, which have been buried by younger rocks. Paleokarstic features at various scales can be recognized within most carbonate successions. More rarely they may be exhumed by the effort of later uplift and erosion (Lowe 1995), which means that the features can be recognized in outcrops at landsurfaces.

It is important to understand the general processes that develop modern cave systems since the scale, geometries, and spatial complexities of paleocave systems are influenced by their initial near-surface scale, geometries and complexities (Loucks 1999).
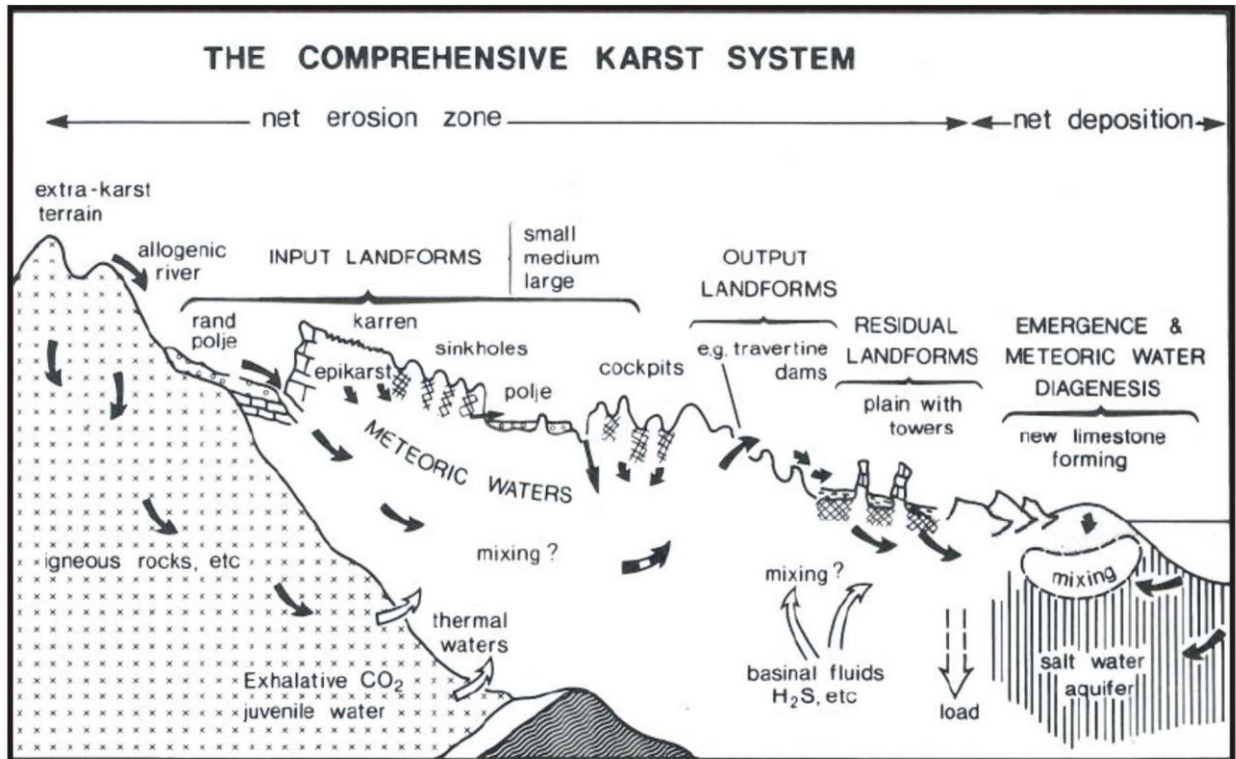
Figure 1.1: The comprehensive karst system. The composite diagram shows the major phenomena encountered in active karst terrains. The diagram illustrates karst features developed at the surface, called exokarst. Endokarst are karst features developed underground, which is often divided into hyperkarst (underground dissolution by circulating meteoric waters) and hypokarst (dissolution by juvenile or connate waters). Reproduced from hydrology (Ford and Williams 1989).

1.2.2 Origin and distribution of karst landscape

The distribution of an aggregate of surface and near-surface karst globally is about 20% of the planet dry- ice-free land (Ford and Williams 1989). Karstification of these surfaces can be called a process of destruction (White 1988), and karst landscapes are the foremost examples of groundwater erosion on the earth (Ford et al. 1988).

The sculpturing and removal of bedrock is mostly done by solution, and in some cases aided by soil piping and collapse. Karst landforms develop best in limestones, dolomites, gypsum and salt (Ford et al. 1988). Highly soluble rocks such as gypsum and salts are transformed into karst landscapes at a faster rate than for less soluble carbonate rocks (White 1988), where gypsums solubility with respect to limestone is 100 times as great (Warren 2006).

The dissolution and chemical weathering of limestone and dolomite shapes the landscape by creating sinkholes, caves, and a penetrating multistory drainage system underground consisting of

shafts, passages, canyons and chambers (Palmer 1991). The regions underlain by evaporite subcrop exhibit dissolution landforms similar to carbonate karst (Ford and Williams 1989; Warren 2006). But unlike the carbonate karst, the effect of near surface evaporite solution on cavern formation and land surface subsidence are much faster and can take years, not millennia (Warren 2006).

1.2.3   Development of karst landscape

A common dissolution product of karst meteoric diagenetic environment is caves and many reservoirs are known to produce from intervals with paleocaves (Loucks 1999; Lucia 1999). Therefore the focus of this thesis will emphasize on the karst development in the subsurface.

Dissolution due to meteoric water is the main factor in formation of karst, but several other factors are recognized. These include climate, microclimate, the presence and thickness of soil, local topography, parent rock structure and texture, tectonic regime, denudation and time (Klimchouk 2004). Nearly all major surface karst features originates from internal drainage, subsidence, and collapse triggered by the development of underlying caves, **Figure 1.2.**
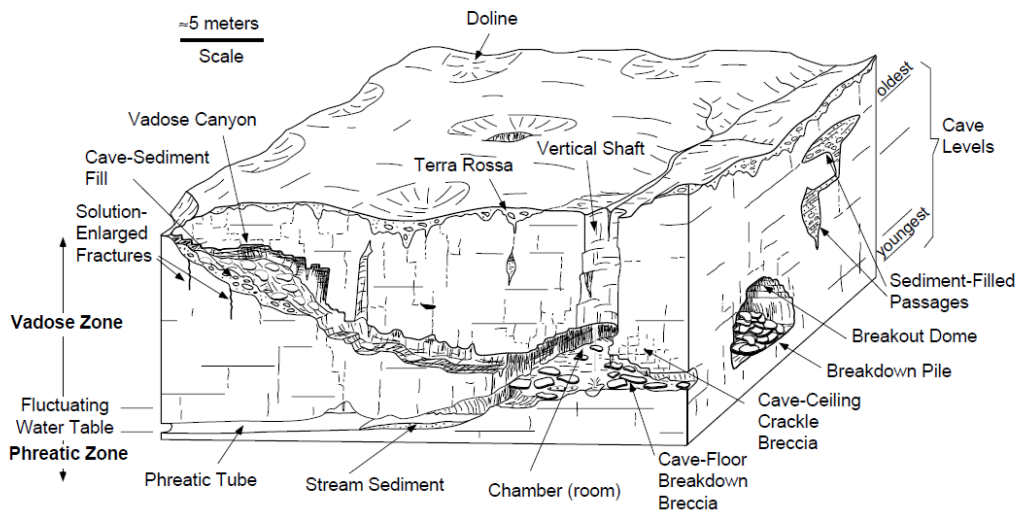
Figure 1.2: The block diagram shows near surface karst terrain with phreatic (below the water table) and vadose (above the water table) cave features. The figure is from Loucks and Handford (1992).

Caves are developed based on the hydrological or geomorphic expression of any karst region (Palmer 1991). Caves are found above, below and along the water table. Most extensive cave systems contain vadose parts draining to phreatic, or water table parts. Systems that have evolved

through several developing stages may contain older phreatic parts and younger water table and vadose passages (Ford et al. 1988).

Dissolution in an evaporite setting typically begins in the shallow subsurface as edges of salt beds are flushed by meteoric or marine waters and continues deeper, wherever and whenever bed egdes are flushed by undersaturated brines (Warren 2006).

1.2.4   Dolines and associated interstratal dissolution – breccia pipes

Dolines (aka. Sinkholes in North America) lead to underground passages that can contain underground streams, and are commonly floored by cave sediments and collapse breccia (Lucia 1999). Dolines are closed circular to elliptical depressions, often funnel shaped, with diameters ranging from a meter to a few kilometres and depth from a meter to hundreds of metres. The dolines indicate subsidence and/ or collapse of underlying salts or carbonates (Warren 2006). There are different types of dolines, **Figure 1.3**. Dissolution, collapse and suffusion are more active, more rapid and more frequent in evaporite terrains compared to carbonates (Warren 2006).
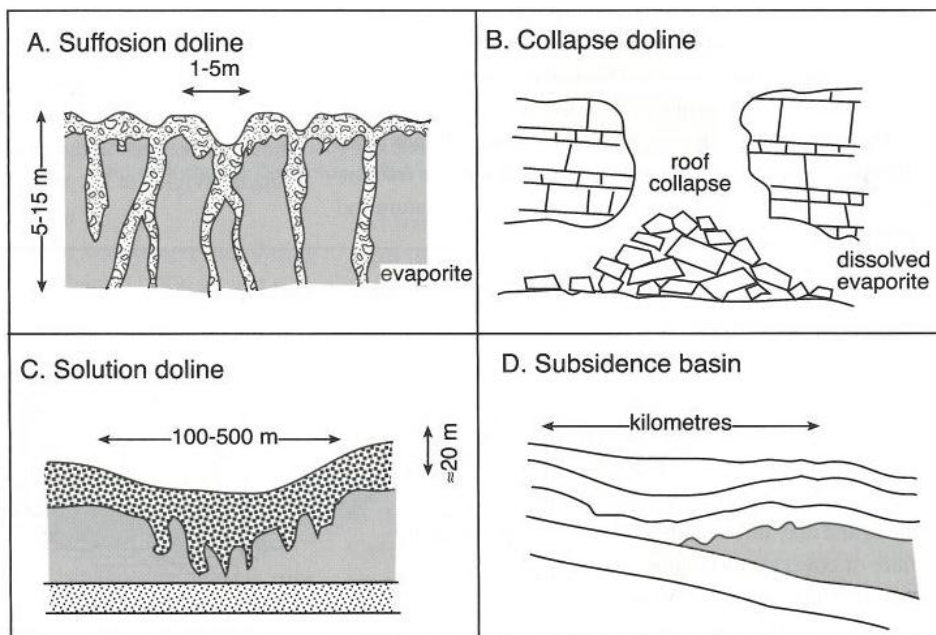
Figure 1.3: Typical evaporite karst features created by-: A) Suffosion, shallow evaporite dissolving rapidly below a soil of insoluble residues. B) Collapse, steep sided sinkholes that often indicates entrance to a cave. C) Solution, subsidence dolines that indicates deep and widespread evaporite dissolution. D) Subsidence on a basin scale. The figure is from (Warren 2006)

Sag structures are circular to subcircular (McDonnell et al. 2007) like dolines and can also be seen in the subsurface. Sag structures are due to underlying collapse mechanism like paleocave collapse, evaporite and hydrothermal dissolution (McDonnell et al. 2007).

Mechanical strength of a rock mass is massive bedrock devoid of jointing and thinly bedded and densely jointed strata. When the bedrock is barely affected by the jointing, the subsidence mechanism is mainly controlled is by the width and size of the cavities. The roof of stratiform cavities with a wide span tend to result in sagging, **Figure 1.4 (a)**. But when cavities have a significant height and a limited width, the collapse processes are controlled by dome shaped failure planes, **Figure 1.4 (b).** With a network of dense jointing, the dominant mechanisms are collapses, and the brecciation controlled by numerous pre-excisting failure planes, **Figure 1.4 (c)**. In **Figure 1.4 (d)** the mechanisms are about the same as in **Figure 1.4 (b)**, but sagging is evident in the stratiform layers next to the open cavity. Sagging and collapse are as well evident when the bedrock is densely jointed and caused by sheet interstratal karstification, **Figure 1.4 (e)**, (Gutiérrez et al. 2008). The main controls in interstratal karstification of evaporite bedrock are sagging and collapse. These processes affect the evaporite bedrock as well as overlying bedrocks such as limestone (Gutiérrez et al. 2008).
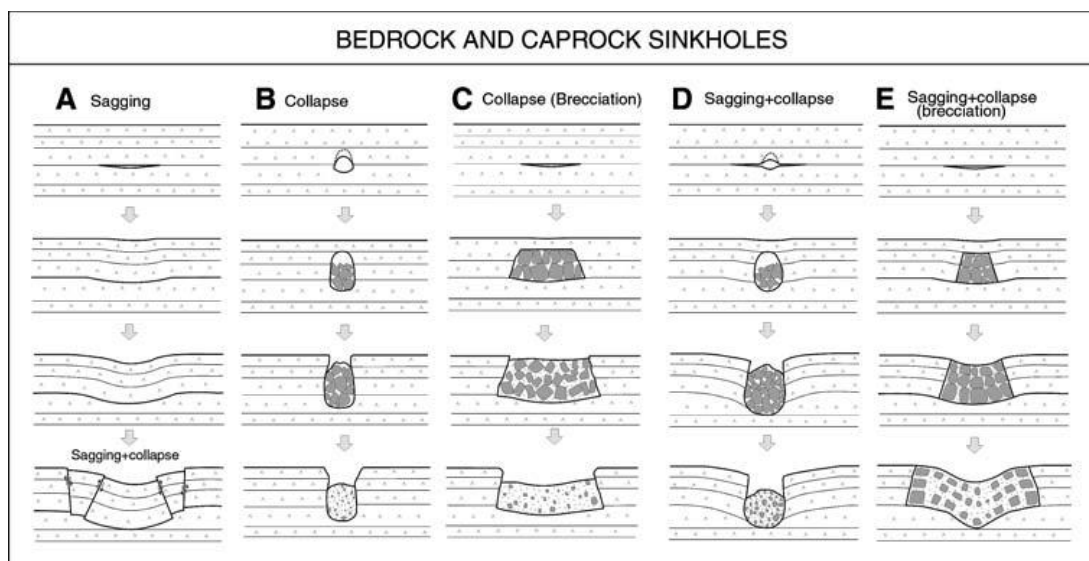
Figure 1.4: The diagrams show the main mechanisms in development of bedrock and caprock sinkholes. The figure is from Gutiérrez et al. (2008).

Breccia pipes develop as landscape features on the same scale as collapse dolines. They are steep sided chimney like features created by progressive upward stoping from in the evaporate case, a basal sulfate or a salt bed. In regions of thick evaporites the stoping process is driven by the escape of undersaturated basinal or deeply circulating meteoric waters leaking from levels below the sealing evaporite bed. The water that create a stoping pipe, may be focused into point or line sources via underlying biogenic buildups or fracture networks (Warren 2006).
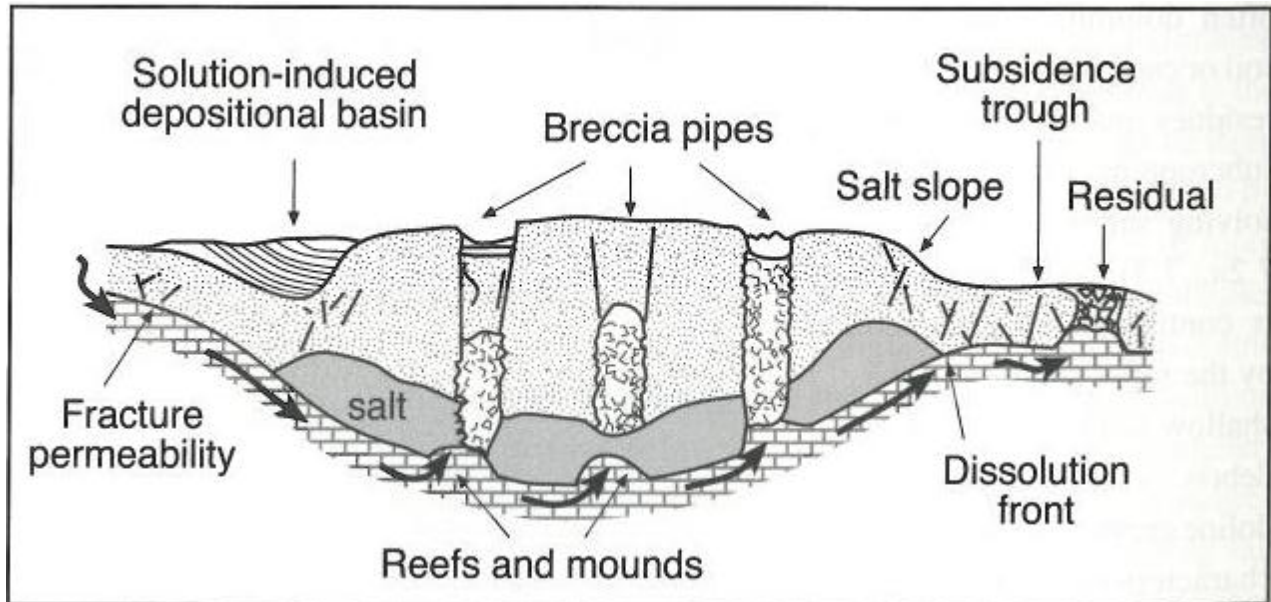
Figure 1.5: Solution subsidence trough which is an elongate depression created by interstratal dissolution. The largest solution-induced depositional basins tend to occur along the margins, creating a solution form that can be represented as a shallow salt slope in the subsurface. Dissolution can occur when the salt is buried and the overlying strata (usually dolomites, gypsum/anhydrite or redbeds) may be comprehensible brecciated. From (Ford and Williams 1989).

Breccia pipes consist of fallen breakdown and debris. The breccia pipes range size from few meters across and tens of meters high, but they can also be of an even larger scale, extending up several hundred meter high through the cover rocks and proportionally many hundreds meter across. These large scale features do not necessarily reach the surface (Waltham et al. 2005). Breccia pipes may exhibit four different states, **Figure 1.5**: 1) Active and prograding upwards towards the surface, but not yet expressed on the surface; 2) Active or inactive, expressed on the surface as a closed depression or as a surface outflow channel from a depression; 3) Inactive and buried by later strata, paleokarst breccia pipe; 4) Inactive and standing up as a positive relief feature on the land surface, as it is more resistant to weathering than the upper strata. The pipe is then a residual pipe, most likely due to cementation of the strata (Warren 2006).

Breccia pipes are not a major feature in limestone karst, and nearly all deep breccia pipes originates from dissolution of gypsum or salt (Waltham et al. 2005). For example there are estimated to be more than 5000 breccia pipes over gypsum and salt in North America (Quinlan Jr 1978; Warren 2006).

1.2.5 Cave sedimentation

Caves are basically giant sediment traps and the sediments can either be allochthonous, which is sediments transported into the cave from outside the cave, or it can be autochthonous which means they originate from inside the cave (Loucks and Handford 1992). Allochtonous sediments are usually water transported and composed sand, clay and rock fragments. Autochthonous sediments are locally derived and can be subdivided into 3 categories which are: chemical sediments, local detritus, and breakdown (White and White 1969).

Chemical sediments consist of locally derived calcite, aragonite and gypsum. Weathered products of limestone such as clay minerals, chert, sand and fossil fragments fall into the local detritus category. Breakdown is the third category and is the general term for the fallen bedrock within the cavity (White and White 1969).

1.2.6 Breakdown

Cave collapse is the product of mechanical failure of cave roofs and is the natural development of karst cave evolution (White and White 2000). Roof collapse can occur during the time of exposure and can continue after exposure as the overlying strata is deposited and the overburden pressure increases (Lucia 1999).

Subsidence mechanism of a rock mass is largely determined by the mechanical strength of the rock itself. The rock strength is largely determined by the density and orientation of bedding planes and joints, the geometry and width span of the cavities, the hydraulic conditions (vadose or phreatic) that will determine the mode of groundwater flow, and the effective weight of cavity roof, as the buoyant support is removed (Gutiérrez et al. 2008).

The cause of all breakdowns within a void is due to mechanical failure within or between rock beds or joint-bounded strata. The distribution of a load (load equals the density of the rock, gravity and the thickness of the rock mass or height of the cliff overhead), as a stress field about a cave cross-section is given in **Figure 1.6 a)**. A tension dome is created in the rock mass above a

passage and the height of the tension dome is determined by the width of the cavity. The rock

beds in the tension dome are subject to sagging, and the overlying weight is transferred to the

adjoining passage walls, greatly increasing the stress there. The tension dome is also within the

floor but have little significance for breakdown in natural caves. Cave breakdown is failures in

the tension dome, and are most regular in form where the strata are well-bedded and horizontal

(Ford and Williams 1989). The **Figure 1.6 b)**, and **Figure 1.6 d)**, indicates different mechanisms

of breakdown in cases where the strata not necessarily are well-bedded and horizontal (Ford and

Williams 1989).
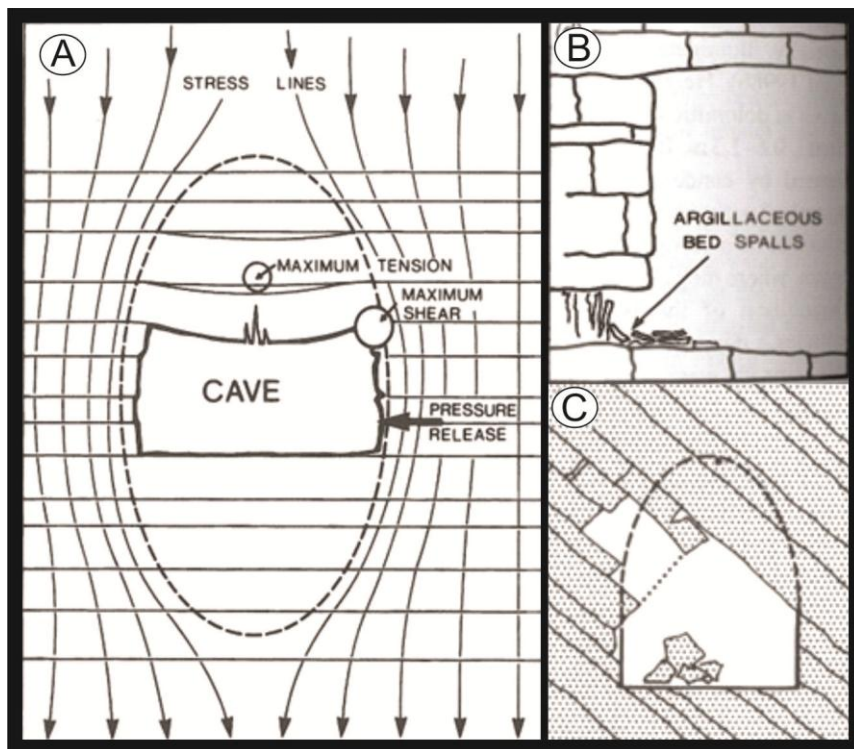
Figure 1.6: A) Distribution of stress lines and a tension dome around a cave. B) Pressure-release spalling where load is maximum, at a pillar or the foot of a wall. C) Deformation of the breakout dome where the stratal dip is steep. Multiple development of cave formation from (Ford and Williams 1989).

Products of collapse that are important for reservoir description are fractures and collapse

breccia. The geometry of the breccia deposits follow the pattern of major cave development

(Lucia 1999). The fracture porosity will be concentrated in the failed roof and flanks of the cave

system (Loucks and Handford 1992; Lucia 1999). Cavern development and collapse can produce

a vertical sequence of fractures and different breccia types (Kerans 1988; Lucia 1999)
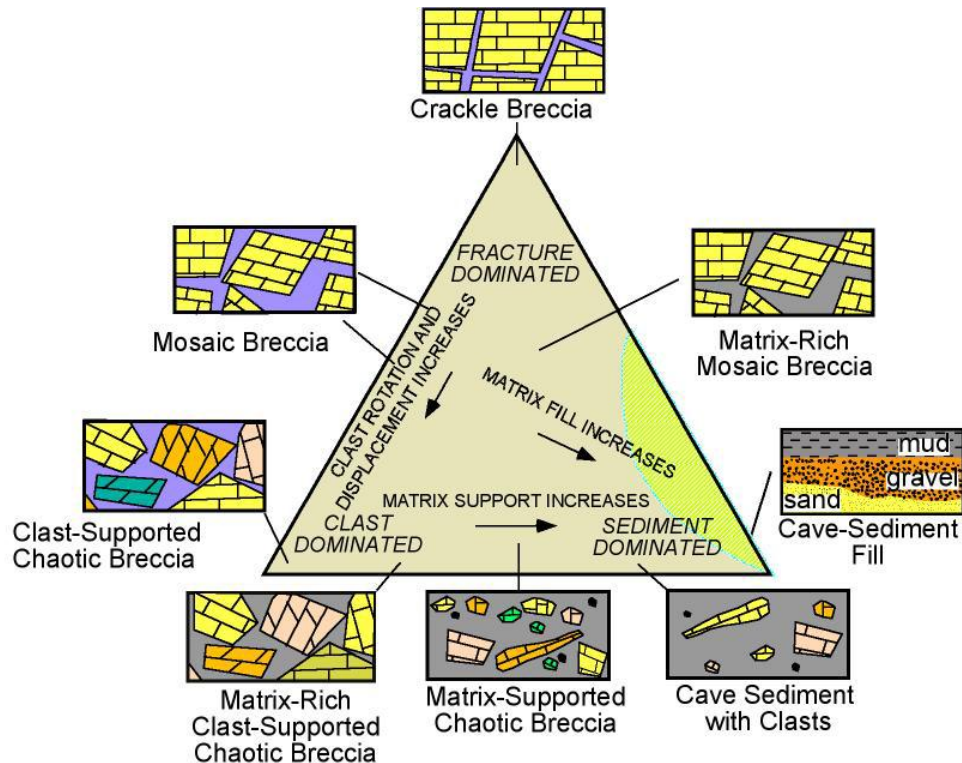
Figure 1.7: Triangle classification showing the breccia and clast deposits within a cave system. Originally from Loucks (1999), modified in Loucks et al. (2007)

Loucks (1999) classified the fractures and different breccia types of cave breakdown, where he used a ternary diagram to show the relationship between crackle breccia, mosaic breccia, chaotic breccia, and cave sediments, **Figure 1.7** (Loucks 2007).

Crackle breccia shows minor displacement between the separate rock fragments and are the product of fracturing due to stress relief in the cave ceiling and walls (Loucks 1999). Mosaic breccia are more displaced and rotated than crackle breccia, but can still be fitted back together (Loucks and Handford 1992). Chaotic breccia cannot be fitted back together and is composed of a mixture of clast that originates from one or several sources. They have been transported vertically by collapse, or laterally by fluvial or density flow mechanism and they range from matrix-free to matrix-rich (Loucks 2007). Sediment fill indicates processes of suspension, traction and mass flow mechanisms and can therefore be of any material texture or fabric (Loucks and Handford 1992).

Due to differential compaction, crackle breccia with loosely fitted clasts are formed in the buried cave-roof. Due to further mechanical compaction, rebrecciation creates a chaotic breccia of

smaller clasts as the voids are closed. In the subsurface, hydrothermal dissolution can give preferred mechanism for mineral deposits. Because of several episodes of rebrecciation and tectonic overprint it can be hard to distinguish between the cave related breccia and the tectonic overprint (Loucks and Handford 1992).

1.2.7   Classifications of cave facies

Karst brecciation is the controlling factor for a paleokarst reservoir`s quality and heterogeneity, and not the tectonic overprint (Kerans 1988). A model of karst facies is therefore important in order to understand the heterogeneity of the reservoir (Loucks et al. 2004). Loucks and Mescher (2001) proposed a general classification of six common paleocave facies, described below, and shown in **Figure 1.8**.

1. **Continuous strata,** is characterized by undisturbed bedding continuity for tens to hundreds of meters. The strata can show minor deformation such as titling and fracturing and solution holes with breccia and /or sediment fill.
2. **Discontinuous strata**, is characterized by high continuity of the bedding with small scale folding and faulting that is commonly overprinted with crackle and mosaic brecciation. This facies is interpreted as disturbed host rock around collapsed cave passages.
3. **Highly disturbed strata**, is highly disturbed, very discontinuously bedded strata with pockets and layers of chaotic breccia. Small scale folding and faulting is common with significant overprint of crackle and mosaic breccia. This facies is interpreted as lithified collapsed roof and wall rock at the top of the caverns.
4. **Coarse-clast chaotic breccia**, is poorly sorted, matrix to clast-supported, granule- to boulder sized chaotic breccia that is 0.3 to 3 meter long. It is commonly clast supported, but can contain matrix material. It forms ribbon- to tabular-shaped body as much as 15 meter across and hundreds of meters long. The facies has been interpreted to be deposited in-situ as collapsed-breccia cavern fill which has not been transported by stram or mass-flow processes. Interclast pores in the matrix-free chaotic breccia have good reservoir quality when not cemented.
5. **Fine-clast chaotic breccia**, is poorly to well sorted, matrix- to clast-supported, granule- to cobble-sized chaotic breccia with varying amounts of matrix. The clasts can be imbricated or graded and forms ribbon- to tabular shaped body as much as 15 meters

across and hundreds meter long. It consists mostly of cavern fill that has been transported either by mass flow or stream flow processes.

6. **Finer grained sediment**, consists of fine silt-to granule-sized sediments that contain less than 10 % granules, and are carbonate and/or siliclastic debris. Sedimentary structures can be common. The facies ranges from 0,3 to 0,8 meter in thickness and is interbedded with chaotic breccia facies. The fine grained material that make up this facies is interpreted to have been transported by traction, mass-flow, and suspension mechanism (Loucks et al. 2004).
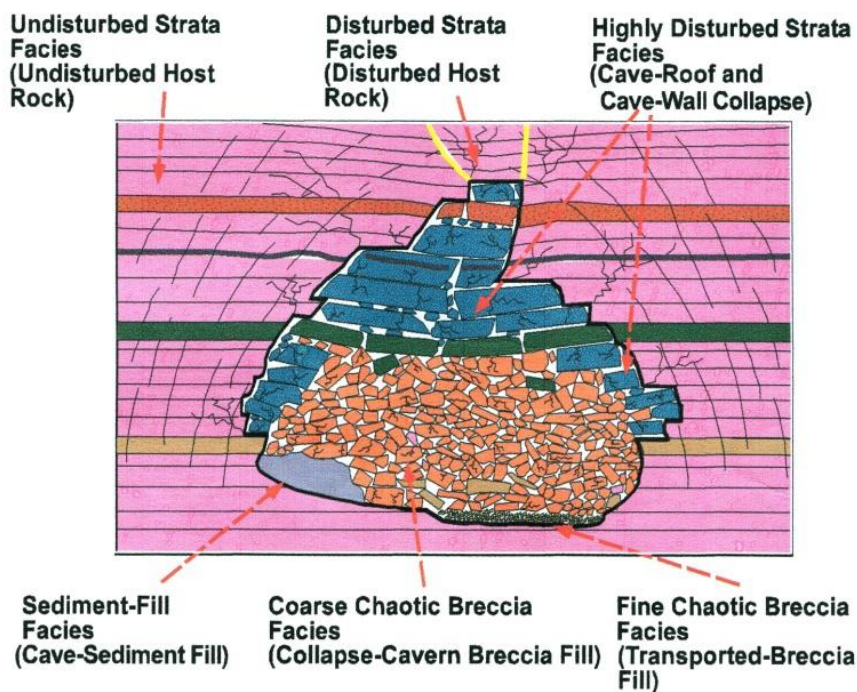
Figure 1.8: Cross sectional view of a collapsed cave passage and facies classification. Originally from Loucks and Mescher (2001), modified in (McDonnell et al. 2007).

The facies classification proposed by Loucks and Mescher (2001) was un-obtainable, but the classification was re-stated in (Loucks et al. 2004). However since the classification originally was published in Loucks and Mescher (2001), it will in this thesis be referred to Loucks and Mescher (2001).

1.2.8 Evolution of paleocave reservoirs

When there is a high density of cave passages, the expanded area of breccia and fractures from each passage may intersect with each other. The result is interconnection of cave passage chaotic breccia with crackle, mosaic and fractures, creating a large-scale, coalesced, collapsed paleocave system (Loucks 1999). This large scale system may be hundreds to several thousand of meters across, and tens of meters to more than 100 meter thick (Loucks 2007).

Large scale breccia can also be formed due to stratiform brecciation, where the general style of interstratal collapse is typified by blanket aquifers and broad areas of gentle sagging where diffuse flow of undersaturated flow over large areas has slowly removed evaporites. The blanket aquifer can lie within, below or above the dissolving evaporite bed. Larger interbed and overburden clast tend to be tabular, and dominated by mosaic to crackle breccias. In areas with focused dissolution, large caverns and solution planes have formed within the dissolving evaporite bed, so that the whole of the overlying unit can be reduced to a breccia pipe (Warren 2006).

1.3 Petrophysical properties

Reservoirs in karstified carbonate rocks are usually heterogeneous. The heterogeneity is the result of the irregular distribution of porosity zones and complex nature of pore systems (Chilingar et al. 1996). The heterogeneity causes problems in reservoir development as the karst related dissolution that has overprinted pre-existing porosity systems complicates reservoir petrophysical characterizations (Chilingar et al. 1996).

1.3.1 Porosity

Porosity is defined as the void part of the rocks total volume that is unoccupied by rock grains or mineral cement (Zolotukhin 2000). From a reservoir engineering point of view, porosity is one of the most important of the rock properties (Amyx et al. 1960), due to hydrocarbon storage potential.

Porosity can be divided into primary porosity, secondary porosity and effective porosity. Primary porosity is defined as developed during deposition of the rock (Zolotukhin 2000). Primary pores can be divided into interparticle and intraparticle, **Feil! Fant ikke referansekilden.**. The interparticle pores are initially present in all sediments, but are quickly lost in carbonates due to

the combined effects of compaction and cementation. The intraparticle pores are found within skeletal grains of carbonate sands, and are thus often *cul-de-sac* pores, but are usually also absent due to compaction and cementation (Selley 1985).

The absolute porosity is the total volume of pores irrespective whether the pores are interconnected or not. Absolute porosity is given, in percentage, as the ratio of the total void volume, V_T, to the bulk volume, V_B.

$$\emptyset_A = 100 \times \frac{V_T}{V_B} \qquad\qquad (1.1)$$

The effective porosity gives the volume of interconnected pores, and is dependent on rock type, grain size range, grain packing and orientation (fabric), cementation, weathering and leaching (Zolotukhin 2000). Effective porosity is the ratio between the total pore volume of the interconnected pores, V_P, to the bulk volume of the rock, V_B.

$$\emptyset_E = 100 \times \frac{V_P}{V_B} \qquad\qquad (1.2)$$

For highly cemented materials and limestone, there can be a significant difference in the total and effective porosity. The effective porosity is usually the quantitative value desired since it represents the void space occupied by mobile fluids (Amyx et al. 1960).

1.3.2   Secondary porosity

Secondary porosity is produced during geological processes subsequent to the deposition of the rock. Processes includes diagenesis, fractures, fissures and channels within the formation (Ford and Williams 1989). Secondary porosity in limestone is typified by the vugs or solution cavities. Rocks with original porosity have more uniform characteristics than rocks that have their porosity enhanced (Amyx et al. 1960).

Paleokarst is reworked carbonate and evaporite rock, and can therefore have induced porosity with a complex pore geometry configuration. This means that two or more pore systems may occur. The basic rock material is fine intercrystalline and referred to as the matrix, with one pore system consisting of uniformly small pores. Larger voids and pores are due to leaching or fracturing of the primary rock material, and can be variable in size and distribution (Amyx et al. 1960). The secondary porosity can therefore be classified into several pore types.

Solution-induced pores are common in carbonates and generally a distinction is made between moldic and vuggy porosity, **Table 1.1**. Moldic porosity is fabric selective, which means that only the grains or only the matrix has been leached out. Whereas vugs, are pores whose boundaries cross-cut grains, matrices, and/or earlier cement, and are generally larger than moldic pores. With increasing size vuggy porosity can increase into cavernous porosity (Selley 1985).

Table 1.1: Classification of porosity found in sediments. Modified from (Selley 1985)

Time of formation	Type	Origin
Primary of depositional	Interparticle and intraparticle	Sedimentation
	Intercrystalline and Fenestral	Cementation
Secondary or postdepositional	Vuggy and moldic	Solution
	Fracture	Tectonics, compaction, dehydration and diagenesis

Microporosity is porous cement or interstitial matrix and fracture porosity which is secondary pores shaped by open microfractures (Zolotukhin 2000). Vugular openings and fractures can be large and are attributed to the rock after its deposition. Both fractures and vuggy porosity can be partially closed or fully closed by infill of cement such as precipitated calcite or other material (Amyx et al. 1960).

Secondary porosity can be caused by the effects of cementation(Selley 1985). Fenestral pores occur where there is a primary or penecontemporaneous gaps in the rock framework, which is larger than the grain-supported interstices, **Table 1.1** (Selley 1985; Tebbutt et al. 1965). Therefore can fenestral pores appear to be primary rather than secondary, and are typically found in carbonates (Selley 1985).

Intercrystalline porosity is pores occurring between the crystal faces of crystalline rocks, **Table 1.1**. Most limestones that are recrystallized contain negligible porosity. But is more common in dolomites that have gained intercrystalline porosity due to replacement of calcite (Selley 1985).

Fracture porosity is one of the most important of the pore geometries to consider as they increase the storage capacity of a reservoir, as they enhance the permeability in the reservoir, **Table 1.1**. Fractures are most common in brittle rock such as limestones (Selley 1985).

1.3.3 Permeability

The permeability is a measure of the ability of a porous medium to transport a fluid through its network of interconnected pores (Amyx et al. 1960). Permeability can be considered as a static parameter if there is only a single fluid flowing through the medium (Zolotukhin 2000), thus absolute permeability is a rock dependent property. The absolute permeability is defined through Darcy`s law, **Equation 1.3**, for an incompressible fluid and for a horizontal flow in the direction of decreasing pressure (Lien 2004):

$$Q = -\frac{K \cdot A}{L \cdot \mu} \Delta p$$

$$(1.3)$$

Where:

Q = Volumetric fluid flow rate

K = Absolute permeability

A = Cross-sectional area of the porous medium

μ = Fluid viscosity

Δp = Pressure drop across the flow

When several fluids flow through the interconnected pores, the permeability depends strongly on each of the fluids relative saturation. This is called the effective permeability. Because the non-miscible fluids would inhibit the flow of each other, the effective permeability can be considerable lower than the absolute permeability (Zolotukhin 2000). The Darcy equation has to be applied for each phase.

The relative permeability is the ratio between the effective permeability of each fluid phase and the absolute permeability of the medium (Lien 2004). The relative permeability gives the direct measurement for a porous medium to conduct one fluid when one or more fluids are present. The flow properties are then a composition of the effects of pore geometries, wettability, fluid distribution and saturation history (Anderson 1987).

2   Regional Geology

This chapter will summarize the regional geology of the study area, which is situated in the northernmost part of Billefjorden at Spitsbergen. A brief background of the geological setting and development within the region will be given, with the emphasizes on the formation of the Billefjorden trough and the geological formations. In the end, an introduction to the breccia bodies within the Billefjorden Trough will be given.

2.1 Regional overview

The Svalbard archipelago, **Figure 2.1**, is situated at latitudes 74˚ to 81˚ North, and longitude 10˚ to 35˚ East and includes all the islands within these latitudes (Nøttvedt et al. 1993; Steel and Worsley 1984).
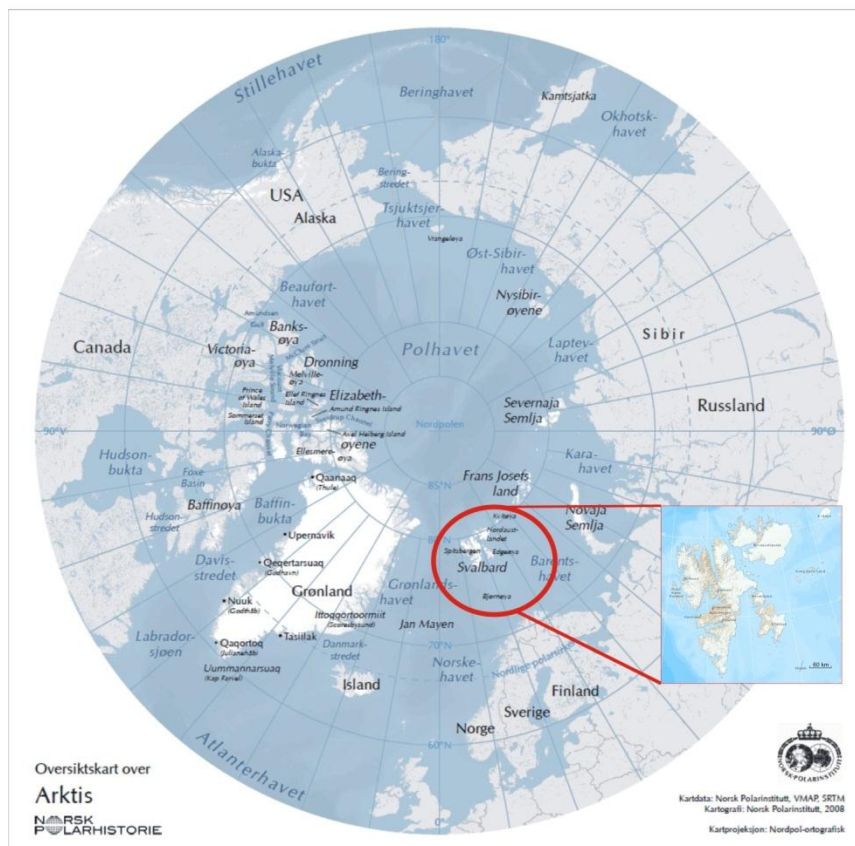
Figure 2.1: Map showing the location of The Svalbard Archipelago (inset) situated in the Arctic region in the Northern Hemisphere. The Arctic region map is retrieved from polarhistorie.no/seksjoner/Ressurskart and the map of the Svalbard Archipelago is retrieved from TopoSvalbard at polarinstituttet.no.

The Svalbard Archipelago includes Spitsbergen, Nordaustlandet, Edgeøya, Barentsøya, Bjørnøya and innumerable smaller island and skerries. The islands combined comprises of a total land area of 62,700 km^2 (Worsley 1986). The Svalbard Archipelago form the subaerially exposed north-western margins of the Barents Sea shelf. Even though it covers less than 5 % of the Barents Sea, it gives a comprehensive overview of the geology of the entire region (Harland 1997; Steel and Worsley 1984; Worsley 2008, 1986). Approximately 60 % of Svalbard archipelago is permanently covered by glaciers and inland ice, but at summer time, successions ranging from the Precambrian to the Paleogene are well exposed in the coastal regions(Steel and Worsley 1984).

2.2 Geological setting

The basement of Svalbard, The Hecla Hoek Formation, was formed as a part of the Caledonian orogeny. In this period the faulting, folding, thrusting and metamorphism of Pre-Cambrian to middle Ordovician sediments and igneous rocks, were at the most intense(Nøttvedt et al. 1993). In the post-Caledonian of Svalbard, tectonic setting has been an important controlling influence on sedimentation patterns. The tectonic framework of the largest island of Svalbard, Spitsbergen, is by N-S to NW-SE structural lineaments on which repeated differential movement or inversion took place since Devonian times. The lineaments are centered around The Lomfjorden Fault Zone, Billefjorden Fault Zone (BFZ) **Figure 2.2**, as well as Hornsund and Paleo-Hornsund fault zones (Steel and Worsley 1984). The tectonic movement along these lineaments varied from slight flexuring to discrete faulting, where the faulting varied from dip-slip to strike-slip dominance (Steel and Worsley 1984).
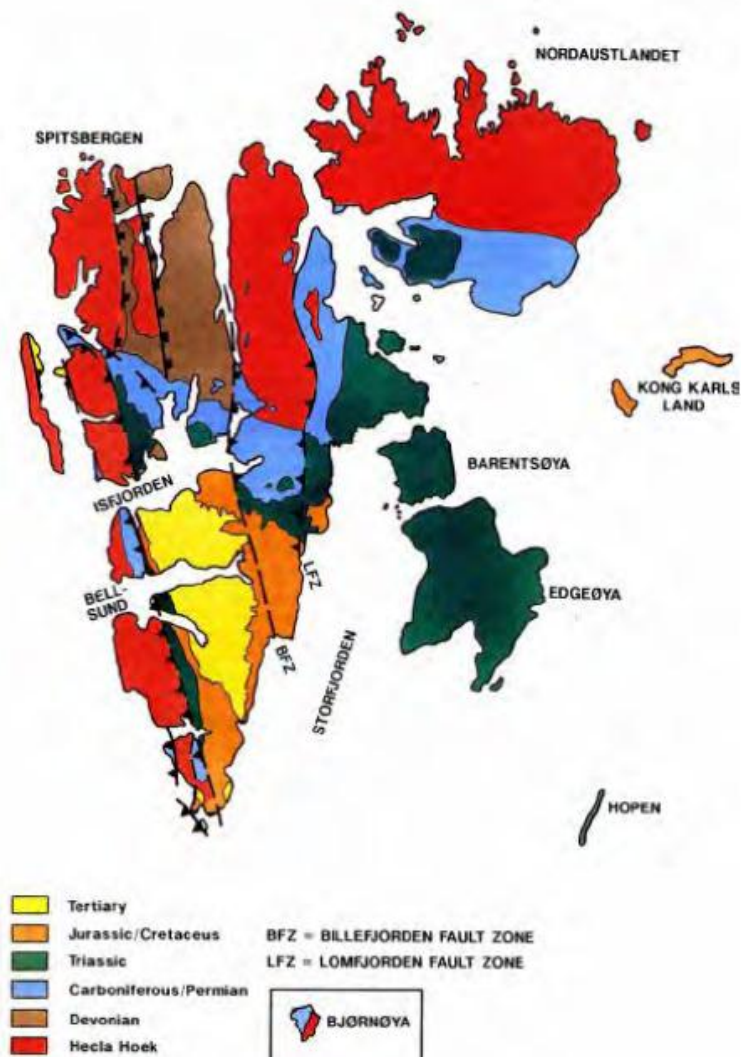
Figure 2.2: Geological map showing the deposits deposited under different geological time periods. The map is from (Nøttvedt et al., 1993).

In the late Devonian, the Devonian succession consisting mostly of continental red beds, was partly deformed and overthrusted, resulting in an angular unconformity to the overlying Carboniferous (Nøttvedt et al. 1993). The early to middle Carboniferous was a period of extension along the N-S to NW-SW lineaments, creating a number of narrow rift basins, like the Billefjorden graben (Nøttvedt et al. 1993). In the middle Carboniferous the extensional rift basins shows an *en echelon* distribution, indicating that it has resulted from oblique-slip movements, **Figure 2.3** (Johannessen and Steel 1992; Steel and Worsley 1984). The narrow Carboniferous basins developed into broader basins, and from the early to the middle Carboniferous there was a

shift from coarse clastic red-beds to carbonates and evaporites (Johannessen and Steel 1992). During this time the climate had changed from humid to arid conditions, and from continental to marine conditions, resulting from a regional rise in sea level (Gjelberg and Steel 1981). During the late Carboniferous, Permian and Mesozoic, Svalbard became a stable platform and drifted slowly northward to higher latitudes.

 The focus of this chapter is one of the characteristic Carboniferous asymmetric and narrow basins, Billefjorden (Gjelberg and Steel 1981), including the Billefjorden trough located in the area of present day Billefjorden (Eliassen and Talbot 2003b; Johannessen and Steel 1992).
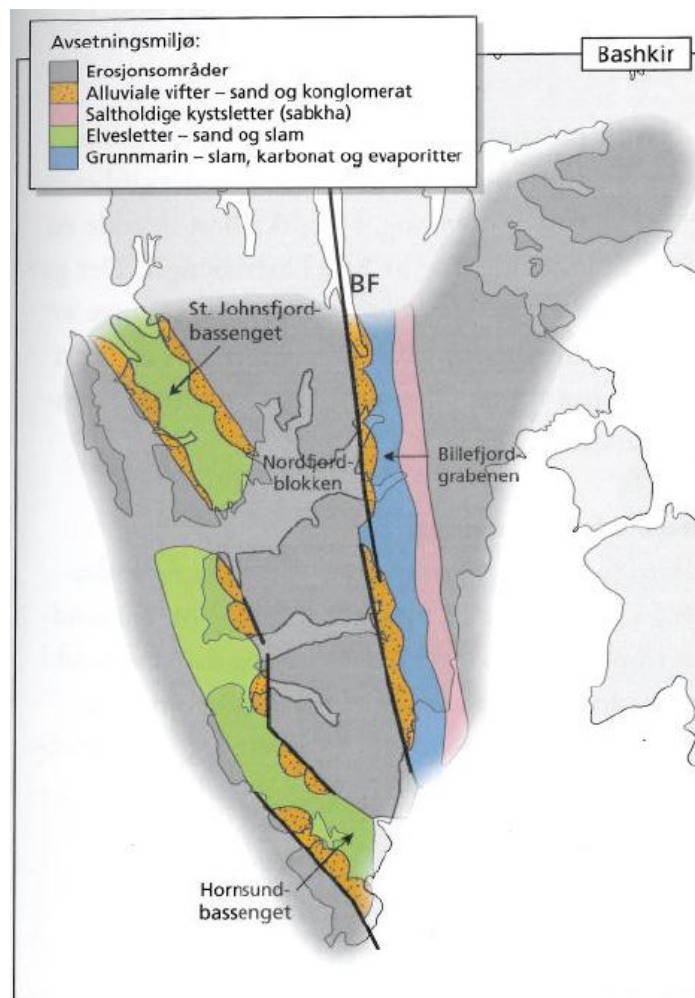
Figure 2.3: Geography and the main depositional environment in Middle Carboniferous. The grey areas indicate where there was mostly erosion of the strata. from (Steel and Worsley 1984) and modified in (Ramberg et al. 2008)

2.3 Tectonic setting

The onset of Carboniferous extension as a result from transtensional tectonic movement in the Bashkirian times to Gzhelian times (Eliassen and Talbot 2003b; Gjelberg and Steel 1981; Steel and Worsley 1984), was concentrated along a few major lineaments like the Billefjorden Fault Zone (BFZ) (Nøttvedt et al. 1993). The Billefjorden Trough is a half-graben developed along the eastern side of the (BFZ), between the footwall of the Nordfjorden block and hanging wall of the Ny Friesland block (Johannessen and Steel 1992). The syn-tectonic nature of the basin fill is evident from the marked thickening and coarsening of strata towards the fault zone, creating a distinct asymmetry of the basin. The asymmetry is evident from the 700 meters of syn-tectonic strata close to the faulted zone in the west and pinching out to only a few tens of meters at the eastern side, **Figure 2.4** (Johannessen and Steel 1992).
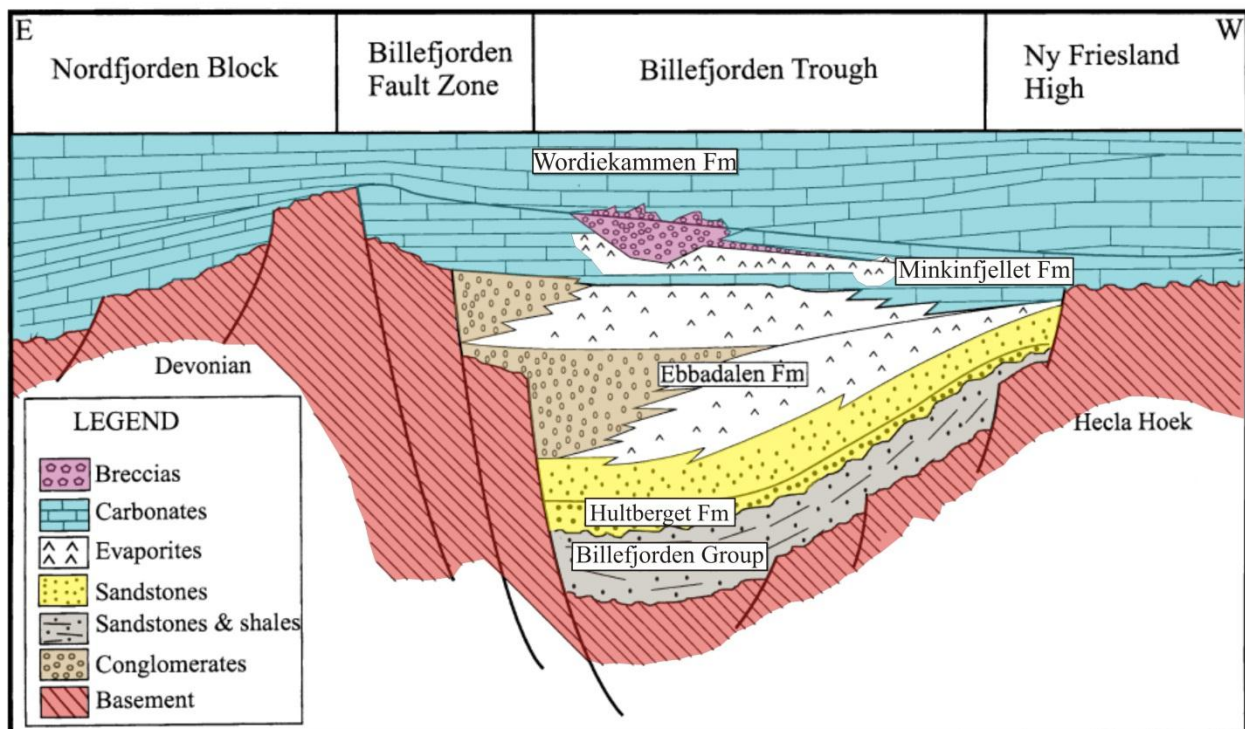
Figure 2.4: The Billefjorden Trough and the adjacent structural heighs and the stratigraphic position of Minkinfjellet and Wordiekammen Formation breccias, Modified figure from (Eliassen and Talbot 2005), originally published in (Johannessen and Steel 1992)

During the Moscovian, active rifting ceased, and the syn-tectonic basin was filled up with sediments. In the early Kazimovian, regional subsidence caused drowning of the structural heights, causing a widening of the basin, **Figure 2.4** (Eliassen and Talbot 2005). The entire rift

fill succession of the Billefjorden Trough is described as approximately 1 km thick (Braathen et al. 2011). By the end of the Carboniferous and Permian, a large stable platform developed that persisted through the Mesozoic (Steel and Worsley 1984), into Tertiary times (Nøttvedt et al. 1993). In the **Figure 2.5**, the geological stratigraphy and the tectonic framework of the study area are indicated.
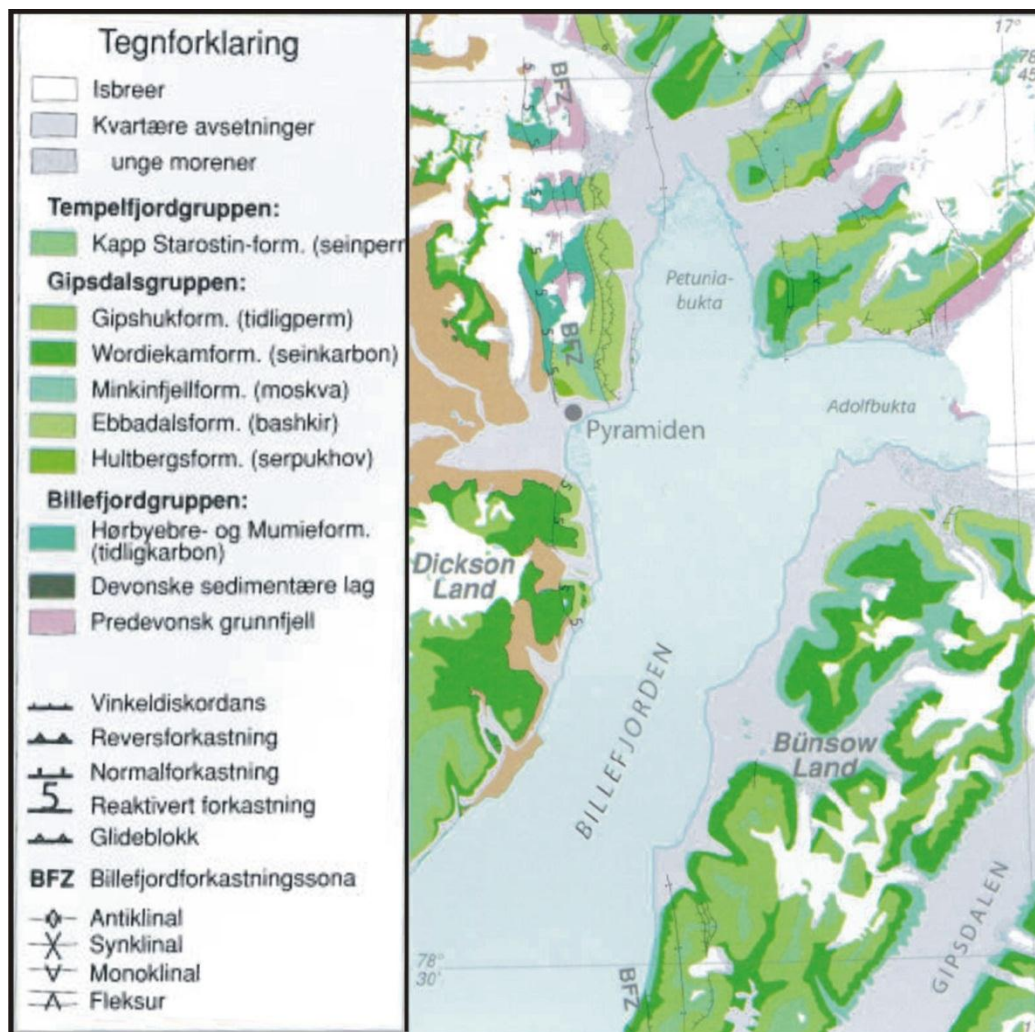
Figure 2.5: Geological map over Carboniferous and Permian stratigraphy in Billefjorden, from (W.Dallmann) and modified from (Ramberg et al. 2008).

2.4 Basin Geometry

The Billefjorden trough is located between the footwall of Nordfjorden block and the hanging wall of Ny Frieslandblock (Johannessen and Steel 1992). The Billefjorden Trough trends N-S, and is a half graben developed in the hanging wall of a steeply east-dipping fault, the Billefjorden Fault Zone. The BFZ is an array of subsidiary faults that link up with each other through soft or hard link structures (Braathen et al. 2011).

The western boundary of the BFZ is a basement horst developed between the Balliolbreen and Odellfjellet faults, whose vertical movements controlled the western margin of the mid-Carboniferous basin, mainly shifting the basin margin eastward throughout time. The eastern margin of the Billefjorden trough is defined by differential onlap of the Middle Carboniferous formations onto the Ny Friesland Platform (McCann and Dallmann 1995). Faulting in the eastern part of the Billefjorden basin is represented by the Lemstrømfjellet Fault Zone (LFZ). There the general gentle western dip of the basin succession towards the BFZ is disrupted by several west-dipping normal faults, where some shows a monocline or drag-fold structure (Braathen et al. 2011).Within LFZ the Løvehovden fault represent the southern termination of the Lemstrømfjellet fault, **Figure 2.6** (Maher and Braathen 2011) Although the Wordiekammen Formation is considered a post-tectonic unit, thickness changes along the Løvehovden fault suggest continued fault-controlled basin subsidence. The stratiform breccias in the area are most common on the footwall side of intra-basin faults (Maher and Braathen 2011).

Figure 2.6: Photo-panorama of Billefjorden Trough. The picture shows the extent of the faults with the Balliolbreen Fault (BBF) and Odellfjellet Fault (OFF) to the west, and to the east the Løvehøvden Fault (LHF)(de Boer et al. 2011).

2.5 Stratigraphic setting

The stratigraphy of the Billefjorden trough is shown in **Figure 2.4**, and shows the Carboniferous pre-, syn- and postrift successions. The successions range from continental through sabkha into marine strata (Eliassen and Talbot 2005). In the area studied, the uppermost stratigraphic unit at the outcrop sites were the Gipshuken Formation, deposited in the early Permian (Lauritzen 1981; Steel and Worsley 1984). This section will only focus on the syn-rift to early post-rift successions, because these were the area of study.

2.6 Late syn-rift deposits

From the late Serpukhovian to early Bashkirian time, there was a dramatic change from humid to arid conditions and the change from continental to marine conditions from a regional sea-level rise (Gjelberg and Steel 1981). Rapid subsidence and faulting occurred along the BFZ, and the general trend was regression in the area (Steel and Worsley 1984).The syn-rift fill of the Billefjorden Trough consist of Hultberget Formation, Ebbadalen Formation (composed of Ebbaelva, Odellfjellet and Tricolorfjellet members) and the Minkinfjellet Formation (Braathen et al. 2011; Cutbill and Challinor 1965; Dallmann et al. 1999; Johannessen and Steel 1992).

The Odellfjellet Member is up to 400 meter thick and onlaps the faulted basin margin in the west. It consists of red, grey and yellow conglomerates and sandstones, red shales with some gypsum nodules and yellow dolomite. These strata are interpreted to be clastic wedges building out from the BFZ as alluvial fans, fan delta, shoreline and shallow marine carbonates. Laterally interfingering the Odellfjellet member is the Tricolorfjellet Member (>240 m thick) (Dallmann et al. 1999), which represents the basinal facies consisting of sabkha deposits like gypsum/anhydrite. The sabkha deposits alternates with open marine/lagoonal to intertidal deposits, consisting of black and yellow limestones/dolomites. Odellfjellet and Tricolorfjellet members are time-synchronous (Johannessen and Steel 1992). The deposits of Odellfjellet Member became drowned by evaporites and carbonates of the uppermost Tricolor Member and finally by marine deposits of the overlying Minkinfjellet Formation (Johannessen and Steel 1992).

The Minkinfjellet Formation, up to 300 meter thick (Eliassen and Talbot 2005), is deposited in Moscovian – early Kasimovian times (Dallmann et al. 1999). The succession is carbonate-

dominated, consisting of interbedded sandstones, evaporites and minor shales (Eliassen and Talbot 2003b). Breccias within the formation are widespread, and increasing with the proportion of evaporites to the south (Eliassen and Talbot 2003b; Maher and Braathen 2011). During the Moscovian, active rifting ceased, but the Nordfjorden block remained sub-aerially exposed and deposition of the Minkinfjellet Formation was limited to the west (Eliassen and Talbot 2005). To the east the deposition is characterized as differential onlap onto the New Friesland Platfrom, extending further east than the Ebbadalen formation (Eliassen and Talbot 2005; McCann and Dallmann 1995). By the Kazimovian, regional subsidence led to drowning of both the structural heights, and a wider basin developed (Eliassen and Talbot 2005) The unit is considered retrograding and a part of a transgressive phase of a new megasequence (Johannessen and Steel 1992).

The breccias within the Minkinfjellet Formation has been given an informal name, the Fortet member (Dallmann et al. 1999). The member includes only the breccias within the Minkinfjellet formation, even though brecciation continues into the overlying Black Crag Beds. Due to this the brecciation will be referred to their formal formation names.

2.7   Post-rift

The Wordiekammen Formation overlies the Minkinfjellet Formation, and is represented in the Billefjorden area by Cadellfjellet (thickness 90-250 m) and Tyrrellfjellet (thickness 110-180 m) Members, **Figure 2.7** (Dallmann et al. 1999). The Wordiekammen Formation was deposited from late Moscovian to Sakmarian (Dallmann et al. 1999), and is considered as a post-tectonic unit (Braathen et al. 2011). Although (Maher and Braathen 2011) documented thickness changes, for example around the Løvehovden fault which suggest a continued fault-controlled basin. The Wordiekammen Formation accumulated as a transgressive to regressive unit, and the sediments were deposited in a broad basin covering much of central Spitsbergen (Eliassen and Talbot 2005; Pickard et al. 1996; Samuelsberg and Pickard 1999; Steel and Worsley 1984). The sediments are mainly of marine limestone (Dallmann et al. 1999), mostly deposited on a platform in open to semi-restricted, shallow subtidal marine and intertidal to supratidal enviroments (Dallmann et al. 1999; Eliassen and Talbot 2005; Samuelsberg and Pickard 1999; Sundsbø 1982)

In the Billefjorden Trough and to the east of it, the Cadellfjellet Member forms the lowermost part of Wordiekammen Formation. The lowermost beds of the Cadellfjellet Member is the Black Crag beds (Dallmann et al. 1999) represented in our study, which is sparse to non-fossiliferous dark brown to black mudstone (micrite) units. These units are typically massive and cliff forming (Pickard et al. 1996), interbedded with thinner, yellow and white wackestone- and packstone beds (Braathen et al. 2011). The Black Crags are restricted to the Central part of Billefjorden Trough, and thicken from the south to the north with thicknesses ranging from 20 to 60 meter (Eliassen and Talbot 2005; Pickard et al. 1996; Samuelsberg and Pickard 1999). Locally brecciation in the Black Crags, cut the formation in form of breccia pipes (Braathen et al. 2011; Eliassen and Talbot 2003b), which have been the area of study in the Billefjorden Trough, and will be discussed further.

Lithostratigraphy				Age	
Gipsdalen Group	Wordie-kammen Formation	Tyrrellfjellet Member		Sakmarian	Permian
				Asselian	
		Cadellfjellet Member	Mathewbreen beds	Gzhelian	Carboniferous
			Gerritbreen beds		
			Black crag Beds	Kasimovian	
	Minkin-fjellet Formation	Fortet member		Moscovian	
		Terrierfjellet member			
		Carronelva member			
	Ebbadalen Formation	Odell fjellet Member	Tricolorfjellet Member	Bashkirian	
		Ebbaelva Member			

Figure 2.7: Late Carboniferous to early Permian stratigraphy in Billefjorden area (Eliassen and Talbot 2005), after (Dallmann et al. 1999).

From the Sakmarian to the Artinskian times in the Middle Permian, a major regression event occurred, leading to sabkha progradation. The sabkhas mark the lower boundary of the Gipshuken Formation (Lauritzen 1981; Steel and Worsley 1984). The Gipshuken formation is up

to 280 meter thick, but only the lower third constitutes rhythmic intercalations of sabkha and dolomites. The upper 100-150 meter comprises thinly interbedded dolomites and marls, with only evaporitic near the top of the formation. The formation is generally characterized by supra- to intertidal sedimentation on evaporitic and carbonate flats (Stemmerik and Worsley 2005). The Gipshuken Formation is the highest geological unit in our area of study, and whereas only scattered patches of sabkha deposits remain in northern Billefjorden (Braathen et al. 2011)

2.8 Brecciation

Thick and widespread carbonate breccia occurs within the Billefjorden Trough in both syn-rift and early post-rift deposits. The breccias exhibit a lateral extent over more than 250 km^2. The **Figure 2.8** shows the area of study, and the figure shows that the dominant breccias are the cross-cutting breccias with thicknesses up to 200 m measured in the central part of the basin. In the area in total, the dominant occurrence of breccias are as individual beds of 0,5-15 meter that are interbedded with undeformed limestones and siliciclastics (Eliassen and Talbot 2005). The Breccias are developed throughout the Minkinfjellet formation and in basal parts of the Wordiekammen formation (Eliassen and Talbot 2005). The breccias are polygenetic (Maher and Braathen 2011), and can be divided into two categories (Eliassen and Talbot 2005).

The first category of thick breccia bodies is situated in the central part of the basin. It consists of massive and up to 200 meter thick funnel-shaped breccia pipes, which resembles typical doline breccias. Another feature is large V-structures, which are broken and tilted carbonate beds, showing crackle to mosaic brecciation. The breccias can show subtle bedding or zonation of different types of breccias, which is not laterally consistent (Eliassen and Talbot 2005).

The second category is of stratabound breccia beds interbedded with undeformed carbonate and silisiclastic rocks. The second category has a wider areal extent towards the basin margin than category one, with the dominant occurrence of individual beds with thickness ranging from 30 cm to tens of meters (Eliassen and Talbot 2005). Texturally the clasts are small, ranging from sub-centimeter to meter in size and monomict. They have no zonation or bedding but inverse grading is common. The upper boundary is commonly of disrupted bedding and small scale V-structures (meter size) (Eliassen and Talbot 2005).

The massive breccia bodies of category one are found in the middle and upper parts of the Minkinfjellet Formation and the lower part of Wordiekammen Formation. Category two is only found within the Minkinfjellet formation (Eliassen and Talbot 2005). Studies of breccia deposits supports a solution collapse origin, as interstratal karstification of gypsum and anhydrite beds within the Minkinfjellet and upper Ebbadalen Formations are considered the cause of brecciation at this stratigraphic level (Eliassen and Talbot 2005). The extent of brecciation seems to be directly linked to the amount of gypsum deposited in the basin (Eliassen 2002), with a larger amount of gypsum deposited in the central basin presumably led to thicker solution collapse breccias in this area. Dissolution of thinner gypsum beds presumably produced thinner stratabound breccias towards the basin margin (Eliassen and Talbot 2005). Further, a disconformable surface between the Ebbadalen and Minkinfjellet formations on the eastern side of LFZ is related to fault movement, exposure, and near- or at-surface evaporate dissolution that locally produced stratiform breccias (Maher and Braathen 2011).
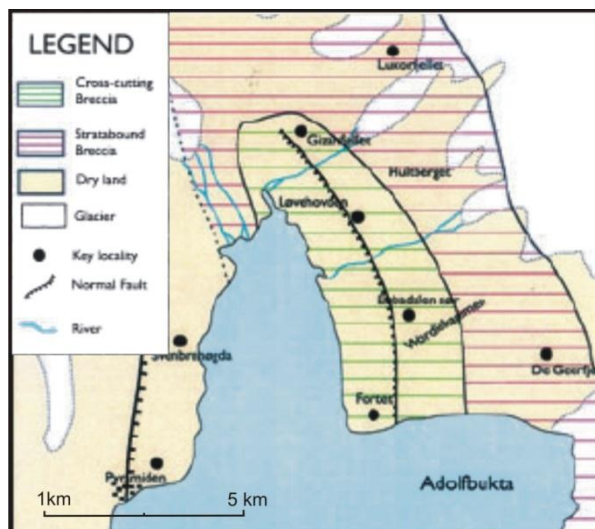
Figure 2.8: The map shows the distribution of breccia types within the study area in the Billefjorden Trough basin. The figure is modified from (Eliassen and Talbot 2005).

2.9   Burial and Diagenesis

The development of the breccia bodies are considered to be Late Carboniferous to Early Permian. This is due to the gypsum dissolution was interstratal by the time brecciation occurred, and the surrounding rocks were lithified and cemented (Eliassen 2002; Eliassen and Talbot 2005). As well as the collapsed breccias developed after dolomitization and formation of chert nodules in the host rock (Eliassen 2002; Eliassen and Talbot 2005). For these reasons the brecciation must

have occurred after deposition of the Minkinfjellet and Wordiekammen Formations, and took place in the subsurface after some degree of burial. Cementation of the breccia bodies must have occurred at similar or slightly greater depths. A burial depth of up to 500 m during brecciation and cementation are not unlikely (Eliassen and Talbot 2005).

The main phase of the dissolution and brecciation was probably related to laterally extensive exposure surfaces detected within the middle and upper part of Wordiekammen Formation (Eliassen 2002). The surfaces were exposed due to a significant fall in sea-level leading during the Late Carboniferous to Early Permian (Eliassen and Talbot 2005). The Gzhelian and Asselian/Sakmarian exposure surfaces are considered to be the best candidates for timing the karstification of Minkinfjellet Formation evaporites, and the brecciation of the Minkinfjellet and Wordiekammen Formation carbonate rocks (Eliassen 2002). Diagenesis in the Late Carboniferous to Early Permian occurred at depth but from waters of meteoric origin (Eliassen and Talbot 2005).

The types of cements presented in **Table 2.1** includes the three generations of cement have been detected in the Minkinfjellet Formation limestone. 1) Early marine fibrous cement, which has volumetrically minor abundance. 2) Drusy calcite spar precipitated during flushing of meteoric water is present around the former exposure surfaces. 3) Coarse crystalline blocky pore-filling spar, which were precipitated during deeper burial (Eliassen 2002). Aggrading neomorphism producing pseudosparitic crystalline limestone, is common in original lime-mudstones and wackestones. Partial or complete dolomitization is widespread within Minkinfjellet Formation and is caused by gypsum precipitation and production of hypersaline brines in the basin. Three mechanisms of silicification are common in the carbonates in Minkinfjellet Formation. 1) Silica replacement of the gypsum nodules. 2) Concretionary growth of silica which has been nucleated by organic matter. 3) Megaquartz that has replaced the calcite spar. The dominant cement in the Minkinfjellet sandstones is quartz. Pore-filling calcite spar are also abundant in the sandstones and post-date the quartz-cementation (Eliassen 2002).

Table 2.1: Cements with increasing burial depth in Minkinfjellet formation, the figure is from (Eliassen and Talbot 2003a).

Sequential evolution of diagenetic events in the Minkinfjellet Formation	
Event	———— Increasing burial depth ———➤
Marine fibrous Cement	
Meteoric drusy spar	
Dolomitization	
Chert formation	
Dedolomitization	
Aggrading neomorphism	
Quartz overgrowth	
Sandstone - calcite cement	
Blocky calcite spar	
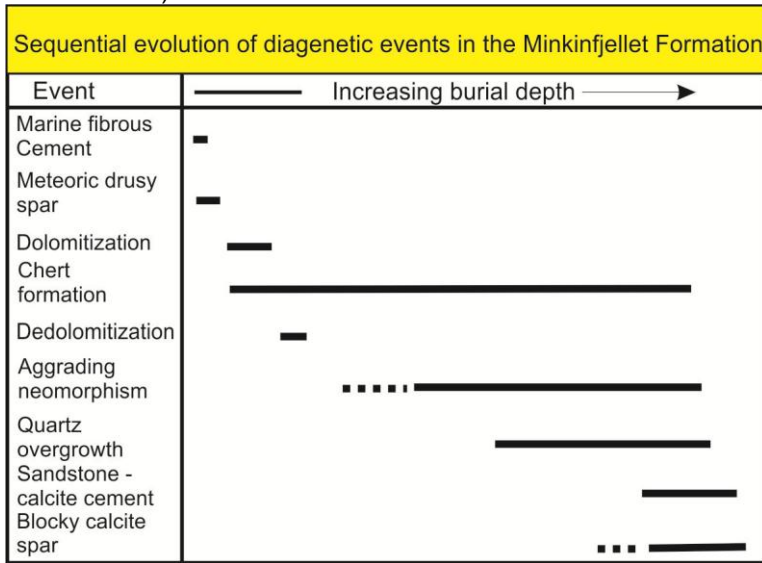
The cementation in the Black Crags of the Wordiekammen Formation took place in near-surface marine and meteoric environments, down to deep burial environments, **Table 2.2** (Aase 2006). The figure shows that the same types of cements as in Minkinfjellet can be found within the Black Crag Beds.

Table 2.2: Sequential evolution of diagenetic events in the Black Crag Beds, the table is from (Aase 2006).

Sequential evolution of diagenetic events in the Black Crag Beds	
Event	———— Increasing burial depth ———➤
Lithification of limemud	
Marine fibrous cement	
Drusy voidfilling spar	
Chert formation	
Dolomitization	
Aggrading neomorphism	
Mechanical compaction	
Chemical compaction	
Silica cement	
Cementation of breccias	
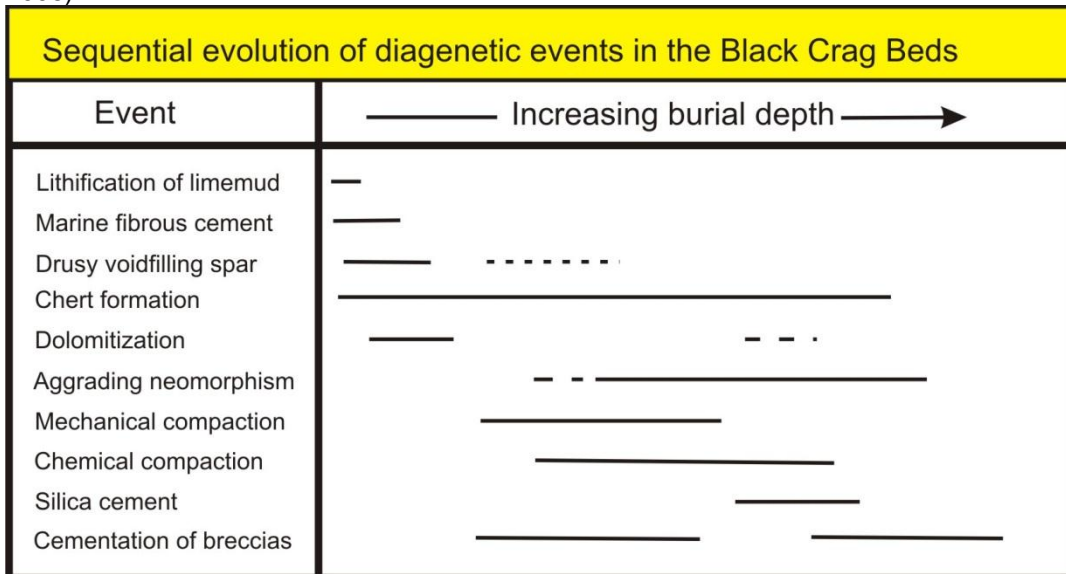
2.10 Breccia Classifications in the Billefjorden area

The breccia classification in the area of study is based upon the facies interpretations from Hege Cecilie Noreides master thesis. Her master thesis, "Spatial distribution and architecture of breccia pipes features at Wordiekammen, Billefjorden, Svalbard", made the classifications for the breccia pipes found within Wordiekammen formation and Fortet of the Minkinkammen Formation.

2.10.1 Breccia facies description

In Noreide (2008), three representative breccia pipes along the western and southern slopes of Wordiekammen were selected for detailed studies of structures and sediment fill. The facies descriptions in (Nordeide 2008) were based upon classification of breccia collapsed caves done by Loucks (1999). In (Noreide 2008), six facies were recognized, and their photo description is indicated in **Figure 2.11** :

Facies A: Brecciated micrite: The facies consists of angular clasts that range in size from 2-10 cm.The color is red and grey and the composition is clast supported micritic breccia. The clasts are brecciated but almost in place.

Facies B: Micritic breccia: The facies consists of angular to sub-angular clasts, ranging from 1-3 cm with occasionally clasts up to 10 cm large. The composition is clast supported grey micritic breccia. The facies is highly fractured and is porous with minor amount of silty matrix.

Facies C: Stratified mixed breccia: The texture of the facies is of angular to ribbon, with clasts ranging from 0.5 m and up to boulders. The color is grey and yellowish. The composition consists of facies F and facies G, with grain and granule sized matrix. Stratification of the facies is with mainly facies F in on sequence, and then facies G in another.

Facies D: Massive mixed breccia: The texture of the facies ranges from angular to ribbon, with gravel to boulder sized rock fragments. The color is grey and yellow and has a chaotic sedimentary structure. The facies consists of facies F and facies G, with grain sized and granule sized matrix.

Facies E: Cemented micritic breccia: The clasts are angular to sub-angular, and consist mainly of 0.3-1 cm clasts, but up to 7 cm clasts were observed. The color is grey and is mainly facies F but with cement around the clasts. The sedimentary structure is fine-clast cemented breccia.

Facies F: Stratified micrite: The texture of this facies is massive and consists of massive clasts. The color ranges from light grey to grey micritic breccia. The sedimentary structure is massive and generally blocky. Horizontal sequences with intervals of light grey and grey color. Farctures around color change were observed.

Facies G: Wackestone/packestone: It has a sedimentary texture and consists of fossiliferous sedimentary rock. The color is yellow and consists of packstone. The sedimentary structure is massive or some sandstone stratification.
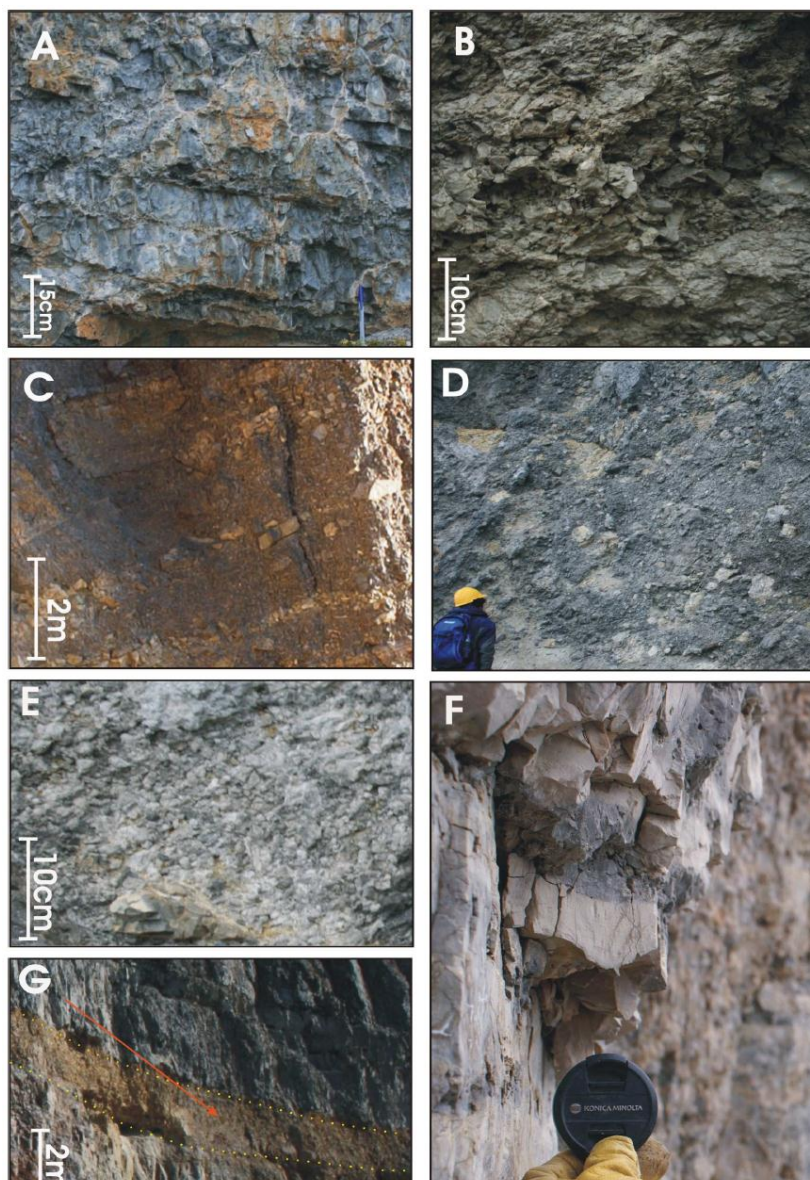
Figure 2.9: Photo description of facies A through G. Picture A, shows facies A and B. Picture B, shows facies B and C. Picture C shows facies C and D. Picture D shows facies D and E. Picture E shows facies E and F. Picture F shows facies F and G, Picture G shows facies G as the darker redder bedding

3 Methods

3.1 Fieldwork

The fieldwork in Billefjorden area in Spitsbergen was conducted from 1st of August to 7th of August 2011. The fieldwork was spent on identifying the paleokarst features in Wordiekammen and Minkinfjellet Formations, in an area ranging from Ebbadalen to Adolfbukta. During this period the size of breccia bodies were identified and mapped. The main focus was on identifying and describing the different facies distribution within a breccia pipe. Positions of the different outcrops within the breccia pipes were made by using GPS, measurement band - and stick.

3.1.1 Equipment

- ✓ Compass
- ✓ GPS (WGS_1984_UTM_Zone_33N)
- ✓ Map: Geological map of Billefjorden, Central Svalbard, Scale 1:50 000
- ✓ Measuring tape (40 meter)
- ✓ Measuring stick (2 meter)
- ✓ Lens
- ✓ Field notebook
- ✓ "Sedimentary rocks in the field" by Maurice E. Tucker, 1996
- ✓ Altimeter

3.2 Mapping techniques

Several techniques have been used in the making a topographic overview over the outcrops in the Billefjorden area. Spitsbergen is badly covered by satellite pictures, so a few mapping programs have been used in order to make a topographic overview picture.

3.2.1 LIME

LIME (Lidar Interpretation and Manipulation Environment) (Buckley et al. 2008) is a lidar interpretation program which is based on terrestrial laser scanning for modelling geological outcrops. The lidar interpretation program integrates photographic 3-D models of geological outcrops (Buckley et al. 2008). The data collected for the 3-D models are based on GPS coordinates. The outcrops at Billefjorden area was scanned in 2007, and careful planning were

done to determine the times when the GPS Constellation was at its best geometric configuration. This is because of the proximity of Svalbard to the North Pole, there are several periods within 24 hour period with poor satellite geometry (Buckley et al. 2010). LIME was used in mapping of the outcrop sites to find the missing GPS coordinates and correct the GPS coordinates taken in the field.

3.2.2 ArcGIS

ArcGIS is a system working with maps and geographic information, and is a group of computer programs based on geographic information systems (GIS), and is produced by Esri. ArcGIS is a complete system for designing and managing solutions for geographic information and knowledge. ArcGIS desktop were used to design a shape file for the GPS coordinates made in the field and constructed from LIME.

3.2.3 Svalbardkartet

Norwegian polar institute does the mapping of the Norwegian areas in Antarctic and in the Arctic, hence Spitsbergen. They have created the interactive maps of Spitsbergen online, called Svalbardkartet and TopoSvalbard (Norsk-Polar-Institutt). The Svalbardkartet shows a detailed topographic base map, equivalent to the topographic main map serie, Svalbard 1:100 000. Into the Svalbardkartet the shape files made in ArcGIS, were incorporated, and a detailed topographic 2-D view of the breccia pipe outcrop site was constructed. The interactive TopoSvalbard map gave coordinates and distance measurements between the localities of study, as well used to make descriptive figures.

3.3 Laboratory technique and methods

3.3.1 TinyPerm

TinyPerm II is a portable air permeameter, **Figure 3.1**. It is a portable hand-held instrument to measure the rock matrix permeability or effective fracture apertures on outcrops, or at samples in a laboratory.

Since all of the samples had a rough surface, an artist`s kneaded-rubber was applied to the nozzle to prevent airflow along the surface of the sample and ensure accuracy. To calculate the permeabilities, **Equation 3.1** was used:

$$T = -0,8206 \times log_{10}(K) + 12,8737 \tag{3.1}$$

The tiny perm measurements were performed five times at each point of measurement, in order to sort out anomalous measurements. The points of measurements taken were indicated with the letters from A to G, see Appendix 1 1. Standard deviation was used to find the probability of the results, **Equation 3.2**.

$$S_x = \frac{\sum_{k=1}^{n}(x_i - \bar{x})^2}{n-1} \tag{3.2}$$

The uncertainties in the measurements could be quite large since the best way to measure tiny perm is on a flat surface. Most of the samples had a rough surface, and reliability values are hard to achieve, but they give an approximation of the permeability. The permeability of these samples is in a wide range due to the heterogeneity and degree of fracturing in the samples. For the more homogenous sample, more equal permeability results were achieved.

Figure 3.1: TinyPerm II, a portable air permeameter.

3.3.2 Total volume measurements of samples

Due to the highly irregular shape of the samples, their volumes were measure with mass balance and Archimedes law. The Archimedes law states that buoyancy equals the weight of the displaced fluid (Lien and Løvhøiden 2004). The formula for buoyancy is.

$$\overrightarrow{F_b} = -\rho V \vec{g} \tag{3.3}$$

In order to get the volume, the Archimedes law, **Equation 3.3**, was incorporated in the mass balance equation, shown in **Figure 3.2**. The mass balance equation is:

$$Mg_{down}=(\rho_w Vg+mg)_{up} \tag{3.4}$$

The reference fluid is distilled water, with density, $\rho = 1$ g/ml. Converting **Equation (3.4),** gives the equation for the total volume of the rock.

$$V_{total} = \frac{m_{down} - m_{up}}{\rho_w} \tag{3.5}$$

The setup for the measuring of the total volume, **Figure 3.2** show the different parameters put into the **Equation 3.5**.
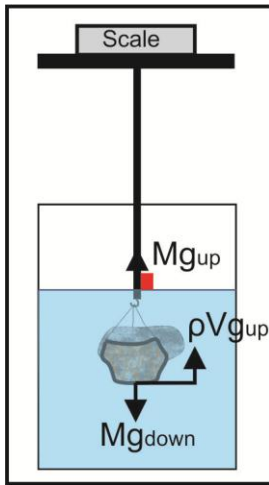
Figure 3.2: The setup for the total volume measurements on both saturated and dry samples.

The measurements of the total volume were performed several times, on both dry samples and saturated samples. The procedure was performed as follows for the dry samples:

1. The samples were dried at 80 ˚C, until the samples had a constant dry weight.
2. The weighted dry weight in air was called, m_{down}.
3. A string was put around the sample and the sample was lowered into the water. The weight in water was then read off the scale, m_{up}.
4. The samples weight was weighted after the experiment, to measure the excess water the samples gained during the measurement, as the samples were measured without a packing.

Distilled water was used because of its neutral ion composition. The samples were not packed, as a result of all the packages were torn apart because of the samples rough surface. By weighing the samples after the measurements the error of the excess water was corrected, as described in section 3.3.6.

For the volume measurement on the saturated samples, setup in **Figure 3.2**, the procedure is mainly the same as for the dry samples, whereas the second step is added. The saturation procedure:

1. The samples were dried at 80 ˚C, until the samples had a constant dry weight.

2. The samples were saturated in a desiccator. The desiccator was evacuated with the
    samples, until the pressure was below 1 Torr. After the pressure was below 1 Torr, the
    desiccator was filled with distilled water. Then the water filled desiccator with the
    samples was left for 6-7 hours, before the samples were taken out.

3. The samples were then taken out and weighted. Which gave the saturated weight in air,
    $m_{down.}$

5. Then a string was put around the sample and the sample was lowered into the water until
    it is totally covered. The weight in water was then read of the scale, m_{up}.

6. Finally the samples were weighted one more time in air.

The pore volume of the samples was measured simultaneously, as both the dry weight and the
saturated weight of the sample was weighted during the procedure. After the saturation procedure
had been completed, the total volume was measured with volume displacement method, since
they would not take up any water in the pore system. Two different containers were used, one for
the small samples and one for the larger samples. The use of two different containers were due to
the volume displacement was insignificant for the small samples in the large container. Volume
displacement is often used when the sample has an irregular shape. The measurements gave an
indication of the total volume.

3.3.3 Porosity measurements on samples

The porosity of the samples was performed as simultaneously as the measurement of the total
volume in the saturation procedure described in section 3.3.2. By creating vacuum in the sample,
the water will instantly be sucked into the pore space of the rock, due to forced imbibition.
However, to ensure that the samples were saturated completely, then stayed in the desiccator for
6-7 hour on average. The pore space of the samples was calculated by subtracting the dry sample
weight from the weight of the saturated sample using the equation below.

$$V_p = \frac{m_{sat} - m_{dry}}{\rho_w} \qquad\qquad (3.6)$$

In the **Equation 3.6** the density of water, ρ, equals 1 g/ml. The porosity of the samples was then
gain by using **Equation 1.2**, thus gaining the effective porosity.

The porosity measurements were executed twice for the small samples (less than 1000 cm^3), and once for the large samples (over 1000 cm^3), due to their fragile state.

3.3.4 Cutting of core plugs

For the permeability testing, the samples were cut into 1 inch cores. The length of the core samples varied due to the original size and the original state of the samples.

The lengths of the core plugs are mostly less than 4 cm. This is because of the fragile state and/or void space of the samples. During cutting of core plugs the samples often cracked to pieces. This is because of larger void space in between the clasts where they are not compacted and cemented completely. Cement can also hold a rock together, but in large quantity it also separates the clasts, and put under stress, the rock often crumbles. Since the breccia samples also can contain different clasts from different origin, these have not been undergone a total lithification, and therefore cracks under stress.

The core plugs which were cut out from the samples were mostly from the most cemented and compacted part. The permeability values can therefore be lower than generally for the whole sample.
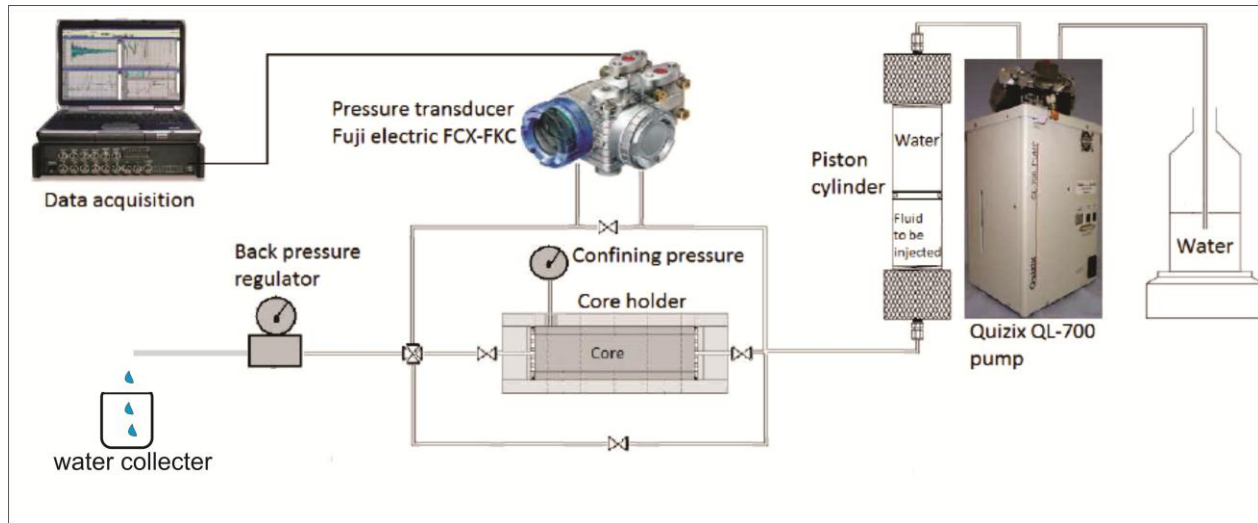
3.3.5 Permeability and porosity measurements on core plugs

The core plugs were first dried at 80˚C, until their weight became constant. Their volume was measured with the use of slide caliper and then calculated by **Equation 3.7** for a cylinder.

$$V_{total} = \pi r^2 h \qquad\qquad\qquad (3.7)$$

First the porosity of the core plugs were gained by the saturation method. To measure the porosity of the cores, **Equation 3.7** and **Equation 1.2** were used, thus gaining the effective porosity.

For the permeability testing, the main experimental setup used during flooding experiments is schematically shown in **Figure 3.3**. To make sure that the core is totally saturated and no air is trapped inside the core, a back pressure was connected to the exit side of the core. This back pressure was set to 8.2 Bar. The setup is shown is **Figure 3.3**.

Figure 3.3: Experimental setup for the permeability measurements. The figure is modified from (Solbakken 2010).

The absolute permeability is measured based on Darcy's law, **Equation 1.3**. By knowing the viscosity of the injected fluid, the length and diameter of the core plug, the permeability can be estimated by measuring the differential pressure at different flow rates. The rate can then be plotted as a linear function of the differential pressure, and the slope is used to calculate the permeability. For example, **Figure 3.4**, show that only 3 of the measured points have been used in further calculations for the sample 6.
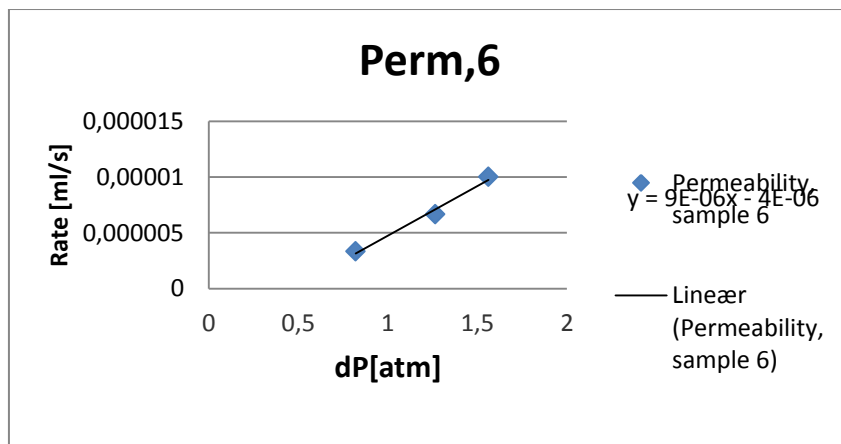
Figure 3.4: Permeability measurement of sample 6, where 3 values have been used in further calculations.

For the first 2 samples, it was hard to achieve a constant pressure at a constant rate. For these samples, distilled water was used, with a viscosity of 1.0 ±0.01 cp. The reason for using distilled water was due to the fact that the samples have been taken from outcrop and the natural fluid has been rain water. Unstable pressure drop profile could be due to swelling of clays, detachment of particles or dissolution. Therefore the injection fluid was changed to syntetic sea water. The viscosity used in, **Equation 1.3**, was then 1.05±0.02 cp for the syntetic sea water. The viscosity is highly dependent on temperature and the viscosity value used is the average of the viscosity values from 20-22˚C. The composition of syntetic sea water is listed in, **Table 3.1**.

Table 3.1: The composition of syntetic sea water

Salt	M_{salt} (g)
NaCl	124,45
CaCl$_2$·6H$_2$O	8,63
MgCl$_2$·6H$_2$O	55,62
NaHCO$_3$	0,96
Na$_2$SO$_4$	20,28
KCl	3,34

It was still hard to get good readings and is mainly due to the lithology of the core plugs, which is very cemented and compacted. To achieve a reading of the differential pressure at a constant rate, it would often take days as very low rates have to be used. Different procedures were performed in order to gain a constant rate at a different pressure. These were:

- *Turn the flow through the core:* performed under the suspicion that loose grains had closed several pore throats and inhibited the flow.
- *Increase the confining pressure:* the confining pressure should always lie about 10 bar higher than the injection pressure. If this is less, it may cause bypass of flow in the core holder.
- *Run the measurement for a longer time:* when the permeability is low, it takes longer time to achieve a constant rate.

3.3.6 Uncertainties in laboratory methods

When working in a laboratory there are several uncertainties involved in every step of the measurements. The uncertainty in the scale is 0.1 gram, however the uncertainty in the methods used are greater. Therefore the uncertainties in the scale are considered to be negliable. The aim here is to give a quantitative approach to the error estimation.

The errors in calculation the porosity of the sample lies in the measurements of the total volume and the volume of the pore space of the sample. The procedure for measuring the total volume of the sample was executed in 3 different procedures. The procedures were described in **section 3.3.2**. The uncertainties in the measurements are:

Total volume based on volume displacement: In this procedure a measurement band was attached to one of the insides of the containers. The reading of the measurement band was hard due to capillary forces adhered to the measurement band. This had a large effect, as the error in reading of the measurement band is estimated to be 0.1 cm. Two containers were used, one for the largest and one for the small samples, with errors:

- $\pm 100 \text{ cm}^3$ for the samples used in the large container.
- $\pm 20 \text{ cm}^3$ for the samples in the smaller container.

Due to the high uncertainties of this method the volume displacement was the most inaccurate of the volume measurements, and the method was discarded as a procedure for measuring the total volume of the samples.

Total volume based on Archimedes law for dry samples: In this procedure the samples was first weighted dry, and then submerged dry. The samples were weighted submerged dry without packing due to:

- Rough surface and an irregular shape; caused tearing of packing.
- Air trapped inside packing; would overestimate the total volume.

The samples became saturated, some more than other due to the brecciation and fracturing. The excess water the samples gained lead to an inaccurate total volume measurement, and the samples were weighted after to correct the error. By doing this the error was eliminated and the uncertainty in this method is estimated to be 1% based on the mechanical work done on the

sample. The method was used to give an indication of the total volume of the sample, however, not used in the calculations to find the porosity of the samples.

Total volume measurements based on Archimedes law for saturated samples: This method is the same as the one in the previous section, but the difference here is that the samples have been saturated first. With this method the pore volume of the samples were also measured. As both the total volume and pore volume of the samples were measured using this method, these values have been used in the porosity calculations. In the measurements of calculating the total - and pore volume there were several non-measurable errors such as:

1. Loss of rock fragments during measurements: This occurred during stress put on the sample, as it was being saturated in the desiccator and during the buoyancy measurement. This was especially the case for the most brecciated and unconsolidated samples.
2. The degree of saturation: In the measurement of the saturated sample, an overestimation of the weight due to the extra water on the surface. But also, an underestimation could be made if the samples were less saturated. This could occur if the samples were taken out of the desiccator too quickly. On average, they stayed in the desiccator for 6-8 hours, but for the unbrecciated samples, the time should have been longer. Or there could have been a leak during the measurement.

Due to these errors a quantitative approach was used to estimate the uncertainties in the measurements. The error in the total –and pore volumes is estimated on the individual samples and measurements. The estimations are based on the observations made during laboratory work. The results from the total and pore space measurements are presented in the Appendix 1. The total volumes used in the calculations to find the effective porosity are presented in the petro-physical chapter 5.

The uncertainty of the porosity of the samples are calculated based on the estimated uncertainties of the total volume and pore space volume. The equation used to find the uncertainty of the measurements is:

$$S_\varphi = \sqrt{\left(\frac{\partial \varphi}{\partial V_p} S_{V_p}\right)^2 + \left(\frac{\partial \varphi}{\partial V_t} S_{V_t}\right)^2} \tag{3.7}$$

The calculated uncertainty varies according to the uncertainties in the method during measurements. The uncertainty of the effective porosity is presented in the Petro-physics chapter 5.

3.3.7 Uncertainties in the porosity and permeability of the core plugs

The total volume for the core plugs were measured accurately with a slide caliper, and 6 measurements of the length and the diameter were carried out. To find the uncertainty, standard deviation, Equation 3.2, was used to find the uncertainty of the length and diameter. Then Equation 3.8 was used to find the uncertainty of the total volume.

$$S_{V_{total}} = \frac{\pi}{4} \sqrt{\left(\frac{\partial V_{total}}{\partial D} S_D\right)^2 + \left(\frac{\partial V_{total}}{\partial L} S_L\right)^2} \qquad (3.8)$$

For the uncertainty of the pore volume, the uncertainty of the scale, 0.01g was used. The uncertainty of the porosity of the core plugs was then gained by using **Equation 3.7**.

For the uncertainty in the permeability measurement was carried out using following equation.

$$S_K = \sqrt{\left(\frac{\partial K}{\partial q} S_q\right)^2 + \left(\frac{\partial K}{\partial \mu} S_\mu\right)^2 + \left(\frac{\partial K}{\partial L} S_L\right)^2 + \left(\frac{\partial K}{\partial A} S_A\right)^2 + \left(\frac{\partial K}{\partial \Delta P} S_{\Delta P}\right)^2} \qquad (3.9)$$

4   The results from the field observations

This chapter presents the results from the fieldwork conducted in Northern Billefjorden, Spitsbergen. The chapter is divided into three sub-chapters that give an overview to the geological outcrop sites in the Wordiekammen Formation and in the Minkinfjellet Formation.

4.1   Introduction

The geological fieldwork was conducted at several localities, which have been divided into three study areas. The study areas have been named; Area 1, Area 2 and Area 3, **Figure 4.1**. The aim of the fieldwork was to map, sample and describe well exposed breccia deposits within the Minkinfjellet and Wordiekammen Formations.
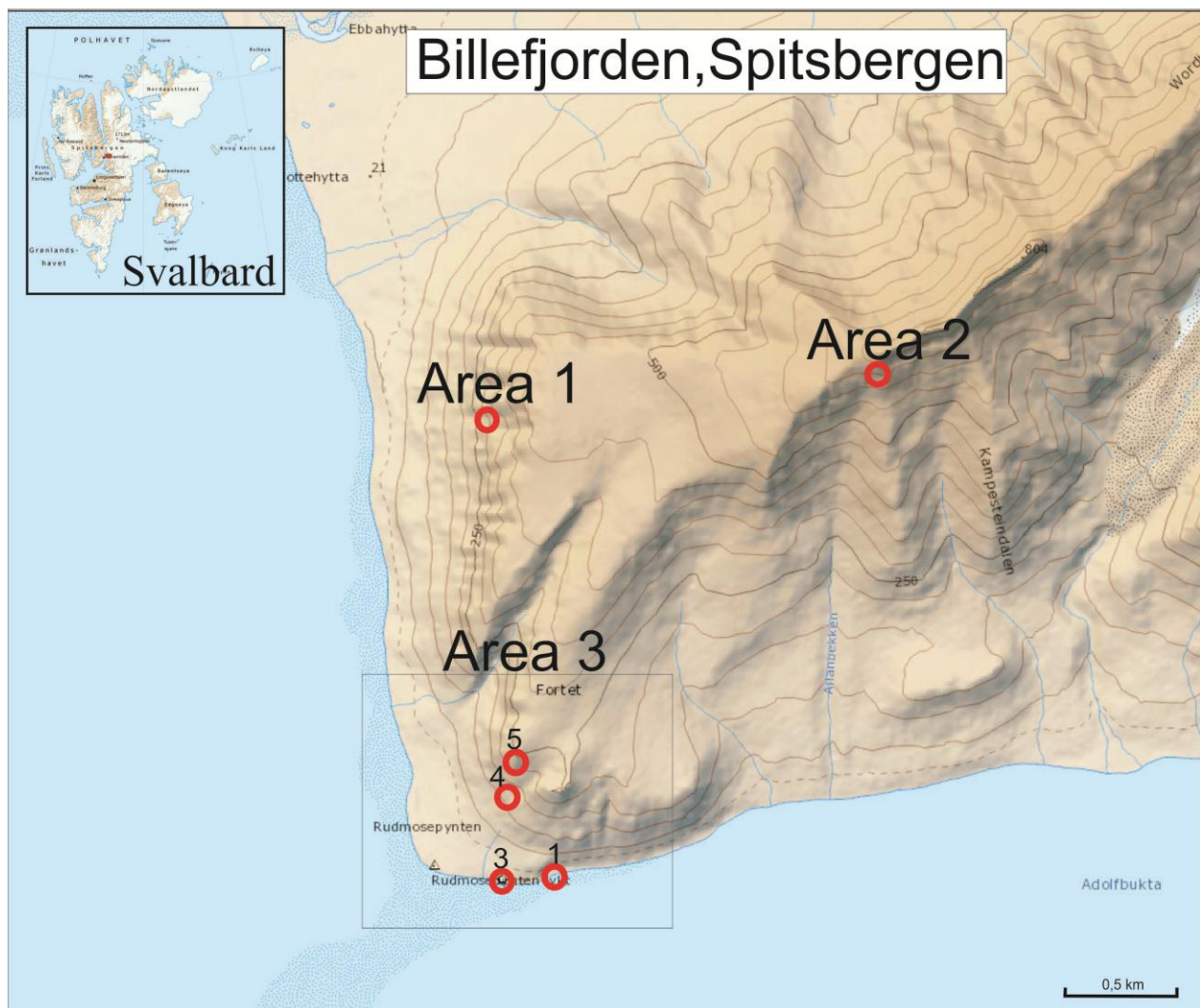

Figure 4.1: The figure shows the locations of the fieldwork based on UTM coordinates. The basemap is modified from Toposvalbard.npolar.no at norskpolarinstitutt.no.

The focus of the fieldwork was Area 1, which was a well exposed breccia pipe within the Black Crag Beds in the lower part of the Wordiekammen formation. Area 2 is a locality of stratiform breccias of the Wordiekammen Formation situated around The Løvehovden Fault Zone. Area 3 consists of localities from both the Minkinfjellet and Wordiekammen Formations. The objective of sampling was to do experimental testing in order to get petrophysical properties such as porosity and permeability from the study areas. The purpose of this is to be able to put the petrophysical properties in context with the different breccia deposits. Each of the areas is presented separately based on the data collected in the field. This chapter will introduce the geological descriptions for each study area (Area 1, Area 2 and Area 3).

4.2 Area 1 - The Red Breccia Pipe

The area was first described and interpreted as a breccia pipe in (Nordeide 2008), where the area was referred to it as Breccia Pipe nr 2. The area is here referred to as The Red Breccia Pipe because of the distinct red color of the breccia sediments at the east side of the pipe. The marked red color can be seen in picture, D, in **Figure 4.3**. The location of Area 1 indicated as The Red Breccia pipe is showed in **Figure 4.3 g)**.

The Red Breccia Pipe is exposed on a slope, with a over 90 meter vertical distance. No cavern floor is exposed in the area. Parts of the roof and wall are observed in the central-east side of the pipe (Nordeide 2008). However the roof can also be interpreted as a local "overhang" in the wall of the pipe. The apparent roof structure of The Red Breccia Pipe is indicated by the red line

above D, in **Figure 4.3**. The reason for the line being drawn here is that the upper limit of layer L4, in **Figure 4.3**, can be traced to the northern side of the Red Pipe.
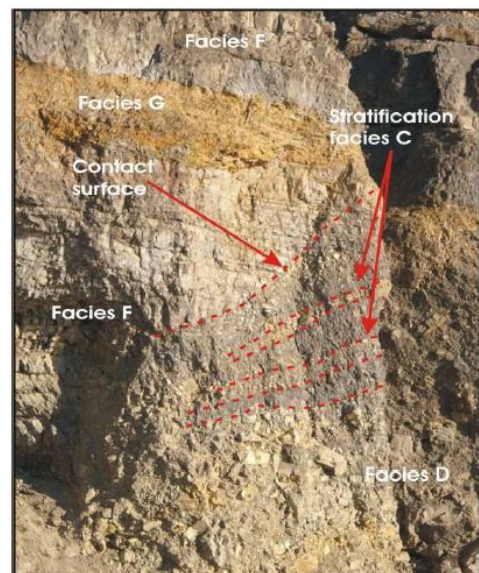
Figure 4.2: Contact between wall and Red breccia, Facies F-G and facies C (Nordeide 2008)

The red outline the brecciated area, and the red and red striped lines in **Figure 4.3**, mark the outline of the Red Breccia Pipe which gives the area a funnel-like shape in the vertical view. The contact between the Red Breccia Pipe and the wall rock was not exposed except in the Red Breccia Pipe margin located to the N-E **Figure 4.2**. The brecciation resembles the style of a typical doline brecciation, as there are sharp lateral boundaries into un-brecciated flat lying strata (Eliassen and Talbot 2005).
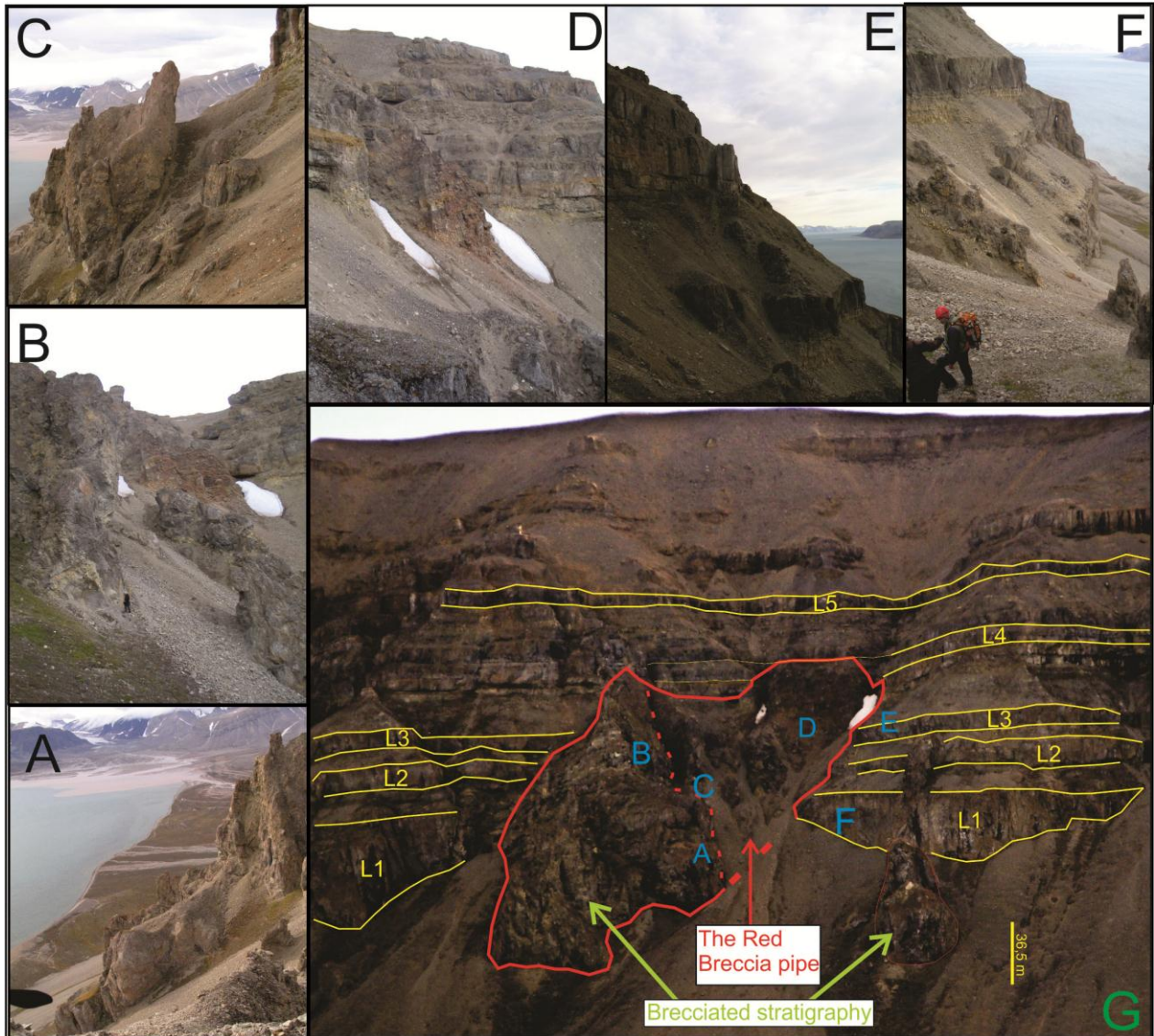
**Figure 4.3**: The Red Breccia Pipe in the Black Crags Beds. The pictures numbered from A to F show the areas within The Red Breccia Pipe observed from different locations, and the blue letters within picture G correlates to each of the numbered pictures (A-F). The cliffs of the Black Crag Beds are numbered from layer 1 (L1) to Layer 5 (L5), where only the top layer 5 can be traced undisturbed at each side of the Red Breccia Pipe.

Much of the pipe has been eroded away and is covered by talus, but individual breccia bodies remain exposed in the pipe at both upper and lower levels. The breccia bodies are separated by scree. In Nordeide (2008) the focus of the facies descriptions were the largest breccia bodies at the locations 12, 13 and 18, **Figure 4.5**. **Figure 4.5** was based on UTM coordinates in the field and those gained from LIME, **Figure 4.4.** In **Figure 4.5** the total 20 mapped locations are outlined. The irregular red shapes give the area of the preserved breccia bodies within the pipe. The map gives a 2-D view of the pipe, which also shows that the breccia pipe has an approximately circular shape seen in plane view.
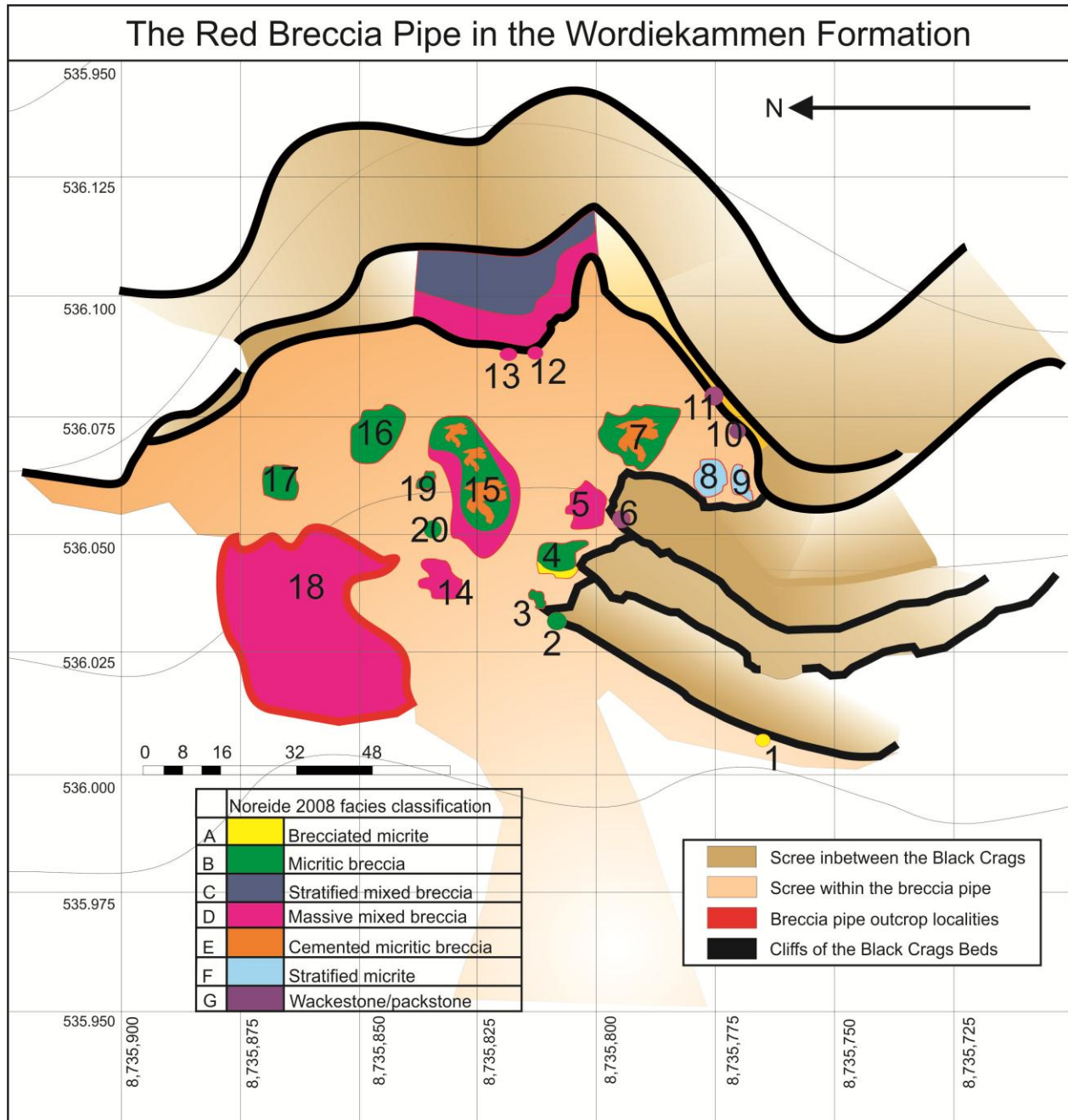
In (Nordeide 2008) a facies classification was presented for the breccia pipes in the Black Crag beds, described in chapter three. The logging and interpretations of the outcrops within the Red Breccia is based on (Nordeide 2008) facies classification. The **Figure 4.6** shows the localities described in Chapter 5, classified after (Nordeide 2008) facies classification. The different colors describe the facies A to facies G. Nordeide (2008) made her classification system for the regional setting based on the classification presented by (Loucks and Mescher 2001).
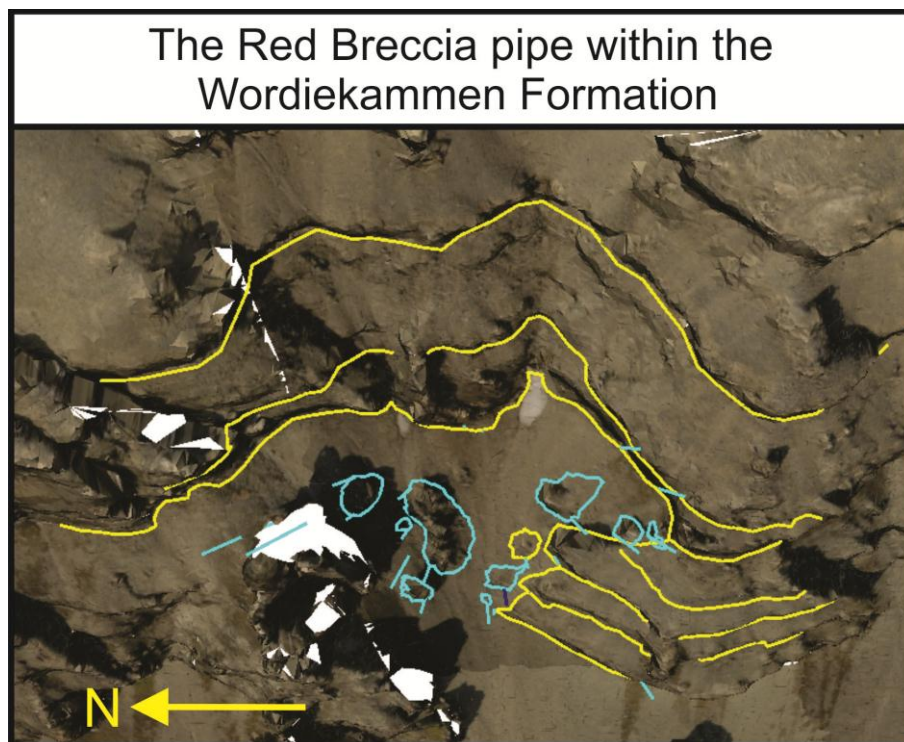
Figure 4.4: The cliffs of the Black Crag Beds and the outcrop locations within the Red Breccia Pipe are outlined in LIME. The lines gave the UTM coordinates in the Area 1.
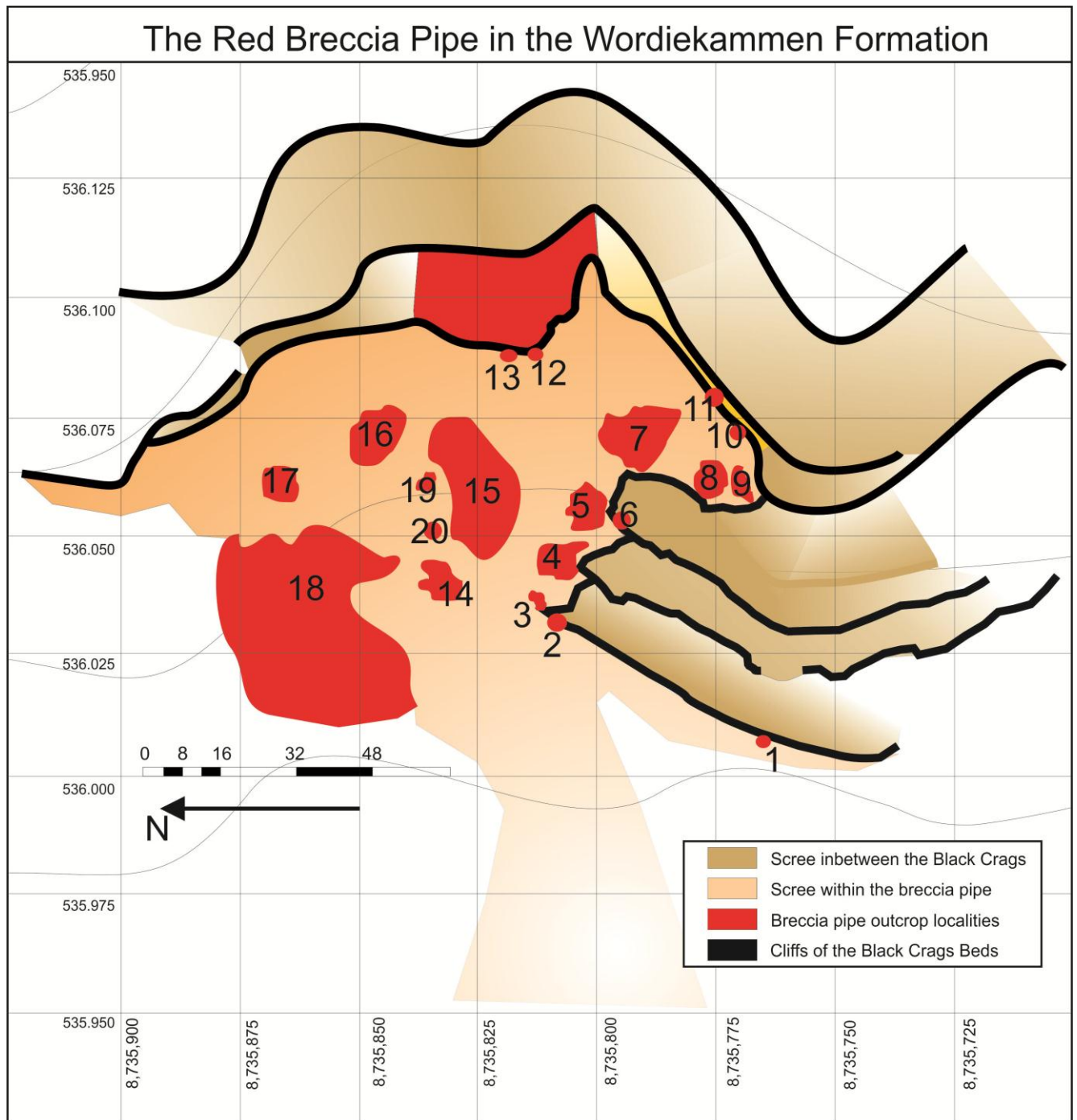
Figure 4.5: Topographic 2-D map over The Red Breccia Pipe. The map shows the different localities within the area, numbered from 1 to 20.

Figure 4.6: The breccia exposures classified by using the scheme of Nordeide (2008). The colors indicates the different facies. At outcrop number 7 and 15, the orange and green indicated that a mix between different facies.

A classification of the outcrop sites was also done with Loucks and Mescher (2001). The facies classification was published in (Loucks et al. 2004), which is used in this thesis. **Figure 4.6** and **Figure 4.7** shows the result of using the different classification systems.
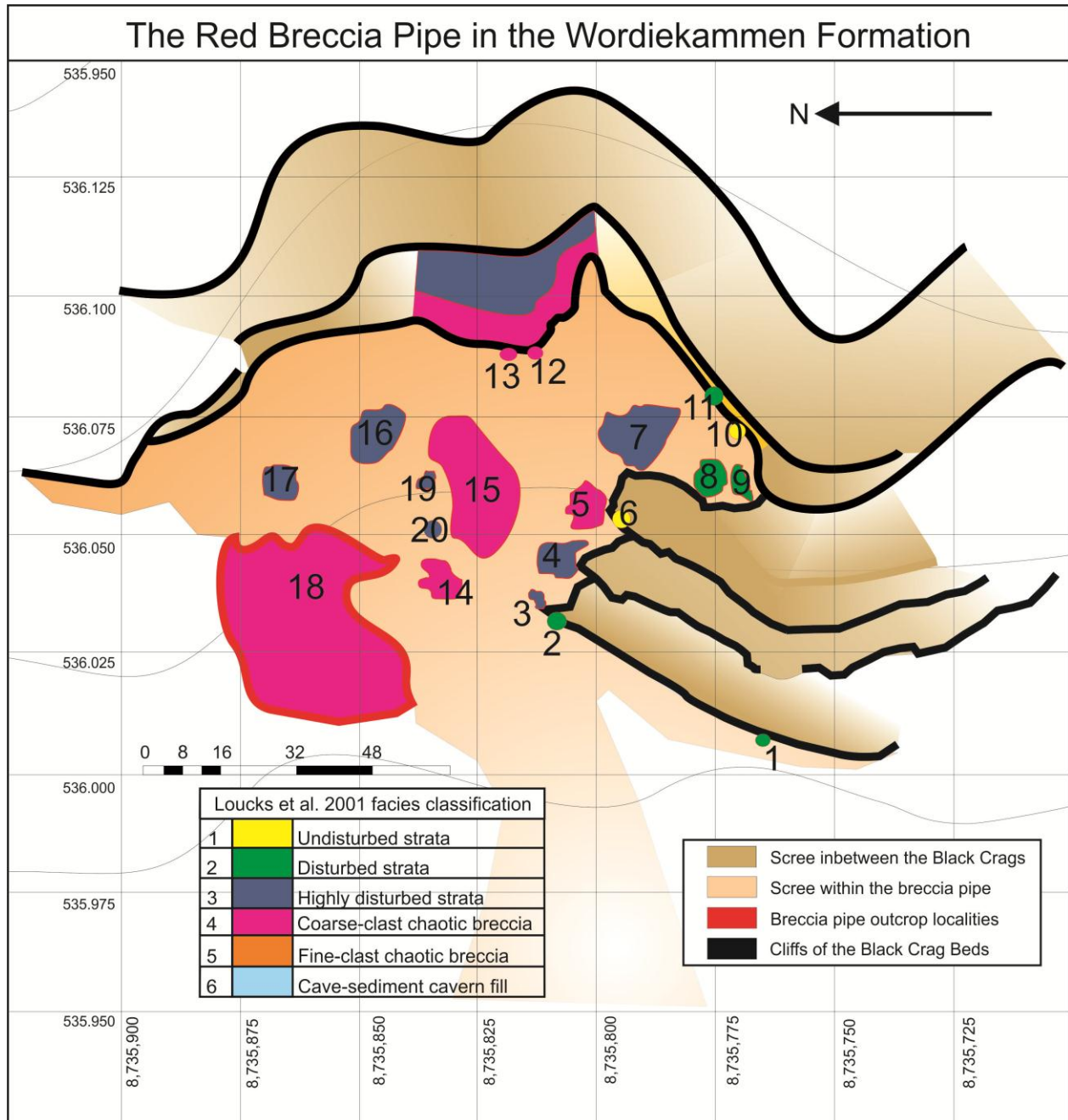
Figure 4.7: The breccia exposures classified by using the scheme of Loucks et al. (2004). The different color represents the different facies.

The aim by classifying the outcrop sites was to evaluate which one had the best approach to classify the deposits within the pipe. The interpretation of the pipe, based on both classification systems shows that no floor were observed and only parts of the roof or a "hanging wall" of the pipe was observed in the eastern direction. All the deposits within the pipe were transported a short distance, as the composition of the brecciated rocks resembles the surrounding stratigraphy. The pipe classifications in **Figure 4.6** and **Figure 4.7** indicate a pattern in the breccia

distribution. However, neither of the classifications indicates how far up the pipe prograded, nor any cave floor facies deposits have been classified. As no cave floor deposits were observed at The Red Breccia pipe, the lower extent is uncertain.

There is evidence that the brecciation occurred in more than one stage. It could have been affected by the faulting in the area. But the most likely reason is that large fractures are developed within the breccia deposits as the breccia are compressed by overlying breccia deposits. Large fractures cross-cut the localities (16, 15, 14 and 7) and the area around the fracture plane showed intense brecciation. Evidence for multiple stages of brecciation is observed in the two mosaic breccia samples from location 15. Mosaic breccia is developed in cavern roof and wall, and the samples were situated in a matrix-rich clast-supported chaotic breccia, which is the facies of the cavern fill classified after the classification by Loucks and Mescher (2001).

4.3 Area 2

Area 2 is located in an area around Løvehovden Fault Zone in The Black Crag Beds of the Wordiekammen Formation, **Figure 4.8 i**. The breccia consists of stratiform breccias, which extends along the Black Crag Bed to the west and ends in the eastern direction.
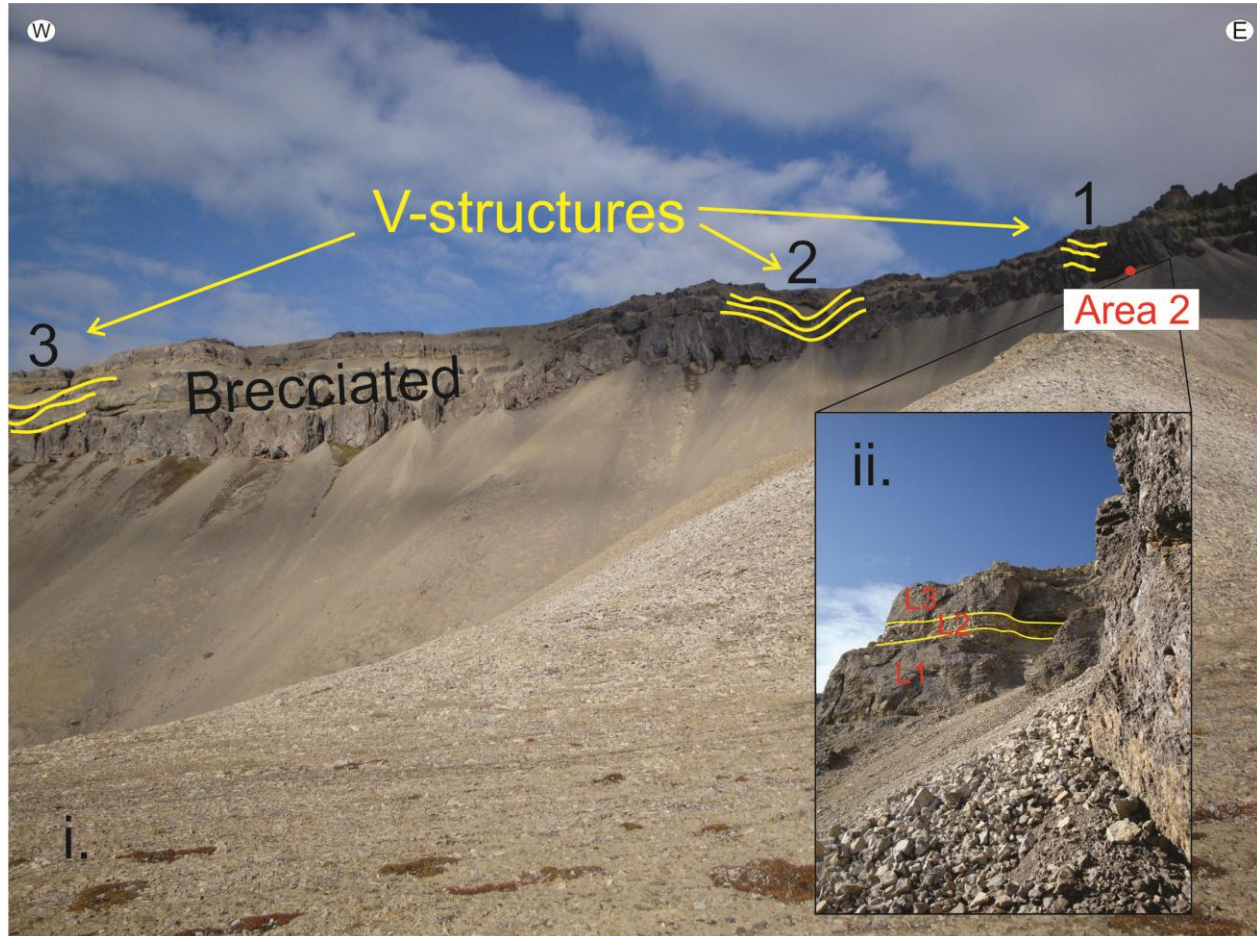
Figure 4.8: i) Indicates the location of Area 2 and V-stuctures in the area. ii) Crackle-mosaic in the stratigraphic layers occurred in-situ, without causing any breaks between the layers.

The location Area 2, **Figure 4.8 i.** shows disrupted layers in a V-shaped geometry close to a fault related monocline. The field observations showed that the V-shaped geometry was related to a brecciated interval, which contained broken and tilted carbonate beds having a crackle and mosaic texture. To the west there are several monoclines related structures that can be seen as the V-structures, **Figure 4.8 i**. No measurements of the V-structures were performed, however by visual observations of the size are in the same range as stated in Eliassen (2002), whom stated that the sizes of the V-structures are tens of meters in vertical direction, and extend for more than

100 meters laterally. **Figure 4.8 ii** indicates that the brecciation has not caused any breaks in the stratigraphic layers, but has occurred in place.

The V-structures associated with the stratiform breccia are interpreted to be a result of the faulting, as fracture density scan-line analysis was executed, **Figure 4.9**. The fracture density scan- line analysis showed a high degree of fault related fractures around the monocline at location "Area 2" in both eastern and western direction. Towards the west the fracture lines first decreased, then increased as the second monocline indicated by the V-structure number 2, **Figure 4.8 (i)** was approached**.** Towards the east the fracture density decreased, and the observed brecciation of the lower cliffs of the Black Crag beds ended. These observations show that the brecciation in the area being fault related. The observation is also consistent with (Maher and Braathen 2011) where they state that the Løvehovden fault was active during deposition of the Minkinfjellet Formation. As the stratiform breccia interval ends towards the east it is in coherence with less impact of the Løvehovden Fault Zone in the eastern direction.
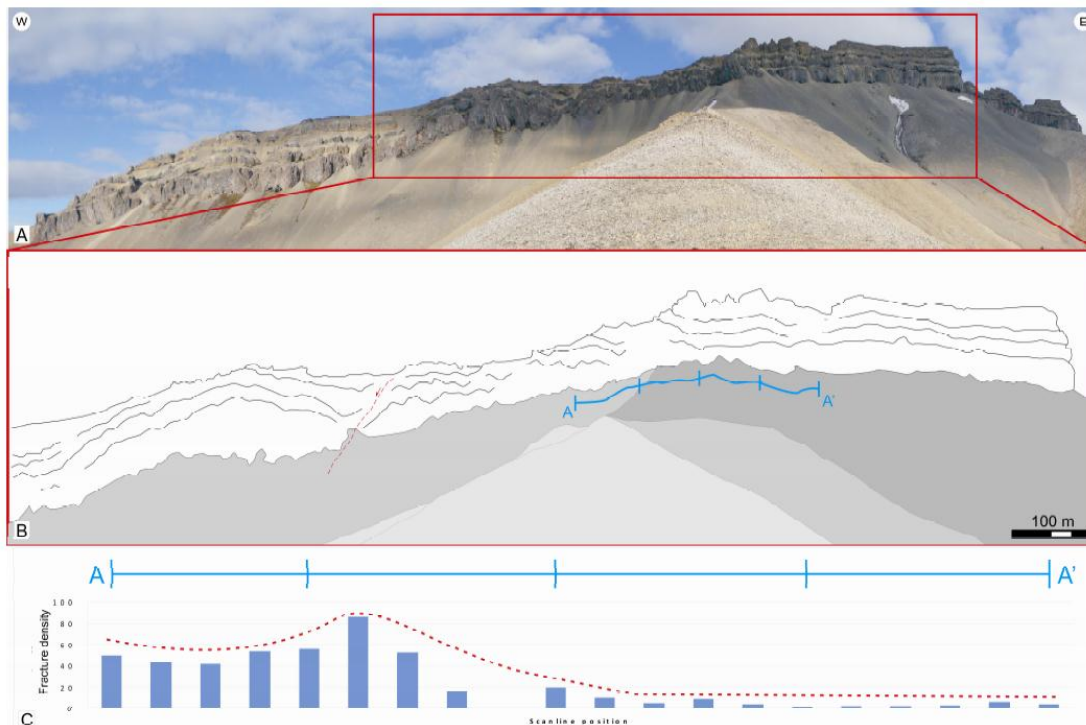
Figure 4.9: A) Panorama-mosaic photo of the Black Crag beds North of Adolfbukta. B) Line interpretation of the red box indicated in picture (A) with the faults indicated with red and the blue indicates the area of the fracture density scan – line (A – A`). C) Shows the density fracture lines along the lowest cliff of the Black Crag beds, with a high density of fractures in the monocline top and limb, as well as influence of a second monocline to the west. The figure is made by Jord de Boer, from a unpublished report Katrine Slotnæs was involved in. (de Boer et al. 2011)

4.4 Area 3

Localities 1 and 3 are breccia outcrops along the coastal escarpement at Rudmosepynten south of Fortet and are interpreted to lie within the Minkinfjellet Formation. Location 4 are a high pinnacle standing on a talus slope west of the Fortet locality and it belongs the Minkinfjellet Formation. Location 5 is grey micritic limestone cliff at the contact with the breccia North of Fortet locality and are within the Black Crag beds of the Wordiekammen Formation (Dallmann et al. 1999), **Figure 4.10**. At Area 3 the brecciated units within the Minkinfjellet and Wordiekammen Formations show subtle bedding, or zonation of different types of breccias. The degree of brecciation (clast size and lithology) is variable both laterally and vertically, giving the breccias distinct zonations.

The base of a breccia body is well exposed a Locality 1. The base is sharp and flat with a dip 14˚W, and lies immediately above a dark micritic limestone. The breccias directly above the basal contact have clasts of similar lithology to the underlying limestone (W. Wheeler, 2011 unpubl. Field notes). Sample 1C was sampled in the strata below the breccia base. Sample 1B comes from the contact between the micritc layering and the breccias, in a relatively thin fine-grained layer. Sample 1A comes from directly above the contact, within the brecciated strata.

The breccia continues laterally for several hundreds meters to the west above this sharp basal contact. A lateral distance of 0.26 km westwards along the coastal escarpment, lies the Locality 3 (estimated from TopoSvalbard from norskpolarinstitutt.no). The samples are taken from a small breccia pinnacle (1.5 meter) above the wrack line. The samples have a more polymict composition, and have several dissolution voids on the surface.

Locality 4 is situated 0.41 km North of Locality 3 (estimated from TopoSvalbard from norskpolarinstitutt.no), and is approximately 100 meter highler up in the topography.There is no clear genetic relationship between the breccia at locations (1- 3) along the coastal escarpment and the Locality 2, due to scree and soil cover. But indicated in (Eliassen 2002) the evaporite-solution collapse form an interconnected system in the central part of the basin, and that the brecciation process was a part of one large karst system rather than small isolated systems. The Locality 4 is an isolated pinnacle standing on a talus slope, the observations of the location showed that it consisted of angular and rounded clasts and boulders, some fluvialy reworked sediments and

some north-dipping layering. The pinnacle is interpreted to be in-fill in a larger cave system that has been cemented, thus is more resistant to weathering than the original host rock that has been eroded away.

Further up in the topography, and 0.16 km in a northward direction lies Locality 5. Locality 5 lies adjacent to a breccia pipe, and the samples are taken from the vertical contact within the breccia wall rock approximately 2 meter from the breccia pipe. The locality consists of micritic limestone and is affected by faulting as slicken-slides are observed. The faulting may be due to faulting in the area or affected by fractures in the breccia wall. Samples are taken from the base at base of the lowest cliff of Black Crag Beds.
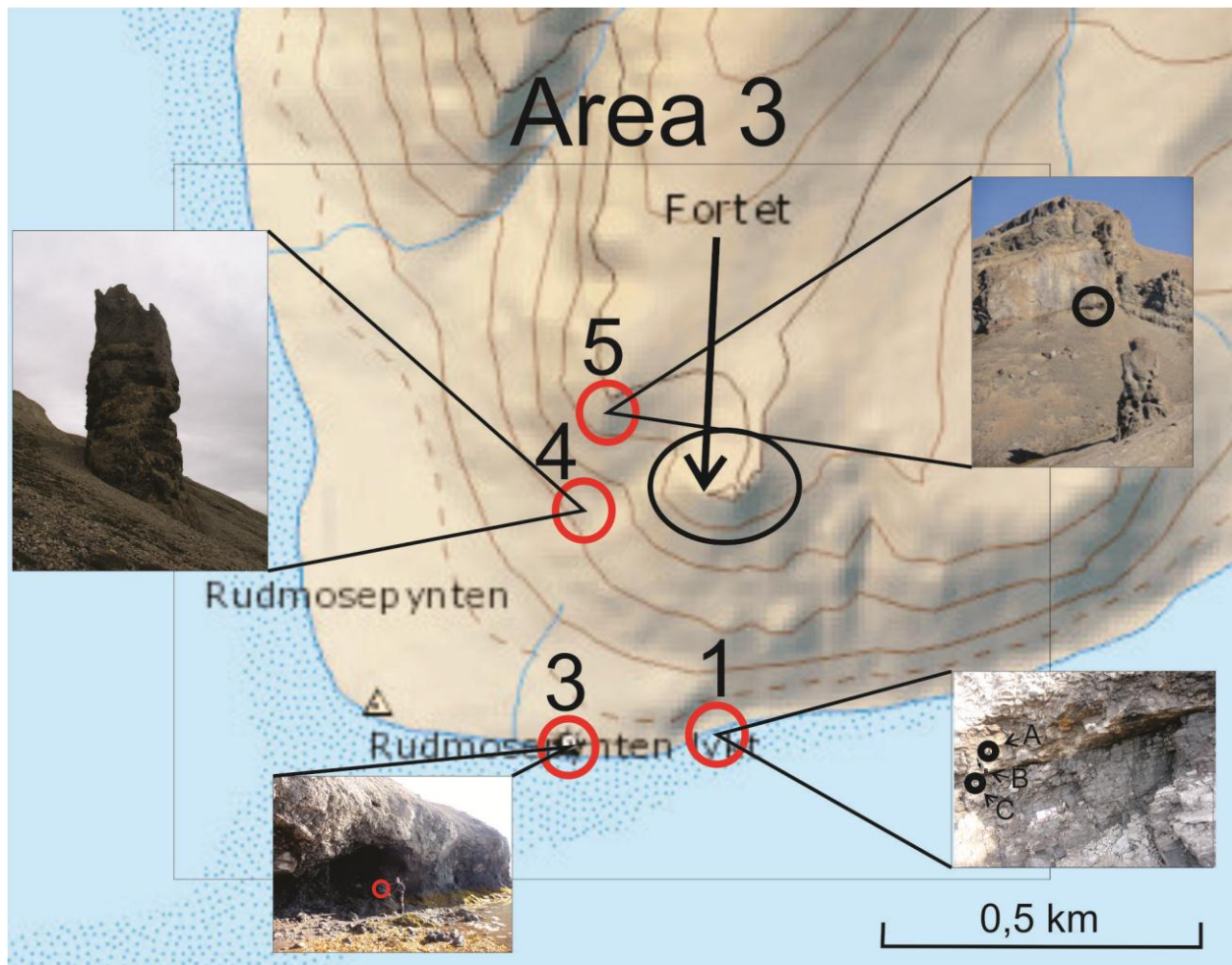
Figure 4.10: Locations at Area 3. The red circles indicate the breccia outcrops. The black arrow indicates a prominent breccia body known by the name "Fortet".

4.5 Facies description

The samples taken from Area 1, Area 2 and Area 3 reflect the wide range of breccia bodies in the area. The facies within these samples have been identified based on their composition. The aim of this was to recognize and correlate the different samples and a total of 11 facies were distinguished. The facies are described in **Figure 4.11** and **Figure 4.12**. The detailed facies interpretations for the individual samples are in the Appendix 1, applied to each of the samples sides.

Facis 1: Heavily dissolved breccia

The surface of the facies is heavily pitted, inferred from dissolution. Several visible voids between cemented fractures and vuggy pore space are observed on the surface. Both the pore system may occur within a sample, however one of the systems are usually the dominating one. The voids between the cemented fracture lines have an angular geometry. In some these open voids partially-dissolved clasts are commonly observed. The partially-dissolved clasts are inferred here to have a composition with high gypsum content. Partially dissolved clasts are also observed within the vuggy porosity (vuggy pores > 4 cm). The observed vuggy pores are often not touching-vug porosity, as most of the pores are not connected with each other. Some to no clasts can be distinguished. The color ranges from light grey to dark grey. The dark grey is more dominant when there are most cemented fracture lines on the surface. The dissolution voids are mostly in mm scale, but open voids from 1 cm to 4 cm occur as well.

Facies 2: Clast-supported breccia

Well cemented to slightly cemented very angular clasts to sub-rounded clasts. The clasts range in size from 1 cm to 3 cm, but clast up to 7 cm large are observed as well. The clasts can be loosely to densely packed, with open voids between the clasts. No dissolution to small scale dissolution in the clasts, and/or between the clasts. But some cemented fracture lines and be seen on the surface but most common as cement infilling between the brecciated clasts. The cement infilling ranges from none to a large degree (approximately 5 % of the total volume, visually estimated) of cement infilling. The clasts can be coated in mudstone and clasts matrix, or smaller brecciated rocks in mm-scale in between the larger clasts. The latter tend to be most the common. Fracture

lines overprint the clasts, which gives them a more cracked texture. Color can be grey or dark grey.

Facies 3: Highly dense and cemented breccia

The composition is of monomictic limestone clasts or of a polymictic composition. However there is not a wide range of different composition of the clast when the breccia is polymictic, usually just two different types, which can be hard to distinguish from each other. The exact size of the clasts are hard to distinguish as the fractures overprints the clasts size and/or the high content of cements precipitated within and on the surface of the sample makes it hard to estimate the exact size. The observed clasts can be from 2 cm up to 6, but also as small as less than 1 cm. The largest clasts tend to dominate, and the smaller clasts make up the clasts matrix. On the surface there are none too little dissolution, creating voids or enlarging fractures. The surfaces range from moderately to highly fractured. The color is grey. The surfaces characterized as either highly dense and/or highly cemented. When it is highly cemented, veins of cements crosscutting the surface are common, and seams of cements. The color is grey. This facies slightly resembles facies 4 (Mudstone-matrix dominated chaotic breccia), but is more highly dense and/or cemented.

Facies 4: Mudstone matrix dominated chaotic breccia

On the surface there are few voids from dissolution observed. The voids are in some cases dissolved clasts, whereas others look like they are along fracture lines between the breccia clasts. The clasts can be lithologically heterogeneous, with some of the clasts with a more dissolvable composition, which gives a more polymictic composition. The degree of compacted and cemented clasts and mudstone matrix varies. The clasts have an angular to rounded shape and the sizes are mainly 2 mm to 0.5 cm large, but clasts as big as 2 cm occur as well. Consist mainly of mudstone matrix with clasts, and small fossils are observed in some of the samples. The brecciation is chaotic, but locally the clast can be similarly orientated. To differentiate between clasts and secondary fractures can be hard in some areas, as well as between clasts and the mudstone matrix. On the surface, white precipitated spots are observed. The color is dark grey.

Facies 5: Crackle breccia

Highly fractured monomictic limestone. Fractures cut the brecciated clasts and the fractures are mainly parallell. Angular to some sub-rounded clasts are situated in between the fractures, where clasts have fractured more than others. The clasts ranges from 1 mm up to 3.5 cm in size. On the surface there is little to none dissolution, and if there is, it appears as mm-scale voids. Cements have infilled the fracture lines between the clasts. But there are still some open voids between the brecciated clasts, which have not been infilled with cements. Some white rounded spots can be seen on the surface and appear to be of gypsum. The color is mainly light grey.

Facies 6: Fault surface breccia

Even, flat surface, with slickenslides, which could infer that it is a fault or fracture surface. The brecciated clasts appear crushed. The clasts are mostly 1 mm large, but can be up to 3 mm. The clasts are sub-rounded to rounded, and loose silty material and cement can be found in-filling between the clasts. The surface is smooth, and has often a glazed look. No dissolution on the surface. Color is mainly light grey.

Facies 7: Matrix-rich clast supported breccia

Angular clasts with sizes ranging from less than 1mm and up to 2 cm large. Variable amount of interclast matrix. In some areas the matrix is only around the mm scale clasts, whereas when there is much matrix, this is also around the largest clasts. But the matrix and the small clasts may also coat the largest clasts. The matrix can consist of mudstone, that is very dense and with a heterogeneity composition of the clasts. But the matrix can also be clast supported with mainly 1 mm large clasts. The surfaces range from slightly to heavily compacted and cemented. But voids that are from 1 mm up to 2 mm, occur mostly around the largest clasts and the matrix around them. In some areas weathering has overprinted the breccia clasts. The color ranges from grey to dark grey. The facies resembles facies 4 (Mudstone-matrix dominated chaotic breccia), but is more rock dominated than mudstone dominated.

Facies 8: Weathered surface

Very weathered surface. The surface can either be artic weathered surface, minerals precipitated on the surface, or iron precipitated on the surface. The weathered texture covers the surface and

the original texture cannot be distinguished. The weathered surface is mainly arctic, which can be distinguished by dots of precipitated minerals sticking out of the surface. Only a few places limestone mudstone, fractures and/or clasts can be distinguished. The color is white or red.

Facies 9: Fine clast breccia

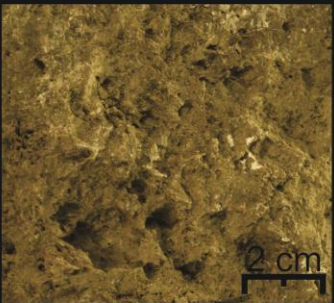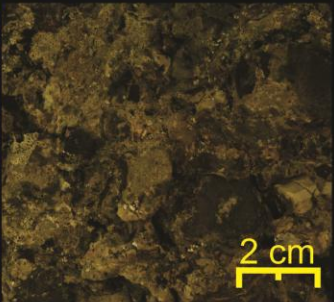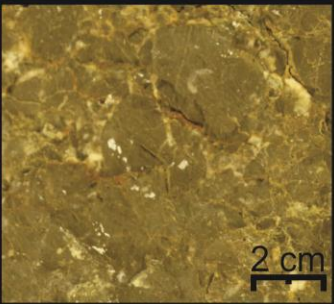Small angular clasts to sub-rounded clasts, that ranges from less than 1 mm up to 2 mm in size. Some of the angular clasts are heavily dense and cemented, whereas others have small open voids between them. In some areas the clasts are coated in mudstone matrix or cements. It is hard to distinguish between the separate clasts in some areas due to cementation and minerals that have precipitated on the surface. This facies mostly occur in small areas and can be interpreted as the matrix-fill in facies 8. The color is mainly grey.

Facies 10: Mudstone/ Wackestone
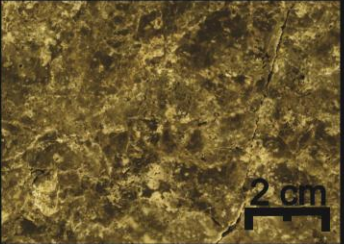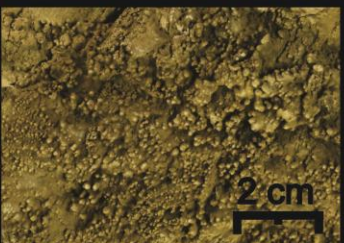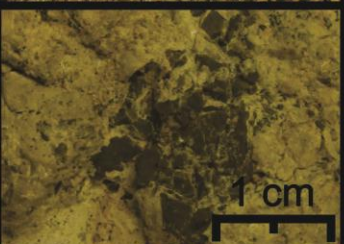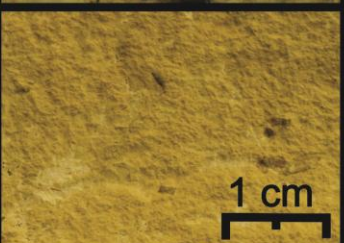
The composition of the facies is of mudstone or wackestone. Few to no surface voids from dissolution. The composition is massive, and the surface has no internal structure. But show fossils and/or sedimentary grading structure that is neither coarsening or fining upwards. There are few to no clasts, but the few that is seen are 1 mm or less in size. Mineral precipitation of calcite, creating white spots on or oth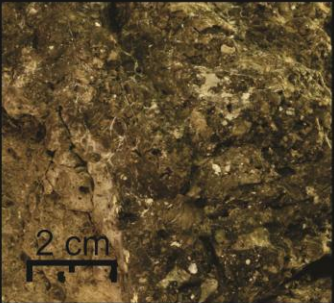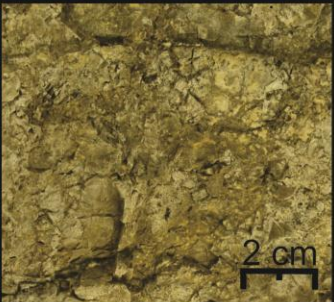er types of precipitated minerals can be observed. Frw fractures. The color can be either yellow or grey. The facies is mainly unbrecciated rock.

Facies 11: Sedimentary fill

The surface shows layering, occasionally slightly graded. Can be some dissolution voids on the surface. Grains can be distinguished, with texture ranging from silty to very fine. But the texture can also range from no distinguishable grains to fine grained. The composition can be from very homogeneous to heterogeneous. The sediments are loosely packed to more densely packed and lithified. The sediments are not very dense or cemented. The sedimentary fill often occur in the middle or up to the top of more densely packed sediments. The sedimentary fill is often seen in a mudstone and/or matrix supported sample. The grains within this sample look transported, as they often infill between the other facies, and flow structures have been observed. The color is light grey and grey to white.

Facies	Color	Texture	Description
1.Heavilily dissolved breccia			Vuggy pores and voids with cemented fractures between. Light grey to dark grey color. Void and vuggy pores are mostly in mm-scale, but can range from 1-4 cm. Few clasts can be distinguished.
2.Clast-supported breccia			Large clasts (1-3 cm), but clast up to 7 cm are observed. Mostly clast - supported breccia. Well cemented to slightly cemented, very angular to sub-rounded clasts. Loosely to tightly packed clasts. Little dissolution. Color can be grey and dark grey.
3.Highly dense and cemented breccia			Very homogeneous clasts. Hard to distinguish the exact clast size,but the distinguishable ones are dominated by clasts from 2 to 6 cm, with a lot of mm scale clasts in between. Very fractured and/or cemented. The color is grey.
4.Mudstone-matrix-dominated chaotic breccia			Mudstone supported chaotic breccia. The clasts have an angular to rounded texture of mainly 2 mm to 0.5 cm large clasts. The cementation and compaction ranges from a low to a high degree between the clasts and matrix. The color is dark grey.
5.Crackle breccia			Parallell linear fractures with angular to occasional sub-rounded clasts in between. The size is from 1 mm up to 3.5 cm. Cement infilling between the brecciated clasts. Light grey color.

Figure 4.11: Facies classification for the breccia samples. From the left to the right: Facies name, color indicating the facies 1- 5 where the different colors marks the area of the facies on the samples, photo-description of the facies and main descriptions for the individual facies to the right.

Facies	Color	Texture	Description
6. Fault surface breccia		2 cm	Fault surface distinguished by slikenslides. Flat and smooth Sub-rounded to rounded clasts, with sizes ranging from 1mm to 3 mm. The color is light grey.
7. Matrix-rich clast supported breccia		1 cm	Angular clasts, from less than 1 mm to 2 cm scale. Matrix-rich with either; Mudstone and polymictic matrix that are densely packed or clast-supported, matrix with mainly 1 mm large clasts. The color is grey to dark grey.
8. Weathered surface		2 cm	Weathered surface, mainly of artic or iron precipitated origin. No clasts can be distinguished. The color is red or white.
9. Fine-clast breccia		1 cm	Small angular to sub-rounded clasts, in the size range from 1 mm up to 2 mm large. Closely spaced clasts and heavily cemented. The color is grey. The facies is interpreted as the matrix-fill in facies 8.
10. Mudstone/ Wackestone		1 cm	Mudstone or wackestone, with a massive texture. Few fractures, mainly unbrecciated rock. The color is either yellow or grey.
11. Sedimentary fill		1 cm	Sedimentary fill, with a texture ranging from silty to very fine grains. The sediments are often loosely packed. They are transported and flow structures have been observed. The color is light grey or grey to white.

Figure 4.12: Continuation of the facies classification, **Figure 4.11**. From the left to the right: Facies name, color indicating the facies 6 - 11 where the different colors marks the area of the facies on the samples, photo-description of the facies and main descriptions for the individual facies to the right.

5   Petrophysical Results and Interpretation

5.1   Introduction

This chapter will present the result of the petro-physical experiments described Chapter 3. The aim is to put the petrophysical properties of the samples in the context of the karsted area, which from they were collected. The sample descriptions are given under Area 1, Area 2 and Area 3. The samples will here be described in detail with descriptive photos and interpretation. The facies classification presented in Section 4.5 has been applied to each sample and is presented here and the Appendix 1. In the Appendix 1 the samples are presented with the facies interpretation in a 3-dimensional view.

The results will be given in the same order as in chapter four. First in every sub-chapter, the permeability and porosity measurements taken at the sample as a whole will be presented. Then the porosity and permeability results from the 1 inch core plugs will be presented in the end. The samples were classified after the ternary diagram (Loucks 1999) which shows the relationship between crackle breccia, mosaic breccia, chaotic breccia, and cave sediments, **Figure 1.7**.

The tiny permeability values will not be emphasized too much. The reason is a correlation value between the tiny permeability values and the permeability from the flow measurements was not attained.

5.2 Area 1 – The Red Breccia Pipe

A suite of samples were collected from both the breccia pipe wall and inside the breccia pipe. The samples were sampled from the outcrop locations 6, 9, 14, 15, 16 and 19, **Figure 4.5**. The samples were all small, in the range of $35 – 700$ cm^3, except from location 14, which had a size of 3800 cm^2. Due to the size of the samples and the size of the outcrops, the samples does not always represent the whole localities as some the localities were very heterogeneous. Sample size was in many cases limited by the high degree of fracturing in the outcrops. The sample size was also limited by the degree of matrix as the matrix was none consolidated. Due to this it was difficult to get a large sample out without breaking.

All the samples were composed of micritic limestone. The samples collected from the middle section locations (19, 15 and 14), contained more void space than the samples from the locations (6, 9 and 16) such as interclast and vuggy pore space. These clasts are interpreted to be composed of earlier brecciation events. Eliassen (2002) also reported evidence re-brecciation commonly in larger clasts showing earlier breccia generations. In some paleokarst examples, abundance of interclast and vuggy pores may give as high porosity as 20 % and the permeability can be in darcys for the collapsed breccia cavern fill (Loucks 2001).

The samples represent the lithology in the area since the brecciated clasts originate from a combination of rockfall and short-transpoted debris/rock slides within the pipe, which is in coherence with the observations done in (Nordeide 2008). The composition of the clasts is micritic limestone, which indicates low porosity and permeability. The interpretation is based on primary interparticle pores are quickly lost in carbonates during compaction and cementation (Selley 1985). Deeply buried paleocave reservoirs mainly have secondary crackle and fracture porosity (Loucks 1999). This is generally the case for the samples taken from the localities close to the breccia pipe wall and within the wall.

5.2.1   Location 6 - Sample 6

Sample 6 was collected at Location 6, inferred to be the south wall of the breccia pipe **Figure 4.5**. The location consists of light yellow to grey layers of fossiliferous limestone interbedding the mudstone benches of the Black Drag Beds. The wall rock at Location 6 is highly fractured with 1 meter thick massive layers and 0.5 meter highly fractured layers towards the top. At the basal part, all the layers are highly fractured, **Figure 5.1 (a)**. The sample was unbrecciated and massive and from the middle and yellow layer at the location **Figure 5.1 (b)**. The facies interpretation of the whole sample is in the Appendix 1.
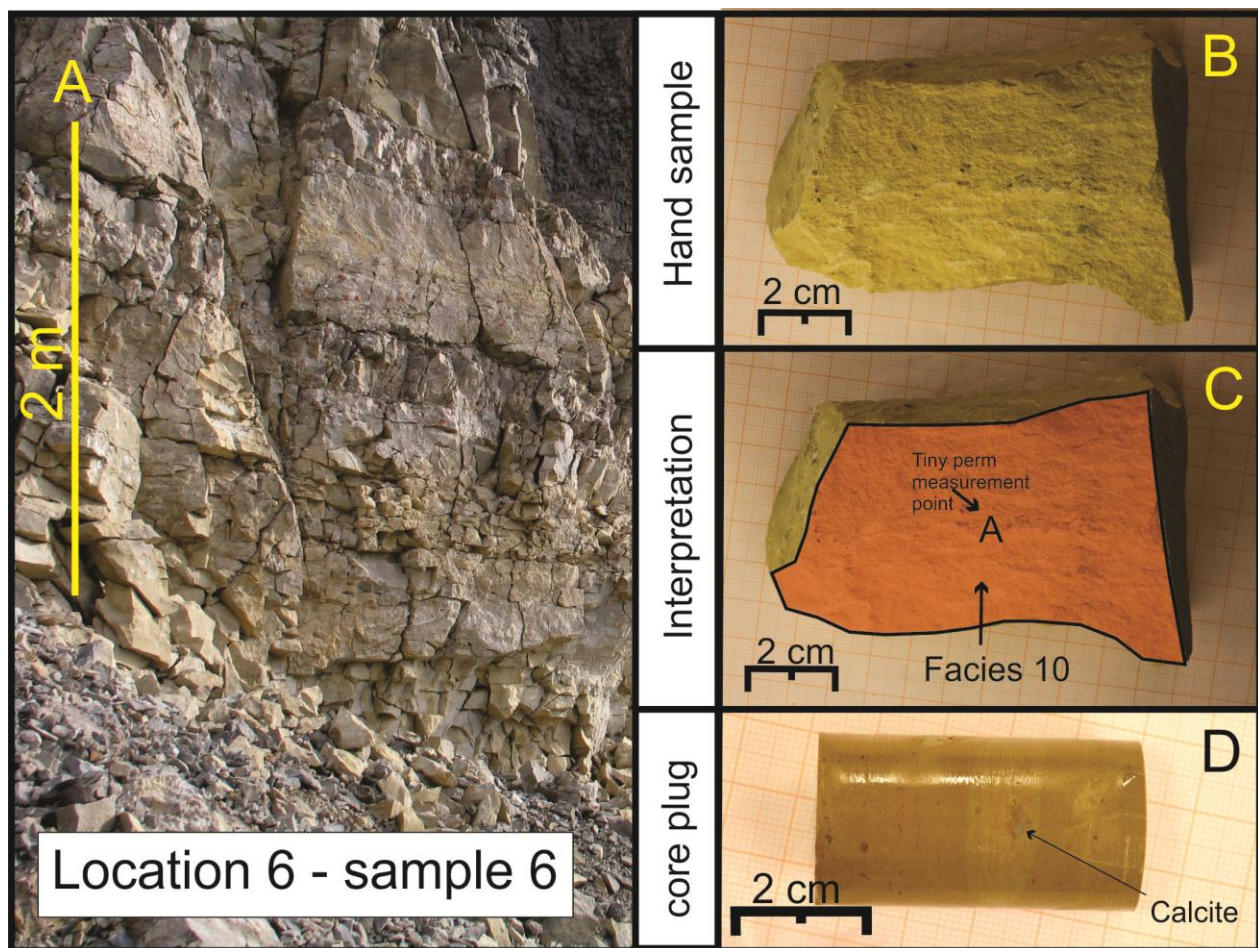
Figure 5.1: A) Photo showing the outcrop, which is unbrecciated but highly fractured. B) The sample taken from the outcrop, is massive and unbrecciated. C) The facies 10 indicated by red color, however the color looks orange due to the yellow color of the texture of the sample. The whole sample was classified as facies 10. D) Core plug from the sample 6, thus a wackestone.

Table 5.1: The table shows the 3 tiny perm values measured at different surfaces of the sample (see Appendix 1 for all points of measurements). Facies 10 (F10) was the main facies at each point of measurement.

Sample 6	A (F10)	B (F10)	C (F10)
K [mD]	3	5	15
ΔK	±2	±2	±14

Table 5.2: Volume and petrophysical properties of sample 6.

Sample 6	Vtotal, [cm3]	ΔVtotal	Porosity,φ [%]	Δφ	Permeability, K [mD]	ΔK
Sample	226	±1	2.0	±0.4	-	-
Core plug	23.7180	±0.0001	5.52	±0.06	0.009	±0.001

The tiny perm values, **Table 5.1**, gave a higher permeability than the water flow testing on the core plug, **Table 5.2**. As the sample was massive and cemented the latter is likely to be a more correct value. However, the tiny perm values indicate permeability variations within the sample and the flow measurement indicate that cement can occlude the pore space. Only small parts of the pore space of the core plug need to be occluded with cement, for the flow through the core to be inhibited. As long as the cement occludes the pore space at any cross-section it will inhibit the flow and the permeability value gained would be low, in this case around zero. **Figure 5.1** shows that the permeability lies in the fractures rather than in the pore space of the rock. The location lies adjacent to the breccia pipe and fractures at this locality are interpreted to be due to the formation breccia pipe. The measured porosity for the core plug was almost 3 times higher than the measured porosity for the sample **Table 5.2**. The variations in the measured porosity can have several reasons; natural variations in the pore throat distribution yielding difference in the effective porosity within the sample, mistakes during the saturation method where the sample should have stayed in the water-filled desiccator under pressure for a longer amount of time and/or the composition of the sample had started to dissolve as the sample had been saturated 4 times previous to the flow measurement of the core plug. The latter is the most unlikely since the solutional denudation of carbonates would have taken longer time in more aggressive waters than used during the experiments.

5.2.2 Location 9 - Sample 9

Sample 9 was collected at the southernmost extent of the upper part of the outcrops within the Red Breccia Pipe **Figure 4.5**. The colors of the locality range from yellow to brown towards the top. The outcrop consists of laminated layers of massive micritic limestone that are thinning towards the top of the outcrop, and is heavily fractured. It is not brecciated but may be a block that has slide down or a remaining part of the breccia wall, **Figure 5.2 (a)**. **Figure 5.2 (b)** shows that the sample has a homogeneous composition and unbrecciated.
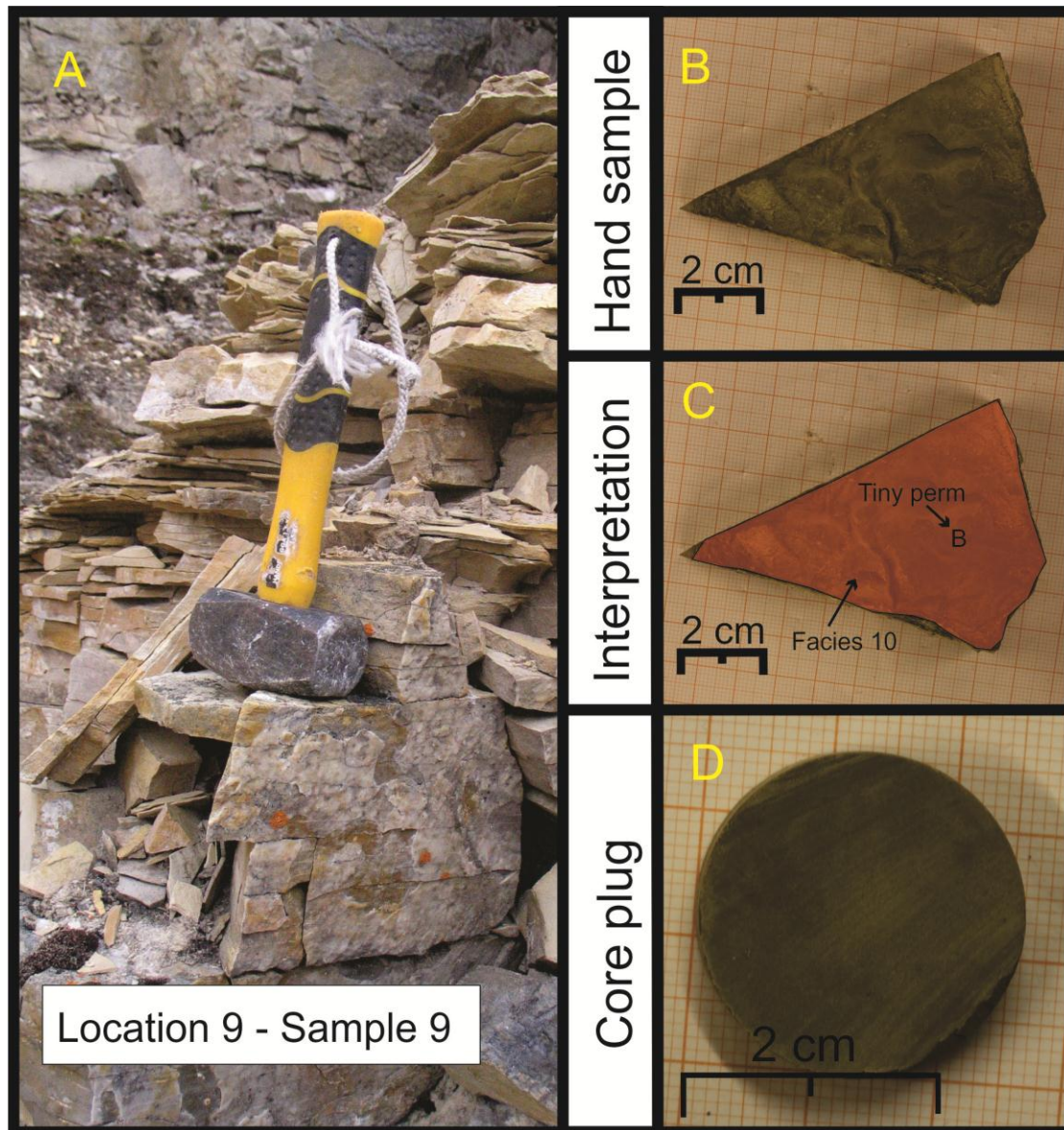
Figure 5.2: A) The photo shows that the outcrop was small, and highly fractured but unbrecciated. B) Hand sample taken from the outcrop. C) Interpretation on the sample, a mudstone (facies is 10) which is descriptive for the whole sample, except for one side which had mineral precipitation. D) As the sample was thin, core plug with length > 1 cm was cut out.

Table 5.3: The table shows the 2 tiny perm values measured on 2 of sample nines surfaces (see Appendix 1 for all points of measurements). Facies 10 (F10) was the main facies at each point of measurement A and B.

Sample 9	A	B
K (mD)	3	2.0
ΔK	±1	±0.7

Table 5.4: Volume and petrophysical properties of sample 9.

Sample 9	Vtotal [cm^3]	ΔVtotal	Porosity, φ [%]	Δφ	Permeability,K K [mD]	ΔK
Sample	36.5	±0.2	2.4	±0.5	-	-
Core plug	3.2808	±0.0003	3.4	±0.4	3.8	±0.2

Table 5.3 gives the measured tiny perm values. These are in the range from 2 to 3 mD. Whereas **Table 5.4** gives the value for the permeability from the flow measurement which is nearly 4 mD. Usually the tiny perm gives an overestimation, but in this case the water flow gives an overestimation. The reason is due to the short length of the core plug, led to cracking during the experiment. The cracking led to one fracture that cut through the cross-section of the core plug. The fracture would then have become the main path of flow since the water would always migrate in the direction of least resistance.

For the porosity measurements, **Table 5.4** the porosity of the sample and core plug are low and similar results for the porosity were gained in both the flow and saturation measurements. The porosity would be around 2 – 3 %.

Based on visually observations, the outcrop in **Figure 5.2 (a)** shows the permeability would be more likely to be in the fractures than in the pore systems of the rock approximately 2 from mD and possible into darcys range. The dominant pore space would be within the fractured zone.

5.2.3 Location 14 - Sample 14

Sample 14 was sampled from Location 14, at the lowest topographically outcrop location within the Area 1, **Figure 4.5**. The outcrop is characterized by clast-supported breccia, with sizes ranging from 2 cm clast up to boulder.
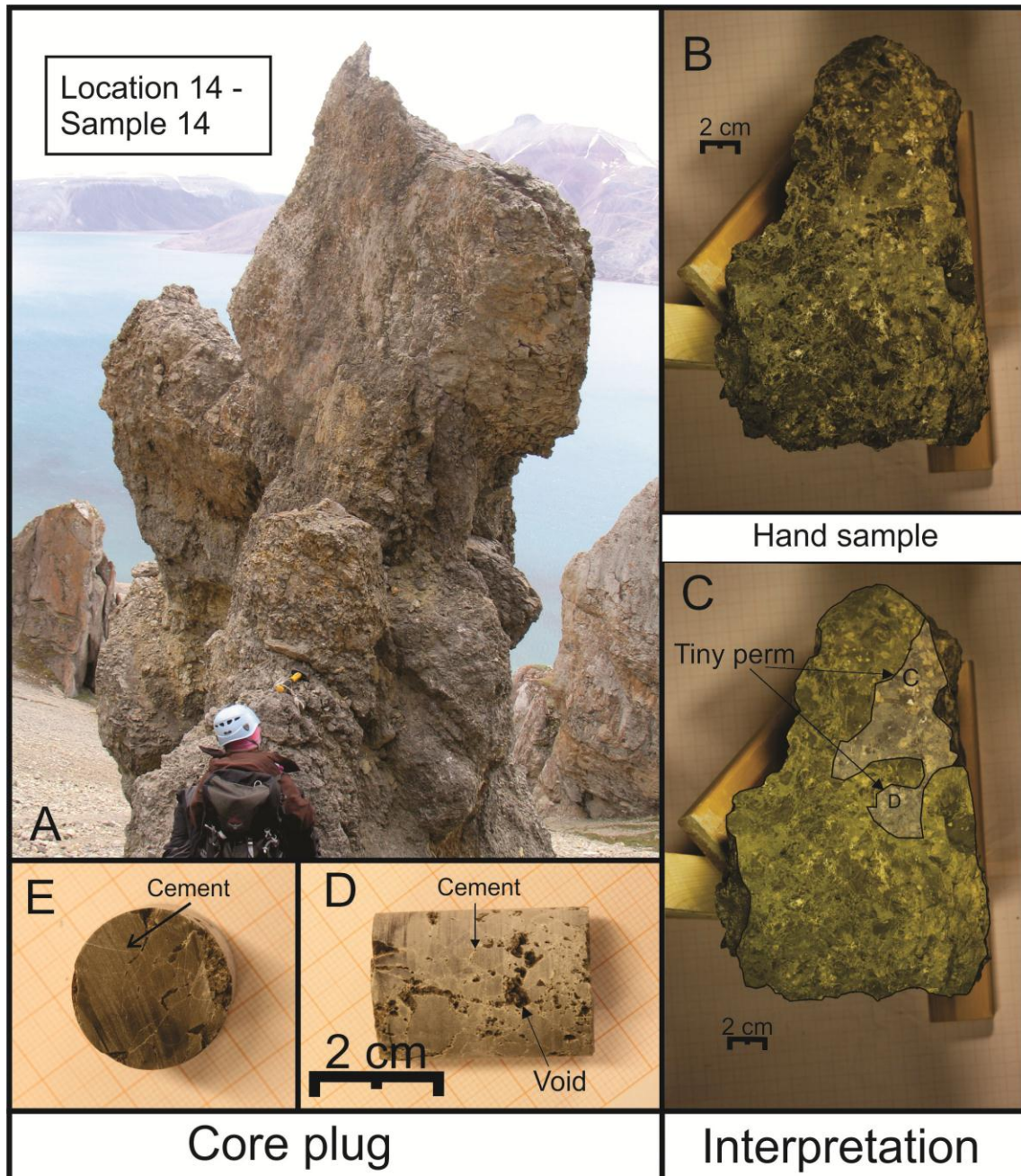
Figure 5.3: A) Coarse chaotic breccia at the lowermost part of the breccia pipe. B) Hand sample taken from the location, and as the scale show, the sample was big. C) Interpretation of the sample, with facies 2 and 4. The Facies 4 was only observed on a small part of the sample, as the Facies 2 was the main facies of the sample. D) Several 1 mm – 5 mm vugs, visually observed are these mainly none connected vugs. E) Cross-section of the core plug shows cemented fracture lines

The breccia is chaotic with a domination of angular-very angular clasts (2-20 cm) and few boulders. The boulders are rounded and have a grey or yellow color, which also is the overall color for the whole location. The breccia is well cemented and has a low degree of matrix. The outcrop site was classified as coarse clast chaotic breccia, **Figure 5.3 (a)**. The sample is monomictic and cemented, **Figure 5.3 (e)**. The sample is interpreted as clast-supported chaotic breccia.

Table 5.5: The table shows 6 tiny perm values measured (A-F) on Sample 14`s surfaces (see Appendix 1 for measurement locations). 4 facies were distinguished on the sample surfaces (see Appendix 1).

Sample 14	A (F6)	B (F6)	C (F4)	D (F4)	E (F7)	F (F2)
K [D]	1.1	0.131	0.07	0.02	18.4	0.08
ΔK	±0.4	±0.009	±0.07	±0.02	±2.9	±0.007

Table 5.6: Petrophysical and volume properties of sample 14.

Sample 14	Vtotal [cm³]	ΔVtotal	Porosity, φ [%]	Δφ	Permeability,K [mD]	ΔK
Sample 1	73.4	±0.7	4.3	±0.6	-	-
Sample 2	2620	±26	7	±2	-	-
Core plug	17.572	±0.004	5.97	±0.08	0.84	±0.07

The tiny perm gave a range in the permeability, **Table 5.5**. The points of measurement (A and E) were measured near fractures and thus yield high permeabilities. The flow measurement of the core plug yielded permeability less than 1 mD. Visually observed voids and vugs in the core plug, **Figure 5.3 (c)** are thus not connected. The migration path of fluids is through the primary pore space, voids and vugs, thus these voids and vugs do not contribute a great deal to increase the permeability. Another factor that restricts the flow through the core plug are cemented fractures, **Figure 5.3 (b)**. Since the core plug just covers a small area of the sample, the permeability of the sample can be in the darcys due to non-cemented fractures as indicated by the tiny perm measurements, **Table 5.5**.

The porosity measurement of the sample gave porosity in the range of 4 – 7 %. The average porosity for the whole sample would be nearly 6 %, as **Figure 5.3 b-e** shows there are several pore systems present within the sample, as well as the composition is different. Comparing the measured porosities indicates that there are low porosity zones and higher porosity zones. The cut

Sample 2 has 7 % porosity; this higher porosity is attributed due to several uncemented fractures within the sample.

The tiny permeability measurements might reflect the permeability of the outcrop, as it was proposed in (Loucks and Mescher 2001) facies classification that the permeability can be in the darcys range for the facies clast-supported chaotic breccia. It was also inferred in Loucks and Mescher (2001) classification that the porosity can exceed 20 %, which is not the case at location 14, where the porosity may be as high as 10 %. However, this value is not confirmed by measurements.

5.2.4 Location 15 – samples 15

Samples 15.1 and 15.2 were sampled from the center of the Red Breccia Pipe, situated just above location 14 and below locations 12 and 13, **Figure 4.5**. The outcrop had a vertical length of 36.5 meter. The outcrop showed a transition in the brecciation style from the lower to the upper section. The lower section is dominated by yellow boulders that are highly fractured and the matrix around these yellow boulders consists of loosely packed grey clasts, silty and fine material. The texture of the outcrop is chaotic and the shape of the rock fragments ranges from rounded to very angular. Little cement is observed and the amount of yellow boulders decreases towards the middle of Location 15. From the middle part and up, there is more cementation and a homogeneous composition of highly fractured grey limestone. The composition is dominated by angular clasts that are only a few centimeter large, some yellow boulders are observed in the upper section as well. Some layering is observed. At the upper section some large scale fractures cross-cut the location in E-W direction. Both the collected samples came from the upper part.

The location was classified as coarse clasts chaotic breccia after the Loucks and Mescher (2001) classification. As there was a transition between lower and upper part of location 15, the lower part was classified as massive mixed breccia and the upper part was classified as micritic breccia in a mix with cemented micritic breccia after Nordeide (2008) facies classification.
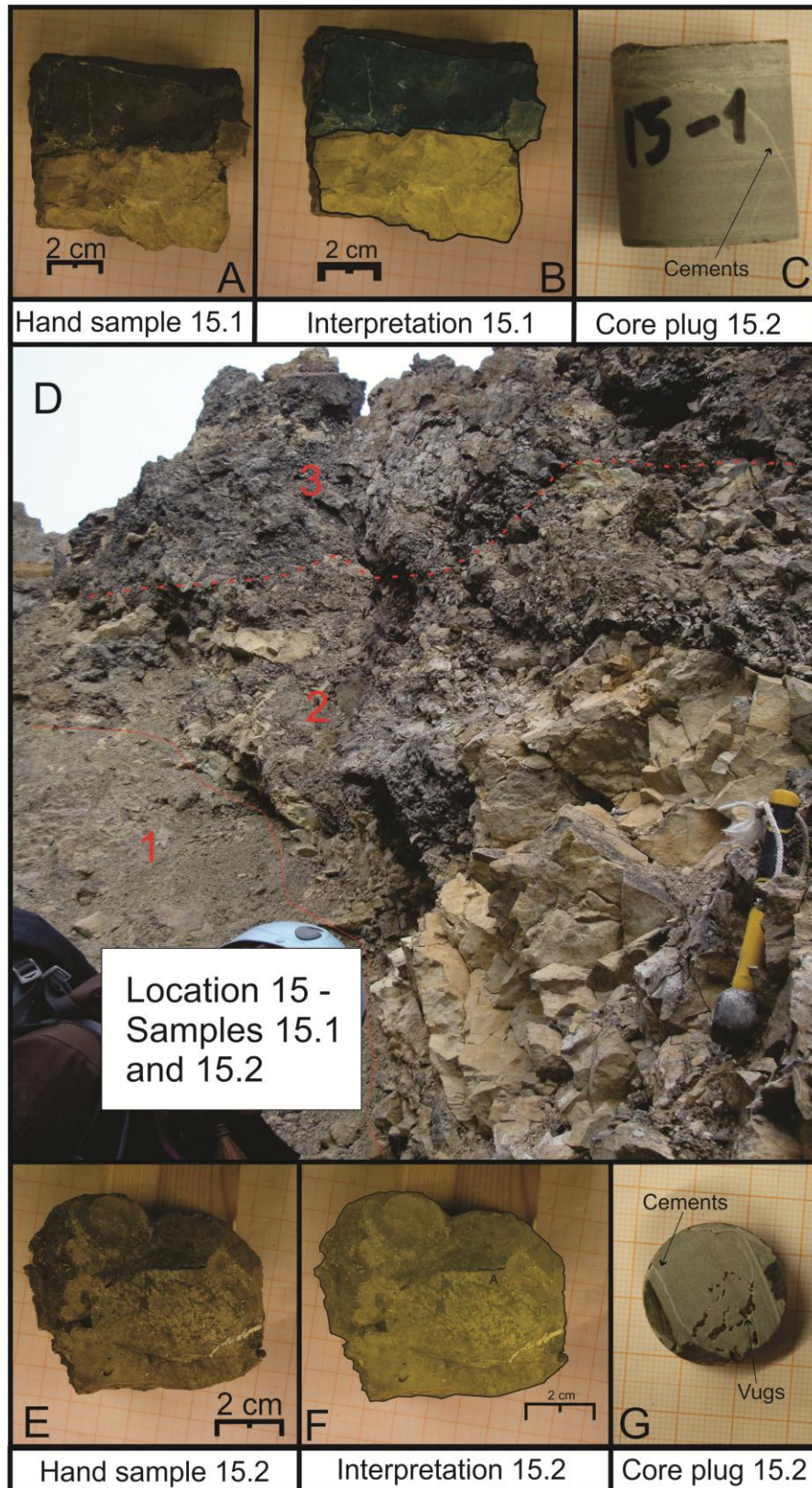
Figure 5.4: A) 15.1 is the first hand sample taken from the outcrop, and is mosaic breccia B) Interpretation of the sample and is representative for the whole sample with facies 2 and 3. C) Is the cut core plug from sample 15.2 and is massive with cemented fracture lines. D) Photo of the outcrop location, it shows that the outcrop could be divided into 3 categories: 1) Scree dominated, only a few clasts could be distinguished. 2) A marked transition was between part 2 and part 3 of the outcrop. Section 2 was boulderdominated. Loucks and Mescher (2001) classification had limitations in order to classifiy the distinct transition. By using (Noreide 2008), the middle part 2 is classified as massive mixed breccia. 3) The samples were taken from this upper part, and is classified after (Noreide 2008) facies classification as the Micritic Breccia facies with parts containing Cemented Micritic breccia facie. E) 15.2 is the second sample taken from the outcrop, and is a mosaic breccia. F) The interpretation of 15.2, with only facies 2 is pictured. G) Only a small core plug was cut from the sample and shows cemented fracture lines and vugs (1 mm-3 mm).

Table 5.7: The table shows 3 tiny perm values measured (A-C) on Sample 15.1`s surfaces (see Appendix 1 for measurement locations). 2 facies were distinguished on the sample surfaces (see Appendix 1).

Sample 15.1	A (F2)	B (F2)	C (F3)
K (mD)	134	70	3.5
ΔK	±8	±31	±0.8

Table 5.8: Petrophysical and volume properties of sample 15.1

Sample 15.1	Vtotal [cm^3]	ΔVtotal	Porosity, φ [%]	Δφ	Permeability,K [mD]	ΔK
Sample	295	±1	4.3	±0.9	-	-
Core plug	14.134	±0.002	0.5	±0.1	0.00163	±0.00004

Table 5.9: The table shows 3 tiny perm values measured (A-C) on Sample 15.2`s surfaces (see Appendix 1 for measurement locations). 3 facies were distinguished on the sample surfaces (see Appendix 1).

Sample 15.2	A (F3)	B (F8)	C (F2)
K (mD)	19	6	488
ΔK	±16	±3	±309

Table 5.10: Petrophysical and volume properties of sample 15.2.

Sample 15.2	Vtotal [cm^3]	ΔVtotal	Porosity, φ [%]	Δφ	Permeability,K [mD]	ΔK
Sample	75.6	±0.8	1.9	±0.4	-	-
Core plug	4,60	±0.05	3.0	±0.3	4.0	±0.5

The samples from location 15 are very similar in composition, as both are mosaic breccia consisting of homogenous limestone clasts, **Figure 5.4 (c)** and **(e)**. The mosaic breccia of the samples have fractures between the clasts that are generally cemented as observed in **Figure 5.4 (c)** and **Figure 5.4 (g)**.

The tiny perm values showed a wide range as measurement B for sample 15.1 and measurement A and C for sample 15.2 is taken in proximity to fractures between the clasts. The tiny perm gives an indication on permeability differences, due to the wide range of values. The samples compositions were dense and cemented fractures, but also had several voids and a few vuggy pores. Visually observed some voids and vugs were connected. Due to this smaller core plugs were drilled with visually observed non-connecting vugs and voids, as larger voids made the sample crack during drilling. **Table 5.7** shows that the core plug from sample 15.1 had no flow permeability. Whereas the flow permeability measurement **Table 5.9** gave a high permeability values, but this was because the core plug fractured, and the flow increased, as the flow chose the path of least resistance.

 Table 5.8 and Table 5.10 show the measured porosities, which are less than 5 %. The porosity of the samples gave a range in the porosity from 0.5 to 4.3 %. The range in reflect that the porosity is not uniform. For sample 15.1, the low value of the core plug can be due to porosity heterogeneities within the sample like cementation or mistakes during the saturation method. However, as **Figure 5.4 c)** shows the core plug had a dense composition and a cemented fracture line cross-cutting the sample, which was probably the reasons why the core plug from this sample yield low porosities and permeabilitys. Sample 15.2 also show differences in the porosities and is probably due to a non-iniform pore distribution. The values measured reflect the composition of the samples rather than the outcrop they were taken from, **Figure 5.4 (d)**.

5.2.5 Location 16 - Sample 16

Sample 16 is from location 16 and situated in the N-E direction of the Red breccia Pipe and the whole outcrop location is surrounded by scree, **Figure 4.5**. Observations of the location showed that it consisted of thin layers of highly fractured grey micritic limestone. A fault plane went through the outcrop (E-W direction) and the micritic limestone was more intensely brecciated to the north of this fault plane **Figure 5.5 (a)**. The location consisted of crackle and mosaic breccia, which were densely packed and consisted on angular and very angular rocks. Cement was observed as well.

The faulting is in the east west direction and is most likely to be a fault caused by the brecciation. The outcrop is classified as the facies Highly disturbed strata after Loucks and Mescher (2001). The hand sample **Figure 5.5 (c)**, is interpreted as crackle breccia.
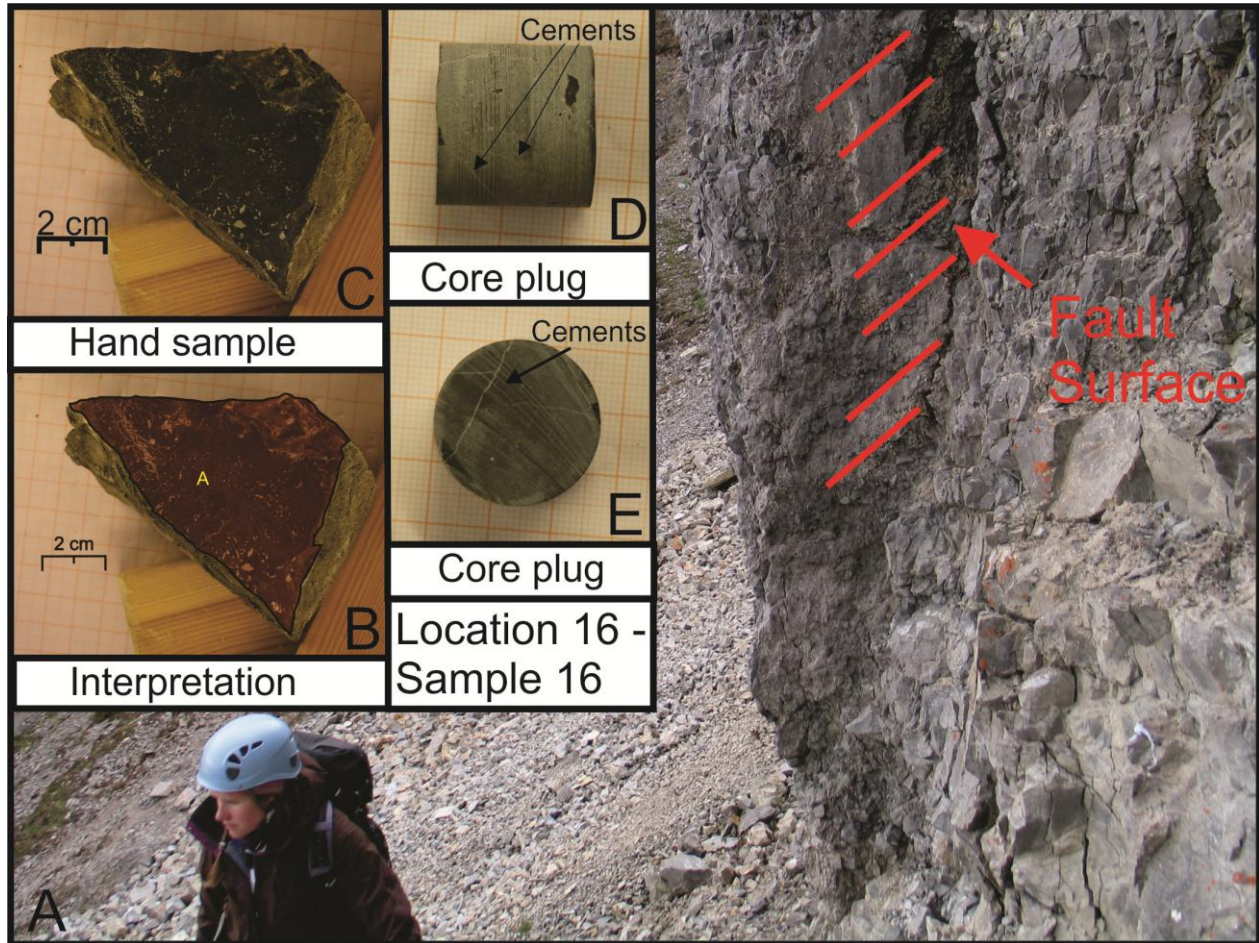
Figure 5.5: A) Photo of the outcrop with the fault surface indicated in red. B) Interpretation of the sample with facies 10 and is descriptive for the whole sample as many of the other surfaces consists of facies 1 and facies 8. C) Hand sample taken from the outcrop. D) Length of the core plug from sample 16 which is massive with a few cemented fracture lines. E) The end of the core plug shows cemented fracture lines.

Table 5.11: The table shows 3 tiny perm values measured (A-C) on Sample 16`s surfaces (see Appendix 1 for measurement locations). 3 facies were distinguished on the sample surfaces (see Appendix 1).

Sample 16	A (F10)	B (F1)	C (F10)
K (mD)	4.7	3	6
ΔK	±0.6	±1	±2

Table 5.12: Petrophysical and volume properties of sample 16.

Sample 16	Vtotal [cm³]	ΔVtotal	Porosity, φ [%]	Δφ	Permeability,K [mD]	ΔK
Sample	197	±2	1.0	±0.2	-	-
Core plug	11.9370	±0.0005	0.67	±0.12	0.0	±0.0

75

The sample looked homogeneous, slightly fractured and unbrecciated. The tiny permeability measurements gave a generally low permeability, **Table 5.11** and the permeability from the flow measurement **Table 5.12** gave no permeability value. The core plug was massive and unbrecciated with cemented fracture lines which would inhibit the flow **Figure 5.5 d), e)**.

The sample has low porosity, **Table 5.11**, from both the core plug and sample measurement. The porosity is around 1% which explains the low permeability measurements.

The sample is unbrecciated but has fractures running through the sample. Since the sample is limestone and unbrecciated the porosity of the sample is mainly primary porosity. Primary porosity is quickly lost in carbonates due to compaction and cementation (Selley 1985), as is in good agreement with the observed measurements on sample 16.

5.2.6 Location 19 - Sample 19

Sample 19 was taken from Location 19, the location was in the center of the Red Breccia Pipe just to the North of Location 15, **Figure 4.5.** The total visible area of location 19 was approximately 4 meters high and 4 meters wide. The brecciated rocks are very densely packed and consist of angular rock fragments. Some layering (> 10 cm) of brecciated clasts, however the layering is highly fractured.

The outcrop is classified as Highly Disturbed Strata after (Loucks and Mescher 2001). The location was very fragmented and fractured and the sample from the location is interpreted as clast-supported chaotic breccia.

The surface of the sample indicated a crackle to mosaic sample. After the cutting of the sample, the observations indicated that the sample was a Clast-supported chaotic breccia.
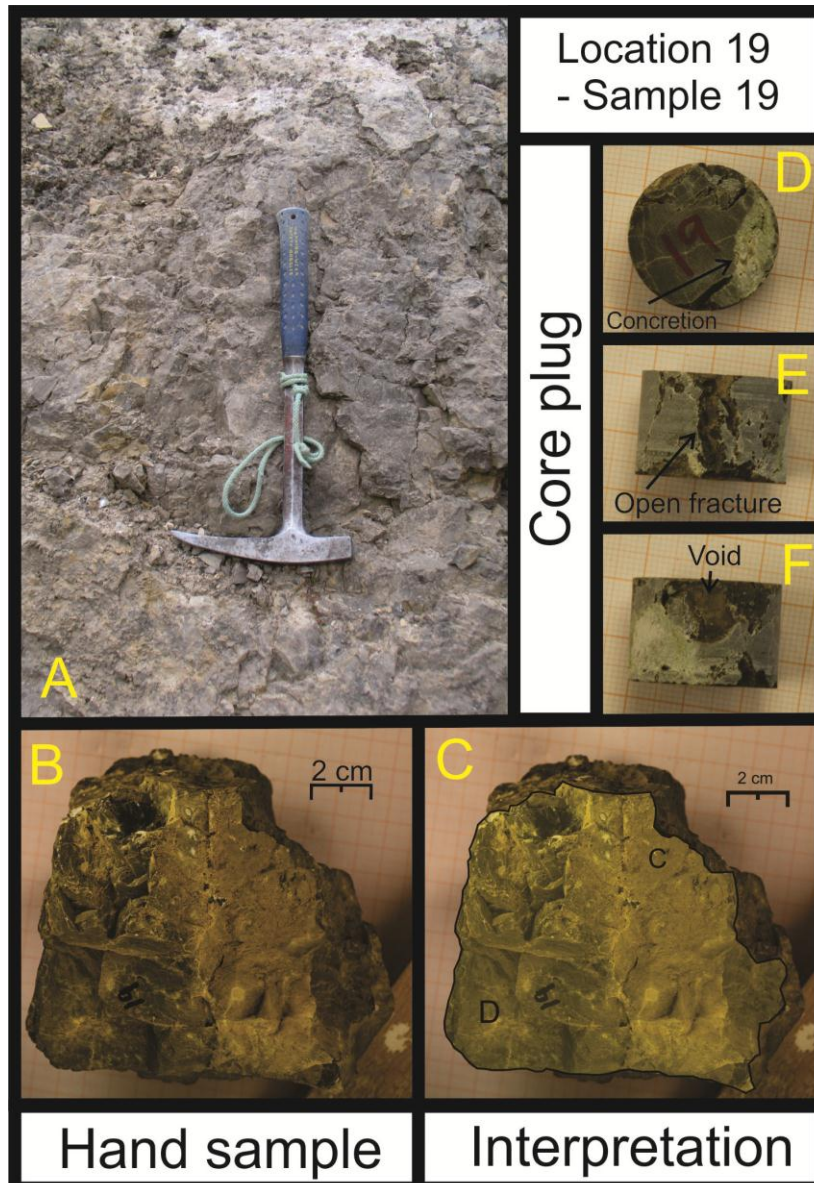
Figure 5.6: A) Photo of the outcrop, no stratigraphy could be seen, however the location was very dense. B) Hand sample of the rock, the color of the rock is grey. C) Interpretation of the sample; facies 2, was the most dominating facies. D) Cross section of the core plug. E) The length of the core showing open fractures. F) The length of the core seen from the other side, also with several voids.

Table 5.13: The table shows 5 tiny perm values measured (A-E) on Sample 19`s surfaces (see Appendix 1 for measurement locations). 3 facies were distinguished on the sample surfaces (see Appendix 1).

Sample 19	A (F10)	B (F10)	C (F2)	D (F2)	E (F2)
K (mD)	67	4	118	41	14
ΔK	±78	±2	±42	±25	±9

Table 5.14: Petrophysical and volume properties of sample 19.

Sample 19	Vtotal [cm^3]	ΔVtotal	Porosity, φ [%]	Δφ	Permeability,K [mD]	ΔK
Sample	700	±7	4.5	±0.5	-	-
Core plug	8.67	±0.01	5.3	±0.2	0.099	±0.009

The tiny perm measurements, **Table 5.13**, gave a wide range in the permeabilities, measurement A can be discarded as the uncertainty of the measurement is larger than the measurement itself. The sample was dense and had a variable composition in clast sizes and cementation. Although voids are observed in the in the core plug, **Figure 5.6 C), d)** and **e)**, none of the voids were connected through the length of the core plug as the flow measurement yielded low permeability. The low permeability (around zero) also indicates that the core plug is cemented. Visual observations when cutting revealed that the sample had larger voids (> 1 cm) within the sample, some were connected. The measured tiny perm and the visual observations show that the sample may have greater permeability than measured in the flow measurement.

Table 5.14 shows the porosities from the saturation method for the sample and the flow measurement on the core plug. Both the measurements gave approximately the same porosity. An interpretation of the porosity of due to the observed void space within the sample, is that all of these voids were not filled during the porosity measurement as a higher porosity would have been expected. Therefore the absolute porosity of the sample is probably higher than the effective porosity which was measured.

5.3 Area 2

The location, **Figure 4.1**, lies at the southern cliff of the Black Crag Beds of Wordiekammen Formation. The area of sampling is indicated as Area 2 in **Figure 5.7** which is located at the top of the Minkinfjellet Formation and at the base of the Black Crag Beds. The samples Q1 and Q2 were taken approximately 5 meters apart. The samples resembles crackle and mosaic breccia. These were the largest samples collected: sample Q1 weighed 11 kg and Q2 weighed 16 kg. The sample 1.M with weight 1.8 kg was taken at the uppermost part of the Minkinfjellet Formation and has a solid and homogenous mudstone composition, with few fractures. The interpreted facies of this location is classified after the classification by Loucks and Mescher (2001) disturbed strata facies.

The samples, Q1 and Q2, have a monomict micritic composition and are heavily fractured. The fractures are characterized by 1 - 4 mm thick sparry calcite, and the clasts appear to be "floating" in cement. This vein network could indicate an early state of cementation, with a probable meteoric origin. As stated in (Eliassen 2002) the diagenesis in the breccia, developed in the Late Carboniferous to Early Permian, occurred at depth from water of meteoric origin, as the vertical permeability was enhanced by faults. Another possibility is precipitation due to hydrothermal water migrating through the pore network of these samples during burial as underlying gypsum beds are dehydrating into anhydrite. However, both type of cementation model might have occurred as Eliassen and Talbot (2003a) detected 3 generations of cementation, where both the cementation models proposed here was included.
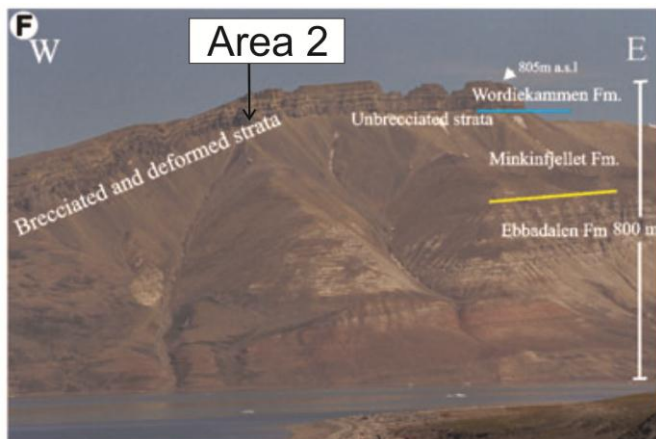
Figure 5.7: Picture of the location of Area 2. The figure indicates the brecciated and deformed strata to the west and the un-brecciated strata to the east. The picture is from (Eliassen and Talbot 2005), with location of Area 2 indicated on the figure.

5.3.1 Area 2 – sample 1M

The sample 1M was sampled just below the Black Crag Beds and is of Minkinfjellet Formation. It had few fractures, and was solid and unbrecciated. The texture of the sample was yellow mudstone without internal structures, but with 1 mm sized rock fragments "floating" within the mudstone.
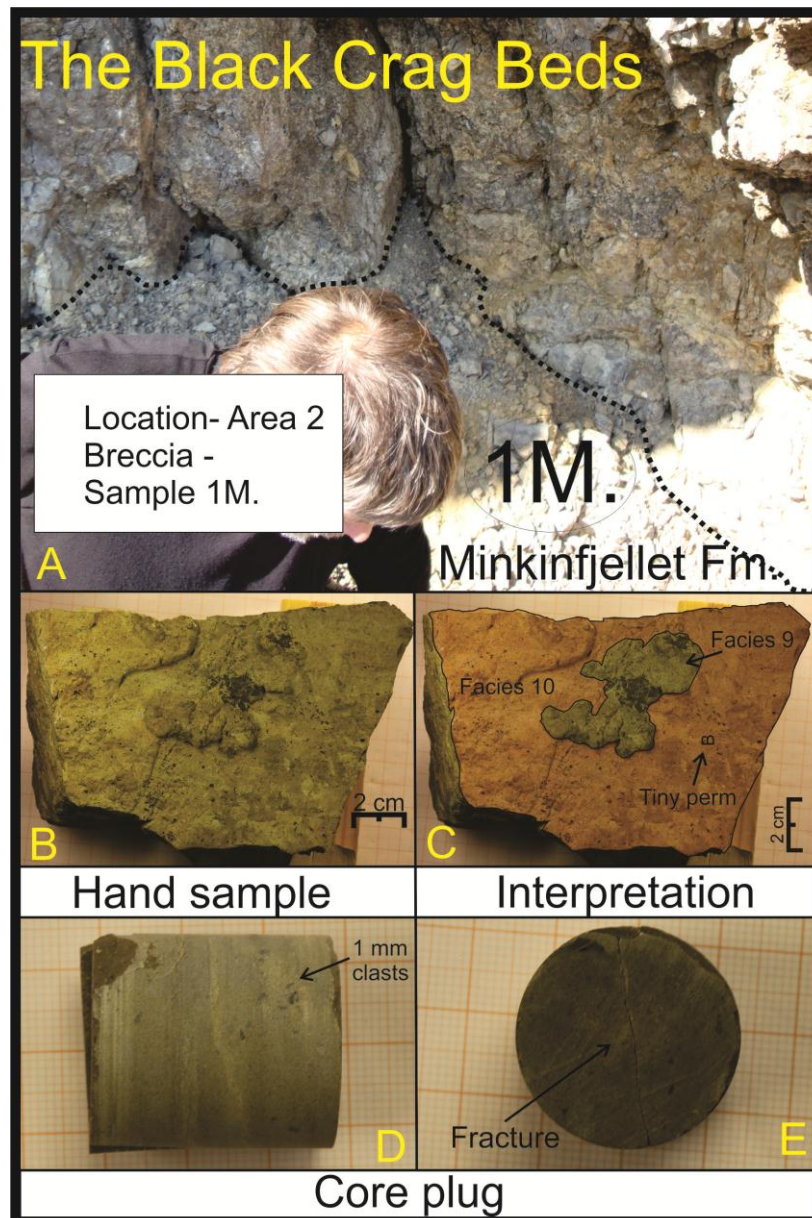
Figure 5.8. A) Location of the sample 1M right below the Black Crag Beds, where the black line indicates the break between the formations. B) Hand sample with a yellow unbrecciated color. C) The facies 10 is indicated on the sample with a red color (due to transparency the red color looks orange). Facies 10 was the main facies and facies 9 was observed only at the spot indicated in the photo. D) Length of the core plug with the floating clasts in the mudstone as indicated. E) Cross-section which shows a fracture. The fracture did not do through the length of the core plug.

Table 5.15 The table shows 3 tiny perm values measured (A-C) on Sample 1M`s surfaces (see Appendix 1 for measurement locations). 2 facies were distinguished on the sample surfaces. The tiny perm was only measured on facies F10 (F10) (see Appendix 1).

1.Mink	A (F10)	B (F10)	C (F10)
K (mD)	6	2.1	19
ΔK	±5	±0.6	±12

Table 5.16: Petrophysical and volume properties of sample 1M.

Sample 1M	Vtotal [cm^3]	ΔVtotal	Porosity, φ [%]	Δφ	Permeability,K [mD]	ΔK
Sample	693	±3	3.1	±0.2	-	-
Core plug	14.4853	±0.0003	3.9	±0.1	0.035	±0.004

The tiny permeability measurements gave a range of low permeabilities, **Table 515**. The sample appears to be homogeneous, **Figure 5.8 a)**, however cements can occlude the pore space in areas which leads to the different tiny permeability values. Based on the flow measurement through the core plug **Table 5.16**, there was little flow through the core as the permeability was less than 1 mD. An interpretation is that the permeability would be low, and if one include the uncertainty on tiny pern measurement A and B, the permeability of the sample would be around 1 mD.

The porosity measurements of both sample and core plug gave a porosity of 3 − 4 %, **Table 5.16**. The porosity reflects a dense and cemented sample, since the porosity is low. As the sample had few fractures the migration of fluid would be through the mudstone, and thus the low permeability value as well.

5.3.2 Area 2 – sample Q1

The sample was taken approximately 5 meter from the fault core, where sample Q2 was taken from, **Figure 5.10 a).** The sample is crackle to mosaic breccia, and has been brecciated in place. The sample was heavily cemented which separated the clasts due to the large infill of cements. The cements hold the sample barely together, and the whole sample shattered under the drilling for a core plug. Only a core plug less than 1 cm long was retrieved.
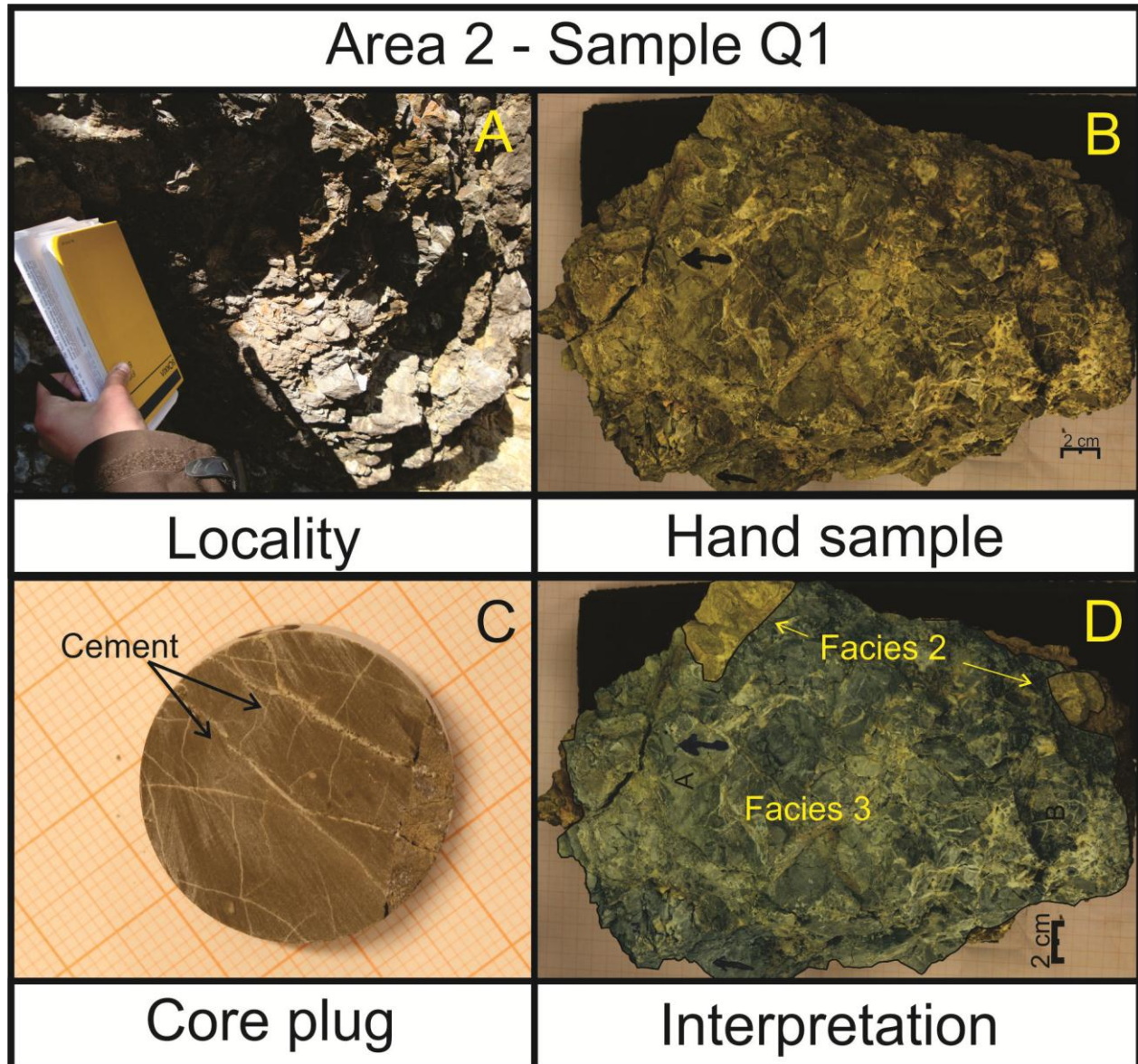
Figure 5.9: A) the locality of the sampling. B) The hand sample, and the large size of it, is indicated by the scale. The high degree (>5%) of cements can be clearly seen in the picture. C) Cross-section of the core plug, which shows how fractured the sample is. D) Facies 2 and 3 were the main facies of the whole sample.

Table 5.17 The table shows 3 tiny perm values measured (A-C) on Sample Q1`s surfaces (see Appendix 1 for measurement locations). 2 facies were distinguished on the sample surfaces. The tiny perm was only measured on facies F3 (F3) (see Appendix 1).

Sample Q1.	A (F3)	B (F3)	C (F3)
K (D)	12	0.3	0.005
ΔK	±5	±0.2	±0.003

Table 5.18: Petrophysical and volume properties of sample Q1

Sample Q1	Vtotal [cm^3]	ΔVtotal	Porosity, φ [%]	Δφ	Permeability,K [mD]	ΔK
Q1A	2400	±12	5.2	±0.5	-	-
Q1B	625	±6	2.2	±0.5	-	-
Q1C	292	±3	5.4	±0.5	-	-
Q1D	183	±2	3.7	±0.2	-	-
Q1E	49.2	±0.5	2.4	±0.2	-	-
Q1F	51.3	±0.5	3.4	±0.7	-	-
Q1G	67.4	±0.7	4.8	±0.5	-	-
Q1H	127	±1	7.7	±0.2	-	-
Core plug	4.0	±0.4	3.3	±0.5	6.6	±0.7

The tiny permeability, **Table 5.17**, show a wide range in the permeability measurements as there was hard to get a good reading due to the state of the sample. This is because of the measurement procedure of the tiny perm. Since one has to put a lot of pressure onto the area one is measuring in order to avoid a leakage. In this case it was difficult to perform the procedure as the Sample Q1 constantly loosed clasts. The permeability measured on the core plug measurement, **Table 5.18** is similar to measurement C of the tiny perm. There are some uncertainties to the permeability value in **Table 5.17**, as the sample was less than 1 cm, and bypass flow of the core might have occurred since the length of the core plug should be between 1- 5 cm long.

The sample Q1 was heavily cemented, and the cement appeared to separate the clast. The sample was not dense but rather loosely packed. As the original size of the sample was too large to perform porosity testing on, the sample was cut into smaller pieces. When performing the cutting several small pieces of rock fell off in the process. The largest of these was taken to be tested for porosity, as well as the cut sample. From **Table 5.18**, the porosity lays in a range of, 2-5 % in the whole sample. The only exception was the piece Q1H, which had a porosity of nearly 8%. The porosity of the core plug correlated well with the range the rock pieces lay in.

The average porosity of all the samples (Q1A-Q1H) is 4.4 ± 1%. As **Graph 1** show, the porosity measurements were not depended on the size of the pieces (Q1A-Q1H) of the sample Q1, but are natural variations within the sample Q1.
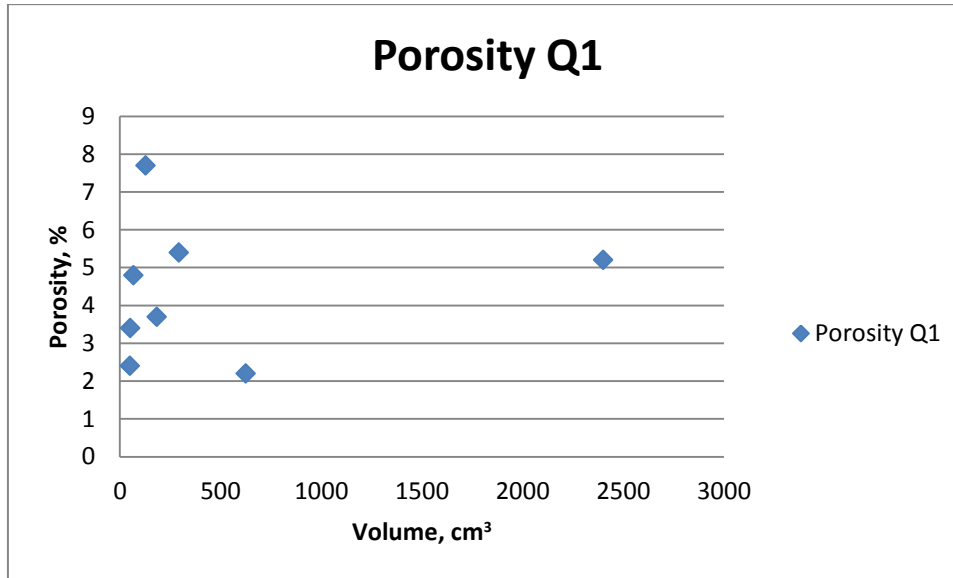
Graph 1: Pieces (QA-QH) of Q1 and their correlating porosity values.

The large amount of cement could decrease the porosity and permeability of the samples, but assumed here only to a minor degree. The reasoning for this is that both of the samples fractured and crumbled easily and it were hard to transport without breaking. Due to these observations the porosity and permeability are considered to be slightly higher than the values measured.

5.3.3 Area 2 – Sample Q2

The sample Q2 was taken approximately 5 m in horizontal direction to the west of sample Q1.
The sample is as cemented but has a more dense composition than sample Q1 as the clasts do not
fracture and fall off as easily. The sample is situated in a fault core and has a more heterogeneous
composition in the clast sizes than sample Q1. The sample is interpreted as fault induced breccia.
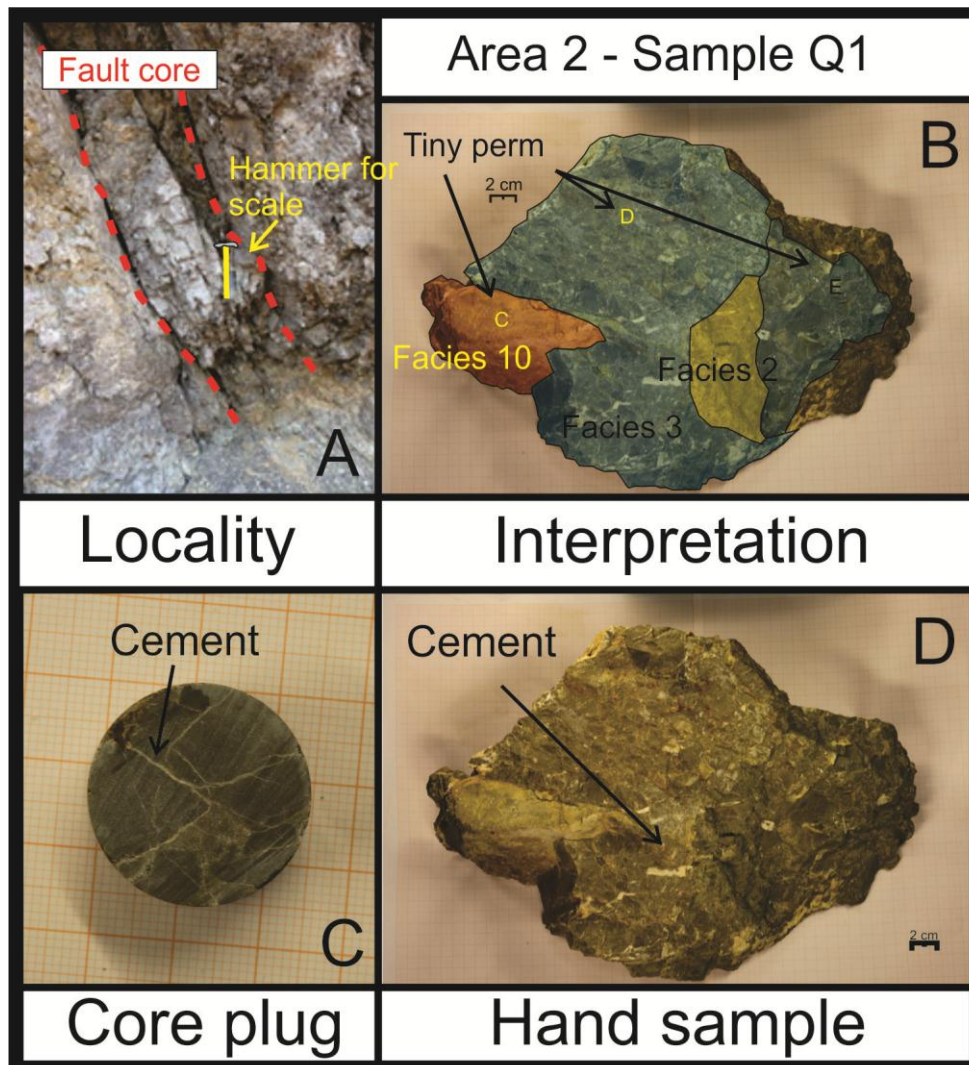
Figure 5.10: A) Sample taking is within the fault core. Hammer in picture for scale. B Interpretation of the
sample wirh facies, 2, 3 and 10. The facies 7 was also observed. C) Cross-section of the core plug, C)
Clast observed in the core plug ranges from 2 mm to 2 cm large. D) Hand sample with a grey color and
distinct white cement seams.

Table 5.19: The table shows 5 tiny perm values measured (A-E) on Sample Q2`s surfaces (see Appendix 1 for measurement locations). 4 facies were distinguished on the sample surfaces. The tiny perm was only measured on 2 of these, Facies 3 and Facies 10 (see Appendix 1).

Sample Q2	A (F3)	B (F3)	C (F10)	D (F3)	E (F3)
K (mD)	7	27	4	37	254
ΔK	±2	±31	±1	±27	±102

Table 5.20: Petrophysical and volume properties of sample Q2

| Sample Q2	Vtotal [cm³]	ΔVtotal	Porosity, φ [%]	Δφ	Permeability,K [mD]	ΔK
Q2A	176	±2	2.0	±0.4	-	-
Q2B	2535	±51	1.79	±0.10	-	-
Q2C	3050	±30	1.6	±0.2	-	-
Q2D	271	±3	2.4	±0.2	-	-
Q2E	620	±6	2.2	±0.2	-	-
Core plug 1	8.13	±0.04	0.9	±0.2	0.005	±0.001

The tiny permeability measurements, **Table 5.19** indicate the permeability in the range 4 - 40 mD. The measurement E, is probably too high due to the uneven surface at the point of measurement. The permeability measurement, **Table 5.20**, gave zero in permeability, which does not necessarily reflect the whole sample as the core was small, and the porosity was below the average.

The porosity measurements of the different pieces showed less than 1 % difference, with a porosity ranging from 1,5 – 2,5 %. The average porosity for the sample was 2.0 ± 0.3 %. The measurements support the observations where few voids were observed and the fracture lines were cemented together.

In sample Q2 the porosity was generally low, which explains the low permeability measurements, **Table 5.20**. The porosity of the sample lies then within the primary pore space of the clasts which is generally low, due to cementation and compaction. The reason for the sample do not have a lot of secondary fractures is that the clasts are crushed and smeared against each other, creating a dense texture as they are situated within a fault core. The porosity of the core plug yield a lower porosity than for the samples which reflects that the core plug was drilled out from one of the most compacted and cemented parts of the sample Q2.

When performing the saturation procedure, the large sample could be harder to saturate due to their size. However, as **Graph 2** shows, the porosity of the largest pieces of sample Q2 gave only a slightly lower porosity than the measurements performed on the smaller pieces of sample Q2.
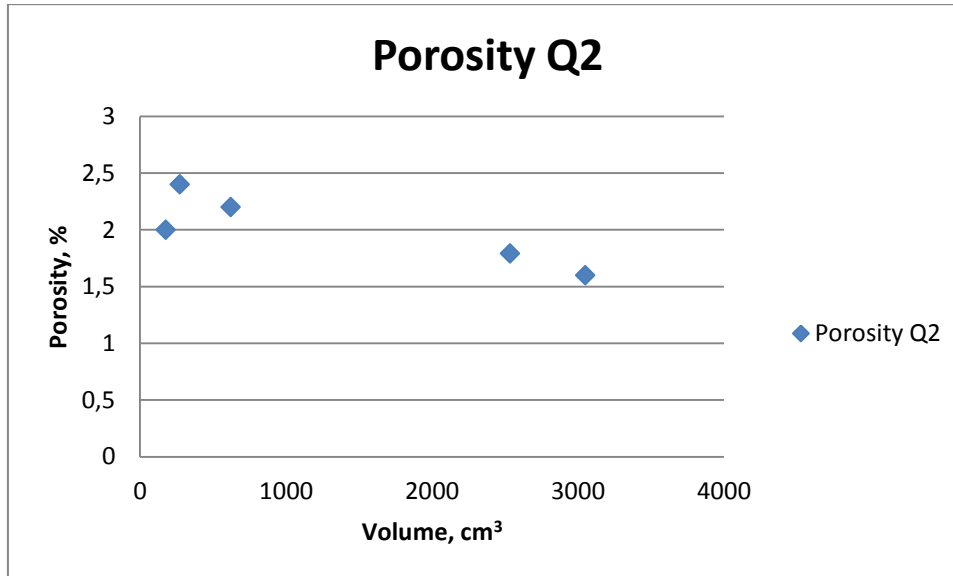
Graph 2: Volume of pieces of Q2 and their correlating porosity values

5.4 Area 3

There are a wide range of the breccia bodies at Area 3, **Figure 4.10**. The texture of the samples ranges from vuggy pores to loosely packed to very cemented and dense breccia. The degree of brecciation (clast size and lithology) is very variable both laterally and vertically, giving the breccias distinct zonations.

At the Locality 1 the sample **Figure 4.10**, 1C, is taken from a succession of micritic limestone. The porosity of this sample, and thus the permeability are going to be low. This is because mud starts to loose porosity during burial, mainly due to compaction (Selley 1985). The sample 1B, show more loosely packed sediments consisting of mainly breccia, but has a surface of compacted sediments that have started to become dissolute. The sample 1B and the totally brecciated sample of 1A, have probably good porosity and permeability based on visually estimations. Sample 1A broke apart under sampling and is categorized as the sub - samples; 1Aa, 1Ab, 1Ac, and 1Ad. The samples 1A and 1B are composed of carbonate rubble. The figure citing refers to Rudmosepynten within Area 3, as sample 1 was along the coastal escarpment at Rudmosepynten.

The samples collected at Location 3 have a polymictic composition and large matrix content. Within these samples several voids were seen on the surface and within the sample caused by dissolution, here inferred to be due to dissolution (see Section 1.3.2). Most of these voids create a separate vuggy porosity. Even if the voids create a touching-vug pore space, the porosity and permeability are low. Touching-vug systems typically control fluid flow through their conduits, but contribute less than 1 % to the reservoir porosity, due to most of the reservoir pore space is located in the matrix. This creates a bimodal pore system where most of the storage is within the matrix and most of the flow capacity is within the vug system (Lucia 1999). Samples at location 3 will be referred to as Rudmosepynten as they were situated is a western direction along the coastal escarpment.

The sample collected at locality four, is from a coarse-clast chaotic breccia. The locality has been classified as fine-clasts chaotic breccia after the classification scheme by Loucks and Mescher (2001) since the breccia showed flow transported breccia structures. The facies classification partly matches the locality, as it is one of the facies not accounted for in Nordeide (2008). As

mentioned in section 1.2.4, collapsed breccias can stand as a positive relief on the surface, more resistant to weathering due to cement. The limiting factor to porosity and permeability would be cements. But the in general the porosity and permeability values can be high as stated in (Loucks 2001), with abundant interclast pores the porosity can exceed 20 % and the permeability can be in darcys.

The samples collected at Location 5 are within the wallrock, but affected by fractures ans faults of undetermined offsets. Each the 2 collected samples shows slikenslides on one or more surfaces, but no fault core was observed. For these samples the fractures would be the main conduits of flow. As for classification these would correlate to the disturbed host rock strata with minor matrix pores and crackle to mosaic fracture pores, with porosity less than 5 % and permeability as much as tens of millidarcys (Loucks 2001).

5.4.1 Location 1 - Sample 1Aa

The sample 1Aa, **Figure 5.12 (e)**, was a part of the larger sample 1A, which broke apart under sampling. The sample is heavily brecciated and situated right above the base of the brecciated unit, **Figure 5.12 (a).** The sample has a large mudstone matrix content and the composition is polymictic. The sample is mainly matrix-supported chaotic breccia.
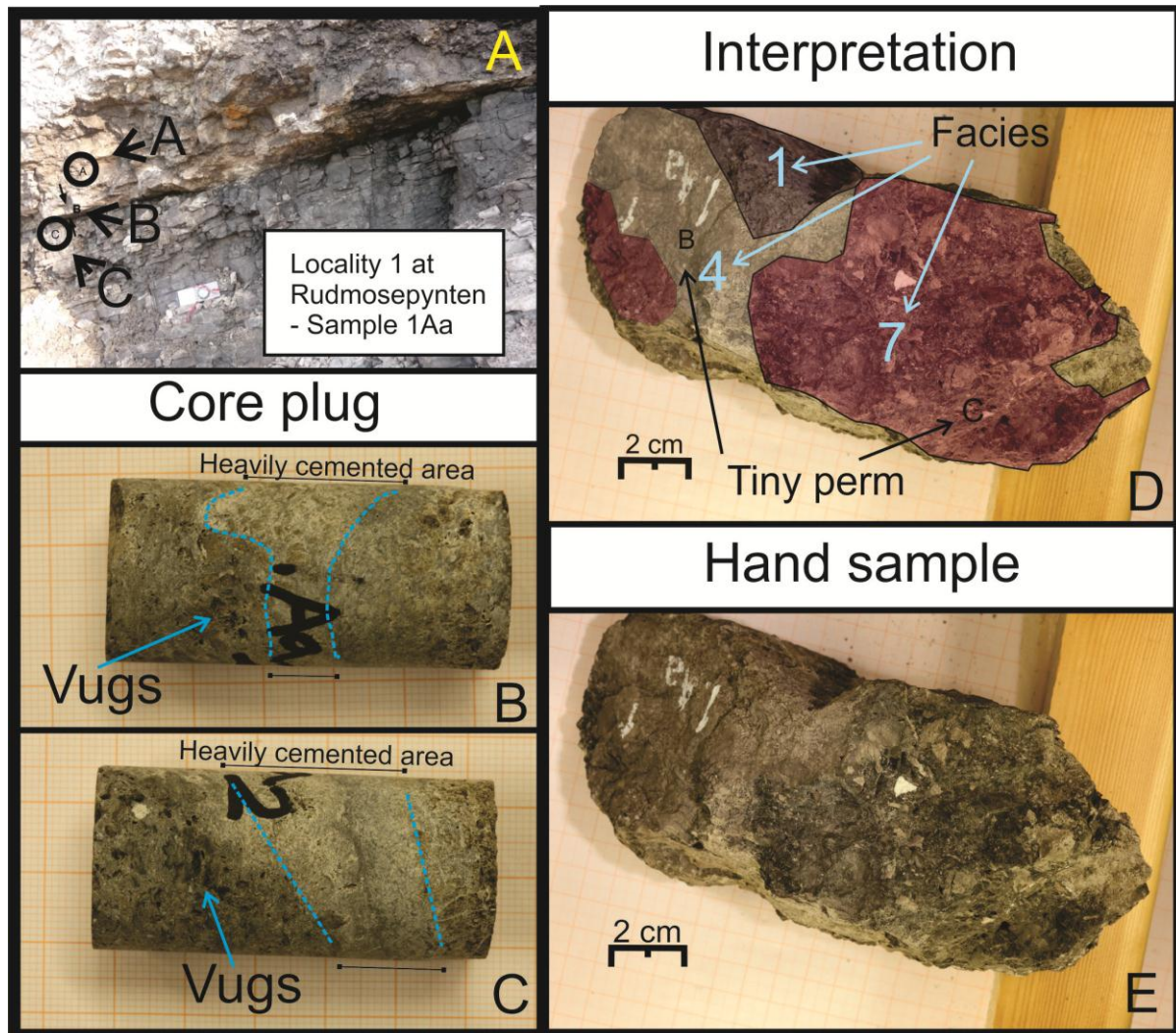
Figure 5.11: A) The picture shows distinct layering. The sample 1Aa has been sampled from the uppermost section indicated as A. B) From sample 1Aa a long core was drilled, this core shoved vugs, and a distinct layer that was heavily cemented running through the cross-section of the core. C) Description in B) applies here. D) The sample with the interpreted facies 1, 4 and 7. These were the main facies of the sample. E) Hand sample collected from the locality, and has a dark grey color.

Table 5.21: The table shows 3 tiny perm values measured (A-C) on Sample 1Aa`s surfaces (see Appendix 1 for measurement locations). 3 facies were distinguished on the sample surfaces. The tiny perm was measured on all 3, Facies 1, Facies 4 and Facies 7 (see Appendix 1).

Sample 1Aa	A	B	C
K (mD)	865	244	246
ΔK	±562	±167	±225

Table 5.22: Petrophysical and volume properties of sample 1Aa.

Sample 1Aa	Vtotal [cm^3]	ΔVtotal	Porosity, φ [%]	Δφ	Permeability,K [mD]	ΔK
Sample 1Aa	734	±4	13.9	±0.3	-	-
Core plug 1Aa	26.82	±0.01	14.47	±0.05	0.030	±0,005

The tiny perm measurements, **Table 5.21**, indicated permeability in areas of the sample. However, as the core plug measurement in **Table 5.22** measured a permeability less than 1 mD. The core plug had a heavily cemented layer cutting the core plug across. The cementation is believed to not only be located in the area from where the core plug was cut out from. Cementation seams are most quite dominating in this sample as it was hard to evacuate the sample under the porosity measurements. Therefore the permeability measurement in **Table 5.22** is the most adequately for the whole sample. The porosity measurements **Table 5.22**, gives about the same result for the porosity in the sample, around 14 %. This indicates that the porosity is good, but cements have occluded the effective permeability in areas of the sample.

5.4.2 Location 1 – Sample 1Ab

The sample 1Ab was taken from the same location as sample 1Aa, as it originally was one big sample. The locality is indicated in **Figure 5.12 (a)**, is at the bottom of the brecciated stratigraphy of the Minkinfjellet Formation. In **Figure 5.12 (b)**, the clasts of the hand sample is loosely packed, and little cements were observed. Otherwise its composition is very similar to 1Aa. The sample is mainly matrix-rich clast-supported chaotic breccia.
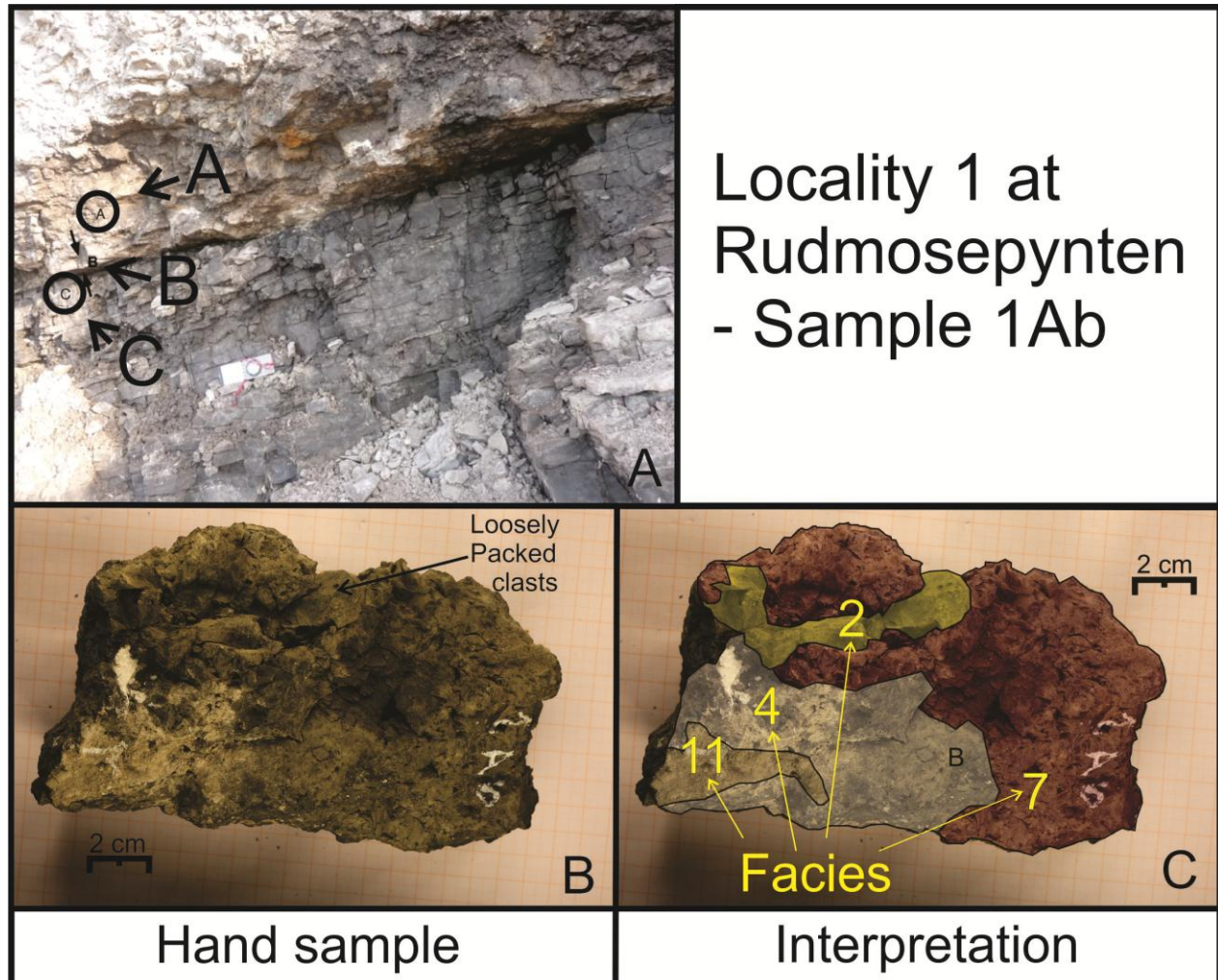
Figure 5.12: A) The location of the sampling, indicated with A and an arrow to the sampling point. B) Hand sample sampled from the outcrop. C) Facies interpretation, where facies 7 and 4 were the main facies for the whole sample. Facies 2 and 11, were only observed at the small parts indicated in the picture.

Table 5.23 The table shows 2 tiny perm values measured (A-B) on Sample 1Ab`s surfaces (see Appendix 1 for measurement locations). 3 facies were distinguished on the sample surfaces. The tiny perm was measured on 2 of these, Facies 4 and Facies 7 (see Appendix 1).

Sample 1Ab	A	B
K (mD)	0.09	35
ΔK	±0.02	±9

Table 5.24: Petrophysical and volume properties of sample 1Ab.

Sample 1A	Vtotal [cm^3]	ΔVtotal	Porosity, φ [%]	Δφ	Permeability,K [mD]	ΔK
Sample 1Ab	674	±3	10.2	±0.5	-	-

The sample can have high permeability, **Table 2.23**, and the permeability can be even in Darcys. This interpretation was made on the basis of a core plug analysis was not performed as the whole sample cracked to pieces under cutting for a core plug. As the sample was so loosely packed, the tiny permeability values obtained in **Table 5.23** seems probably based on the observations. However in the range of tiny perm value (A) is the most reasonable, since it also was hard to conduct a proper measurement of the tiny perm as well due to the composition of the sample.

The porosity of the sample **Table 5.24**, was expected to be greater due to the observations of the composition of the sample. But water might have dripped off during the experiments as the sample was transported to the scale after saturation in the desiccator.

5.4.3 Location 1 – sample 1Ac

The sample 1Ac is the third piece of sample 1A, taken from locality 1 at Area 3, **Figure 5.13 (a)**, at the uppermost brecciated layer. The sample is mainly matrix-supported chaotic breccia, as it has a similar composition as the other brecciated pieces of 1A.
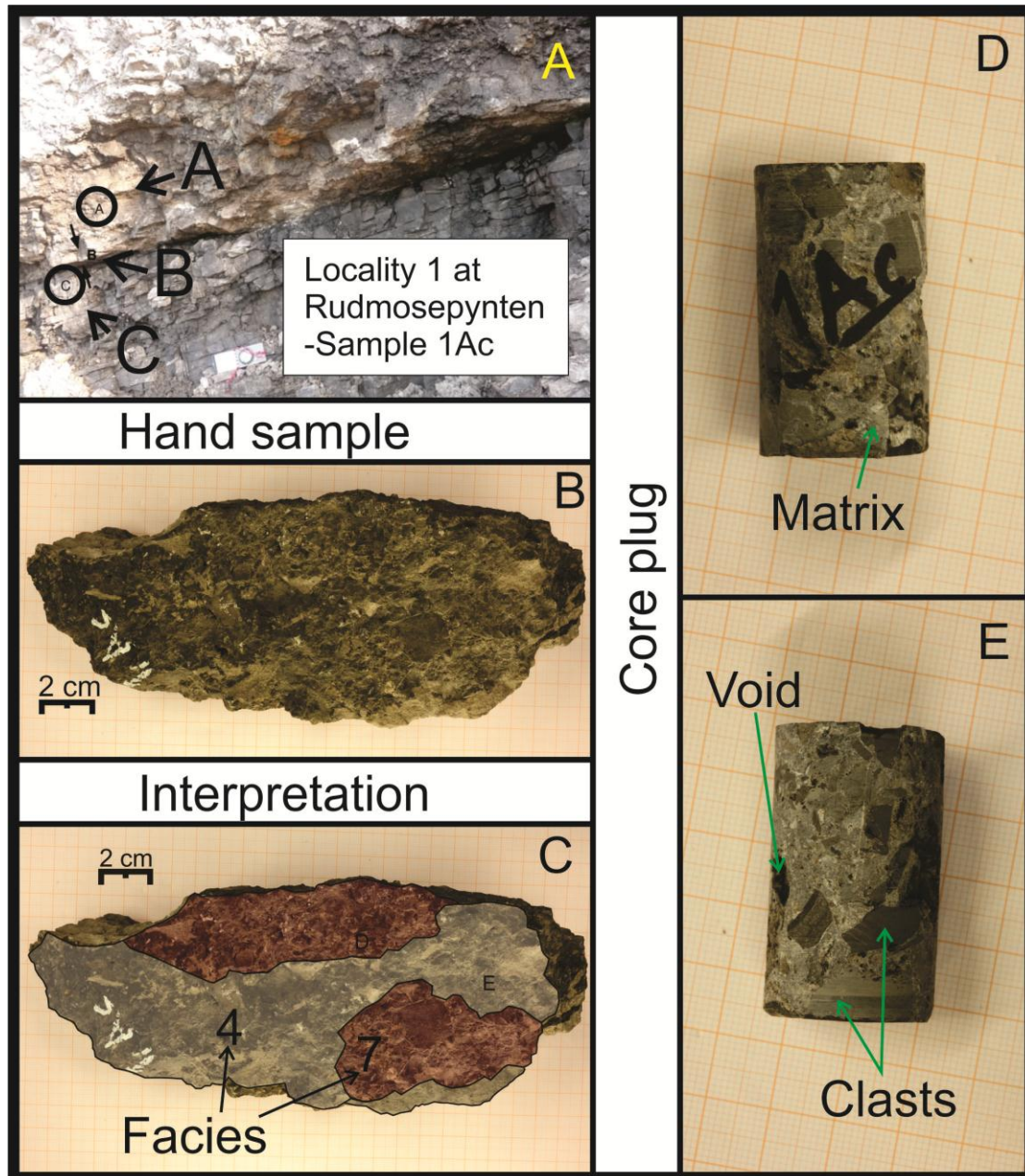
Figure 5.13: A) The locality of sampling,The sample 1Ac is taken from the uppermost layer indicated with the A and the arrow showing site. B) The hand sample taken from the outcrop with dark grey color. C) Facies interpretation of the sample, with the main facies 4 and 7. Facies 1 and 11 were also observed D) Core plug with the matrix of the sample indicated which consists of fine rounded clasts (< 1 mm) and some vuggy pores are observed. E) Voids within the matrix and <1 cm clasts coated I matrix in in another side of the core plug.

Table 5.25: The table shows 5 tiny perm values measured (A-E) on Sample 1Ac`s surfaces (see Appendix 1 for measurement locations). 4 facies were distinguished on the sample surfaces. The tiny perm was measured on 3 of these, Facies 1, Facies 4 and Facies 7 (see Appendix 1).

Sample 1Ac	A (F11)	B (F7)	C (F7)	D (F7)	E (F4)
K (mD)	102	722	151	307	171
ΔK	±38	±661	±94	±162	±74

Table 5.26: Petrophysical and volume properties of sample 1Ac

Sample 1Ac	Vtotal [cm^3]	ΔVtotal	Porosity, φ [%]	Δφ	Permeability,K [mD]	ΔK
Sample 1Ac	696	±3	11.4	±0.2	-	-
Core plug 1Ac	21.07	±0.05	19.51	±0.08	6.5	±0.4

The tiny permeability values, **Table 5.25**, of sample 1Ac showed generally much greater permeabilities than the flow measurement executed on the core plug, **Table 5.26**. The permeability, **Table 5.26** is likely the most true permeability of the sample as a representable plug was drilled from the sample, **Figure 5.13 (d)** and **(e)**. The porosity measurement gave almost twice as high porosity in the flow measurement, and is probably the most correct. This is because a casing was wrapped around the core plug. This enabled the voids on the surface of the core plug to be saturated without draining off before the scale is reached. As well as the pore space of the core plug could be filled even more with an injection pressure, which led to the pore space being even more filled.

5.4.4 Location 1 – sample 1Ad

The sample 1Ad was the smallest piece of sample 1A, taken from the uppermost brecciated layer at location 1, **Figure 5.14 (a)**. The sample is interpreted as matrix-supported chaotic-breccia, as the other samples from location 1, however this sample showed less dissolution and generally smaller size of clasts as facies 7 was the dominant one.
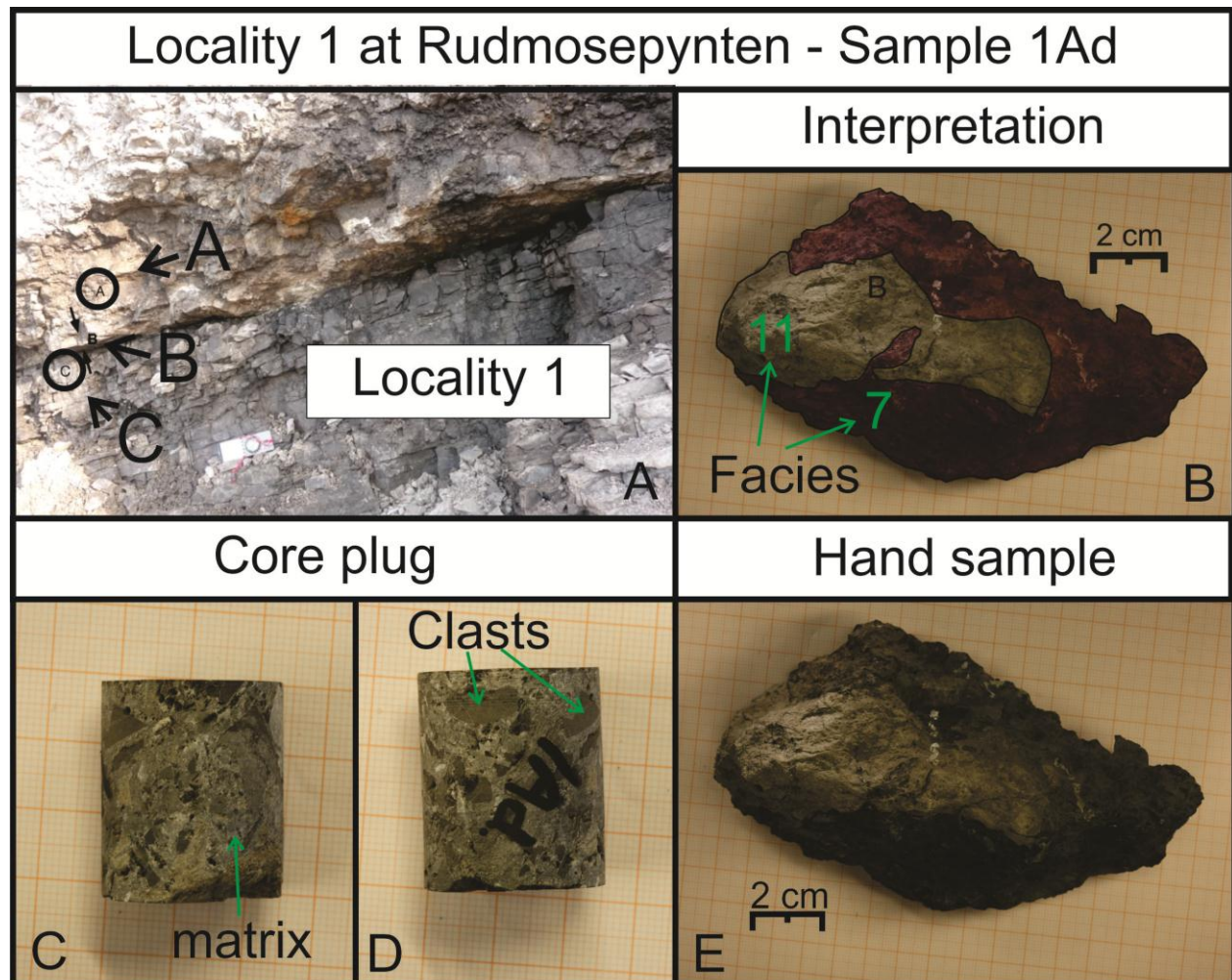
Figure 5.14: A) The uppermost brecciated layer, with site of sampling indicated with A and arrow. B) Interpretation of the sample with facies 11 and 7, which were the representative facies. C) Matrix with <1mm rounded clasts. D) Clasts <1 cm large coated in matrix observed in the core plug from another side. E) Hand sample, showing the dark grey color of the sample.

Table 5.27: The table shows 2 tiny perm values measured (A-B) on Sample 1Ad`s surfaces (see Appendix 1 for measurement locations). 2 facies were distinguished on the sample surfaces. The tiny perm was measured on 2 of these,Facies 7 and Facies 7 (see Appendix 1).

Sample 1Ad	A (F7)	B (F11)
K (mD)	601	170
ΔK	±379	±33

Table 5.28: Petrophysical and volume properties of sample 1Ad.

| Sample 1Ad	Vtotal [cm^3]	ΔVtotal	Porosity, φ [%]	Δφ	Permeability,K [mD]	ΔK
Sample 1Ad	232	±1	12.0	±0.4	-	-
Core plug 1Ad	15.109	±0.008	8.67	±0.09	0.55	±0.03

The tiny permeability measurement, **table 5.27**, gave higher permeabilities compared to the result from the core plug, **Table 5.28,** which gave permeability less than zero. The core plug was drilled through the middle of the sample and would therefore reflect the composition of the whole sample, however as shown in **Figure 5.14 (c) and (d)** the fine grained material interpreted as sediment fill (facies 11) **Figure 5.14 (b)** is not a part of the core plug. The facies 11 are assumed to have good porosity and permeability. That can be a reason for the core plug yield lower porosity, and therefore lower permeability than for the whole sample. Areas with greater permeability might occur, but probably not give as high permeability as the tiny perm gave. The porosity of the sample is probably 12 ±0.4 % , **Table 5.27**, which was the measured porosity for the sample.

Summary 1A

For the 1A an average porosity is 12 ± 2 %. This is in the same range as for the core plugs 13 ± 5 %. A higher porosity on average was expected for the cores. But can be explained by the most compacted and cemented parts of the samples were cut out.

5.4.5 Location 1 – sample 1B

The sample 1B was sampled in the contact zone between the unbrecciated mudstone stratigraphy and the upper brecciated zone, **Figure 5.15 (a)**. The sample 1B, shows a texture with few clasts and is classified as cave sediment-fill. The texture of the sample indicates sedimentary flow structures.
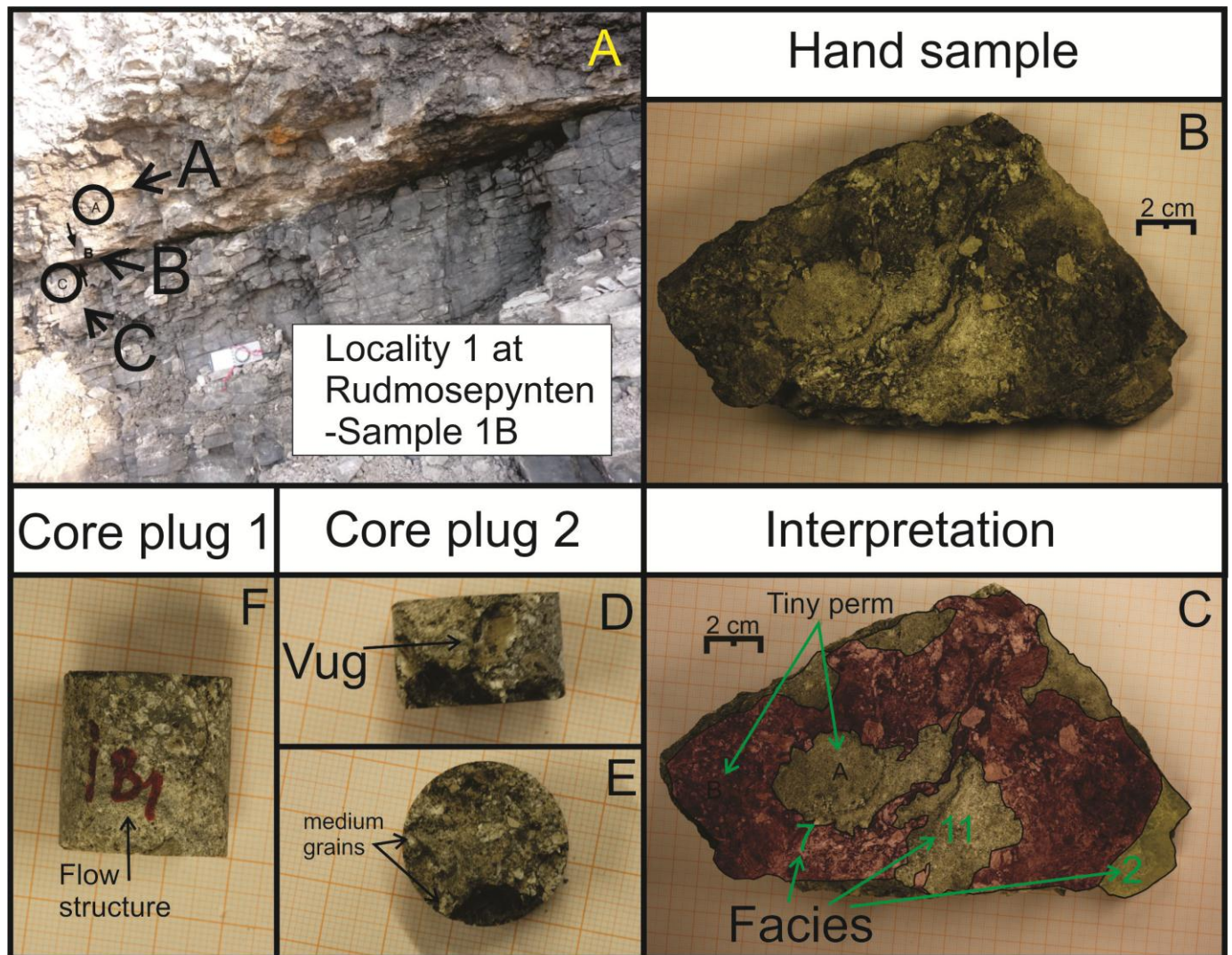
Figure 5.15: A) The locality of sampling. The letter B and an arrow indicate the site of sampling. B) Hand sample taken from the outcrop location, which has a grey and white color. C) The Facies interpretation with three of the main facies (7, 11 and 2). Facies 1 was also observed on the surface of the sample. D) Core plug 2, with several large vuggy pores. E) Cross section of core plug 2, shows that the core plug is mainly grain supported. F) Core plug 1, cut from a different area of the sample. Internal flow structures can be seen.

Table 5.29: The table shows 5 tiny perm values measured (A-E) on Sample 1B`s surfaces (see Appendix 1 for measurement locations). 4 facies were distinguished on the sample surfaces. The tiny perm was measured on these 4, Facies 1, Facies 2, Facies 7 and Facies 11 (see Appendix 1).

Sample 1B	A (F11)	B (F7)	C (F1)	D (F2)	E (F2)
K (mD)	1137	416	27	8	4884
ΔK	±389	±191	±20	±3	±5978

Table 5.30: Petrophysical and volume properties of sample 1B.

Sample 1B	Vtotal [cm^3]	ΔVtotal	Porosity, φ [%]	Δφ	Permeability,K [mD]	ΔK
Sample	546	±5	15.4	±0.5	-	-
Core plug 1	13.218	±0.001	10.3	±0.1	1.20	±0.08
Core plug 2	7.1	±0.7	18	±2	27	±8

The tiny permeability values B to D, **Table 5.29,** show likely permeability values of the sample. The values A and E gave too high permeability values than what is expected for this type of composition as it is consolidated and consist of carbonate mud, sand fine-medium grains and a few clasts. This assumption is based upon the high porosity values, **Table 5.30**. The permeability measurements performed on the two core plugs, **Table 5.30**, show how much the porosity and permeability can vary within the sample. The range in permeability is mainly due to the amount of cements within the sample. Cement growth can close the pore throats and decrease the effective porosity and permeability. The average porosity of the sample is 15 ± 0.5 % based on the porosity measurement performed on the whole sample.

5.4.6 Location 1 – sample 1C

The sample 1C was sampled at locality 1, at the lowermost unbrecciated layer. The sample 1C is sampled right below the breccia body contact at the coastal escarpment at Rudmosepynten, **Figure 5.16 (a)**. The sample is unbrecciated mudstone, **Figure 5.16 (b)**.
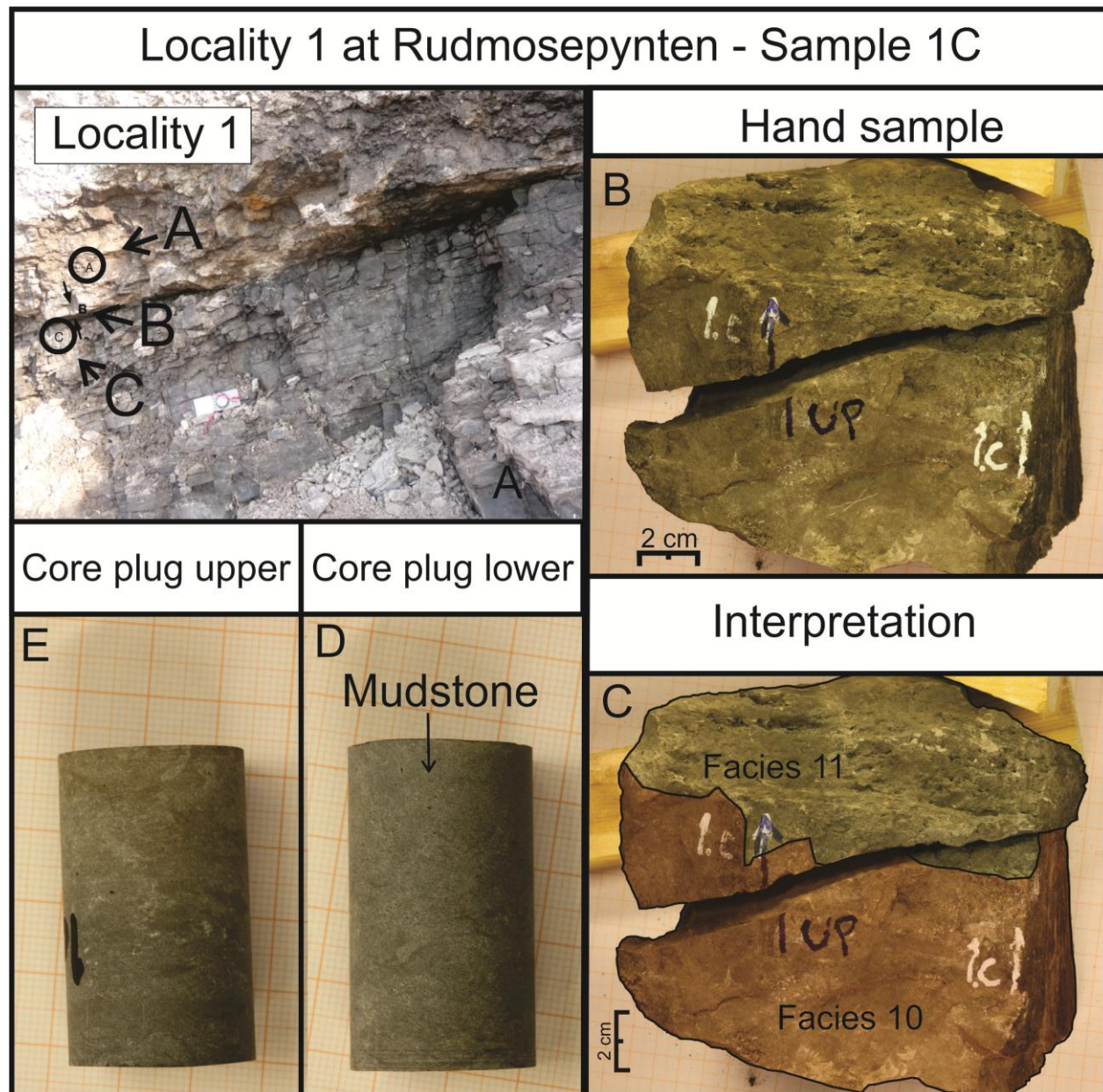
Figure 5.16: A) Locality for sampling indicated by the C and an arrow. The locality consisted of carbonate mudstone strata. B) Hand sample sampled at the locality. C) Facies interpretation where facies 10 was the dominate facies, and the facies 11 was only observed at the upper part of the sample. D) Structureless mudstone. The core plug was drilled out from the lower part of the sample. E) Core plug drilled out from the upper part of the sample. It has a distinct color change from grey to brown. The upper part of the core plug has a more disturbed texture.

Table 5.31 The table shows 4 tiny perm values measured (A-D) on Sample 1C`s surfaces (see Appendix 1 for measurement locations). 2 facies were distinguished on the sample surfaces. The tiny perm was measured on both, Facies 10 and Facies 11 (see Appendix 1).

Sample 1C	A (F10)	B (F10)	C (F11)	D (F11)
K (mD)	16	5	12	14
ΔK	±15	±3	±8	±15

Table 5.32: Petrophysical and volume properties of sample 1C.

Sample 1C	Vtotal [cm^3]	ΔVtotal	Porosity, φ [%]	Δφ	Permeability,K [mD]	ΔK
Sample upper	374	±2	10.4	±0.5	-	-
Sample lower	870	±4	3.7	±0.4	-	-
Core plug upper	21.2738	±0.0002	10.76	±0.07	0.000308	±0.000006
Core plug lower	22.2153	±0.0003	2.03	±0.06	0.0089	±0.0002

The tiny permeability, **Table 5.31**, gave low permeability. Based on the composition of the sample which was nearly homogeneous and had several flat surfaces, good readings were achieved. By contrast the even lower permeability values gained from the core plug, **Table 5.32**, are the most likely ones. These show that there were about no flow through the core plugs. However, the core plug drilled from the upper piece of sample 1C gave a high porosity compared to the lower piece of the sample 1 C and a greater permeability had been anticipated. But when performing the flow measurement on the upper core plug, only one reading could be used to calculate the permeability. This was because there was no flow through the permeability, thus low permeability. Only one reading was achieved for the core plug from the lower piece, and is due to the same reasons as for core plug Upper. Another reason for low permeability for core plug Upper was that all the silty material on the uppermost part of this sample was not a part of the core plug, thus only micritic mudstone.

5.4.7 Location 3 – Sample 3A1

The location 3 was within a brecciated stratigraphy along the coastal escarpment at Rudmosepynten. The sample 3A1, **Figure 5.17 (c)**, collected at the locality, **Figure 5.17 (a)**, is classified as cave sediments with clasts.
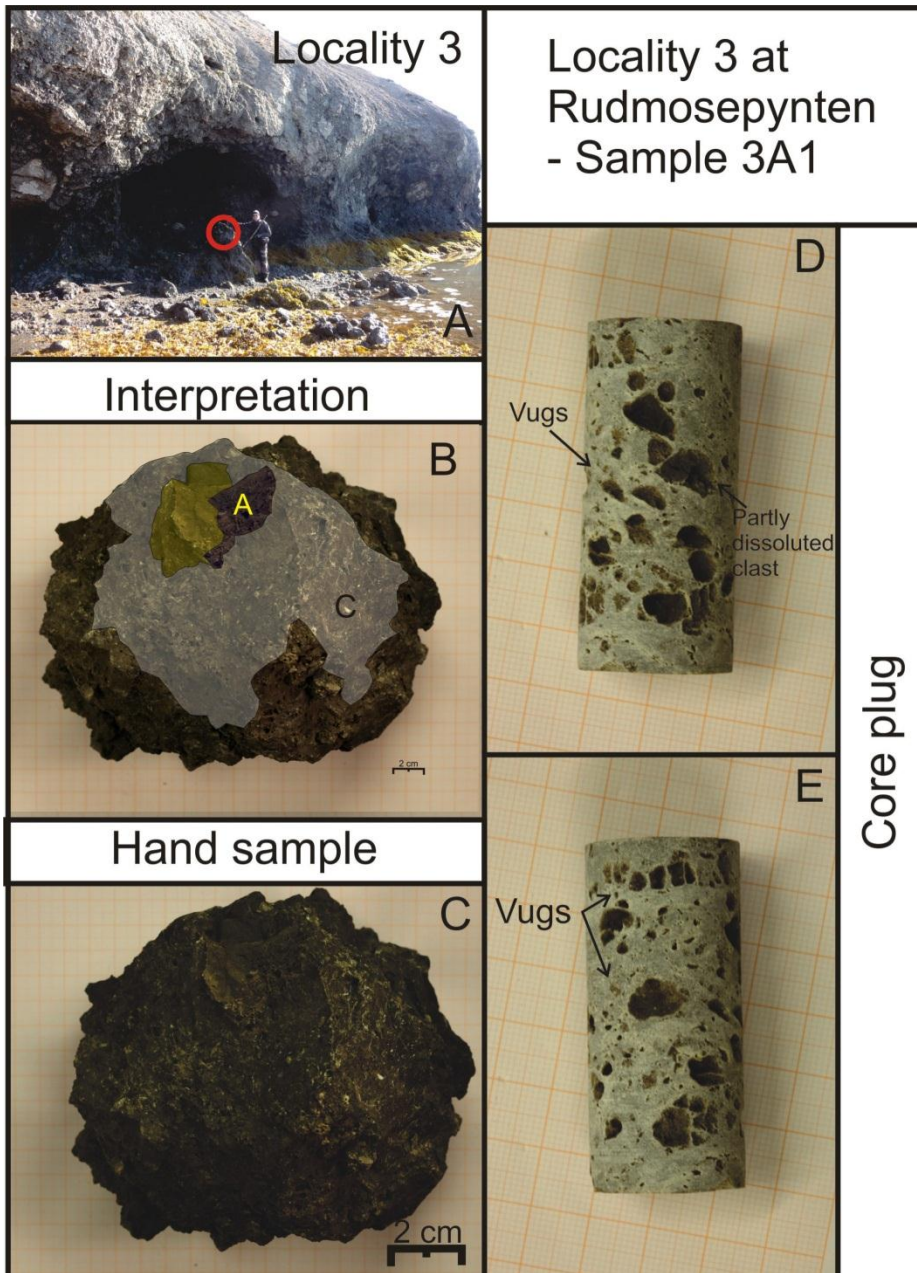
Figure 5.17: A) The red circle at the top of the pinnacle indicates the locality of the sampling. B) Interpretation of the sample with the facies 1,2 and 4 which were the main facies of the sample. C) Hand sample collected at the locality. The sample had a dark grey color. D) Core plug, with vuggy pores, and partly dissolved clasts within the pores was observed. E) Vuggy pores within a carbonate mud matrix. Few clast could be distinguished.

Table 5.33: The table shows 3 tiny perm values measured (A-D) on Sample 3A1`s surfaces (see Appendix 1 for measurement locations). 3 facies were distinguished on the sample surfaces. The tiny perm was measured on all, Facies 1, Facies 2 and Facies 4 (see Appendix 1).

Sample 3A1	A (F1)	B (F2)	C (F4)
K (mD)	75683	1659	83
ΔK	±21865	±790	±49

Table 5.34: Petrophysical and volume properties of sample 3A1.

Samples 3A1	Vtotal [cm^3]	ΔVtotal	Porosity, φ [%]	Δφ	Permeability,K [mD]	ΔK
Sample 3A1	1147	±11	12.9	±0.7	-	-
Core plug 3A1	28,11	±0.01	17.57	±0.05	0.42	±0.04

The tiny permeability, **Table 5.33**, gave to high permeability for this sample. This assumption is due to the fact that it was hard to make good measurements on the sample, as it had vuggy pores that were 1 mm and up to 1 .5 cm large. The flow permeability measurement, **Table 5.34**, gave a better estimation of the permeability, due to visually observations, the pores observed at the surface were mainly non-touching and the pore system would be within the matrix of the core plug. As **Figure 5.18 (d)** and **(e)** shows that the vuggy pores are not touching vugs. The porosity of the sample is therefore within the mudstone matrix. There are areas with touching vugs, however just in small areas. Therefore this would not lead to greater permeability extending over large areas.

The porosity value, **Table 5.33**, gave a higher porosity value in the core plug and is the best estimation. This is due to a casing was put on the core plug, so that the water filling the pores would not leak out before weighting the saturated core plug. The sample did not have such a casing and gave an underestimation of the porosity. The porosity presented of the core plug is the porosity measurement of the sample before the permeability measurement. After the permeability measurement the core plug gave a lower porosity which indicates that there was little flow through the core plug.

5.4.8 Location 3 – Sample 3A2

The sample 3A2 was the second sample collected from the pinnacle at the coastal escarpment at Rudmosepynten, **Figure 5.18 (a)**. The sample collected at the location, **Figure 5.18 (c)**, is interpreted to be cave sediments with clasts.
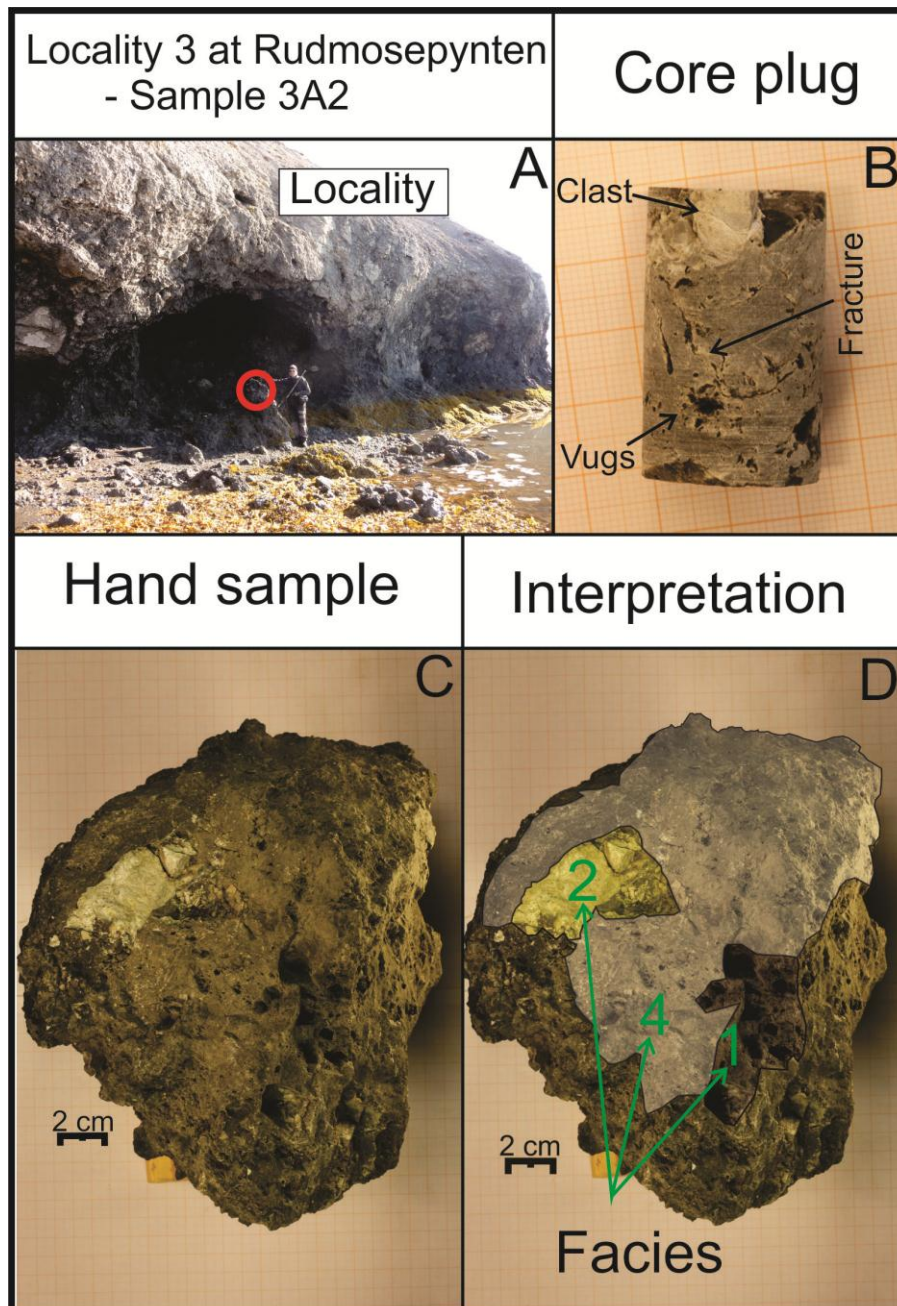
Figure 5.18: A) The location 3 of sampling, at the top of the pinnacle indicated with the red circle. B) Core plug drilled out from the sample, shows a heterogeneous composition, vuggy pores and a fracture. C) The hand sample collected at the outcrop location. D) Interpretation of the sample, which shows the main facies of the sample, 1, 2 and 4.

Table 5.35: The table shows 5 tiny perm values measured (A-E) on Sample 3A2`s surfaces (see Appendix 1 for measurement locations). 3 facies were distinguished on the sample surfaces. The tiny perm was measured on all, Facies 1, Facies 2 and Facies 4(see Appendix 1).

Sample 3A2	A (F2)	B (F4)	C (F1)	D (F4)	E (F1)
K (mD)	11	40	102	186	40
ΔK	±12	±27	±36	±80	±25

Table 5.36: Petrophysical and volume properties of sample 3A2.

Samples 3A	Vtotal [cm^3]	ΔVtotal	Porosity, φ [%]	Δφ	Permeability,K [mD]	ΔK
Sample 3A2	3802	±38	6.8	±0.5	-	-
Core plug 3A2	19.57	±0.21	6.95	±0.10	0.073	±0.002

The tiny permeability measurements, **Table 5.35**, indicate higher permeabilities of this sample compared to the permeability measured through the flow measurement, **Table 5.36**. Although the permeability varies within the sample, the tiny perm values C and D are unlikely. This assumption is based on the same reasoning as for sample 3A1. **Figure 5.18 (b),** indicates the sample has vuggy pores, but most of them appears to be none touching vugs. When executing the permeability measurement, it was hard to gain a constant rate at a constant pressure, which indicated that the sample had low permeability. The porosity of the sample lies around $6 - 7\,\%$, **Table 5.35**, and the porosity is within the same range. However, the porosity of the sample can be greater as it would vary with the amount of the vuggy pores.

Even if the voids create a touching-vug pore space, the porosity and permeability are low. Touching-vug systems typically control fluid flow through their conduits, but contribute less than 1 % to the reservoir porosity, due to most of the reservoir pore space is located in the matrix. This creates a bimodal pore system where most of the storage is within the matrix and most of the flow capacity is within the vug system (Lucia 1999)

5.4.9 Location 4 – sample 4

The location 4 has been classified as the Fortet member of the Minkinfjellet Formation, **Figure 5.19 (a)**. But the lithology of the outcrop consists of clasts and matrix of the Wordiekammen Formation. The locality four is a large pinnacle consisting of angular and rounded clasts and boulders, some fluvial reworked sediments and some north-dipping lineation. Based on the composition of the pinnacle the breccia has been transported and is believed to have been a part of a greater connected cave system, and not only caused by an upward prograding breccia pipe. The sample is interpreted to be matrix-rich clasts-supported chaotic breccia.
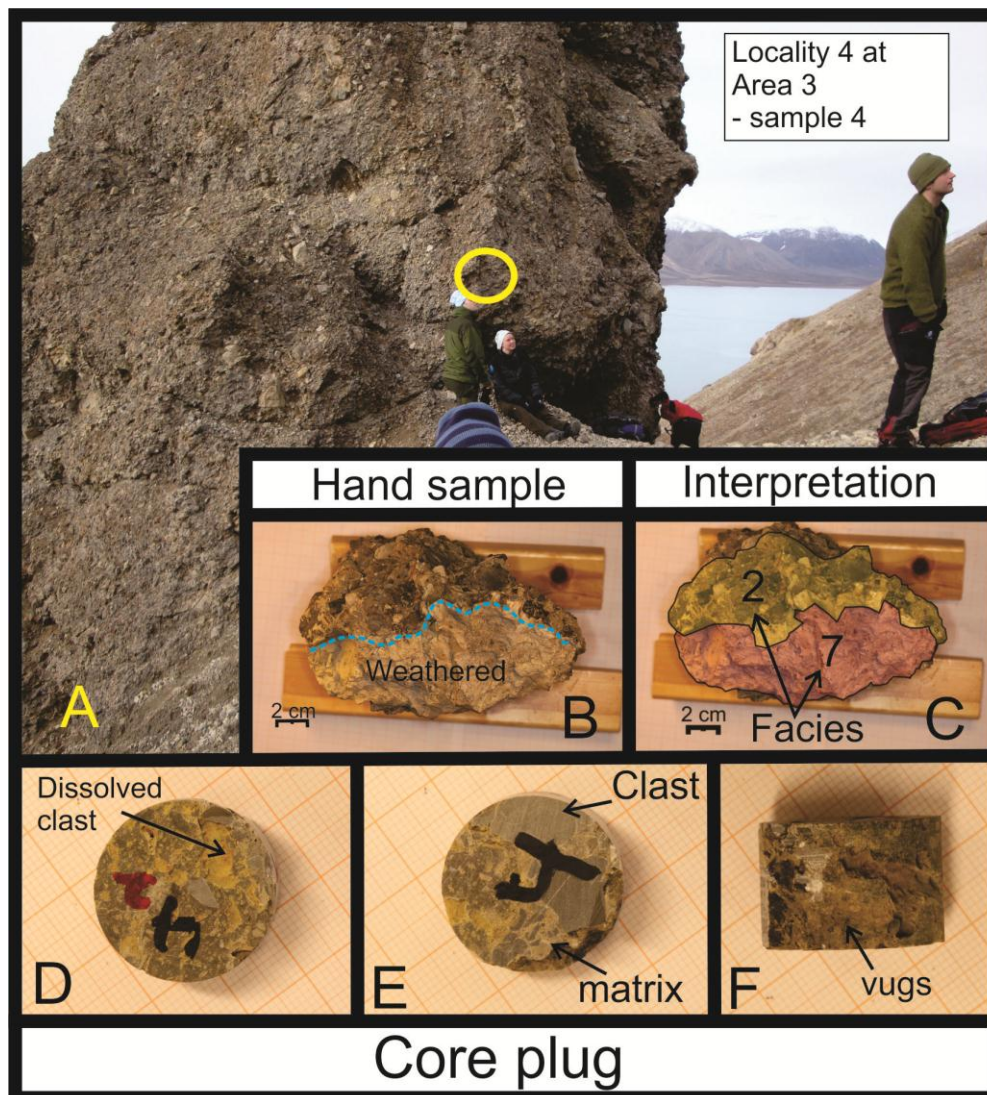
Figure 5.19: A) The location of sampling, indicated by the yellow circle. B) Hand sample taken from the outcrop, which indicates a weathered surface. C) Facies interpretation of the sample, where facies 2 and 7 were the main facies. D) Cross section of the core plug which indicates a heterogeneous composition. E) < 2 cm large clasts observed at the cross section on the other side of the core plug. F) Large vuggy pores within the core plug.

Table 5.37 The table shows 4 tiny perm values measured (A-D) on Sample 4`s surfaces (see Appendix 1 for measurement locations). 3 facies were distinguished on the sample surfaces. The tiny perm was measured on all, Facies 1, Facies 2 and Facies 7(see Appendix 1).

| Sample 4	A (F7)	B (F7)	C (F2)	D (F1)
K (mD)	101	7	60	104
ΔK	±76	±3	±28	±69

Table 5.38: Petrophysical and volume properties of sample 4.

Samples 4	Vtotal (sat), cm^3	σ	Porosity, %	σ	Permeability, (mDarcy)	σ
Sample 4	1774	±18	7.2	±0.7	-	-
Core plug 1	8.27	±0.57	9.19	±0.65	3.41	±0.02

The sample 4 appeared to be mainly clast supported, with little matrix content. When performing the cutting, it was observed that the sample had a large matrix content and voids, thus it was hard to drill larger core plugs. The sample had a heterogeneous composition and clasts sizes ranges from 1 mm up to 7 cm. The tiny permeabilities, **Table 5.37**, gave generally low permeabilities, compared to the composition of the sample. The tiny permeability values give generally greater permeabilitis than flow measurements. Which is due to gas is used to measure the permeability instead of water, the tiny permeabilities is thus low. This is because the surfaces the tiny permeability was measured on were mainly the flat limestone rock fragments. The permeability of the sample, **Table 5.38**, is likely to be closest to the correct permeability within the sample. The porosity is likely to vary within the sample, the greater porosity gained from the core plug, **Table 5.38**, is due to the core plug had large vuggy pores. The porosity of the whole sample lies therefore around 7 – 9 %.

5.4.10 Location 5 – Sample 5A

The sample 5A was sampled within a fractured zone adjacent to a breccia pipe within the Wordiekammen Formation, **Figure 5.20 (b)**. The sample is a part of a breccia wall and is interpreted to be a crackle breccia.
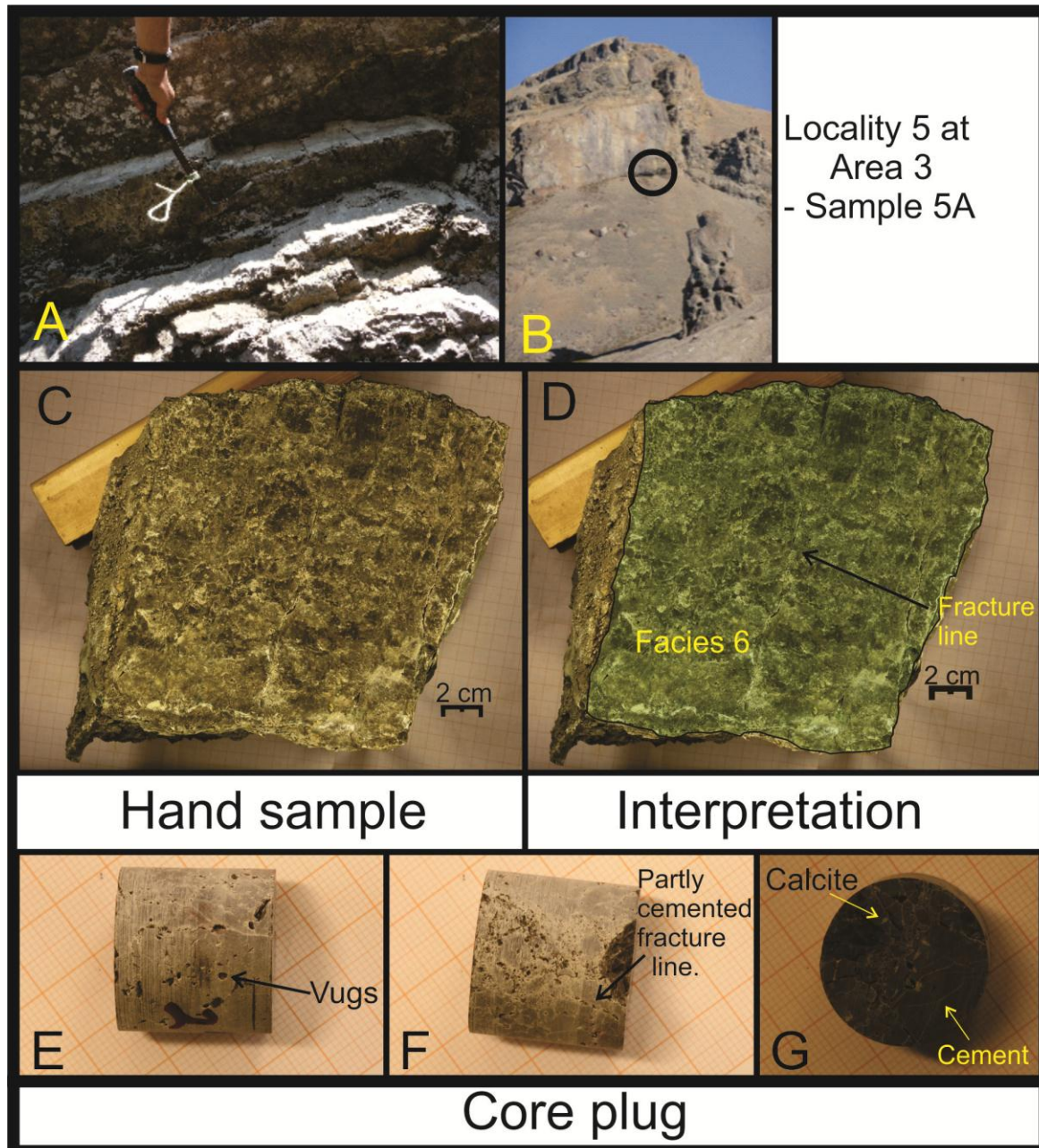
Figure 5.20: A) Close up picture of the location of sampling. B Locality 5b indicated by a black circle adjacent to a breccia pipe to the right. Location 4 is the pinnacle standing in lower right of the picture. C) Hand sample sampled at the locality, the scale indicates the large size. D) Facies interpretation of the sample, with facies 6 represented. Other facies observed were 2, 5 and 8. E) Lengt of the core plug with vuggy porosity. F) Highly fractures with several 1 mm large rock fragments with cemented fracture lines. Vuggy porosity observed. G) Cross section of the sample with white calcite spots on the surface.

Table 5.39: The table shows 7 tiny perm values measured (A-G) on Sample 5A`s surfaces (see Appendix 1 for measurement locations). 4 facies were distinguished on the sample surfaces. The tiny perm was measured on 2 of these, Facies 5 and Facies 6(see Appendix 1).

| Sample 5A	A (F6)	B (F6)	C (F6)	D (F5)	E (F5)	F (F5)	G (F6)
K (mD)	47	238	42	14	88	88	7
	±3	±49	±19	±21	±27	±44	±3

Table 5.40: Petrophysical and volume properties of sample 5A.

Samples 5	Vtotal [cm^3]	ΔVtotal	Porosity, φ [%]	Δφ	Permeability,K [mD]	ΔK
Sample 5A1	2831	±28	3.7	±0.4	-	-
Sample 5A2	2132	±21	4.4	±0.4	-	-
Core plug 5A	11.52	±0.06	3.82	±0.12	1.16	±0.09

The sample 5A was a large sample, **Figure 5.20 (c)**, and cut in two in order to be suited for the porosity measurement, the two pieces was called 5A1 and 5A2. The tiny permeability values, **Table 5.39**, were mainly executed on the unfractured surface. The permeabilities are thus higher than the core plug measurement, **Table 5.40**, which is naturally lower due to it is harder to flow water than air into a sample. An even higher permeability are assumed in the sample as observations during cutting showed that the larger fractured had not been totally infilled by cements. The cements inhibit the flow, and small fractures were partly and totally infilled by cement, **Figure 5.20 (e)** and **(f)**. The large fractures on the other hand would act as good pathways to flow, **Figure 5.20 (d)**. The porosity of the sample would lie around 4 % which is in agreement with the porosity measurements performed on the sample, **Table 5.40**.

5.4.11 Location 5 – Sample 5B

The sample 5B was sampled at the same location as sample 5A, which is adjacent to a breccia pipe within the Wordiekammen formation, **Figure 5.21 (a)** and **(b).** The sample is interpreted as crackle breccia, and has several through going fractures.
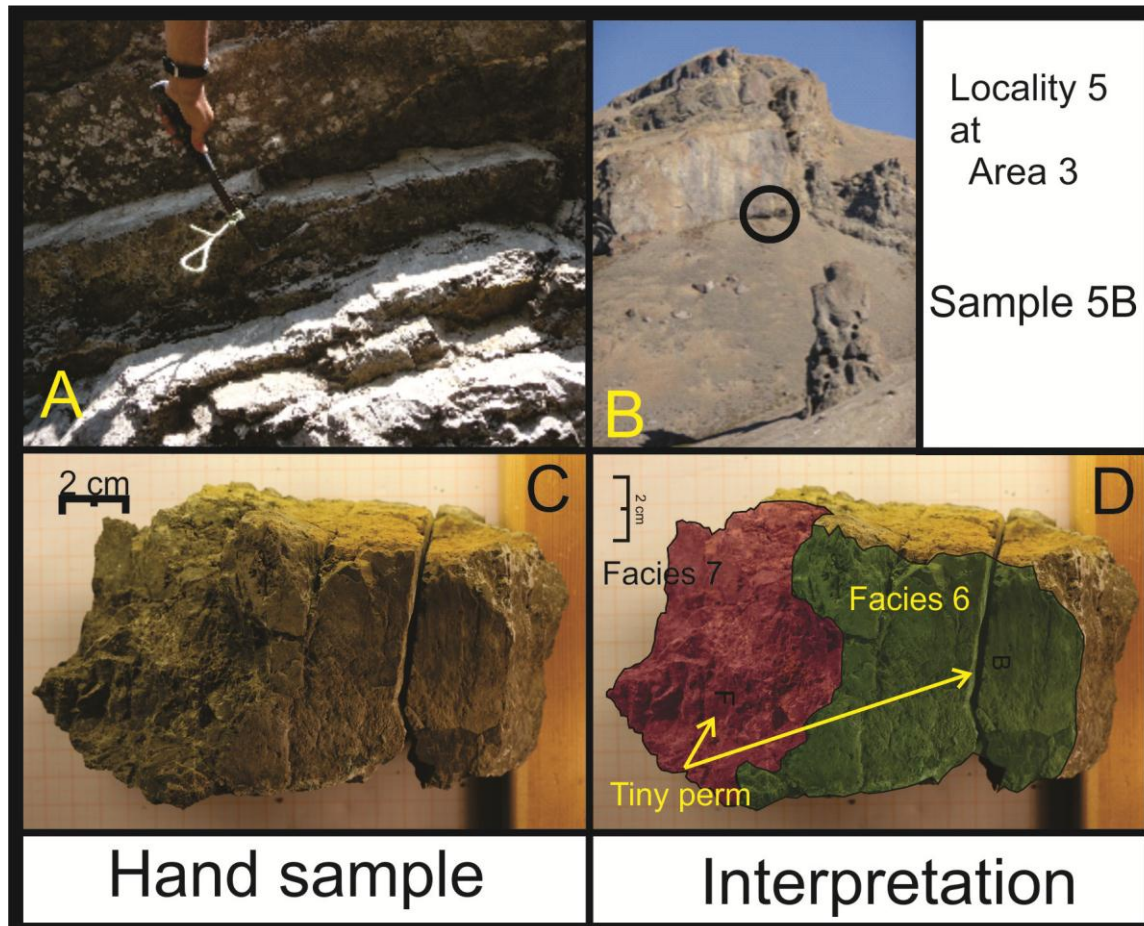
Figure 5.21: A) Close up picture of the locality. B) Locality indicated by the black circle adjacent to the breccia pipe to the right. C) Hand sample sampled at the outcrop locality. D) Facies interpretation of the sample 5B with facies 7 and 6. The facies 1 and 5 was also observed within the sample.

Table 5.41: The table shows 5 tiny perm values measured (A-F) on Sample 5B`s surfaces (see Appendix 1 for measurement locations). 5 facies were distinguished on the sample surfaces. The tiny perm was measured on 4 of these, Facies 1, Facies 5, Facies 6, Facies 5 and Facies 7(see Appendix 1).

Sample 5B	A (F6)	B (F6)	C (F6)	D (F5)	E (F1)	F (F7)
K (mD)	1383	154	2886	184	75	891
	±230	±204	±589	±75	±68	±250

Table 5.42: Petrophysical and volume properties of sample 5B.

Samples 5	Vtotal [cm^3]	ΔVtotal	Porosity, φ [%]	Δφ	Permeability,K [mD]	ΔK
Sample 5B1	520	±5	4.7	±0.1	-	-
Sample 5B2	138	±1	3.7	±0.4	-	-

The tiny permeability values, **Table 5.41**, show a wide range in the permeabilities. This is because measurement A and C were measures adjacent or on a fracture and would therefore yield high permeability. The sample was also cut in two by an open fracture, which would yield high permeability. The measurements B, D, E and F give a higher permeability than expected, this is based upon the observations that the voids between the clasts were filled with cements and the clast were compact, **Figure 5.21 (c)**. The sample 5B was the first sample to be drilled, and due to problems with the drill, it led to the whole sample cracked and no core plug could be drilled out of the sample. However based upon the similar composition and porosity of the samples 5A and 5B, a flow measurement would yield the same value as for sample 5A, which is 1.2 mD. The porosity of the sample 5B was around 4-5 %, in the same range as sample 5A, **Table 5.42**.

6 Discussion

The aim of this thesis is to improve our understanding related to reservoir characterization of the petrophysical properties of a karst reservoir, in this case a system of collapsed limestone strata related to gypsum dissolution. In general, carbonate reservoirs have low porosity due to compaction and cementation as a result of burial (Selley 1985). Karstification of carbonate enhances the porosity and permeability of a reservoir (Mazzullo and Chilingarian 1996). Crucial for well planning and developing a karstified carbonate reservoir is to understand how both karst and karst induced collapse features are distributed and what the expected petrophysical properties are.

The brecciated areas within the study area are of reservoir potential, based on the results. Therefore an estimated extension of a potential karsted reservoir, **Figure 6.1**, in the study area was made. This discussion will focus on the values and the breccia features at Area 1, Area 2 and Area 3, but will mainly concentrate around the Area 1 – The Red Breccia Pipe.
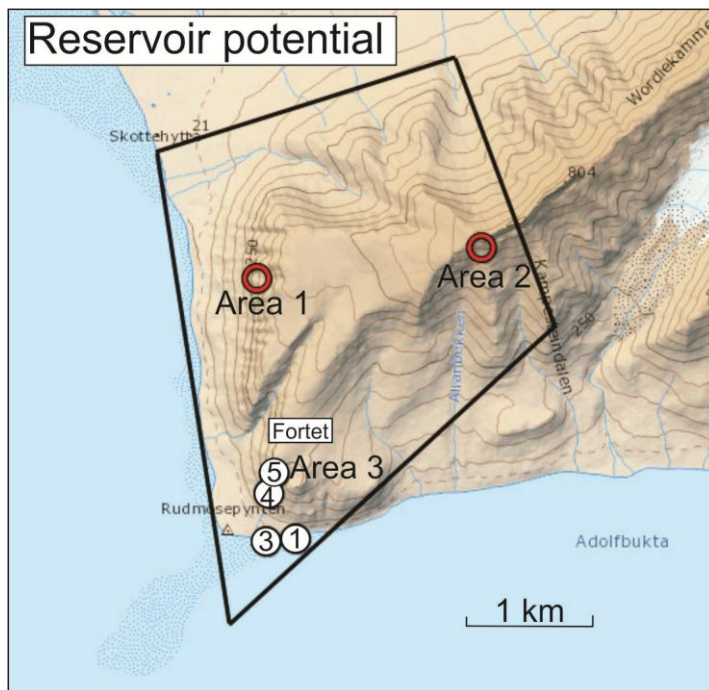

Figure 6.1: Study area with black lines indicating the extended area for which the reservoir potential discussed herein is inferred valid.

6.1 Breccia

The breccia pipes within the Wordiekammen Formation follow the tectonic lineaments which are in the NNW-SSE and NNE-SSW direction (Nordeide 2008; Nøttvedt et al. 1993; Steel and Worsley 1984). The breccia bodies appear to align with the faulting pattern. Similar to observations elsewhere by Lucia (1999), that concentrated dissolution is often formed around an intersection of a fracture system creates karst.

The breccia bodies are interpreted to have been formed by gypsum dissolution within the Minkinfjellet Formation and the upper part of the Ebbadalen Formation. This subsequently caused collapse of the overlying strata. (Braathen et al. 2011; Eliassen 2002; Eliassen and Talbot 2005; Lønøy 1995; McWhae 1953). The brecciation appears to have enhanced the faulting pattern due to removal of material as gypsum and anhydrite, which has been suggested as a possible origin by (Braathen et al. 2011). As stated in Eliassen (2002) the breccias represent a large gypsum paleokarst system where the controlling factors were the distribution of gypsum in the basin and the flow of dissolutional (meteoric) waters. Faults enhance the vertical permeability and large amounts of gypsum of the Minkinfjellet Formation were observed along the shoreline of Billefjorden below the breccia pipes in our area of study. The observations from the fieldwork showed that the breccia pipes were situated towards the center of the Billefjorden Trough. Thinner brecciated strata were situated further to the east and towards the margin of the basin, where no collapse structures such as breccia pipes were observed. The observations are supported by Eliassen (2002) where he states that the distribution of brecciation appears to have been in relation with the distribution of gypsum in the basin (see section 2.8). The interpretation by Eliassen (2002) supports our observations as the brecciation thickens towards the center of the basin and thins and terminates to the east **Figure 6.2 a)**. The brecciated section terminated just east of Area 2, **Figure 5.7**. **Figure 6.2 c)** also indicates that the thicker that evaporite layers are the more void space can be created as gypsum dissolves, and breccia pipes are more likely to occur in these areas. Disturbed strata but not a collapse structure such as a breccia pipe may occur where there are thinner gypsum beds. However, the observation of Area 2 situated towards the east did support a more fault related brecciation at this location as it was situated around a fault related monocline and a fracture density scan-line analysis was executed which showed high density of fractures towards another fault related monocline towards the west. No monoclines

were observed towards the east, and the density of fracture ceased and so did the breccia in the area. Strata at this location showed disturbed layers of crackle and mosaic breccia. The brecciation might have been influenced by gypsum dissolution in underlying Minkinfjellet Formation, although this could not be observed. But Maher and Braathen (2011) stated that Løvehovden fault was active during deposition of Minkinfjellet Formation, and fault movement, exposure, and associated near- or at-surface evaporate dissolution locally produced stratiform breccia.
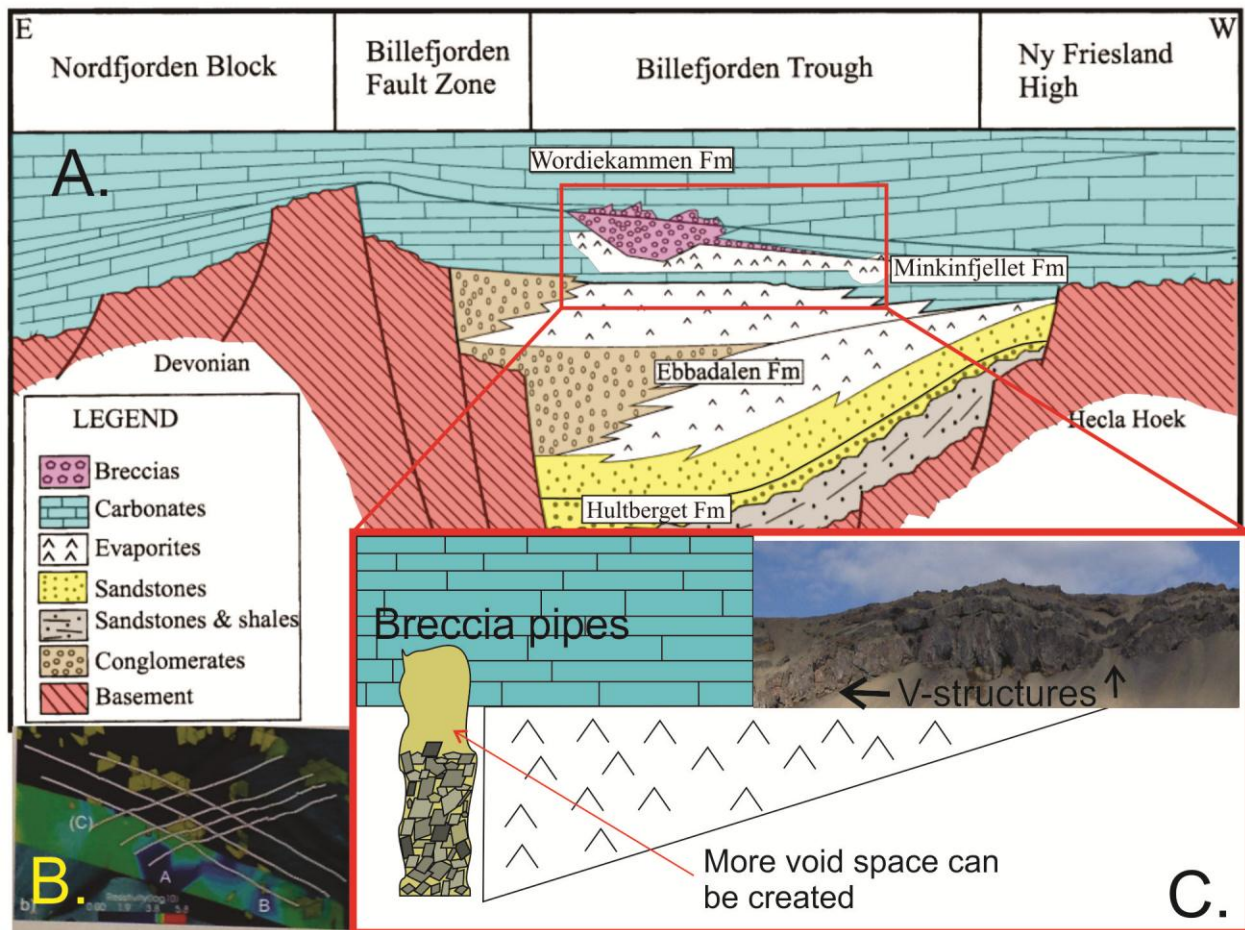
Figure 6.2: A) The figure show the interpreted area on the The Ny Friesland block, indicated with the red square. The modified figure from (Eliassen and Talbot 2005), originally published in (johannessen and Steel). B) The show the breccia bodies within the Wordiekammen Formation, interpreted with?? From ???. C. The interpretation of the pattern of dissolution, which shows that the more gypsum that can be dissolved, the more void space can be created, thus creating breccia pipes. The figure shows that it is more likely to get V-structures which is interpreted as sagging .

At Area 3, a breccia stratigraphy named Fortet locality (Dallmann et al. 1999) has been documented by several authors (Dallmann et al. 1999; Eliassen 2002; Eliassen and Talbot 2005;

McWhae 1953; Nordeide 2008; Sundsbø 1982). In Dallmann et al. (1999) the locality is presented as the type example of a stratigraphic member of the Minkinfjellet Formation called the Fortet Member. In this thesis the area around Area 3 has just been referred to as Minkinfjellet Formation, for simplicity reasons. The chosen localities (1, 3, 4 and 5) at Area 3 were some of the less documented areas of The Fortet locality.

The breccia samples collected at the locality four at Area 3 differ in texture and color from localities five at Area 3, Area 2 and Area 1. Observations of locality 4 were that it was standing as a pinnacle on a scree slope, containing flow structures indicating transported breccia. The breccia deposits indicates a different style of brecciation than of the style of brecciation within a breccia pipe, as the clasts were generally smaller and flow structures were seen cross-cutting the pinnacle. This reflects entries of breccia deposits from the side rather than falling from above. Hence at this locality it appears to have been a collapsed cave forming system within the Minkinfjellet and possible Wordiekammen Formations, as most of the clasts appear to have the same lithology as Wordiekammen Formation but are located at the level of the Minkinfjellet Formation. (Nordeide 2008) made a similar interpretation of the overlying Fortet breccia, where she inferred that the breccia originated from collapse of an extensive cave system in the Fortet Member of Minkinfjellet formation. The interpretation at Locality 4 is in agreements with the interpretation proposed by Nordeide (2008). However here we will infer that the cave system was not restricted to Minkinfjellet Formation, but could have extended into the Wordiekammen Formation and that the breccia pipe adjacent to Locatity 5 could have been affected by this cave system. The reasoning is that dissolution would also have enhanced the fractures which could have led to the extensive cave system. It should however be emphasized that further studies should be made at this locality.

At Locality 1 a sharp contact in the stratigraphy with the underlying carbonate mudstone and the above lying breccia was observed. The contact marked the base of the brecciation. The strata below the contact were thinly (1-3) cm laminated to thicker (20 cm – 1 m) layers of black micritic limestone (ref. personal communication Walter Wheeler). The breccia above the contact is clast-supported with dusty matrix, with a dominant clasts size of 1-5 cm in diameter (ref. personal communication Walter Wheeler). This flat floor geometry is consistent with dissolution of a layer-parallel gypsum bed (Eliassen and Talbot 2005; Simpson 1988). At the base of the cave

the fill would consist of fine-grained, chaotic breccia with a large matrix content (Eliassen and Talbot 2005). The breccia at this site has these features, but has a heterogeneous composition in clast sizes and clast composition. Hence the Locality 1 consists of facies 5 of Loucks and Mescher (2001) facies classification which is fine-clast chaotic breccia; poorly to well sorted, matrix- to clast-supported, granule- to cobble-sized chaotic breccia. The clasts can be imbricated or graded and form ribbon- to tabular shaped bodies as much as 15 meters across and hundreds meter long. The fill has been transported either by mass flow or stream flow processes (Loucks et al. 2004), **Figure 1.8**. Following Loucks and Mescher (2001) classification the Locality 1 mark the base of the collapsed paleo-cave system of Locality 4 and the stratigraphically overlying Fortet. An agreement to this is that the brecciation extends laterally and updip along the coastal escarpment with brecciation of similar texture at locality three of the sampling, a distance of 260 m. Then the locality one and three would mark the bottom facies of this system. It should be emphasized that a more thorough interpretation should be done at these localities, but this is outside the scope of this thesis.

6.2 Area 1 - The Red breccia pipe

The Red Breccia pipe has been interpreted as a breccia pipe, as it is a steep-sided chimney-like feature. It is inferred to have been created by progressive upward stoping from a basal gypsum bed (section 1.2.4). The Red breccia pipe contains short distance transported infill, as the lithology of the infill has the same texture and color as the overlying layers of the Wordiekammen Formation. It can be assumed that the breccia pipe would have infill that reflects the overlying stratigraphy as it progrades upward. The interpretation is consistent with (Eliassen 2002). The classification of the outcropping facies was based upon Loucks and Mescher (2001), **Figure 4.6**. Only four of the facies were identified, **Figure 6.3**.

Classification of Paleocave Facies
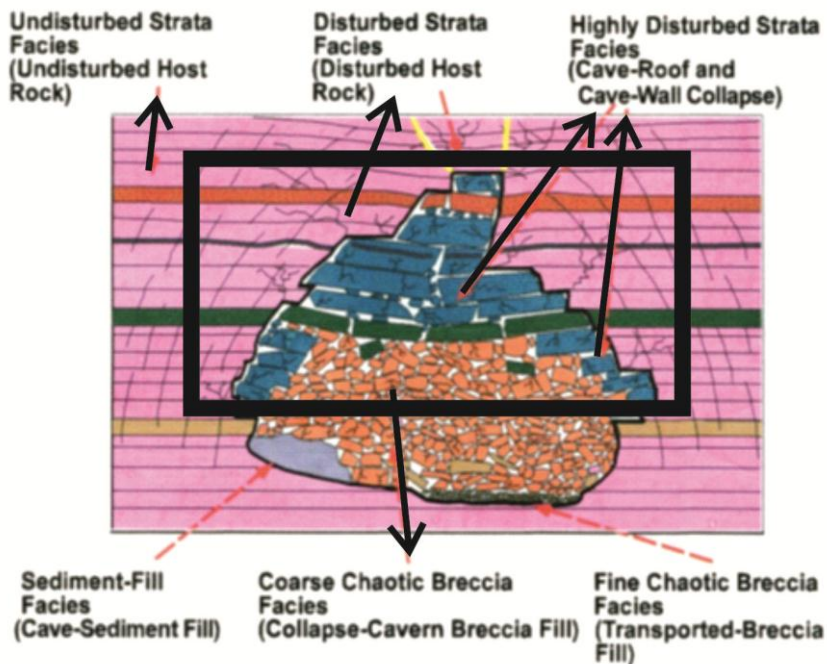
Figure 6.3: The figure highlights the facies used to interpret the breccia pipe, and indicates that only middle and upper facies were identified at The Red Breccia Pipe.

As no basal contact and no roof or sagging structures above the pipe were observed it is hard to estimate the height, The Red Breccia pipe extended through the stratigraphy. If breccia were dissolved by groundwater, the breccia pipe could have extended through the Wordiekammen Formation described in section 2.7. The overlying Gipshuken Formation represents a major regression event, leading to sabkha progradation (Section 2.7). As sabkha environment means restricted influx of water, the collapses might have stopped as the breccia fill could have reached the ceiling as indicated in the black square in **Figure 6.3**. Little is available to document the upward limit of the exposed breccia pipes, such as clasts from overlying formations as the breccia pipes within the study area have undergone considerable erosion.

The observations presented in this study show continuously brecciated stratigraphy between breccia pipe 1 and 2 **Figure 6.4**. Also, compared to Nordeide (2008), the area of breccia pipe

number 2 has been extended about 50 m further to the south. Within the about 50 meter zone, the localities of outcrop 2, 3, 5 and 7 were situated, **Figure 4.5.**

Figure 6.4: Overview of breccia pipes along the western side of Wordiekammen, starting at 1 in the North and ending at 9 in the South. The total area of the Red Breccia Pipe has been outlined with the black line. Photo interpretation is from Wheeler (2007, unpublished) and appeared in Nordeide (2008).

6.3 Petro-physical properties within The Red Breccia Pipe

The facies classification, in conjunction with burial history data has to be used to describe and predict pore type distribution and magnitude of reservoir quality. Pore networks associated with paleokarst systems are interclast pores, matrix pores (thought less common), crackle and mosaic breccia fractures (Loucks 2001). Visual estimations have been performed to estimate the porosity of the breccia bodies in the Billefjorden area by Lønøy (1995) and Nordeide (2008). Petrophysical experiments have been conducted and the aim here is to compare and correlate the results. The results will be compared with the classification of the outcrop sites with respect to Loucks and Mescher (2001), and to Noreide (2008).

6.3.1 Petrophysical characterization with respect to Loucks and Mescher (2001)

Table 6.1 compares the petrophysical values presented in Loucks and Mescher (2001) to values determined from measurements of samples taken from The Red Breccia Pipe (RBP). The RBP porosity values are similar to Loucks and Mescher (2001) averages porosity values for Disturbed and Undisturbed facies. Whereas, the facies Highly disturbed strata and Coarse-clast chaotic breccia, the RBP values are at the low end of the range of the porosity values inferred by Loucks and Mescher (2001). The RBP permeability values are far lower than average for all the facies except for Disturbed strata, which is within the Loucks and Mescher (2001) range. However, the samples were typically small as they cracked during sampling, and often the dense and cemented part remained. Therefore the RBP data may not be representable for the whole outcrop. As the infill in RBP is interpreted as short transported material from the overlying stratigraphy, the measured porosity values of the samples (Loc. 6, 9, 16) would reflect the porosity of undisturbed

strata. The macroscopic appearance of Highly disturbed strata and Coarse-clast chaotic breccia, indicate a much higher porosity than determined from the experiments. In the case that the samples under-represent the porosity and permeability the values proposed by Loucks and Mescher (2001) could be applied.

Table 6.1: Summary of paleocave facies and their correlative petrophysical properties from (Loucks and Mescher 2001). Petrophysical results of porosity and permeability from The Red Breccia Pipe (RBP).

Loucks et al. 2001 facies classification	Pore System/Reservoir Quality	Petrophysical Results From RBP.
1 Undisturbed strata	Fracture pores and minor matrix Ø < 3 & to 5 % K < a few millidarcys	Sample taken from this facies was nr. 6 Ø = 5.52 %, K < 1 mD
2 Disturbed strata	Fracture pores: Crackle to mosaic. Minor matrix Ø < 5 % , K < tens of millidarcys	Sample taken from this facies was nr.9 Ø = 3.4 %, K = 3.8 mD
3 Highly disturbed strata	Pockets or layers of breccia that can have porosity in the range of 5-15 % K = tens to hundreds of millidarcys	Sample taken from this facies were samples nr. 16 and nr. 19 Ø = 1 - 5.3 %, K = 0-0.099 mD
4 Coarse-clast chaotic breccia	Abundant interclast pores. Porosity can exceed 20%, and permeability can be in the darcys	Sample taken from this facies were samples nr. 14, nr. 15.1 and nr. 15.2 Ø = 3 - 5.97 %, K = 0.00163- 4 mD
5 Fine-clast chaotic breccia	Abundant interclast pores. Porosity can exceed 20%, and permeability can be in the darcys	The facies was not observed within The Red Breccia Pipe, thus no samples collected.
6 Cave-sediment cavern fill	Siliclastic fill is commonly tight, but the carbonate fill might be permeable.	The facies was not observed within The Red Breccia Pipe, thus no samples collected.

The permeabilities determined through water flow measurements, indicate a low permeability in the whole of RBP. Many cores broke during drilling and nearly all samples crumbled partially or completely. Thus the cores recovered represent the densiest and best cemented part of the samples. It is not surprising that they typically have lower permeability. Furthermore, large void space (0.1 > 1.5 cm) within the samples was observed during cutting. But since the core plugs were just 1 inch in the diameter, the void space would cross cut the core plug, and a shorter length of a core plug was attained.

The measurements showed that there were few interconnected pores, thus low porosity and permeability, and the lithology of the breccia samples consist short transported clasts from the surrounding the strata of the RBP (section 4.2). Hence, the strata surrounding the breccia pipes would have a low reservoir potential unless brecciated and fractured.

The RBP is inferred to have greater permeability than measured in the petrophysical experiments as the figures (sub-chapters; 5.2.1 to 5.2.5) characterize the localities with high density of

fractures and a higher matrix content than none of the collected samples showed. The loosely packed sediment, especially from location 13, 15 and 18 made it difficult to sample a representative volume at these outcrop locations. Not as great as in the Darcys at any of the localities, but hundreds of millidarcy are possible **Table 6.1**. The fractures observed at the outcrop sites could have been enlarged by frost wedging and during uplift. However the observations indicate that the fractures observed within the breccia pipe would be present in the subsurface as well, but not as large.

Figure 6.5 shows an interpretation of how far the separate facies locations extended in the vertical direction within the RBP. The interpretation is based upon the classification of the outcrop sites and an approximation of how far the outcrops extended in a cross-sectional view and in the North - South direction. As the breccia pipe would protrude through the stratigraphy in a chimney-shaped manner, the interpreted brecciation would produce the facies as indicated in **Figure 6.5**. Undisturbed strata would mark the outer edges of the breccia pipe, then Disturbed strata, so on to Highly disturbed strata before the facies Coarse-clast chaotic breccia would mark the innermost zone of the pipe.

Figure 6.5 is location dependent, as **Figure 6.6** shows that the cross section would not intersect similar breccias in all directions if moved or rotated. However, more of the facies 2 (Distured strata) might have been surrounding the pipe, but due to erosion exposed outcrops of facies 2 were only observed in the southern side of the RBP. **Figure 6.6** also illustrates the field-based inferrence thate facies 1 (Undisturbed strata) is more fractured than described by Loucks and Mescher (2001).
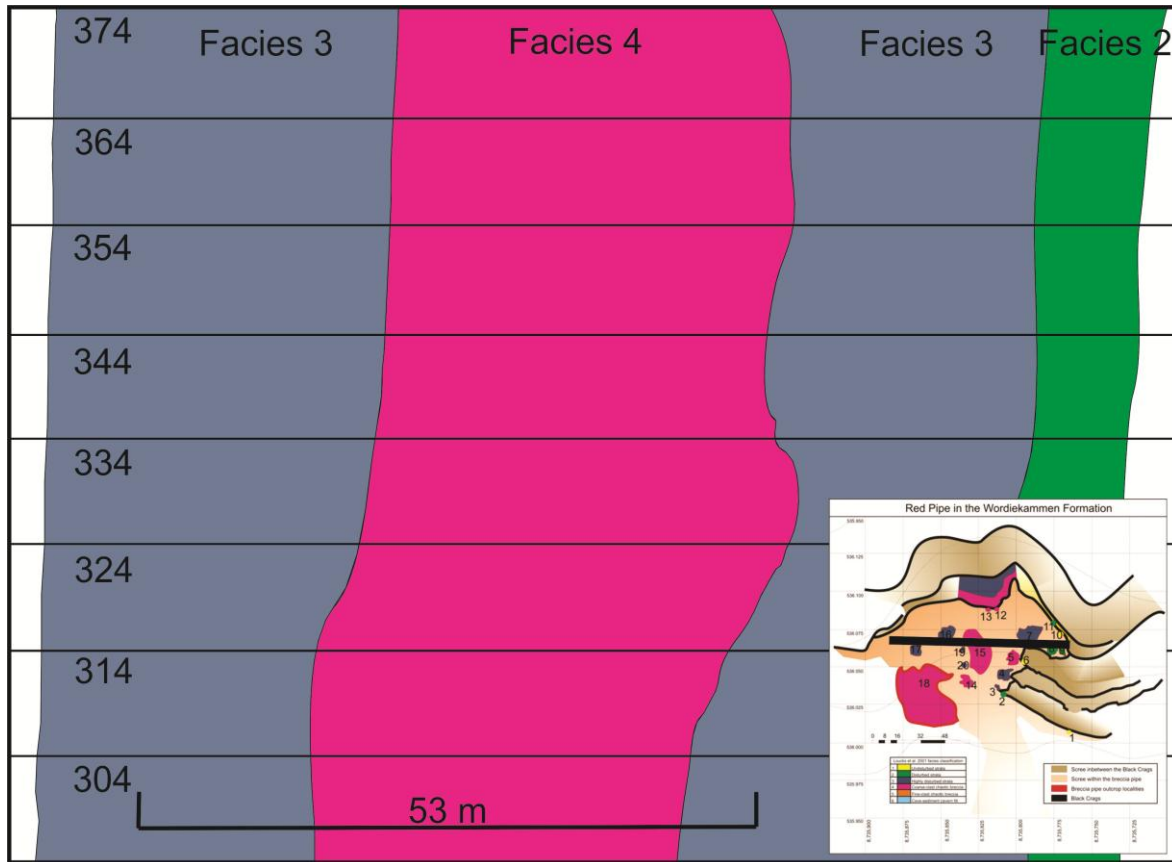
Figure 6.5: Cross-section of the RBP made with an interpreted extension of the facies classification. The picture to the lower right indicates where the interpreted coss-section intersects.
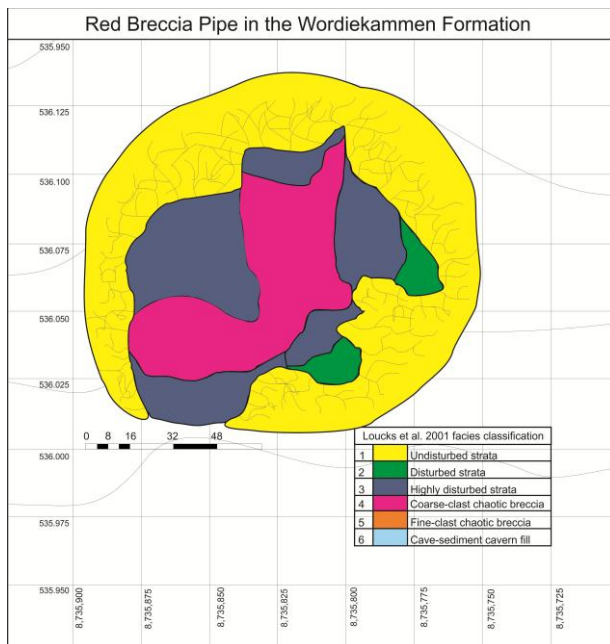
Figure 6.6: Interpretation of the extent of the facies in a horizontal cross-section. The figure is a modified figure of Figure 4.7.

6.3.2 Petrophysical characterization with respect to Noreide (2008)

Nordeide (2008) proposed a facies classification (section 2.10) for the breccia bodies in Northernmost Billefjorden. The facies classification had a basis in the Loucks and Mescher (2001) facies classification. In Nordeide`s (2008) facies classification, three of the uppermost facies (Disturbed strata, Highly disturbed strata and Coarse chaotic breccia) from a collapsed cave, from Loucks and Mescher (2001) were developed in order to correlate to the breccia pipes. The included facies from Loucks and Mescher (2001) into the classification scheme by Nordeide (2008) correlates well with the interpretation of the Red Breccia Pipe, as it was showed in section 6.2 that 4 of Loucks and Mescher (2001) facies were used to classify the outcrop sites and 3 of the same facies was used in Nordeide (2008) as well.

The **Table 6.2** shows the petrophysical properties of the breccia pipe estimated for each facies by Nordeide (2008) give generally much higher values than the values gained from the experimental work. The estimated porosities under Pore Systems/ Reservoir Quality are generally too large, compared to the results gained from the experimental work. Based on the experimental work, the void space creating the pore space will also be within the fractures. As this would be considered a fractured reservoir, the porosity will be low whereas the permeability would be much higher.

Table 6.2: Summary of Breccia pipe facies and their correlative petrophysical properties, from Noreide (2008). Petrophysical results of porosity and permeability from The Red Breccia Pipe (RBP).
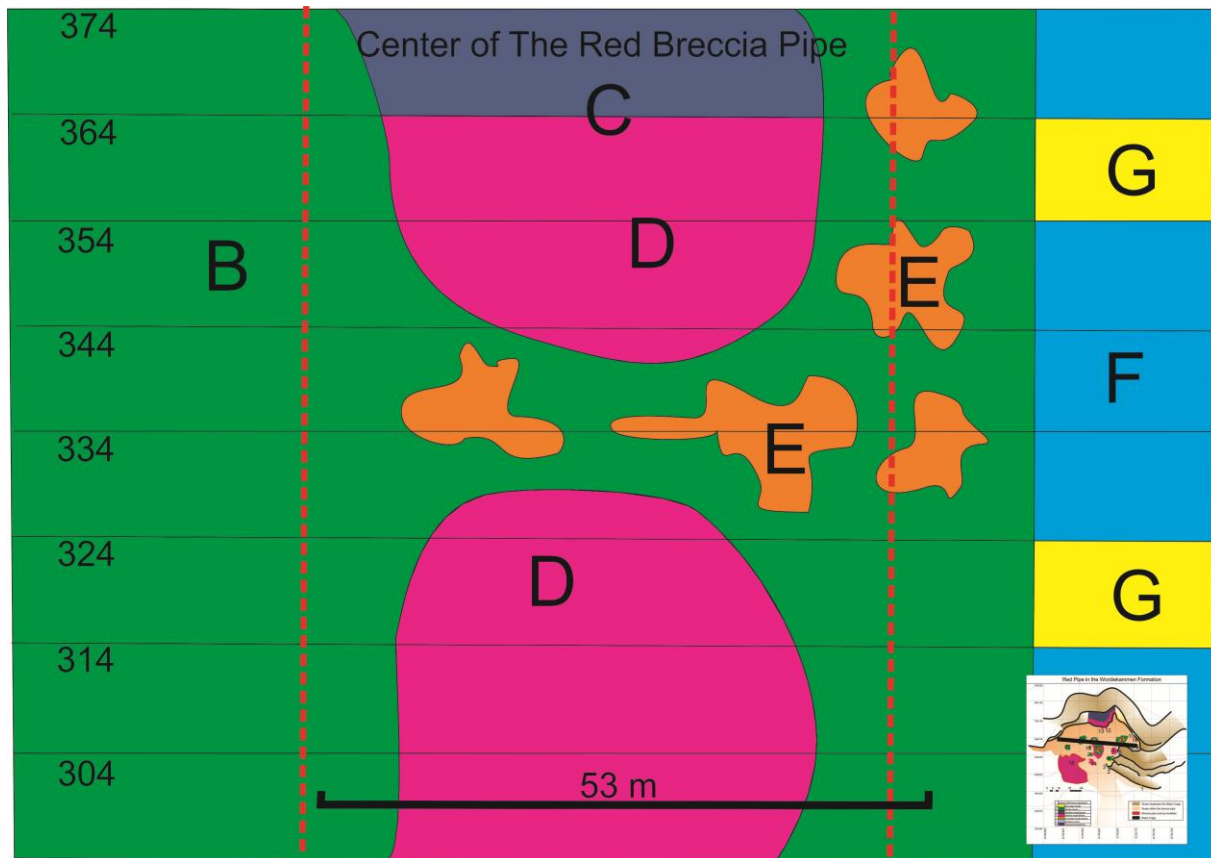
Noreide (2008) facies classification			Pore System/ Reservoir Quality	Petrophysical Results From RBP.
A		Brecciated micrite	Brecciated micrite is in situ breccia, minor displacement fo clasts. Permeability differs a lot. Ø = 2 - 20%, K = 0 - 10 mD	No samples collected from this facies.
B		Micritic breccia	Coarse gravel-sized clasts with little or no matrix. Ø = 25 - 35 %, K = 100 - 1000mD	Samples taken from this facies were samples number 15.1, 15.2, 16 and 19. Ø = 1 - 5.3 %, K = 0.0 - 0.099 mD
C		Stratified mixed breccia	Mixture of large blocks and sand-sized matrix (10% of total volume). Clasts exhibit fissures. Ø = 15 %, K = 10 -20 mD	No samples collected from this facies.
D		Massive mixed breccia	Approximately the same as facies C, but less stratified. Clasts are smaller and higher matrix content. Ø = 10-15 %, K = 5-15 mD.	Sample taken from this facies was sample nr.14. Ø = 5.97 %, K = 0.84 mD
E		Cemented micritic breccia	No values given	Occurs in small zones, mixed with other facies. Observed mixed with facies B.
F		Stratified micrite	Consists of micrite. Ø = 0 - 0.9 %, K = 0 - 0.9	Sample taken from this facies was sample nr.9. Ø = 3.4 %, K = 3.8 mD
G		Wackestone/packstone	Poorly sorted wackestone/packstone. Inner shelf deposits. Ø = 10 - 15 %, K = 20- 40 mD	Sample taken from this facies was sample nr.6. Ø = 5.52 %, K = 0.009 mD

The experimental work just measured the permeability through a solid core plug. The measurements on the matrix of the clasts did in most cases not yield any permeability at all. Only the rocks that fractured under measurement gave permeability with some reservoir potential. The tiny permeability gave a higher permeability, and higher permeability is assumed due to the observations made during field work. On the other hand, as the outcrop has experienced uplift and exhumation, as well as frost wedging during the winter time. The estimated permeability made for facies B and facies G should be lower than given under Pore system/Reservoir Quality, **Table 6.2**.

By using the facies classification by Nordeide (2008), more internal facies changes within the RBP could be identified and distinguished. The general trend of the facies were Stratified micrite (F) and Wackestone/packstone (G) being the undisturbed wall rock. The Brecciated micrite (A) lies adjacent to the breccia pipe and can indicate of being the highly fractured wall surrounding the breccia pipe. The micritic breccia (B) is situated at the outskirts of the breccia pipe. The micritic breccia (B) is also observed closer to the center of the breccia pipe, but then in a mix with cemented micritic breccia (E). The middle part of the RBP mainly consisted of massive mixed breccia (D). Towards the top of the RBP, the facies stratified mixed breccia is situated. The Brecciated micrite (A) was observed in the lower cliffs of the Black Crag beds adjacent to the Red Breccia Pipe outcrop. There were however some difficulties in distinguish some of the facies, due to poorly facies descriptions, this was especially the case for facies A and B.

The interpretation made in Nordeide (2008), **Figure 6.8 ii.** is partly in agreement with the classification made in this thesis of the RBP. A vertical cross-section of the RBP was made based upon the facies classification proposed by Nordeide (2008), **Figure 6.7**. The interpretation indicates the facies B occurred in a greater extent than indicated in **Figure 6.8 ii.** as it was only proposed as a thin lining around the pipe. In Nordeide (2008) it was stated that oil saturated clasts were observed in facies B. The observation is in agreement with the observations made of RBP. The outcrop locations 7, 20 and the upper part of 15 had an oil odor, they were all classified as facies B. The only other place with an oil odor was location 14, classified as facies D. The facies C and D are indicated as composing the center of the RBP, **Figure 6.7**. And Facies B would be a larger part of the outskirts of the RBP. Although facies E is observed within the facies

B, the permeability would not have been completely occluded by cementation overall, as indicated in **Figure 6.7**.

Figure 6.7: Cross-section of the Red Breccia Pipe. Interpretation of the extent the facies within the breccia pipe have, using Noreide (2008) facies classification. The total area covers outcrop locations within the Red Breccia Pipe, as indicated in the map to the lower right.
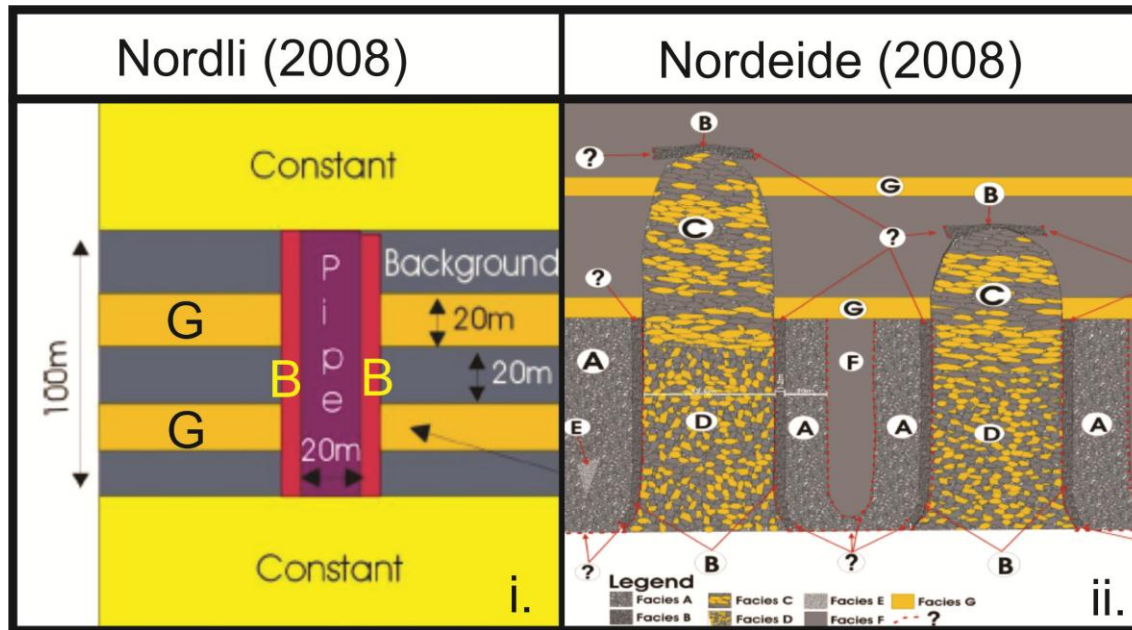
Figure 6.8: i. The figure is from Nordli (2009) and is of reservoir test 7, which was the test model which reflected the Red Breccia Pipe best. ii. The general trend of the breccia pipes, figure is not to scale (Nordeide 2008).

In Nordli (2009) a reservoir simulation of a karst reservoir with collapse features such as a breccia pipes. The simulation was performed based on the petrophysical values estimated in Nordeide (2008). Several tests were performed, and the test model 7 was the one best reflecting the interpretation of the RBP, **Figure 6.8 i.** which was one of the more stratigraphic complex models. The reason why test seven reflected the RBP was due to a high permeable lining (Facies B) surrounding the pipe interval, several cross-cutting layers of the facies G was included. An average value of the facies C and D had been taken and is indicated as Pipe in **Figure 6.8 i.**. As **figure 6.7** shows, the diameter would be greater than the diameter used in the simulation.

The facies B would probably yield lower permeability than used in the simulations as the permeability used here was 3 Darcy, which was three times higher than the estimated value given in Nordeide (2008). As stated, the estimated permeability was probably too high and values in the range of tens to hundreds of millidarcys are probably more likely.

Simulations performed by Nordli (2009) were based on the data available. Future simulations should take these factors into account;

- A karst reservoir is mainly a fractured reservoir, which yield low porosity and high permeability. Wells should be placed in order to optimize production from high fracture

zones such as breccia pipes, as the un-fractured carbonate rock would yield low reservoir potential.

- As the experimental measurements showed, all the samples from the RBP gave low porosities. The clasts of the samples reflect the lithology of the overlying stratigraphy as the samples were transported into a void space below. To set the porosity parameter for the undisturbed wall rock to any greater than 5 % would be too high. Un-fractured carbonate wall rock would have greater seal potential rather than a reservoir potential.

- A correct estimation of the relative permeability requires correct estimation of the relative thickness of the lining and the pipe (Nordli 2009). The **Figure 6.7** and **Figure 4.6** indicates that it would be hard to estimate the thickness of the lining and the pipe, as the thickness of the different facies differs in x,y and z direction.

6.4 Area 2

By Wordiekammen Formation times the basin flanks of the Billefjorden basin were submerged and experienced open marine deposition (Braathen et al. 2011; Pickard et al. 1996). The faults of the basin were mildly reactivated and the faulting could have been thermally driven, controlled by differential compaction of the basin fill, and/or compaction and removal by dissolution could also explain the faulting (Maher and Braathen 2011). The Area 2 breccia location was in the area where a local monocline onlapped the Black Crag Beds (Maher and Braathen 2011). As previously inferred the faulting is believed to be partly due to removal by dissolution.

The samples Q1 and Q2 were sampled from the Black Crag Beds, whereas the sample 1M was sampled from the scree below. The 1M was sampled in the scree of the Minkinfjellet Formation, below the Black Crag beds. Since 1M`s exact location is uncertain, the samples Q1 and Q2 will be emphasized further. The Black Crag Beds are here inferred as of crackle and mosaic breccia, and the composition of the samples reflected the composition of the outcrop. The void space between the crackle and mosaic breccia are filled in with cements. The clasts are also cross-cut by fracture lines, which are also filled in with cements. The large degree of cements are interpreted been precipitated during thermal conditions due to burial. As gypsum beds of the

Minkinfjellet Formations would be altered to anhydrite during burial and water subsequent being released, the water would have flushed through the void space in the overlying breccia stratigraphy. Although the samples fractured easily during sampling, the cements within the pore space could occlude the void space as the breccia body, **Figure 6.9**. Due to burial the weight of the above lying stratigraphy would compress the underlying layers. However as **Figure 6.9** shows are that not all of the fractures filled with cements, some cross-cut the sample. These might have occurred during cutting of the samples, but some are assumed to be a natural part of the sample when sampled from the outcrop site. The porosity of the samples was an average 4.4 ± 1% for Q1 and 2.0 ± 0.3 % for Q2. . The sample Q1 gave a permeability of 6.6±0.7 mD, whereas the Q2 had a permeability of 0.005±0.001 mD. The sample Q2 had a more crushed texture at places and was overall more compacted. This sample was sampled closer to a fault core, and had more compact and crushed texture than Q1. The porosity of the samples lies within the fractures, and the location is interpreted to give low porosity but high permeability. Based on the visual observations, the location could yield tens of millidDarcys. However, the vertical permeability alters much likely around a monocline, as a fault core would yield lower permeability.
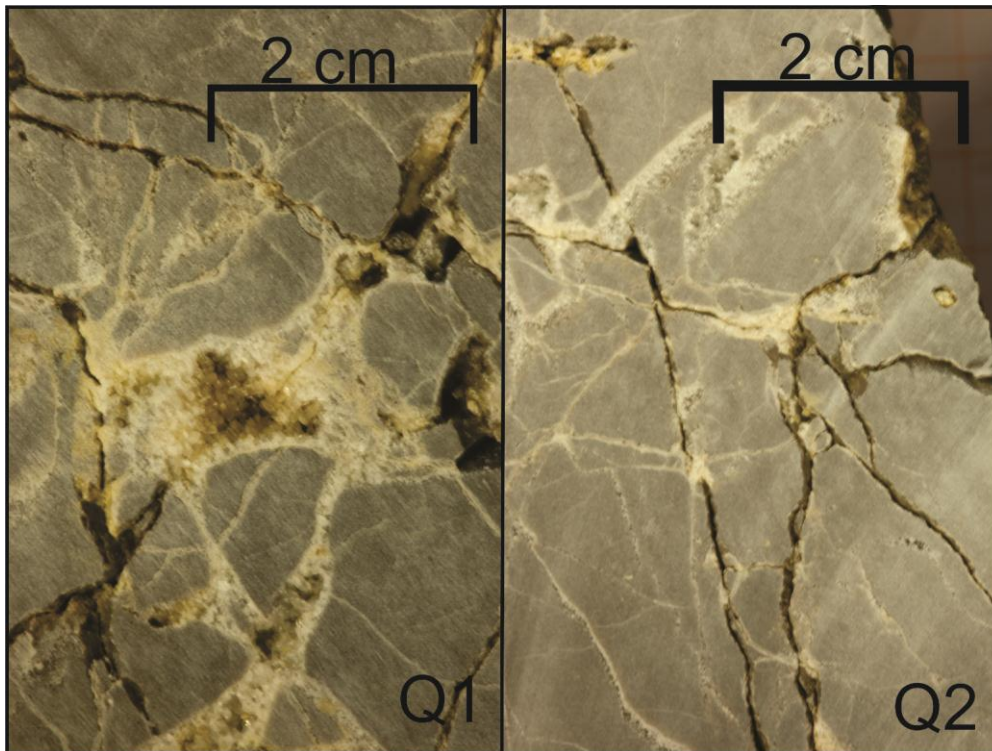
Figure 6.9: The pictures of the samples Q1 and Q2 shows how much cements have filled the void space. Q1 is the sample to the left and have a higher degree of cementation than Q2 to the right.

6.5 Area 3

Although the Area 3 concists of a wide range of breccia composition, it is here inferred that they are all connected in a collapsed paleokarst system (section 6.1). The petro-physical results gave generally the highest porosity and permeability compared to Area 1 and Area 2.
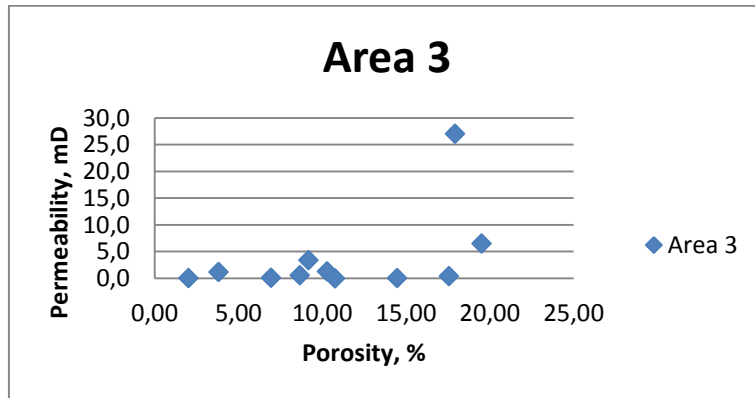
Graph 3: Porosity and permeability measurements from Area 3.

At the Locality 1, the sample 1C marked the base of brecciation and the sample had no permeability. The upper part of the sample yield as high porosity as 10-11%, whereas the lower part of the sample yield porosity around 2%. As this section marked the base of brecciation and was a part of an unbrecciated stratigraphy, the values indicated that the unbrecciated beds below the brecciated section within the Minkinfjellet Formation yield no reservoir potential.

The sample 1B was sampled in the thin transition zone between the unbrecciated and brecciated stratigraphy. The sample yield high porosity and permeability, where core plug 2 (1B) had as high porosity as 18±2 and a permeability of 27±8. The zone is very thin, however the sample 1A have also high porosities with an average porosity 13 ± 5 %. The permeability for two of the core plugs was around zero millidarcy, however the core plugs was often from the most compacted and cemented parts. The core plug from sample 1Ac had a permeability of 6.5 ± 0.4 mD. Based on these measurements the brecciated part of this location would probably yield a permeability of tens of millidarcys and porosities in the range of 10 - 20 %. Some variations would occur due to differential cementation within the section.

The locality 3 lay along the coastal escarpment and has been inferred here as consisting of the same facies as at locality one (Fine-clast chaotic breccia). However the locality showed a more extensively degree of dissolution with around 40 % of vuggy pore space (visually estimated). The porosity of these samples was in the range of 7 % to 17 %. The porosities of the samples varied

due to the density of the vuggy pore space. From both the core plugs the permeability was less than 1 mD. The permeability might be higher where there are touching vugs, but due to the small diameter (1 inch) of the cores, only the most compacted cores were drilled out. As stated in Lucia (1999) most of the reservoir potential pore space would be located within the matrix, creating a bimodal pore system where most of the storage is in the matrix and most of the flow capacity is within the vug system. Lucia (1999) further states that the petrophysical properties of touching-vug reservoirs are difficult to characterize because of the size and shape of the vugs are often larger than those of the core plugs. The porosity of locality three is estimated to be in the range of 7 – 17 %, whereas the permeability is hard to estimate based on the laboratory results alone.

In a higher stratigraphic level lay location 4, standing up as a pinnacle in a scree covered slope. The sample 4 that was taken from this locality appeared to have 80 % of the sample consisting of micritic limestone clasts (1-7 cm). During cutting, the sample reviled to have higher matrix content. For the permeability and porosity testing a core plug, containing a high degree of matrix were used as the flow would rather go through the matrix than solid limestone clasts. The porosity was higher for the core plug than the sample, as the core plug also had vuggy pores. The highest porosity gained was 9.19±0.65 % and the permeability was 3.41±0.02 mD. A reason why the core plug did not give any higher permeability can be due to cementation. The reason is that the location 4, stands up like a pinnacle and all the stratigraphy that have been surrounding the pinnacle has been eroded away. This indicates that to withstand the erosion, the strata are more cemented. The locality will here be inferred to be classified as Fine-clasts chaotic breccia since the breccia showed structures as if the breccia has been transported. The assumed petrophysical values for this locality would be in the range of 10 – 20 % and with permeability in the range of 5 – 100 mD. The reason why an estimation of the permeability is not higher is because the risk of cements occluding the pore space.

At an even higher stratigraphic level within the Wordiekammen Formation, the location 5 lay adjacent to a breccia pipe. Two samples were collected at this locality and the porosity values from the samples were in the range of 4 – 5 %. The samples are classified as crackle breccia and the pore space are within the fracture zones of these samples. Several of the voids between the clasts had been occluded with cements, and the porosity would be within the clasts matrix. However the permeability could can be quite high. Only one permeability value was gained,

1.16±0.09. The permeability at the location would be higher as there were open fractures cross cutting the samples. As the samples were collected in the wall adjacent to a breccia pipe, the facies "Distured Strata" would apply for this location. The porosity of this location is assumed to be > 5 %, whereas the permeability could be in the darcys.

6.6   Reservoir potential

All the measured petrophysical results from Area 1 and Area 2 gave porosities values > 10 % and permeability values > 7 mD. The brecciated clasts within these areas are of the same lithology as the Wordiekammen Formation. The low porosity and permeability indicates that the unbrecciated host rock of Wordiekammen formation would have low reservoir potential. However it would have a higher seal potential.

The samples (1, 2 and 4) from Area 3 gave measured petrophysical values in the range of 2 – 20 % porosity and permeability in the range of 0- 27 mD. The composition of these breccia samples are of clasts originating from both the Minkinfjellet and Wordiekammen Formations. The host rock at these localities might have higher porosities and permeabilities, as the deposits are of the Minkinfjellet Formation (Section 2.6). This could indicate connectivity and a reservoir potential within this formation. However the connectivity within the Minkinfjellet Formation is uncertain in our study area because it was covered by talus and only the brecciated member of the formation was observed.

Based on the characterization of the breccia bodies, the petrophysical results and the field observations, the facies classification made by Nordeide (2008) has been modified. The proposed petrophysical values have also been modified based on the measured values and field observations.

Table 6.3 includes also Loucks and Mescher facies classifications bottom facies of a collapsed cave system. The reason for this is because the localities along the coastal escarpment at Rudmosepynten (Area 3) can be classified as Fine-clasts breccia. The permeability values are not based on the measured but based on visual estimations during the fieldwork.

As the proposed table indicates the reservoir can be classified as a fracture reservoir, where the porosity is low and the permeability is high 1 Darcy. Whenever the breccia bodies are connected, the reservoir potential within the study area can be quite large **Figure 6.1**. Oil odor was observed

in The Red Breccia Pipe, this could indicate that the breccia pipe just acted as a migration path, as the brecciation can have significantly impact on the seal integrity. However the unbrecciated host rock of the Wordiekammen Formation could act like a seal if we infer that the breccia pipes had an upper limit within the carbonate host rock. Then the connectivity would be connecting layers between the breccia bodies. In Noreide (2008) it was proposed that facies G would act like a connecting layer. Whereas the observations of the layer classified at facies G in The Red Breccia Pipe indicated that the fractures within this layer decreases with the distance from the breccia pipe, hence further studies should be executed to establish the fracture density within this area.

Table 6.3: New proposed facies classification for the breccia bodies in Billefjorden, incorporating the classifications of Loucks and Mescher (2001) and Nordeide (2008), and the measured and estimated values from the petrophysical experiments in this thesis.

Facies classification		Description	Pore System/ Reservoir Quality
A	Brecciated micrite	Bedding continuity is high but folded and offset by small faults. Commonly overprinted with crackle and mosaic breccia. Clasts sizes are 2-10 cm. Color is grey and red.	$\varnothing < 8\ \%$, $K < 10\ mD$
B	Micritic breccia	Highly fractured and commonly overprinted by faulting Little or no matrix. Coarse gravel to coarse crackle breccia clast	$\varnothing < 5\ \%$, $K < 1000\ mD$
C	Stratified mixed breccia	Mixture of large blocks and sand-sized matrix (10% of the total volume). Clasts exhibit fissures. Very discontinously bedded strata with pockets and layers of chaotic breccia.	$\varnothing = 5\ \text{-}10\ \%$, $K = 0\ \text{-}\ 15\ mD$ Pockets with higher petrophysical values might occur
D	Massive mixed breccia	Approximately the same as facies C, but less stratified. Clasts are smaller and the matrix content is higher.	$\varnothing = 5\ \text{-}\ 10\ \%$, $K = 0\ \text{-}\ 15\ mD$ Pockets with higher petrophysical values might occur.
E	Cemented micritic breccia	The cements fill the pore space between crackle to chaotic breccia. The cement can also fill the cross-cutting fracture lines.	$\varnothing < 5\ \%$, $K = 0\ mD$
F	Stratified micrite	Consists of micrite. Excellent bedding continuity for tens to hundreds of meters may occur.	$\varnothing < 4\ \%$, $K = 0\ mD$ Areas with larger permeability might occur.
G	Wackestone/ packstone	Poorly sorted wackestone /packestone Inner shelf deposits	$\varnothing < 5\ \%$, $K = 0\ \text{-}\ 40\ mD$
H	Fine-clast chaotic breccia	Mass of clasts- supported, moderately sorted, granule- to cobble-sized clasts with varying amounts of matrix.	$\varnothing = 10\ \text{-}\ 20\ \%$, $K = 0\ \text{-}\ 100\ mD$
I	Cave sediment cavern fill	Consists of fine silt- to granule-sized sediments that contain less than 10 % granules, and are carbonate and/or siliclastic debris.	No values attained
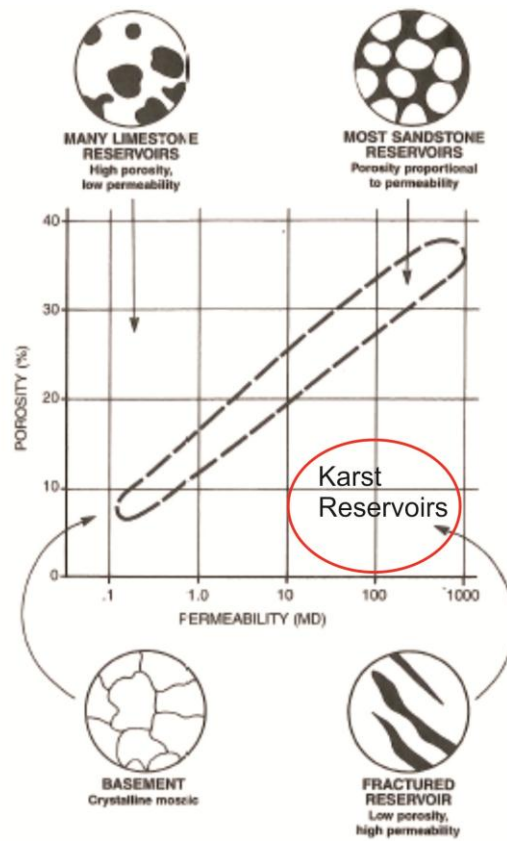
Figure 6.10: Proposed in what area a karst reservoir would lay in comparison to other hydrocarbon reservoirs. Here is karst inferred to be collapse breccia in brittle rock indicated by the red circle. The figure is from (Selley 1985).

7   Conclusion

Field mapping and samples collected from the breccia bodies on Wordiekammen in the northernmost Billefjorden Basin documented a variety of breccia facies characteristic of stratiform breccias in the Carboniferous Minkinfjellet Fm., and collapse- and inferred transported breccias in the Minkinfjellet Fm. and overlying Carboniferous Wordiekammen Fm.

The facies classification presented herein is more detailed than that of Nordeide (2008). My facies classification is made for the study areas, and should be extended to include all the observed facies as proposed in **Table 6.3**. The included measured and estimated values showed that the breccia would create a fracture reservoir.

The samples collected from the breccia bodies in the Northernmost Billefjorden gave low permeability and low porosity through core plug analysis. Based on the low measured porosities and observed fracture permeability, the breccia bodies classified as fracture reservoirs yield low porosity and high permeability. The breccia pipes are interpreted to be caused due to gypsum dissolution and are directly linked to the amount of gypsum deposited within the basin of the Billefjorden Trough. The formation of breccia pipes are due to point sourced of main dissolution of gypsum and anhydrite, and the breccia pipes lines up with the NNW-SSE faulting pattern in the area.

The formation of breccia bodies is inferred to be a part of a connected paleokarst gypsum system. Several mechanisms have influenced the production of breccia bodies in the area. In this model, at Area 3, the extensive brecciation is due to a system of inter-connected caves developed within the Minkinfjellet and lower Wordiekammen Formations.

The results showed that the unbrecciated stratigraphy in the area would have no reservoir potential due to the low porosity of the micritic limestone. However, the stratiform breccia bodies would yield low porosity, but high permeability. The results of the permeability is due to the field observations and tiny permeability values and not on the core plug testing as the permeabilities were small mainly due to cementation

8 Further work

The continuity of fractures should be studied to constrain inter-pipe connectivity. For example, Facies G was proposed as the pathway for fluids connecting the breccia bodies together. The fracture density within this facies should be studied to see if it has a continuation all the way between the breccia bodies within the area.

A correlation value for the tiny permeability and flow measurement regarding breccia deposits should be established. By having a correlation value, the "true" permeability of the breccia deposits could be calculated during fieldwork.

Studies of the locations within Area 3, with a particular focus on the breccia deposits along the escarpment at Rudmosepynten. The aim of this would be to establish if there are genetic relationships between the breccia deposits along the Rudmosepynten escarpment and the breccia bodies situated higher up in the stratigraphy in the Fortet area, as it has been inferred here.

In this thesis the sampling of the samples extended over a large area and of a wide range of breccia deposits. Further studies should choose a smaller area, and take more samples from one location. By doing this the petrophysical results from one locality can be evaluated and compared. Thin sections and cement characterization should be performed on each of the sample in order to gain knowledge of the timing of the cementation. Which means, at what burial depth it might have occurred and the type of depositional environment. A more detailed study will make experimental work more reasonable as well since by performing studies of thin sections, samples best suited for petrophysical experiments can be determined.

9   References

Aase, M., (2006): Sedimentology and sequence stratigraphy of the black crag beds (upper carboniferous) central spitsbergen, Master Thesis, Department of Earth Science, University of Bergen, 163 p.

Amyx, J. W., Bass, D. M., and Whiting, R. L., (1960): Petroleum reservoir engineering - physical properties, McGraw-Hill New York, USA,

Anderson, W., (1987): Wettability Literature Survey Part 5: The Effects Of Wettability On Relative Permeability, Journal of Petroleum Technology, v. 39, no. 11, p. 1453-1468.

Braathen, A., Bælum, K., Maher Jr, H., and Buckley, S. J., (2011): Growth of extensional faults and folds during deposition of an evaporite-dominated half-graben basin: the Carboniferous Billefjorden Trough, Svalbard, Norwegian Journal of Geology, p. 137-160.

Buckley, S., Vallet, J., Braathen, A., and Wheeler, W., (2010): Oblique helicopter-based laser scanning for digital terrain modelling and visualisation of geological outcrops.

Buckley, S. J., Howell, J. A., Vallet, J., Wheeler, W., and Braathen, A., (2008): Oblique helicopter-mounted lidar combined with ultiresolution modelling for the creation of high resolution, wide-area virtual geological outcrops, Abstracts: Annual Meeting - American Association of Petroleum Geologists.

Chilingar, G. V., Mazzullo, S., and Rieke, H. H. e., (1996): Carbonate reservoir characterization: a geologic-engineering analysis, Elsevier Science,

Cutbill, J. L., and Challinor, A., (1965): Revision of the stratigraphical scheme for the Carboniferous and Permian Rocks of Spitsbergen and Bjomoya, Geological Magazine, v. 102, no. 5, p. 418-439.

Dallmann, W. K., Gjelberg, J. G., Harland, W. B., Johannessen, E. P., Keilen, H. B., Lønøy, A., Nilsson, I., and Worsley, D., (1999): Upper Palaeozoic Lithostratigraphy. In Lithostratigraphic Lexicon of Svalbard. Review and recommendations for nomenclature use. Upper Palaeozoic to Quarternary Bedrock, Norsk Polarinstitutt, Tromsø, p. 25-126.

de Boer, J. P., Kalstø, E., Slotnæs, K., Mundal, E., and Dalva, A., (2011): Pyramiden Petroleum - Prospect application, Unpublished Report, UNIS.

Eliassen, A., (2002): Sedimentological and Diagenetic Investigations of the Minkinfjellet Formation, Central Spitsbergen, Svalbard: With Particular Emphasis on the Origin and Evolution of a Large Paleokarst System, Dissertation for the degree of Doctor Scientiarum, University of Bergen.

Eliassen, A., and Talbot, M., (2003a): Diagenesis of the mid-Carboniferous Minkinfjellet Formation, central Spitsbergen, Svalbard, Norsk Geologisk Tidsskrift, v. 83, no. 4, p. 319-332.

Eliassen, A., and Talbot, M., (2003b): Sedimentary facies and depositional history of the mid-Carboniferous Minkinfjellet Formation, central Spitsbergen, Svalbard, Norsk Geologisk Tidsskrift, v. 83, no. 4, p. 299-318.

Eliassen, A., and Talbot, M. R., (2005): Solution collapse breccias of the Minkinfjellet and Wordiekammen Formations, Central Spitsbergen, Svalbard: a large gypsum palaeokarst system, Sedimentology, v. 52, no. 4, p. 775-794.

Ford, D. C., Palmer, A. N., and White, W. B., (1988): Landform development; karst, Hydrogeology, Volume O-2, Boulder, Colorado, Geological Society of America

Ford, D. C., and Williams, P., (1989): Karst Hydrology and geomorphologgy, London, Unwin Hyman Ltd.,2007, 554 p.

Gjelberg, J., and Steel, R., (1981): An outline of Lower–Middle Carboniferous sedimentation on Svalbard. Effects of tectonic, climatic and sea level changes in rift basin sequences, Geology of the North Atlantic borderlands, p. 543-561.
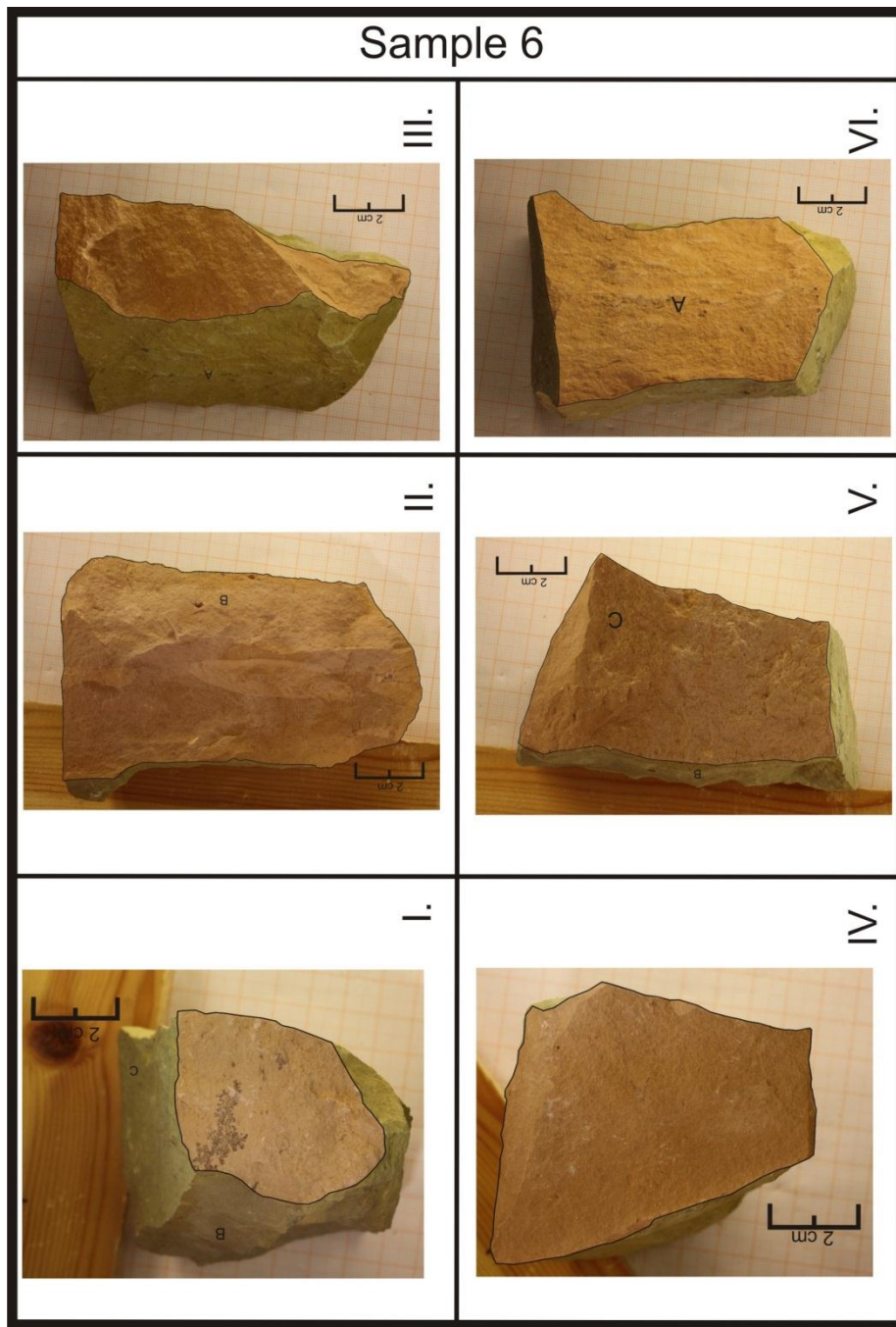
Gutiérrez, F., Guerrero, J., and Lucha, P., (2008): A genetic classification of sinkholes illustrated from evaporite paleokarst exposures in Spain, Environmental Geology, v. 53, no. 5, p. 993-1006.

Hammes, U., Lucia, F., and Kerans, C., (1996): Reservoir heterogeneity in karst-related reservoirs: Lower Ordovician Ellenburger Group, west Texas, Publications-West Texas Geological Society, p. 99-116.

Harland, W. B., (1997): The geology of Svalbard, London, Geological Society,

Johannessen, E., and Steel, R., (1992): Mid-Carboniferous extension and rift-infill sequences in the Billefjorden Trough, Svalbard, Norsk Geologisk Tidsskrift, v. 72, no. 1, p. 35-48.

Kerans, C., (1988): Karst-controlled reservoir heterogeneity in Ellenburger Group carbonates of west Texas: Reply, Aapg Bulletin, v. 72, p. 1160-1183.

Klimchouk, A., (2004): Published, Towards defining, delimiting and classifying epikarst: Its origin, processes and variants of geomorphic evolution, Volume 1, p. 23-35.

Lauritzen, Ø., (1981): Investigations of Carboniferous and Permian sediments in Svalbard, Norsk polarinstitutt,

Lien, J. R., (2004): Grunnleggende reservoarfysikk (kjerneanalyse og logging), Bergen, University of Bergen, p. 72.

Lien, J. R., and Løvhøiden, G., (2004): Generell fysikk, Universitetsforlaget, 400 p.

Loucks, R., and Mescher, P., (2001): Published, Paleocave facies classification and associated pore types, *in* Proceedings American Association of Petroleum Geologists, Soutwest Section, Annual Meeting, Dallas, Texas, p. 18.

Loucks, R., Ruppel, S. C., Contributors: Dembla, D., Julia, G., Holder, J., Kane, J., and Olson, J., (2007): Reviving Abandoned Reservoirs with High-Pressure Air Injection: Application in a Fractured and Karsted Dolomite Reservoir, Department of Petroleum Engineering, The University of Texas at Austin, p.83

Loucks, R. G., (1999): Paleocave carbonate reservoirs: origins, burial-depth modifications, spatial complexity, and reservoir implications, Aapg Bulletin, v. 83, p. 1795-1834.

Loucks, R. G., (2001): Modern analogs for paleocave-sediment fills and their importance in identifying paleocave reservoirs, Transactions-Gulf Coast Association of Geological Societies, p. 195-206.

Loucks, R. G., (2007): A review of coalesced, collapsed-Paleocave systems and associated suprastratal deformation The University of Texas, Austin, Bureau of Economic Geology, J. A., and K.A. Jackson School of Geosciences.-TIME in KARST, p. 121-132.

Loucks, R. G., and Handford, C. R., (1992): Origin and recognition of fractures, breccias, and sediment fills in paleocave reservoir networks, Publication - Society of Economic Paleontologists and Mineralogists, Permian Basin Chapter, v. 92-33, p. 31-44.

Loucks, R. G., Mescher, P. K., and McMechan, G. A., (2004): Three-dimensional architecture of a coalesced, collapsed-paleocave system in the Lower Ordovician Ellenburger Group, central Texas, Aapg Bulletin, v. 88, no. 5, p. 545.

Lowe, D. a. T. W., (1995): A Dictionary of Karst and Caves: A Brief Guide to the Terminology and Concepts of Cave and Karst Science. Cave Studies, London,Britain,

Lucia, F. J., (1999): Carbonate reservoir characterization: An integrated approach, Springer Verlag,edition 2007, 336 p.

Lønøy, A., (1995): A Mid-Carboniferous, carbonate-dominated platform, Central Spitsbergen, Norsk Geologisk Tidsskrift, v. 75, p. 48-63.

Maher, H. D. J., and Braathen, A., (2011): Løvehovden fault and Billefjorden rift basin segmentation and development, Spitsbergen, Norway, Geological Magazine, v. 148, no. 1, p. 154-170.

Mazzullo, S., and Chilingarian, G., (1996): Hydrocarbon reservoirs in karsted carbonate rocks, Developments in Petroleum Science, v. 44, p. 797-865.
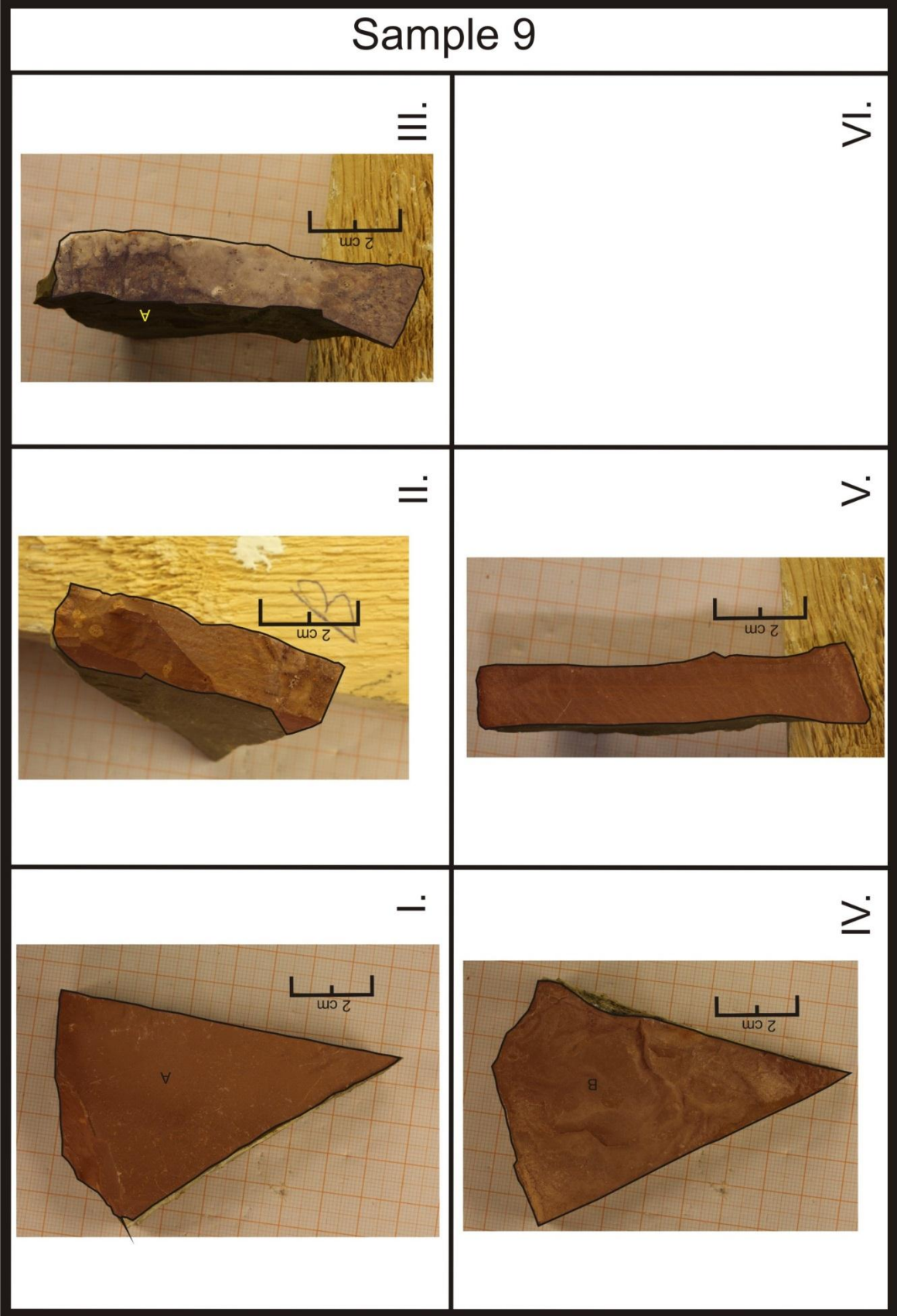
McCann, A. J., and Dallmann, W. K., (1995): Reactivation history of the long-lived Billefjorden Fault Zone in north central Spitsbergen, Svalbard, Geological Magazine, v. 133, no. 01, p. 63-84.

McDonnell, A., Loucks, R. G., and Dooley, T., (2007): Quantifying the origin and geometry of circular sag structures in northern Fort Worth Basin, Texas: Paleocave collapse, pull-apart fault systems, or hydrothermal alteration?, Aapg Bulletin, v. 91, no. 9, p. 1295.

McWhae, J. R. H., (1953): The Carboniferous breccias of Billefjorden, Vestspitsbergen, Geological Magazine, v. 95, p. 287-298.

Nordeide, H. C., (2008): Spatial distribution and architecture of breccia pipes features at Wordiekammen, Billefjorden, Svalbard, Master Thesis, Department of Earth Science, University of Bergen.

Nordli, C., (2009): Fluid Flow in and around collapsed karst structures; breccia pipes, in Petroleum Reservoirs, Master Thesis, Department of Physics and Technology/Department of Earth Science, University of Bergen.

Norsk-Polar-Institutt, http://www.npolar.no/no/.

Nøttvedt, A., Livbjerg, F., Midbøe, P., and Rasmussen, E., (1993): Hydrocarbon potential of the central Spitsbergen basin, Arctic Geology and Petroleum Potential, v. 2, p. 333-361.

Palmer, A. N., (1991): Origin and morphology of limestone caves, Bulletin of the Geological Society of America, v. 103, no. 1, p. 1-21.

Pickard, N. A. H., Eilertsen, F., Hanken, N. M., Johansen, T. A., Lønøy, A., Nakrem, H., Nilsson, I., Samuelsberg, T., and Somerville, I., (1996): Stratigraphic framework of Upper Carboniferous (Moscovian-Kasimovian) strata in Bünsow Land, central Spitsbergen: palaeogeographic implications, Norsk Geologisk Tidsskrift, v. 76, p. 169-186.

Quinlan Jr, J., (1978): Types of karst, with emphasis on cover beds in their classification and development, Doctor thesis, The University of Texas at Austin, 323 p.

Ramberg, I. B., Bryhni, I., Nøttvedt, A., and Rangnes, K., (2008): The making of a land: geology of Norway, Geological Society of Norway, 624 p.

Samuelsberg, T. J., and Pickard, N. A. H., (1999): Upper Carboniferous to Lower Permian transgressive–regressive sequences of central Spitsbergen, Arctic Norway, Geological Journal, v. 34, no. 4, p. 393-411.

Selley, R. C., (1985): Elements of petroleum geology, United States of America, Academic Press, An imprint of Elsevier,2nd edition, 1-463 p.

Simpson, F., (1988): Solution-Generated Collapse (SGC) Structures Associated with Bedded Evaporites: Significance to base-metal and hydro-carbon localization, Geoscience Canada, v. 15, no. 2.

Solbakken, J. S., (2010): An experimental study of low salinity surfactant flooding in low permeability Berea Sandstone, Master Thesis, University of Bergen.

Steel, R., and Worsley, D., (1984): Svalbard's post-Caledonian strata—an atlas of sedimentational patterns and palaeogeographic evolution, Petroleum geology of the North European margin, p. 109-135.

Stemmerik, L., and Worsley, D., (2005): *30 years on: Arctic Upper Palaeozoic stratigraphy, depositional evolution and hydrocarbon prospectivity*, Norsk Geologisk Tidsskrift, v. 85.

Sundsbø, G., (1982): Facies analysis of Late Carboniferous and Early Permian Carbonates in the Billefjorden area, Spitsbergen, Unpublished cand. real. thesis, n, Univerity of Bergen, 161 p.

Tebbutt, G. E., Conley, C. D., and Boyd, D. W., (1965): Lithogenesis of a distinctive carbonate rock fabric, Rocky Mountain Geology, v. 4, no. 1, p. 1-13.

Waltham, T., Bell, F. G., and Culshaw, M. G., (2005): Sinkholes and Subsidence: karst and cavernous rocks in engineering and construction, Springer verlag, 80-81 p.

Warren, J. K. e., (2006): Evaporites: sediments, resources and hydrocarbons, Springer Verlag, 1019 p.

White, E., and White, W., (2000): Breakdown morphology, Speleogenesis: Evolution of Karst Aquifers, p. 427-429.

White, E. L., and White, W., (1969): Processes of cavern breakdown, Nat. Spel. Soc. Bull, v. 31, p. 83-96.

White, W. B., (1988): Geomorphology and hydrology of karst terrains, Oxford university press New York,

Worsley, D., (2008): The post-Caledonian development of Svalbard and the western Barents Sea, Polar Research, v. 27, no. 3, p. 298-317.

Worsley, D., Aga, O. J., Dalland, A, Elverhøi, A., Thon, A., (1986): The Geological history of Svalbard: evolution of an arctic archipelago, Den norske stats oljeselskap as,

Zolotukhin, A. B., and J- R. Ursin, (2000): Introduction to petroleum reservoir engineering, Kristiansand, Høyskoleforlaget AS - Norwegian Academic Press, 402 p.

10 Appendix 1

10.1 Area 1 – The Red Breccia Pipe
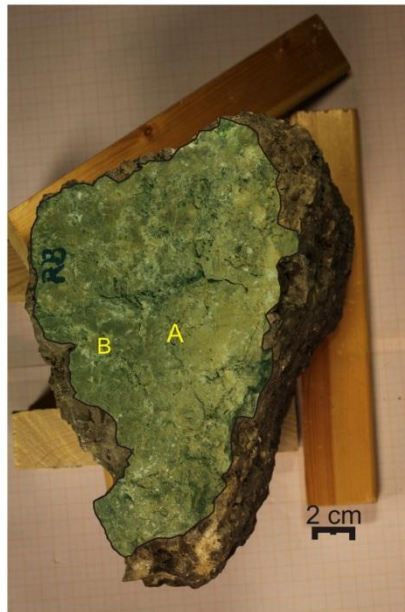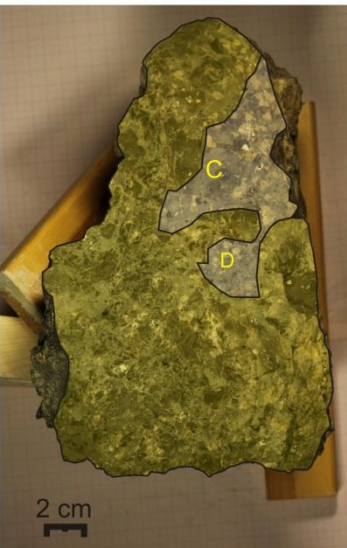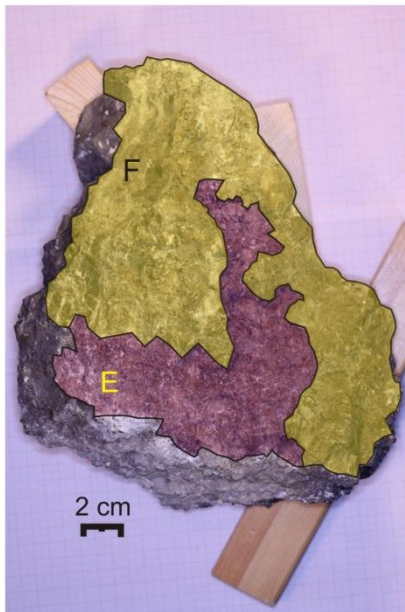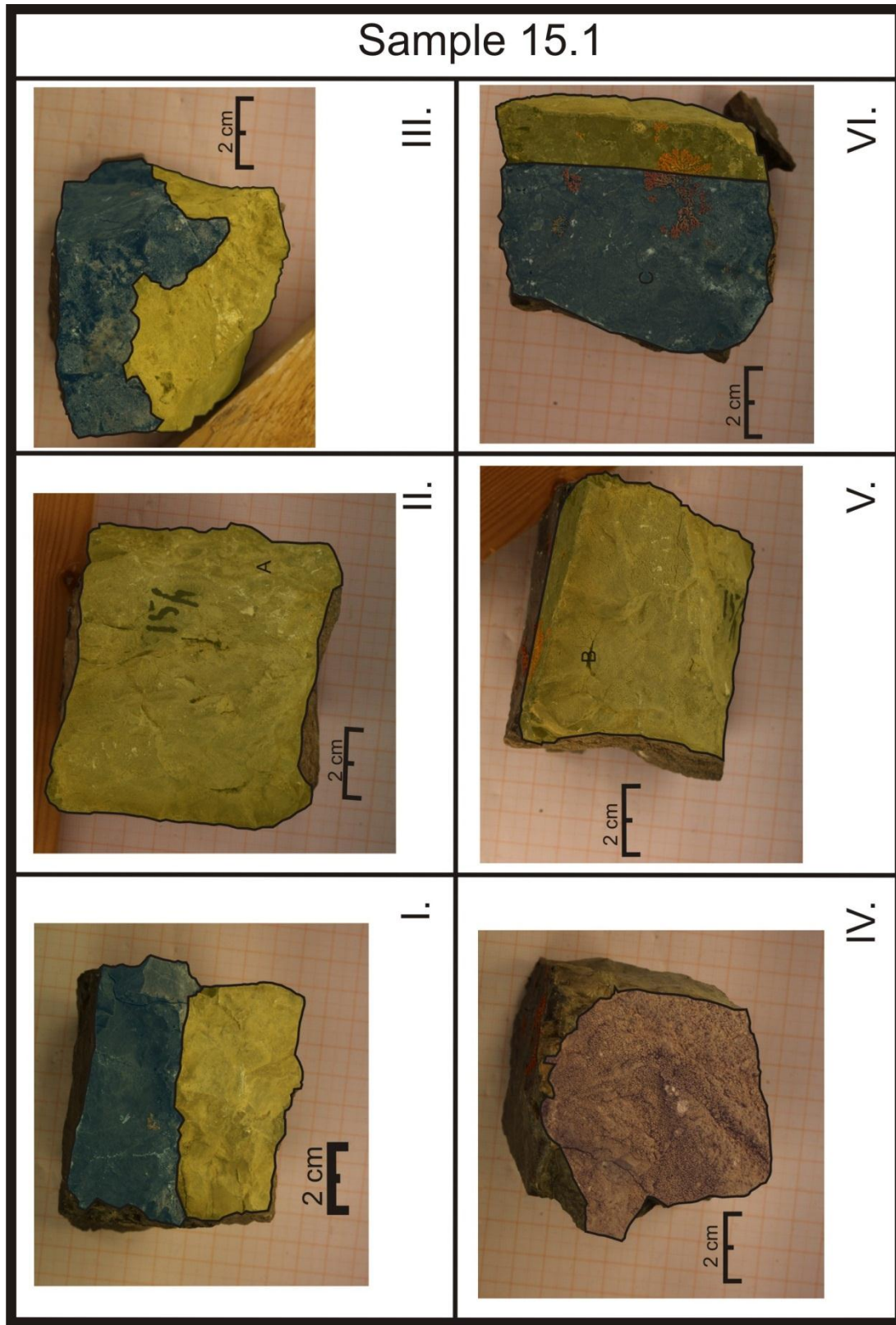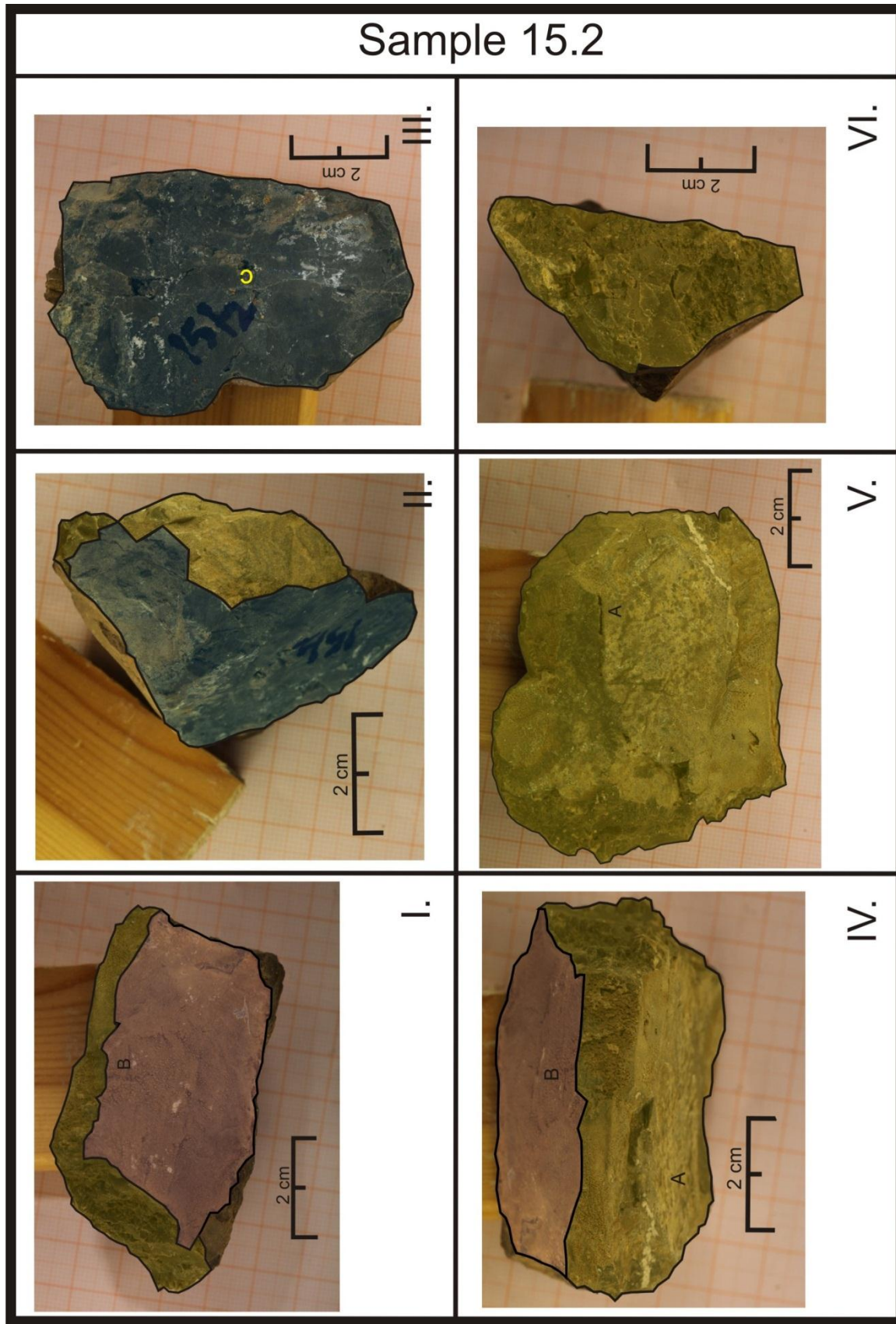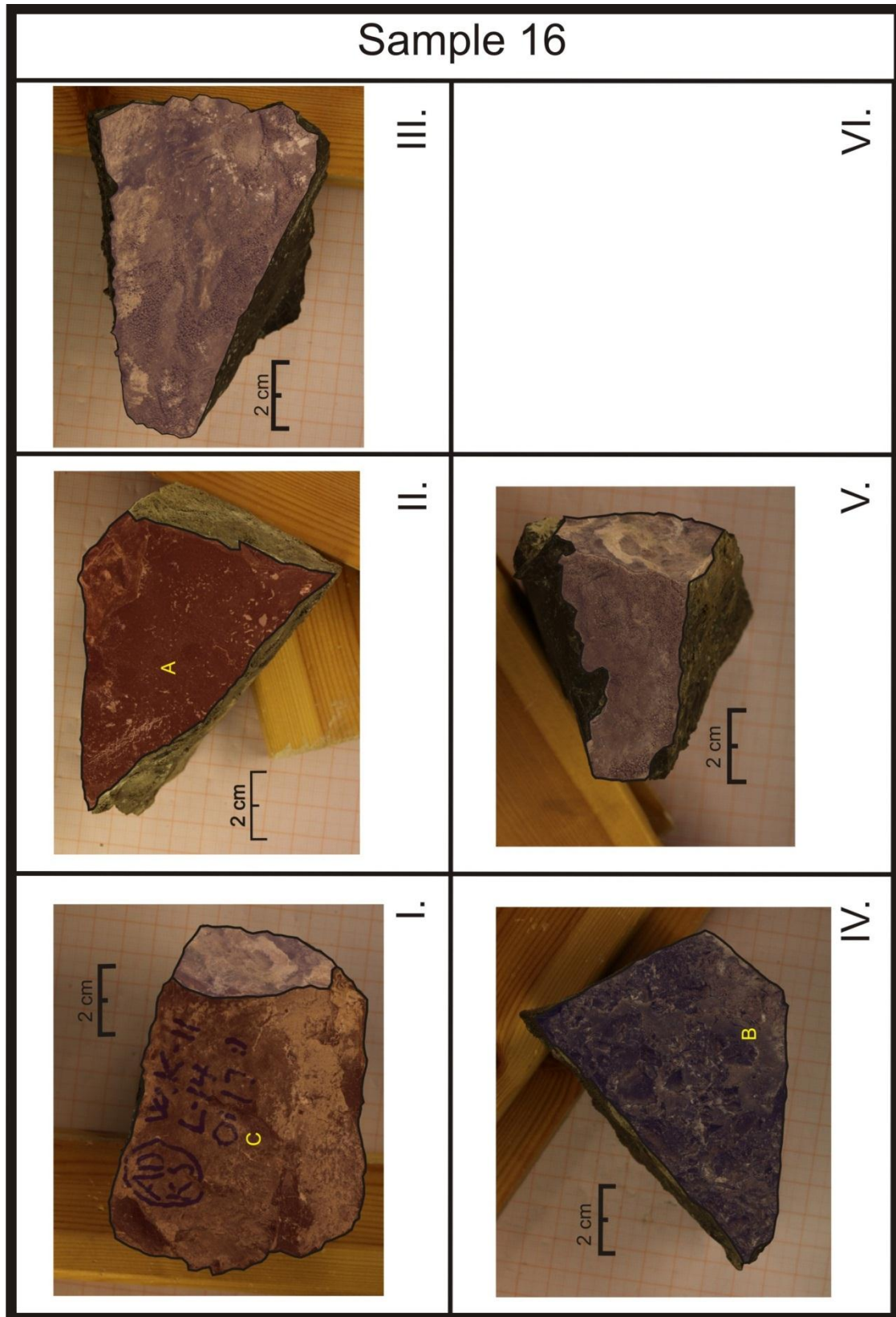
Sample 9

Sample 14

Sample 15.1

Sample 15.2

Sample 16

Sample 19

10.2 Area 2

Sample 1M

Sample Q1

Sample Q2

I.

II.

III.

IV.

V.

VI.

10.3 Area 3

Sample 1Aa

I.

II.

III.

IV.

V.

VI.

VII.

VIII.

Sample 1Ab

Sample 1Ac

Sample 1Ad

Sample 1B

Sample 1C

I.

II.

III.

IV.

V.

VI.

VII.

VIII.

Sample 3A1

Sample 3A2
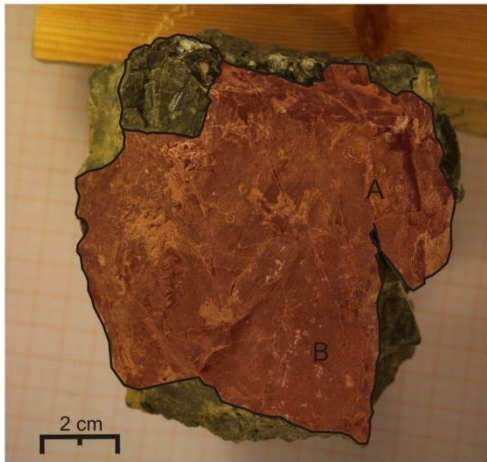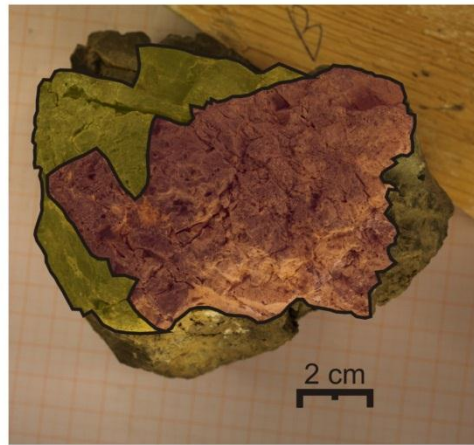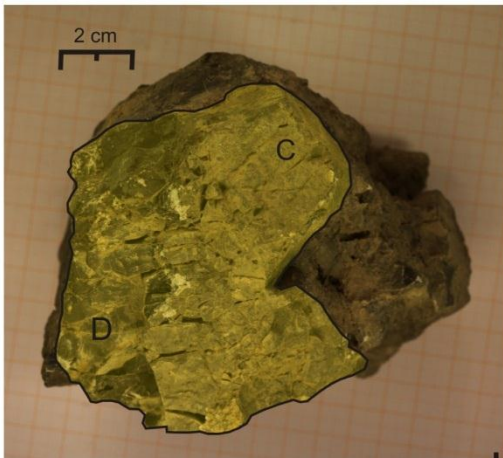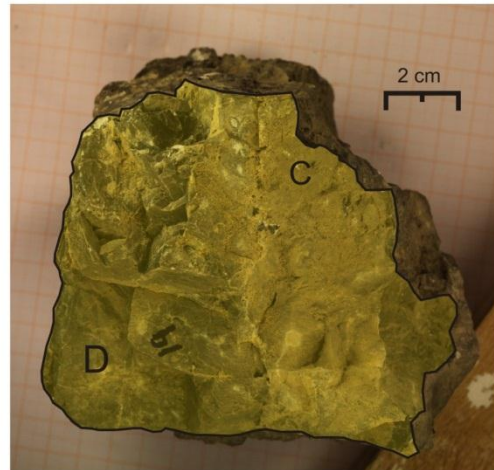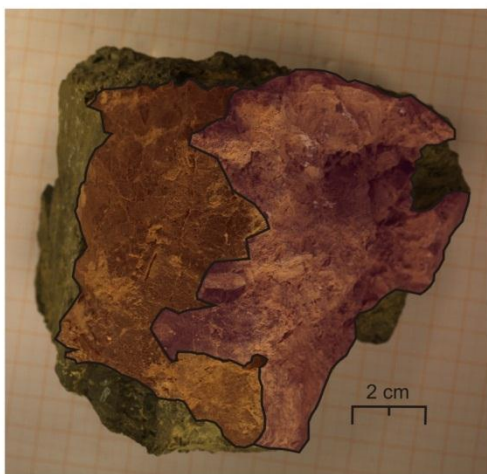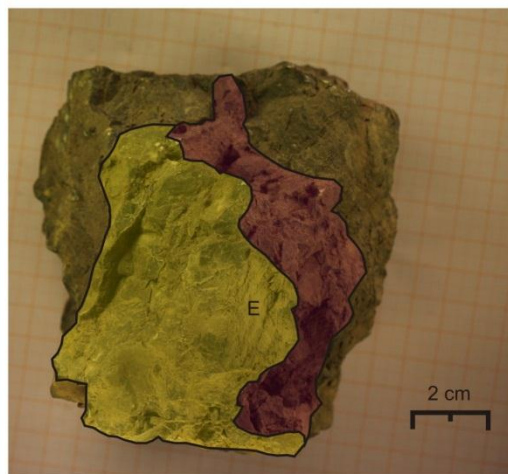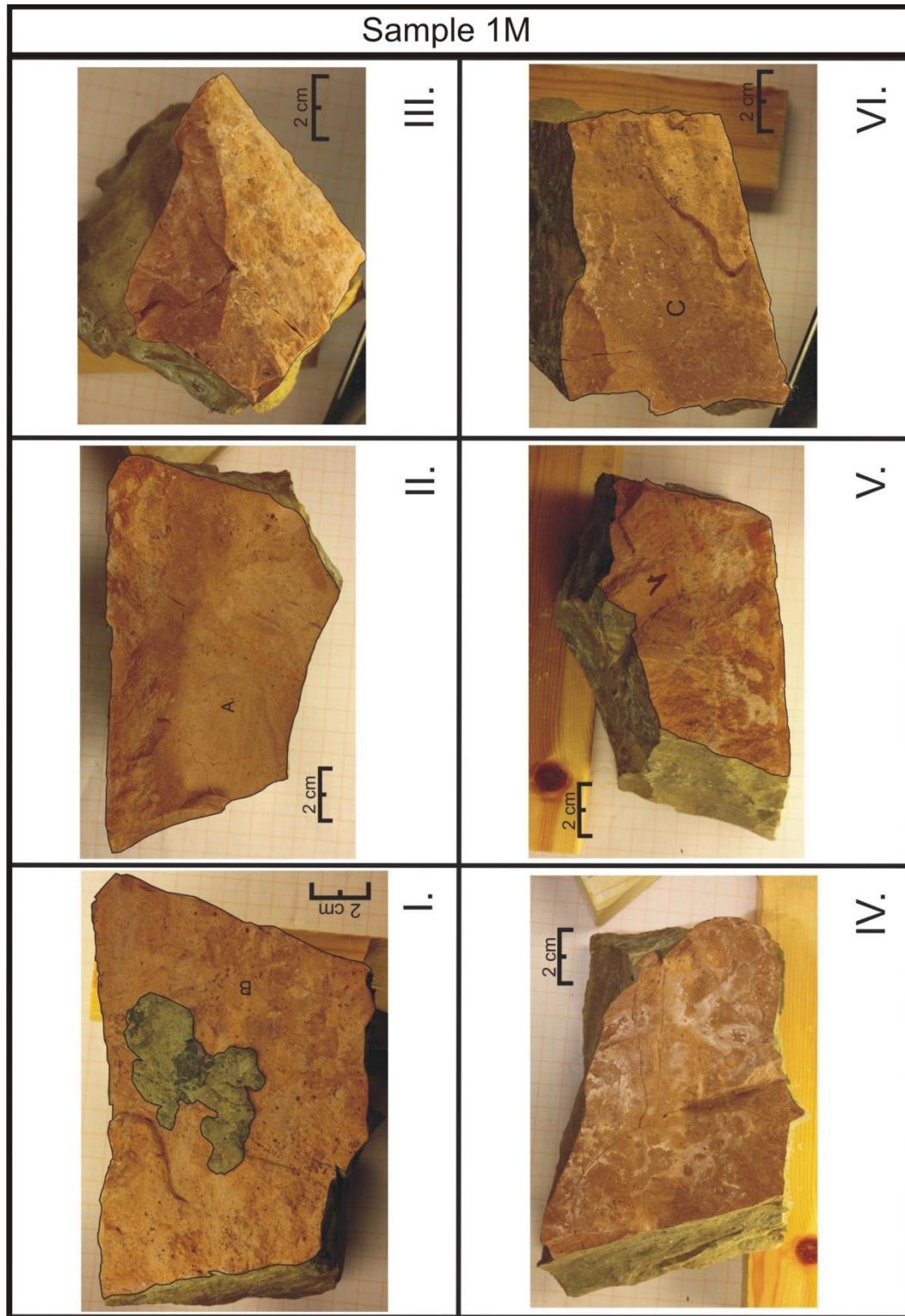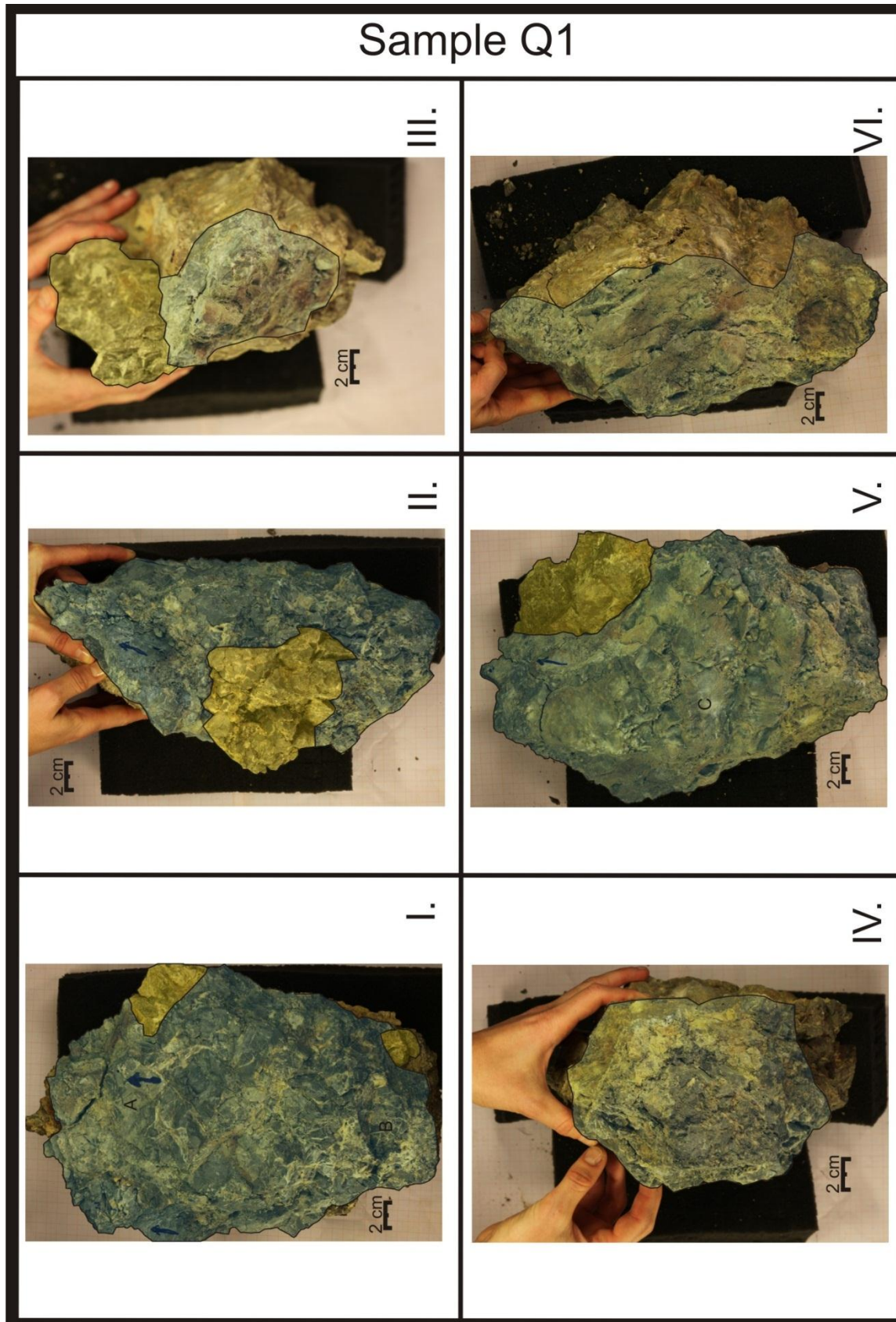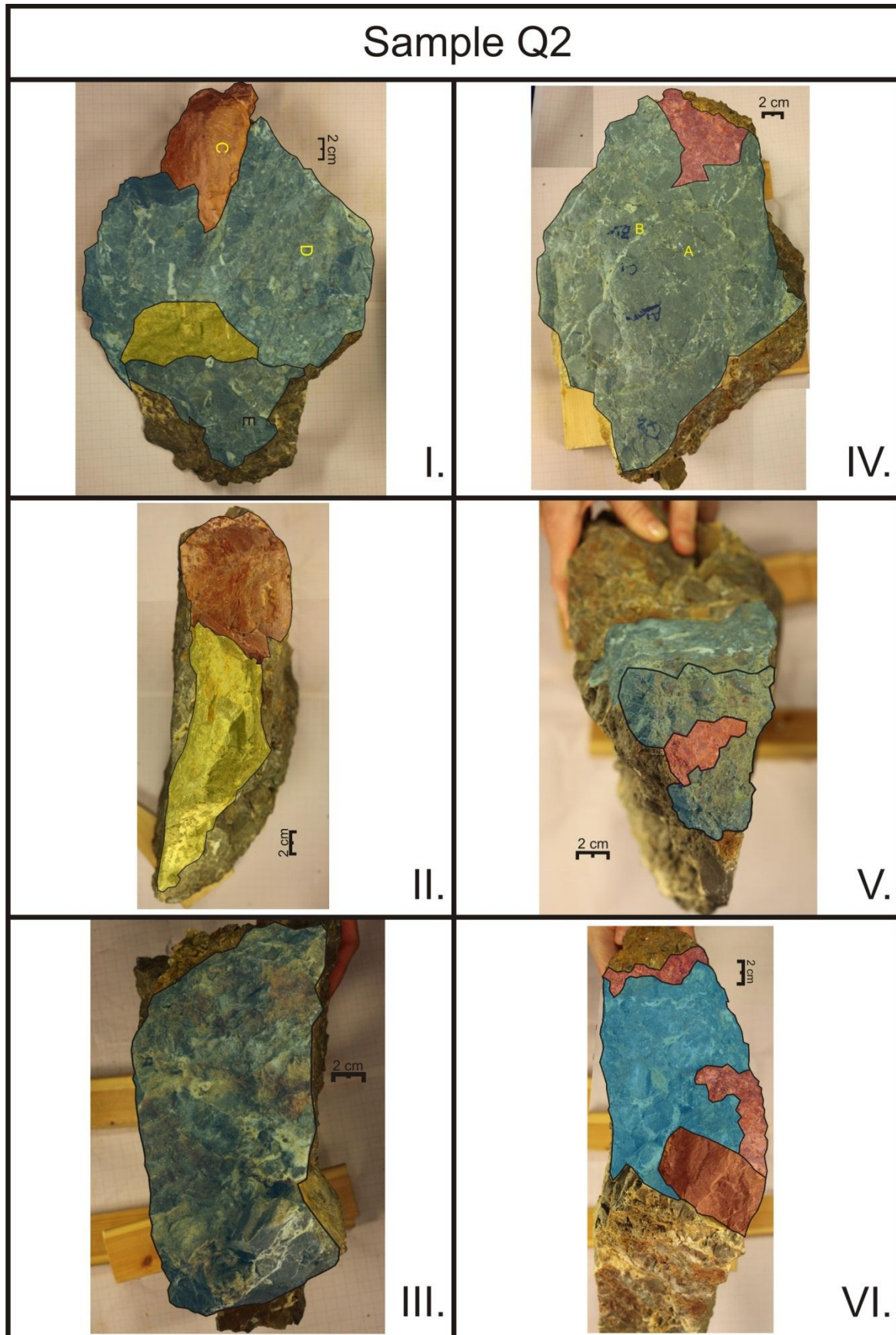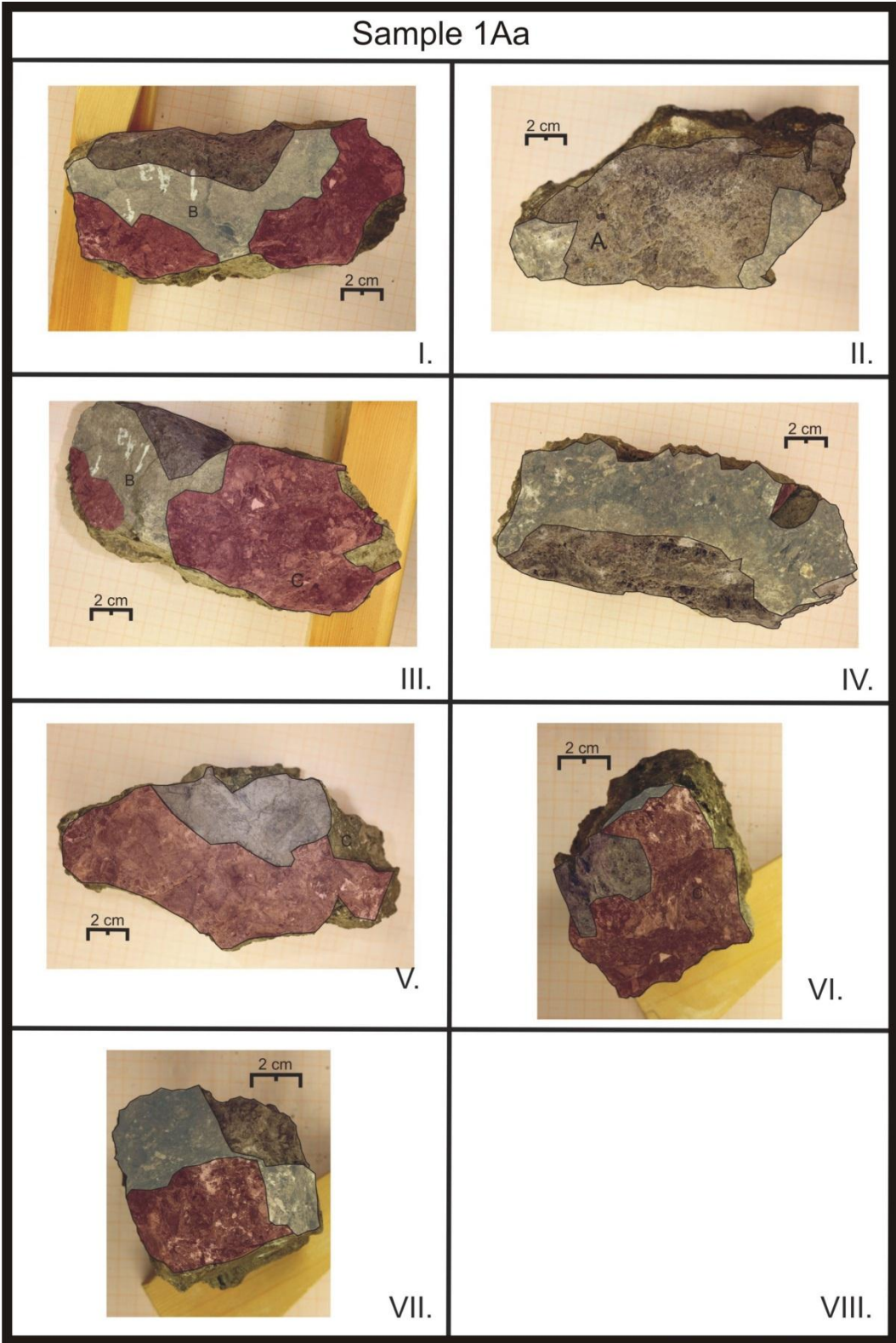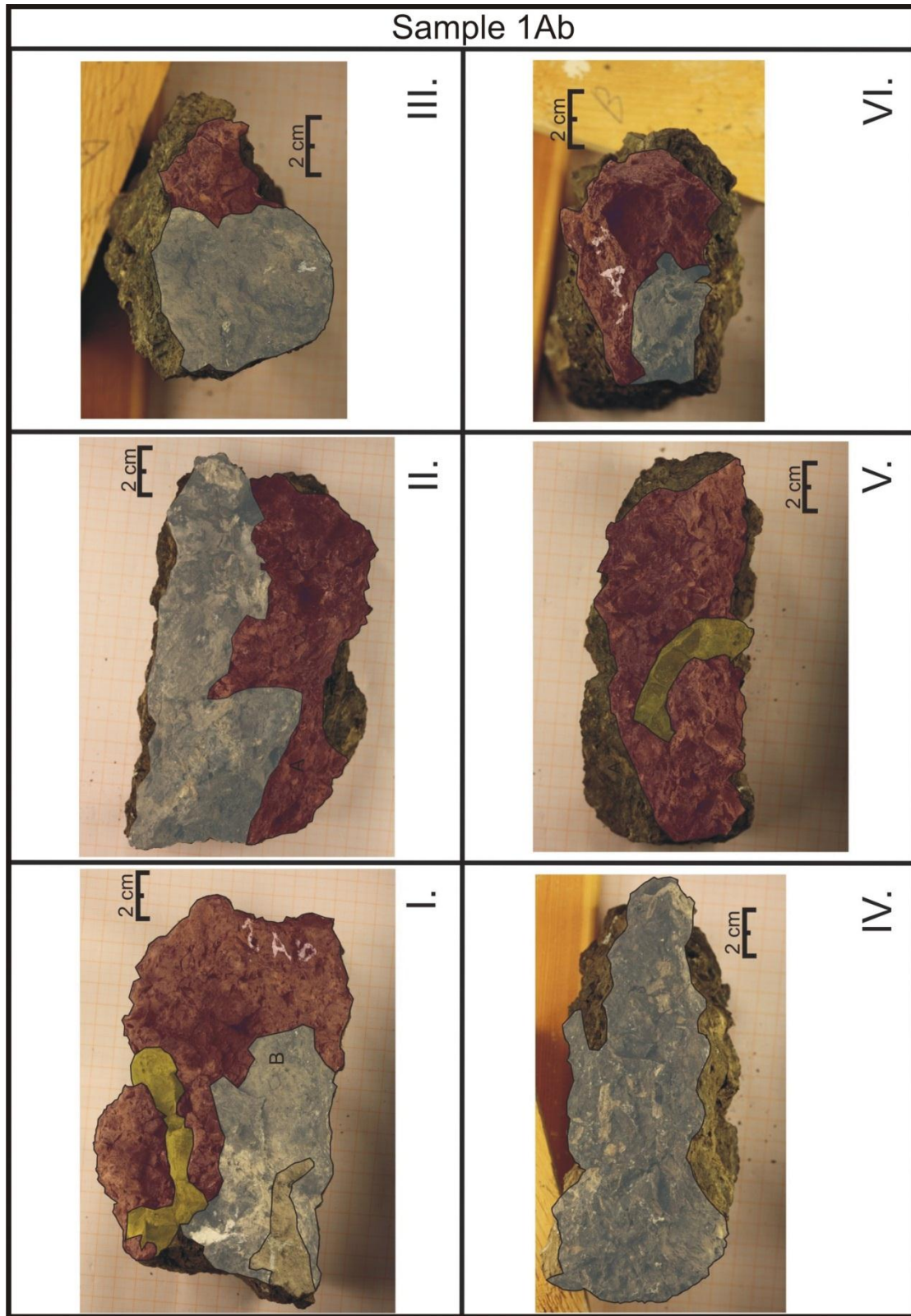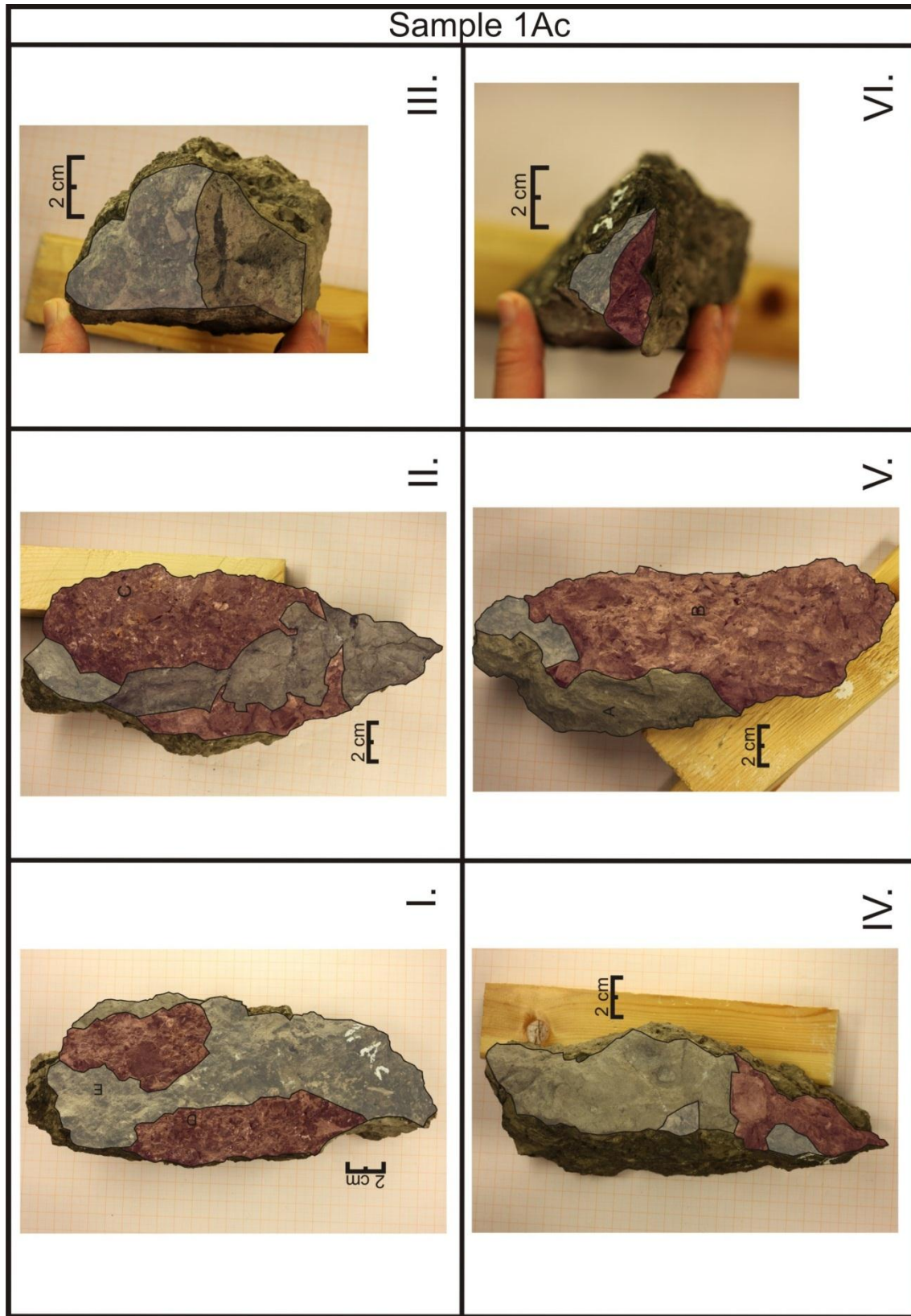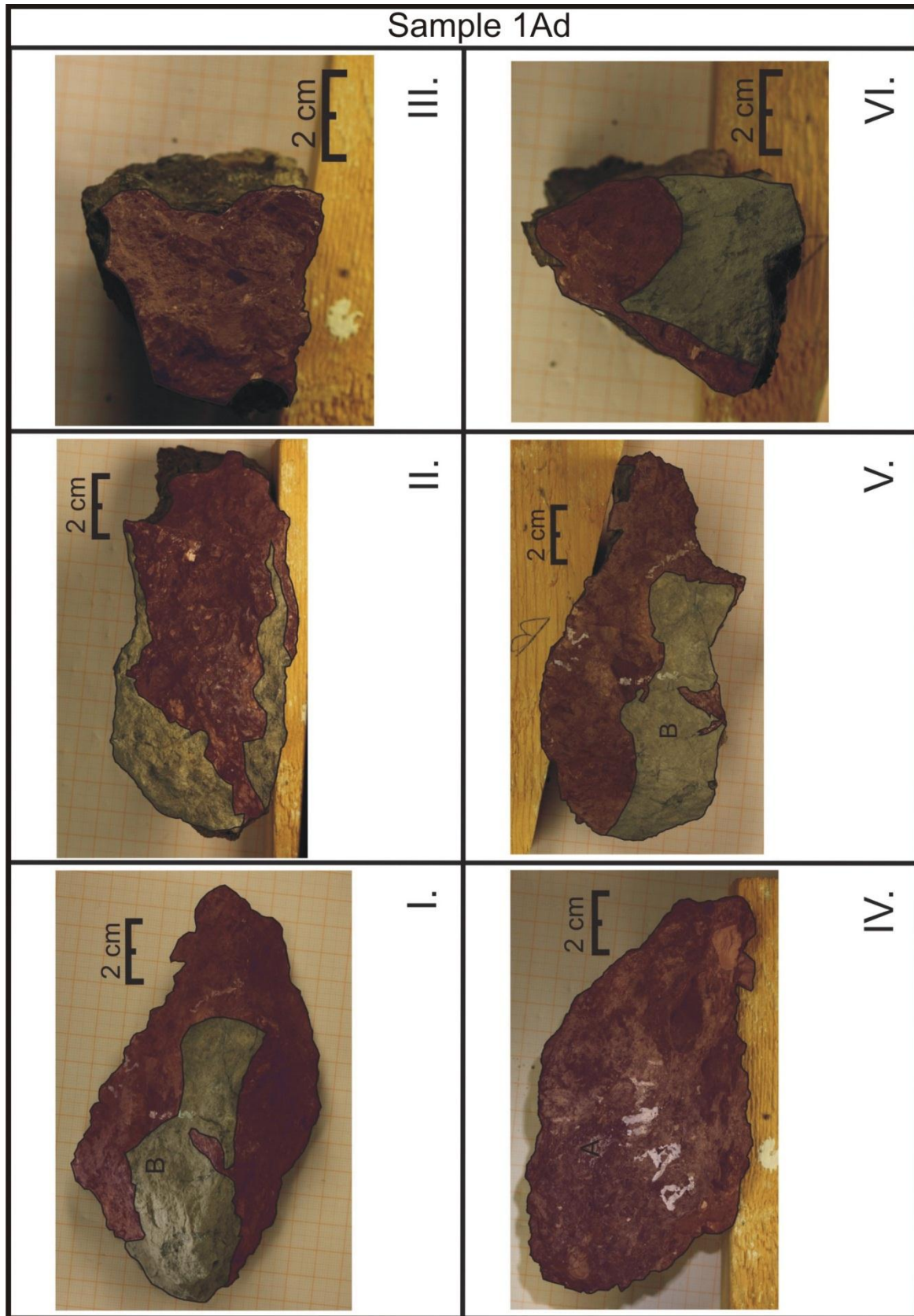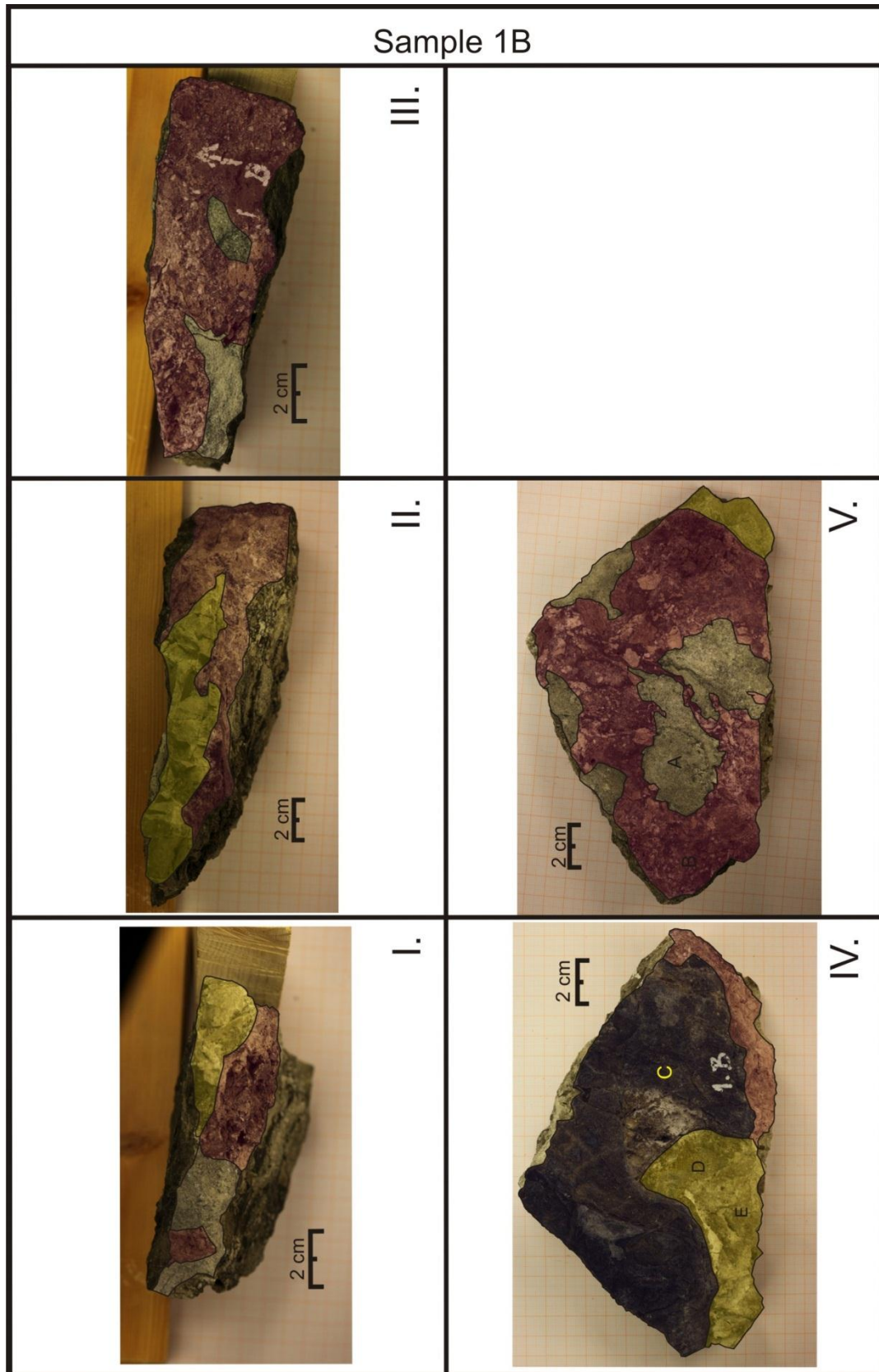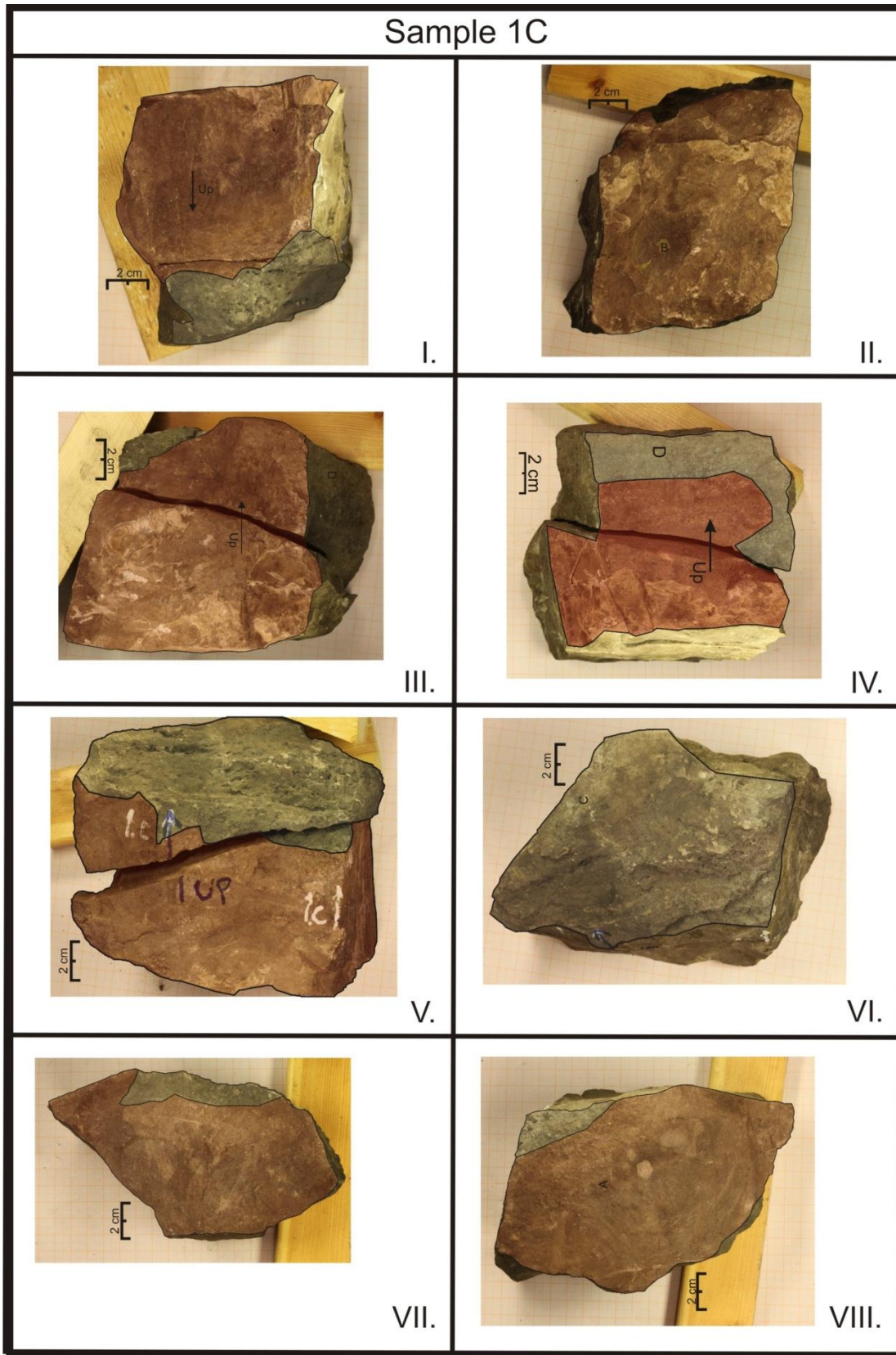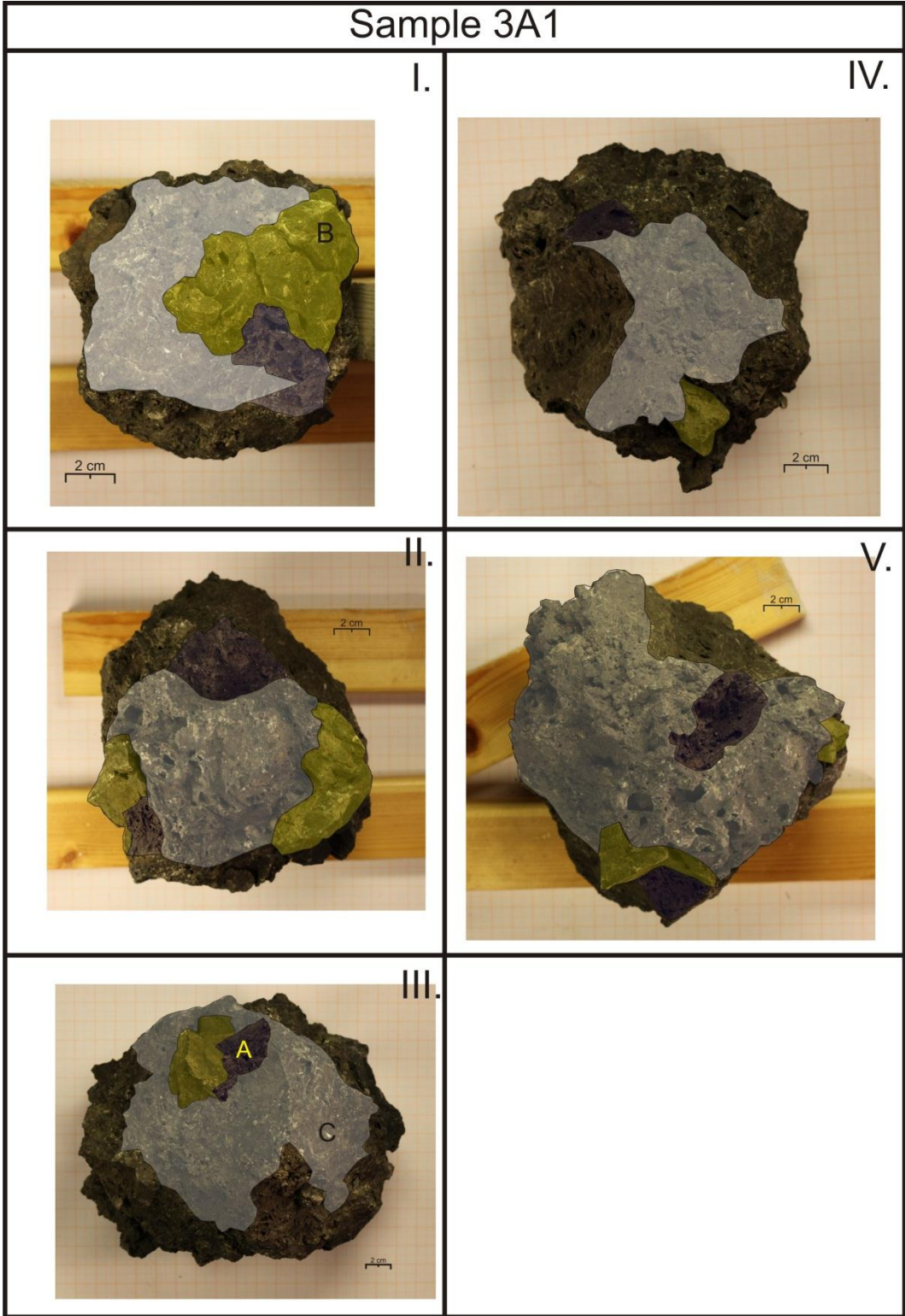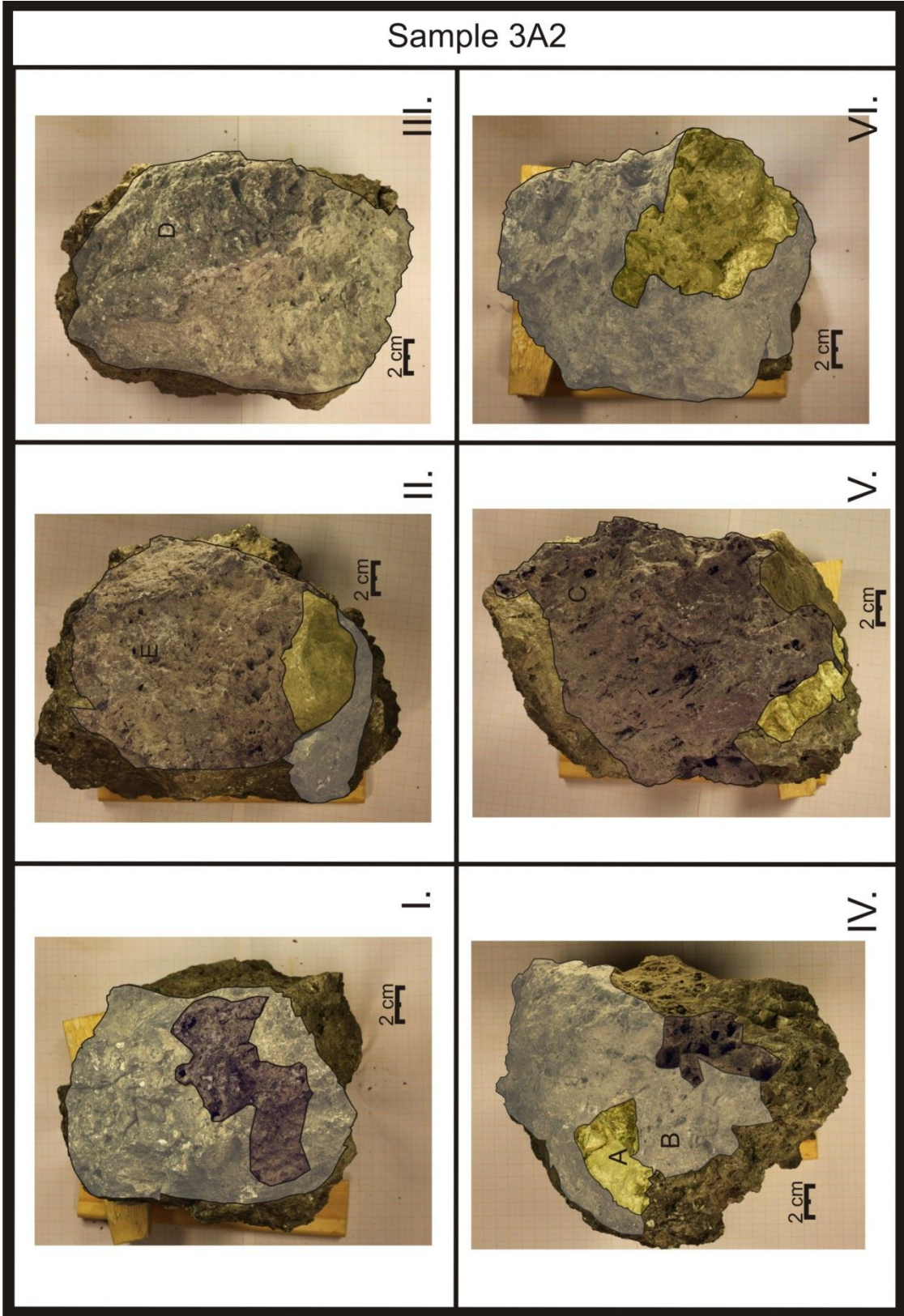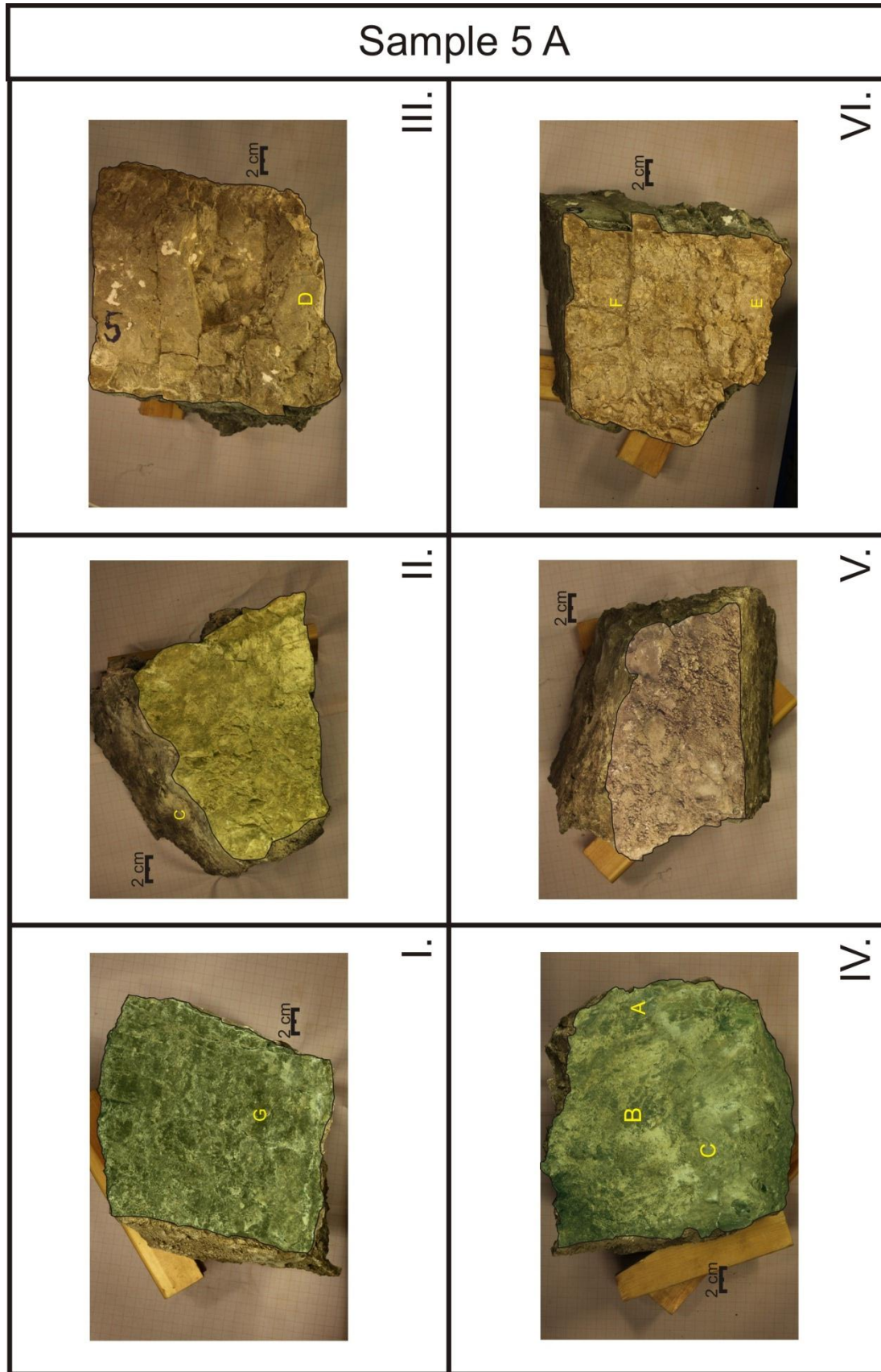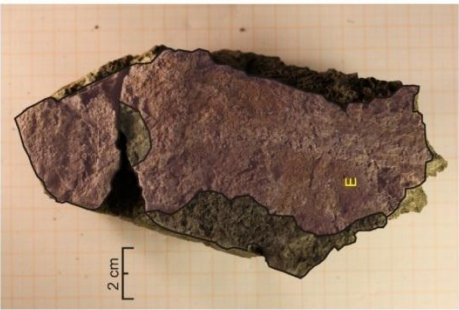
Sample 5 A

Sample 5 B

11 Appendix 2

11.1 Results of experimental measurement

This section will present the measured and calculated values from the lab experiments. The objective of this is that several experiments were carried out for the samples, but some of the results are more credible than the other. The most reliable 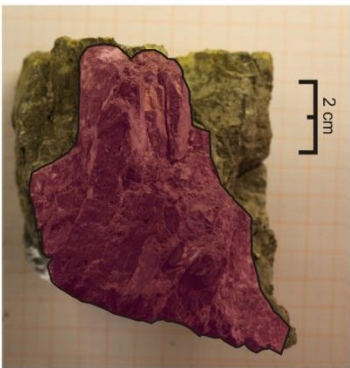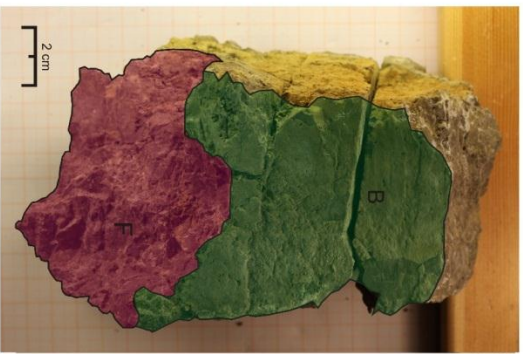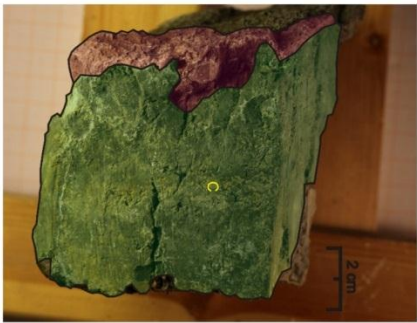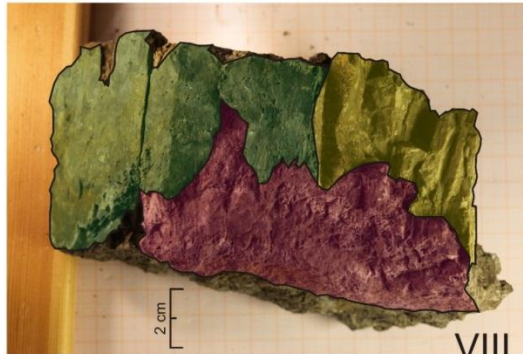values are presented in chapter five. The presentation of the measured and calculated results will follow the same order as the results chapter.

11.1.1 Area 1 – The Red Breccia Pipe

Sample 6	Vm,cm3	Vtot,cm3	Vp, (g)	φ,%	Vtot,disp. (cm3)
1.	226	226	3	1.2	
σ	±2	±2	±1	±0.6	
2.		**226**	**4,5**	**2.0**	290
σ		±1	±0.9	**±0.4**	± 100

Sample 9	Vm,cm3	Vtot,cm3	Vp, (g)	φ,%	Vtot,disp. (cm3)
1.	36.2	-	0.9	-	
σ	±0.4		± 0.2		
2.		**36.5**	**0.3**	**0.7**	44
σ		±0.4	± 0.2	**±0.6**	±18

Sample 14-16	Vm,cm3	Vtot,cm3	Vp, (g)	φ,%	Vtot,disp. (cm3)
1.	195	-	2.3	-	
σ	±2		±0.5		
2.		**197**	**2.0**	**1.0**	290,2
σ		±2	±0.4	**±0.2**	±100

Sample 15/1	Vm,cm3	Vtot,cm3	Vp, (g)	φ,%	Vtot,disp. (cm3)
1.	293	**295**	**4.3**	**1.5**	
σ	±3	±1	± 0.9	±0.3	
2.		295	3,3	1.1	193
σ		±1	± 1.0	±0.3	±100

Sample 15/2	Vm,cm3	Vtot,cm3	Vp, (g)	ϕ,%	Vtot,disp. (cm3)
1.	75.4	-	1.7	-	
σ	±0.8	-	±0.3	-	
2.		**75.6**	**1.5**	**1.9**	88
σ		±0.8	±0.3	±0.4	±18

Sample 19	Vm,cm3	Vtot,cm3	Vp, (g)	ϕ,%	Vtot,disp. (cm3)
1.	698	395	30	8	
σ	±7	±316	±3	±6	
2.		**700**	**32**	**4.5**	773,8
σ		±7	±3	±0.5	±100

RB=14,small	Vm,cm3	Vtot,cm3	Vp, (g)	ϕ,%	Vtot,disp. (cm3)
1.	72.4	74	3	3,49	
σ	±0.7	±1	±1	±0.7	
2.		**73,4**	**3.2**	**4.3**	157,95
σ		±0.7	±0.6	±0.9	±18

Sample RB=14,stor	Vtotal (dry),cm3	Vtotal (sat),cm3	Vp, (g)	ϕ,%	Vtot,disp. (cm3)
1.	2623	**2619**	**179**	**7**	-
σ	±26	±26	±54	±2	-

11.1.2 Area 2

1.mink	Vtotal (dry),cm3	Vtotal (sat),cm3	Vp, (g)	ϕ,%	Vtot,disp. (cm3)
1.	694	692	21	2,99	
σ	±7	±3	±1	±0.2	
2.		**693**	**21**	**3.1**	774
σ		±3	±1	±0.2	±100

Sample Q1A	Vm,cm3	Vtot,cm3	Vp, (g)	ϕ,%	Vtot,disp. (cm3)
1.	2406	**2400**	**125**	**5.2**	-
σ	±24	±12	±12	0.5	-

Q1,B	Vm,cm3	Vtot,cm3	Vp, (g)	ϕ,%	Vtot,disp. (cm3)
1.	620	626	18	2.8	
σ	±6	±6	±4	±0.7	
2.		**625**	**14**	**2.2**	677
σ		±6	±3	±0.5	±100

Q1,C	Vm,cm3	Vtot,cm3	Vp, (g)	ϕ,%	Vtot,disp. (cm3)
1.	320	296	17	5.6	
σ	±3	±6	±2	±0.6	
2.		**292**	**16**	**5.4**	290
σ		±3	±2	±0.5	±100

Q1,D	Vm,cm3	Vtot,cm3	Vp, (g)	ϕ,%	Vtot,disp. (cm3)
1.	182	185	6.6	3.6	
σ	±2	±4	±0.3	±0.2	
2.		**183**	**6.7**	**3.7**	193
σ		±2	±0.3	±0.2	±100

Q1,E	Vm,cm3	Vtot,cm3	Vp, (g)	ϕ,%	Vtot,disp. (cm3)
1.	49.5	50	0.17	0.3	
σ	±0.5	±1	±0.14	±0.3	
2.		**49.2**	**1.2**	**2.4**	53
σ		±0.5	±0.1	±0.2	±18

Q1,F	Vm,cm3	Vtot,cm3	Vp, (g)	ϕ,%	Vtot,disp. (cm3)
1.	51	52	1.1	2.2	
σ	±0.5	±1	±0.3	±0.6	
2.		**51.3**	**1.7**	**3.4**	53
σ		±0.5	±0.3	±0.7	±18

Q1,G	Vm,cm3	Vtot,cm3	Vp, (g)	ϕ,%	Vtot,disp. (cm3)
1.	67.3	68	2.8	4.1	
σ	±0.7	±1	±0.6	±0.8	
2.		**67.4**	**3.2**	**4.8**	70
σ		±0.7	±0.3	±0.5	±18

Q1,H	Vm,cm3	Vtot,cm3	Vp, (g)	ϕ,%	Vtot,disp. (cm3)
1.	127	129	9.9	7.7	
σ	±1	±3	±0.5	±0.4	
2.		**127**	**9.8**	**7.7**	123
σ		±1	±0.2	±0.2	±18

Q2,A	Vm,cm3	Vtot,cm3	Vp, (g)	ϕ,%	Vtot,disp. (cm3)
1.	173	**176**	**3.5**	**2.0**	
σ	±2	±2	±0.7	±0.4	
2.		174	2.7	1.5	193
σ		±2	±0.8	±0.5	±100

Sample Q2,B	Vm,cm3	Vtot,cm3	Vp, (g)	φ,%	Vtot,disp. (cm3)
1.	2489	**2535**	**45**	**1.79**	-
σ	±25	±51	±2	±0.10	-

Sample Q2,C	Vm,cm3	Vtot,cm3	Vp, (g)	φ,%	Vtot,disp. (cm3)
1.	3063	**3050**	**48**	**1.6**	-
σ	±31	±30	± 5	±0.2	-

Q2,D	Vm,cm3	Vtot,cm3	Vp, (g)	φ,%	Vtot,disp. (cm3)
1.	276	271	6.0	2.2	
σ	±3	±3	±0.6	±0.2	
2.		**271**	**6.5**	**2.4**	435,26
σ		±3	±0.7	±0.2	±100

Q2,E	Vm,cm3	Vtot,cm3	Vp, (g)	φ,%	Vtot,disp. (cm3)
1.	609	619	12	1.9	
σ	±6	±6	±2	±0.4	
2.		**620**	**14**	**2.2**	580
σ		±6	±1	±0.2	±100

11.1.3 Area 3

Locality 1

Sample 1Aa	Vm,cm3	Vtot,cm3	Vp, (g)	φ,%	Vtot,disp. (cm3)
1.	734	753	98	13.0	
σ	±7	±15	±5	±0.7	
2.		**734**	**102**	**13.9**	773.8
σ		±4	±2	±0.3	±100

Sample 1Ab	Vm,cm3	Vtot,cm3	Vp, (g)	φ,%	Vtot,disp. (cm3)
1.	676	678	63	9.3	
σ	±7	±7	±6	±0.9	
2.		**674**	**69**	**10.2**	677,075
σ		±3	±3	±0.5	±100

Sample 1Ac	Vm,cm3	Vtot,cm3	Vp, (g)	φ,%	Vtot,disp. (cm3)
1.	710	697	79	11.3	
σ	±7	±3	±2	±0.2	
2.		**696**	**79**	**11.4**	532
σ		±3	±2	±0.2	±100

Sample 1Ad	Vm,cm3	Vtot,cm3	Vp, (g)	φ,%	Vtot,disp. (cm3)
1.	233	232	27.8	12.0	
σ	±2	±1	±0.8	±0.4	
2.		**232**	**27.9**	**12.0**	193
σ		±1	±0.8	±0.4	±100

Sample 1B	Vm,cm3	Vtot,cm3	Vp, (g)	φ,%	Vtot,disp. (cm3)
1.	546	533	82	14.4	
σ	±5	±16	±4	±0.9	
2.		**546**	**84**	**15.4**	580
σ		±5	±3	±0.5	±100

Sample 1C,Lower	Vm,cm3	Vtot,cm3	Vp, (g)	φ,%	Vtot,disp. (cm3)
1.	872	**870**	**32**	**3.7**	
σ	±9	±4	±3	±0.4	
2.		870	29	3.4	774
σ		±4	±3	±0.3	±100

Sample 1C,upper	Vm,cm3	Vtot,cm3	Vp, (g)	φ,%	Vtot,disp. (cm3)
1.	374	375	37	10	
σ	±4	±4	±4	±1	
2.		**374**	**39**	**10.4**	435
σ		±2	±2	±0.5	±100

Locality 3

Sample 3A1	Vm,cm3	Vtot,cm3	Vp, (g)	φ,%	Vtot,disp. (cm3)
1.	1139	-	146	-	
σ	±11	-	±3	-	
2.		**1147**	**148**	**12.9**	1161
σ		±11	±7	±0.7	±100

Sample 3A2	Vm,cm3	Vtot,cm3	Vp, (g)	φ,%	Vtot,disp. (cm3)
1.	3818	**3802**	**375**	**6.8**	-
σ	±38	± 38	±19	±0.5	-

Locality 4

Sample 4	Vm,cm3	Vtot,cm3	Vp, (g)	φ,%	Vtot,disp. (cm3)
1.	1776	**1774**	**128**	**7.2**	1741,05
σ	±18	±18	±13	±0.7	±100

Locality 5

Sample 5A1	Vtotal (dry),cm3	Vtotal (sat),cm3	Vp, (g)	φ,%	Vtot,disp. (cm3)
1.	2833	**2831**	**105**	**3.7**	-
σ	±28	±28	±11	±0.4	-

Sample 5A2	Vtotal (dry),cm3	Vtotal (sat),cm3	Vp, (g)	φ,%	Vtot,disp. (cm3)
1.	2131	**2132**	**93**	**4.4**	-
σ	±21	±21	±9	±0.4	-

Sample 5B,large	Vm,cm3	Vtot,cm3	Vp, (g)	φ,%	Vtot,disp. (cm3)
1.	519	-	24.9	-	
σ	±5	-	±0.5	-	
2.		**520**	**24.6**	**4.7**	484
σ		±5	±0.5	±0.1	±100

Sample 5B,small	Vm,cm3	Vtot,cm3	Vp, (g)	φ,%	Vtot,disp. (cm3)
1.	137	-	5.5	-	
σ	±1	-	±0.5		
2.		**138**	**50**	**3.7**	158
σ		0 ±1	±0.5	±0.4	±18